

**Proceedings of the
16th Australian Space Research Conference
Melbourne
September 26 - 28, 2016**



Australian Space Research Conference Series

1st Edition
Published in Australia in 2017 by
National Space Society of Australia Ltd
GPO Box 7048
Sydney NSW 2001
Fax: 61 (02) 9988-0262
email: nssa@nssa.com.au
website: <http://www.nssa.com.au>

Copyright © 2017 National Space Society of Australia Ltd

All rights reserved. No part of this publication may be reproduced, stored in a retrieval system or transmitted in any form or by any means, electronic, mechanical, photocopying, recording or otherwise, without prior permission from the publisher.

ISBN 13: 978-0-6481570-0-7
Editors: Wayne Short and Iver Cairns

Distributed on DVD



Preface to the Proceedings

The Australian Space Research Conference (2016), held at the RMIT University - City Campus (Melbourne, Australia) from September 26 to 28, 2016 (<http://www.nssa.com.au/16asrc/>), was a very successful event, where over 130 papers from Australian and international groups working in the field of space research, business, policy and culture, were presented. Following the conference some of the works were submitted as full-length papers. These proceedings collect the papers accepted after a rigorous process of peer-review.

Each paper published in these proceedings has been peer-reviewed by two assessors selected by the Chair of the Program Committee with inputs from members of the committee, and revised by the authors accordingly. Final decisions to accept or reject manuscripts in their submitted or revised form were taken by the Editor of these proceedings in consultation with the Editor-in-Chief.

More than 35 scientists, engineers and space professionals from Australian and international organizations participated in the peer-review process, with some referees assessing and providing feedback on more than one manuscript. We list below (in alphabetical order) only the referees who agreed to be identified:

Elias Aboutanious (UNSW), Simon Barraclough (UNSW Canberra), Craig Benson (UNSW Canberra), Adrian Brown (SETI Institute), David Buttsworth (University of Southern Queensland), Robert Carter (University of Southern Queensland), Iver Cairns (The University of Sydney), David Lingard (DSTG), Marc Norman (ANU), Hideaki Ogawa (RMIT University), Li Qiao (UNSW Canberra), Wayne Short (NSSA), Tracey Sletten (Monash University) Lachlan Thomson (RMIT University), Yang Yang (RMIT University)

To all the other reviewers who asked to remain anonymous, but who also responded enthusiastically to our invitation to assess and provided timely reviews, we express our gratitude and special acknowledgments for their generous support: they are highly regarded experts in their disciplines, affiliated to universities, and research and professional organizations all over the world.

All reviewers made constructive criticism and suggestions that greatly improved the manuscripts and

contributed to the quality of these proceedings. Responsibility for the published content remains with the authors of the papers, as well as the intellectual property of the work described. The publisher retains copyright over the published Proceedings. Papers appear in these Conference Proceedings with authors' permission.

We thank the RMIT University, for providing the venue and conference facilities, the ASRC 2016 Organizing Committee, the RMIT University members of the Local Organizing Committee chaired by Kefei Zhang, the members of the Program Committee chaired by Iver Cairns, and all the members of the Australian Space Research Community for giving generously of their time, suggestions, and efforts. The Australian Academy of Science, Mars Society Australia, and University of South Australia co-sponsored various conference events.

We trust that you will find the 2016 Conference Proceedings enjoyable and informative.

Iver Cairns

(Editor, 16th ASRC Proceedings; Chair, ASRC 2016 Program Committee)

Wayne Short

(Editor-in-Chief, ASRC Proceedings)

August 2017

Conference Background

The Australian Space Research Conference (ASRC) is the focus of scientific cooperation and discussion in Australia on research relating to space. It is a peer reviewed forum for space scientists, engineers, educators, and workers in Industry and Government.

The conference is of relevance to a very broad cross section of the space community, and therefore generates an enlightening and timely exchange of ideas and perspectives. The scope of the conference covers fundamental and applied research that that can be done from space and space-based platforms, and includes the following:

- Space science, including space and atmospheric physics, Earth observation and remote sensing from/of space, planetary sciences, astrobiology and life sciences, space-based astronomy and astrophysics, and exoplanets.
- Space engineering and technology, including communications, navigation, space operations, space materials, propulsion, and spacecraft design, testing, and implementation.
- Space industry and business
- Space Situational Awareness (SSA)
- Space archaeology and indigenous sky knowledge (or archeo-astronomy)
- Humanities and social aspects
- Use of space data, including EOS, GNSS, and communications
- Current and future Australian space projects
- Government, international relations and law
- Education and outreach, including a dedicated student session.
- Mars and Planetary Exploration

The 2016 conference included a comprehensive program of plenary talks and special sessions on the national context for space the foci and the programs of Australian Government units with interests in space. In addition, the program contained a special planetary science session, with a strong preponderance of projects involving the Mars Society of Australia. The program also contained multiple sessions of invited and contributed presentations, both oral and poster, on Propulsion, Planetary Science, Earth Observation and GNSS, Space Capabilities, Space Physics, Space Situational Awareness, Space Technology, Space Archeology, Education and Outreach, and Indigenous Sky Knowledge.

Appendix A lists all abstracts accepted for presentation at the conference. A call for abstracts was issued in March 2016 and researchers were invited to submit abstracts intended for presentation at the conference. Following the conference itself, a call for written papers was issued in October 2016: this invited presenters to submit a formal written papers for this Proceedings that covered their conference presentations.

Table of Contents

Preface to Proceedings	page iii
Conference Background	page v
List of Proceedings Papers	page vii
About the NSSA	page x
About the NCSRS	page xi
2016 Program Committee	page xiii
2016 Organising Committee	page xiv
Conference Plenary Speakers	page xv
Program	page xvii

List of Proceedings Papers

Authors	Paper Title	Pages
Jonathan Horner, Belinda Nicholson, Ann Cairns, Wayne Short and Alice Gorman	The Gender Balance of the Australian Space Research Community: A Snapshot From The 16th ASRC, 2016	1-12
Lachlan Thompson, James Murray, Anne Brumfitt	Emerald & Mount Burnett Observatories, New Opportunities for Earth Situational Awareness, Research, Education and Tourism	13-22
Gabriela-Nicoleta Hobbs	The ethics of working with robots	23-38
Gabriela-Nicoleta Hobbs	Educational and Scientific Benefits of Extreme Environments	39-52
Kimberley Norris	Antarctic Behavioural Health as a Space Analogue	53-60
Steven Hobbs, David J. Paull, Jonathan Clarke, Siddharth Pandey	Mobility Trials of a Small Planetary Science Rover for Mars Surface Exploration	61-74
Steven Hobbs, David J. Paull, Jonathan Clarke, Siddharth Pandey	Hands Off Field Work: Comparison of Human and Robotic Methods for Gathering Terrain Data using Structure From Motion.	75-88
S.W. Hobbs, D.J. Paull and J. D. A. Clarke	The Little Blue Rover: Robotic Characterisation of Mars Analogue Sites in Arkaroola.	89-104
Siddharth Pandey, Sean Tuttle, John Young	Designing an Experiment to Improve the Understanding of Thermal Convection to aid Gas Gap Design of Mars Rovers	105-114
Jonathan D. A. Clarke, Anna M. Clarke, Gabi Hobbs, Steve Hobbs, Richard McGuirk, Savannah McGuirk, James Waldie, and Andrew Wheeler	Further Evaluation of the Performance of Field Science in an Analogue EVA suit	115-126
Anne M. Unewisse and Andrew D. Cool	Imagers for Ionospheric Airglow Observations	127-138
Anne M. Unewisse, Manuel A. Cervera, Lenard H. Pederick, Trevor J. Harris and Andrew D. Cool	Airglow Observations from ELOISE	139-150
Li Qiao, Michael Ryan, Mahmoud Efatmaneshnik	Tradespace Exploration for CubeSats Bus Design using Principal Component Analysis and k-medoids clustering	151-162
Victor Lim, Hideaki Ogawa, George Coulloupas Daniel Chadwick	Optimising the Launch and Deployment of a Smallsat Constellation	163-182
Angus T. R. Muffatti, Hideaki Ogawa	Multi-objective Design Optimisation of a small scale Cusped Field Thruster for micro-satellite platforms	183-198
Arunkumar Rathinam , Andrew G. Dempster	Geometrical assessment of Multi-GNSS prospects for Space Service Volume	199-206
Sanat Biswas , Li Qiao, Andrew Dempster	Position and Velocity estimation of Re-entry Vehicles using Fast Unscented Kalman Filters	207-218
Changjiang Hu, Craig Benson, Li Qiao	Contemporary Space-based GNSS Remote Sensing	219-232
George Coulloupas , Hideaki Ogawa, John Mo	A Systems Engineering Approach to Miniaturised Satellite Constellation Design Optimization	233-246
Noor Taofiqu Huq and Andrew G Dempster	Evaluation of Current and Projected CubeSat Propulsion Technologies for Navigating Cislunar Space	247-262
Graham Dorrington	Rationale and Strategy for Lunar and Martian Pit Reconnaissance	247-256



The National Space Society of Australia is the coming together of like-minded space enthusiasts who share a vision for the future in which there is an ambitious and vigorous space program leading to eventual space settlement.

To this end the National Space Society (worldwide) promotes interest in space exploration, research, development and habitation through events such as science and business conferences, speaking to the press, public outreach events, speaking engagements with community groups and schools, and other pro-active events. We do this to stimulate advancement and development of space and related applications and technologies and by bringing together people from government, industry and all walks of life for the free exchange of information.

As a non-profit organisation, the National Space Society of Australia draws its strength from an enthusiastic membership who contributes their time and effort to assist the Society in pursuit of its goals.

For more information, and to become a member:

<http://www.nssa.com.au>

Ad Astra!
Wayne Short
NSSA President



The National Committee for Space and Radio Science (NCSRS) is chartered by the Australian Academy of Science to foster space science, to link Australian space scientists together and to their international colleagues, and to advise the Academy's Council on policy for science in general and space and radio science in particular. The NCSRS was formed in 2012 by combining the former National Committee for Space Science (NCSS) and the National Committee for Radio Science (NCRS). The NCSRS web page can be reached at

<https://www.science.org.au/committee/space-and-radio-science>

NCSRS believes that ASRC meetings provide a natural venue to link Australian space scientists and foster the associated science, two of its core goals. As well as ASRC, NCSRS is also sponsoring the VSSEC – NASA Australian Space Prize.

This is the sixth ASRC meeting following launch of the first Decadal Plan for Australian Space Science. NCSRS encourages people to work together to accomplish the Plan's vision: "Build Australia a long term, productive presence in Space via world-leading innovative space science and technology, strong education and outreach, and international collaborations."

2016 ASRC Program Committee

Jeremy Bailey (UNSW Australia)

Annalea Beattie (Mars Society Australia)

Russell Boyce (UNSW Australia, Canberra)

Iver Cairns (University of Sydney), Chair

Graziella Caprarelli (University of South Australia)

Brett Carter (RMIT University)

Jonathan Clarke (Mars Society of Australia)

Andrew Dempster (UNSW Australia)

Brad Evans (University of Sydney)

Alice Gorman (Finders University)

Duane Hamacher (UNSW Australia)

Trevor Harris (Defence Science and Technology Group, Department of Defence)

Jonathan Horner (University of Southern Queensland)

Alexey Kondyurin (University of Sydney)

Roberto Sabatini (RMIT University)

Michael Smart (University of Queensland)

Kefei Zhang (RMIT University)

2016 ASRC Organising Committee

Sarah Barter
RMIT University (Melbourne)

Annalea Beattie
Mars Society Australia

Cheryl Brown
Australian Centre for Space Engineering Research, UNSW Australia
Conference Secretariat

Iver Cairns
University of Sydney
Co-Chair ASRC 2016
Chair, ASRC Program Committee

Brett Carter
RMIT University (Melbourne)

Jonathon Clarke
Mars Society Australia

Jonathan Horner
University of Southern Queensland

Robert Norman
RMIT University (Melbourne)

Wayne Short
Co Chair ASSC 2016
President, NSSA

Kefei Zhang
RMIT University (Melbourne)
Chair, local organising committee

Conference Plenary Speakers

Professor Frances Bagenal

University of Colorado, Boulder

“Exploration of the Outer Solar System: New Horizons at Pluto and Juno at Jupiter”

Professor Kathleen Campbell

University of Auckland

“Astrobiology of Hot Springs on Early Earth and Mars”

Upulie Divisekera

Monash University

“A New Era Space Exploration”

Dr Bradley Evans

Sydney University

“Big Data for Earth observations and Space”

Dr Gordon Frazer

Defence Science Technology Group

“Wide field of view Surveillance of space”

Conference Plenary Speakers

Dr Douglas Griffin

UNSW Canberra

“The Engineering of Space Flight Programmes in the Australian Context: a sustainable model”

Dr Eriita Jones

University of South Australia

“Identifying Something Which Can’t Be Seen: Holistic Methodologies In The Search For Subsurface Water on Mars and Other Planets”

Dr Peter May

Bureau of Meteorology

“Earth Observations from Space: Critical information used by the Bureau for national benefit”

Dr Robert Norman

RMIT University

“RMIT SPACE Research Centre – overview of past and present research endeavours”

16th ASRC Conference Program September 26 - 28

TIME	MONDAY	TUESDAY	WEDNESDAY	TIME
8:00	Registration	Registration	Registration	8:00
8:30				8:30
9:00	Opening / Plenaries Main Theatre (Level 5)	Plenaries Main Theatre (Level 5)	Plenaries Main Theatre (Level 5)	9:00
9:30				9:30
10:00				10:00
10:30	Break	Break	Break	10:30
(10:50)				(10:50)
11:00				11:00
(11:15)				(11:15)
11:30	National Context Main Theatre (Level 5)	Remote Sensing & GNSS Main Theatre (Level 5)	GNSS Main Theatre (Level 5)	11:30
12:00		Human Factors Conference Rooms 1/2 (Level 7)	Space Physics III Conference Rooms 1/2 (Level 7)	12:00
12:30				12:30
13:00	Lunch	Lunch & Women in Space Lunch	Lunch	13:00
13:30				13:30
14:00	Space Engineering & Cubesats Main Theatre (Level 5)	Space Physics II Main Theatre (Level 5)	Space Engineering Main Theatre (Level 5)	14:00
14:30	Space Physics I Conference Rooms 1/2 (Level 7)	Space Business & Entrepreneurship Conference Rooms 1/2 (Level 7)	Mars Seminar Rooms 1/2 (Level 7)	14:30
15:00		Education, Outreach & Ethics Seminar Rooms 1/2 (Level 7)		15:00
15:30	Break	Break	Break	15:30
16:00	Cubesats Main Theatre (Level 5)	Poster Session Foyer Area & Main Theatre	Space Situational Awareness Main Theatre (Level 5)	16:00
16:30	Indigenous Sky Knowledge Conference Rooms 1/2 (Level 7)		Space Missions & Projects Seminar Rooms 1/2 (Level 7)	16:30
17:00				17:00
17:30				17:30
18:00	Gala Dinner Old Melbourne Gaol (6:30pm for a 2pm start)			18:00
18:30				18:30
19:00				19:00
19:30				19:30
20:00				20:00
20:30			Mars Society of Australia - Public Talk Storey Hall Lecture Theatre (Level 2)	20:30
21:00				21:00
21:30				21:30

The Gender Balance of the Australian Space Research Community: A Snapshot from the 16th ASRC, 2016

Jonathan Horner¹, Belinda Nicholson¹, Ann Cairns^{2,3,4}, Wayne Short⁴ and Alice Gorman⁵

¹ *University of Southern Queensland, Computational Engineering and Science Research Centre, Toowoomba, Queensland 4350, Australia*

² *New South Wales Department of Education, New South Wales, Australia*

³ *Division of Information Technology, Engineering and the Environment, University of South Australia, GPO Box 2471, Adelaide, South Australia, 5001, Australia*

⁴ *National Space Society of Australia Ltd, GPO Box 7048, Sydney, New South Wales, 2001, Australia*

⁵ *Department of Archaeology, Flinders University, GPO Box 2100, Adelaide, South Australia 5001, Australia*

Summary: In recent years, there has been significant debate and discussion about the glaring gender disparity in the physical sciences. In order to better understand and address this issue within the Australian Space Research Community, in 2015 we began the process of keeping a statistical record of the gender balance at the annual Australian Space Research Conference. In addition, we have begun holding annual 'Women in Space Research' lunches at that conference, to discuss the situation, and to search for routes by which issues of equity can be addressed, and the situation improved.

Here, we present an update based on the 16th Australian Space Research Conference, held at RMIT, Melbourne, in late September 2016. As was the case in 2015, male attendees outnumbered female attendees by approximately 3:1. However, there was a small shift (~2.3%) in the balance, with female delegates now making up 26.4% of the total, up from 24.1% in 2015. This shift was mirrored in the gender distribution of talks, with 28.9% of all oral presentations being given by women (up from 25.2%). More striking, however, were the changes in the distribution of plenary presentations (44.4% female, up from 22.2%), poster presentations (31.8% female, up from 7.7%), and the student awards (33.3% female, up from 12.5%). These changes are encouraging, and will hopefully continue in the years to come. The conference organising committee again mirrored the gender balance of the delegates as a whole (27.3 % female vs. 26.4% of delegates), though the program committee was markedly more male-dominated this year than last (82.4% male, against last year's 72.2%).

At each year's meeting, we now hold a 'Women in Space Research' lunchtime event, where the various factors that could contribute to making the field more/less equitable are discussed. At this year's event, a number of suggestions were made that could help to make future conferences, and the wider community, a more equitable place – including increased opportunity for networking and mentoring of early- and mid-career researchers, and travel grants to make it easier for students and early-career researchers to attend the meeting. We will endeavour to put into place such schemes for future meetings, as we continue our push to make our community a more equitable place.

Keywords: Women in STEM (Science, Technology, Engineering, and Maths), gender equity, space sciences

Introduction

Historically, and in the present [1], the majority of science, technology, engineering and mathematical fields have been heavily male-dominated. In recent years, there has been a growing effort to better understand why this gender imbalance persists. Numerous studies indicate that *'people's behaviour is shaped by implicit or unintended biases, stemming from repeated exposure to pervasive cultural stereotypes that portray women as less competent but simultaneously emphasize their warmth and likeability compared to men'* [2].

To begin to address such biases, a number of new schemes have been established to encourage 'best practice', and reward universities that make a concerted effort to address issues of gender equity. Perhaps the most famous such scheme is the Athena SWAN (Scientific Women's Academic Network) charter, which was launched in the UK in 2005 with the goal to *'encourage and recognise commitment to advancing the careers of women in science, technology, engineering, maths and medicine (STEMM) employment in higher education and research'* [3]. The Athena SWAN charter is based on set of ten guiding principles that member institutions agree to uphold¹. Taken together, those principles elucidate an attempt to ensure that academia is as equitable and open as possible, recognising that academia as a whole suffers wherever one part of the community is disadvantaged in comparison to another. Initially, Athena SWAN was intended to address issues of equity in the STEMM subjects, but in 2015, its remit was expanded to also cover work carried out in a number of other fields.

In Australia, the Athena SWAN model has recently been adopted by the Australian Academy of Science, who launched the Science in Gender Equity (SAGE) initiative in 2015. To date, a total of forty Australian organisations² have signed up to the pilot phase of the program, which aims to address the problem that *'Women comprise more than half of science PhD graduates and early career researchers, but just 17% of senior academics in Australian universities and research institutes. The loss of so many women scientists is a significant waste of expertise, talent and investment, and this impacts our nation's scientific performance and productivity.'* [4].

The global astronomical community has been particularly active in recent years in attempting to understand and address issues of gender equity. In Australia, the Astronomical Society of Australia's Inclusion, Diversity and Equity in Astronomy Chapter³ hosts annual Diversity Workshops to build equity, and to raise awareness and understanding of a wide variety of issues that can affect the diversity of the community. In addition, in 2014 the Chapter launched the *Pleiades* awards, which are presented to those Astronomy groups across Australia which have demonstrated a commitment to equity in their workplaces⁴.

A key part of the ongoing drive to make communities more equitable has been a push to gather data to allow researchers to understand the current 'state of play', and to provide a

¹ The ten principles on which the charter is based are detailed on the Athena SWAN website, at <http://www.ecu.ac.uk/equality-charters/athena-swan/about-athena-swan/>

² The forty organisations participating in the pilot phase of the SAGE initiative are listed at <https://www.sciencegenderequity.org.au/athena-swan-charter-members/>

³ <https://asa-idea.org/>

⁴ <https://asa-idea.org/the-pleiades-awards/>

metric against which future initiatives can be assessed to see whether they are proving effective.

In 2014, the gender balance at the 223rd meeting of the American Astronomical Society was investigated in some detail in [5]. The results showed that 78 of 225 oral presentations were given by women (35%). In addition, [5] reported on the manner in which the gender of the session chair impacted upon the gender balance of the people asking questions after talks. When session chairs were male, just 20% of questions were asked by female members of the audience. With female session chairs, that number rose to 34% — a value comparable to the overall percentage of delegates that were women.

Similar results were obtained at the UK's annual National Astronomy Meeting, in 2014 [6]. At that conference, 28% of delegates were female, a gender balance that was reflected fairly in the distribution of both oral presentations and session chairs at the meeting. When it came to the questions asked at the conference, however, the authors reported the same pattern – the percentage of questions that were asked by women was markedly lower than the fraction of the overall attendees that were female.

Following these landmark studies, in 2015 we carried out an analysis of the gender balance of the 15th Australian Space Research Conference [7]. In brief, we found that the conference was male-dominated, with just 24% of attendees at the meeting being female. The overall gender balance of the meeting was mirrored by the distribution of oral and plenary presentations (25% and 22% female, respectively). Both the poster presentations and conference prizes were dominated by male delegates to a level greater than that expected on the basis of the distribution of attendees (male:female ratios of 12:1 and 7:1, respectively), although in both cases the number of presentations/awards was small (13 and 8)⁵. These results were intended to provide a baseline on which future conferences could be judged, to assess whether attempts to make the field more equitable bear fruit.

Here, we present the results from the 16th Australian Space Research Conference, held at RMIT University, in Melbourne, from the 26th to 28th September, 2016, and compare the data to that obtained in 2015. We also present a brief discussion of the key recommendations that came out of the lunchtime 'Women in Space Research' meeting, which we hope to implement in the coming years.

⁵ To get a feel for the degree to which female delegates were under-represented in the 2015 poster and awards categories, we direct the interested reader to the online calculator at: <http://aanandprasad.com/diversity-calculator/>, which was brought to our attention by one of the referees of this work. That calculator shows the probability that X of Y presentations will be given by women, given the fraction of conference attendees that are female. It is based on binomial mathematics, and allows users to get a simple visualisation of the degree to which female presenters are under- or over-represented within a given sample. In the same vein, it is possible to calculate the likelihood that a given distribution of events (such as only having a single female presenter out of 13 posters) would occur by chance using such binomial mathematics. In the case of the 2015 poster presentations, such a calculation (given 24% of delegates are female) suggests that the cumulative probability of one or fewer of thirteen poster presentations being given by a women is approximately 14.4%. Similarly, one or fewer women being included in a total of eight conference awards would be expected to occur approximately 39% of the time, were those awards drawn solely by chance.

The Gender Balance of the 16th Australian Space Research Conference

The 16th Australian Space Research Conference was a meeting with a broad scope, bringing together 174 researchers from a wide variety of disciplines. Stretching over three full days at Melbourne's RMIT University, the conference featured three parallel streams of sessions, although the whole meeting came together for the morning plenaries. As with previous years, the conference featured nine such plenaries, with speakers spanning a variety of disciplines, and career stages⁶. Conference sessions covered space engineering, space physics, cubesats, planetary science, Indigenous sky knowledge, remote sensing and GNSS (Global Navigation Satellite Systems), space business and entrepreneurship, human factors in space research, education, outreach and ethics, space situational awareness, Mars, and other space missions and projects.

As with the results we obtained in 2015, we note here that our data was obtained after the conference concluded, using the list of conference delegates. As such, the gender assignments used to build our statistics are based on our personal knowledge of the individuals concerned. The details of those individuals not personally known to us were located online, on their professional websites, and on the homepages of their institutions or employers. We used the data taken from the 2015 meeting to make this assignment process more straightforward, taking the genders assigned to repeat delegates from that dataset.

We acknowledge that this leaves open the risk that individuals might be misgendered in our dataset. Ideally, in future years, we would hope to be able to obtain this information from an anonymised survey as part of the registration process. However, it was unfortunately not possible to set up such a survey as part of the organisation for this year's meeting, and there remains some concern that delegates might not feel comfortable providing gender information as part of the registration process, even if they can be assured that such data would be anonymised and would not be linked with their abstracts, or used in any way as part of the process of constructing the conference program. This is a particularly challenging issue: on the one hand, it is clearly important to be able to track the demographics of the community as a function of time – but at the same time, we must acknowledge the role of both conscious and unconscious bias in the process by which people assess abstracts for inclusion in a conference program – and we do not wish to expose anyone in our community to discomfort around disclosing their gender. How best to obtain such information is therefore still the subject for debate amongst the organising committee, and we continue to seek advice on how best to proceed to balance these concerns.

In Table 1, we present the results obtained for the 16th Australian Space Research Conference, with the data from the 15th Australian Space Research Conference included (right hand side) for direct comparison.

It is important to note that the results presented here for the 2015 conference are slightly different to those presented in [7]. It was brought to our attention that one delegate had been misgendered as female, when in fact they identify as non-binary. We have therefore adjusted

⁶ The full program for the 16th Australian Space Research Conference can be found online at: <http://www.nssa.com.au/16asrc/resources/ASRC2016-ProgramBooklet-23160923.pdf>; and was last accessed on 15th December 2016 for the purposes of putting together this study.

last year's tallies to take account of this – adding the column 'non-binary' to Table 1, and to Figure 1⁷.

Slightly fewer delegates attended this year's meeting than in 2015 (174 vs. 191), and whilst the number of talks was slightly lower (121 vs. 129), this was offset by an approximately commensurate increase in the number of poster presentations (22 vs. 13). Again, due to the post hoc nature of our data collection, we were unable to break down the distribution of attendees and presenters by career stage. It is possible that such data could be obtained as part of the registration process – though we note again that such data collection could raise concerns amongst those registering for the meeting that the information might be used to discriminate against them in the process of program construction. Such information therefore remains something that we would like to investigate in future years, but was not available for this work.

⁷ Should any other delegates feel that we may have misgendered them in our assessment of either meeting, we encourage them to contact us to let us know, if they feel comfortable doing so, so that the statistics can be as accurate as possible going forward.

Table 1: The gender distribution across the 16th Australian Space Research Conference, compared with amended numbers from the 15th Australian Space Research Conference (italicised).

	16 th ASRC (2016)			15 th ASRC (2015)			
	Male	Female	Total	<i>Male</i>	<i>Female</i>	<i>Non binary</i>	<i>Total</i>
Delegates	128 73.6%	46 26.4%	174	<i>145</i> <i>75.9%</i>	<i>45</i> <i>23.6%</i>	<i>1</i> <i>0.5%</i>	<i>191</i>
Talks	86 71.1%	35 28.9%	121	<i>89</i> <i>74.8%</i>	<i>30</i> <i>25.2%</i>		<i>129</i>
Posters	15 68.2%	7 31.8%	22	<i>12</i> <i>92.3%</i>	<i>0</i> <i>0%</i>	<i>1</i> <i>7.7%</i>	<i>13</i>
Plenary Presentations	5 55.6%	4 44.4%	9	<i>7</i> <i>77.8%</i>	<i>2</i> <i>22.2%</i>		<i>9</i>
Student Awards	4 66.7%	2 33.3%	6	<i>7</i> <i>87.5%</i>	<i>1</i> <i>12.5%</i>		<i>8</i>
Program Committee	14 82.4%	3 17.6%	17	<i>13</i> <i>72.2%</i>	<i>5</i> <i>27.8%</i>		<i>18</i>
Organising Committee	8 72.7%	3 27.3%	11	<i>7</i> <i>70%</i>	<i>3</i> <i>30%</i>		<i>10</i>

In Figure 1, we present the gender balance of the 15th and 16th Australian Space Research Conferences, again amended as described above. From both Table 1 and Figure 1, it is clear that there was a small shift across the conference as a whole to being somewhat less male-dominated. The sole exceptions to this were the gender balances of the Program Committee and Organising Committee, which both skewed somewhat towards a more male-dominated position. This is something that we will attempt to address when organising the 17th Australian Space Research Conference, in the coming months.

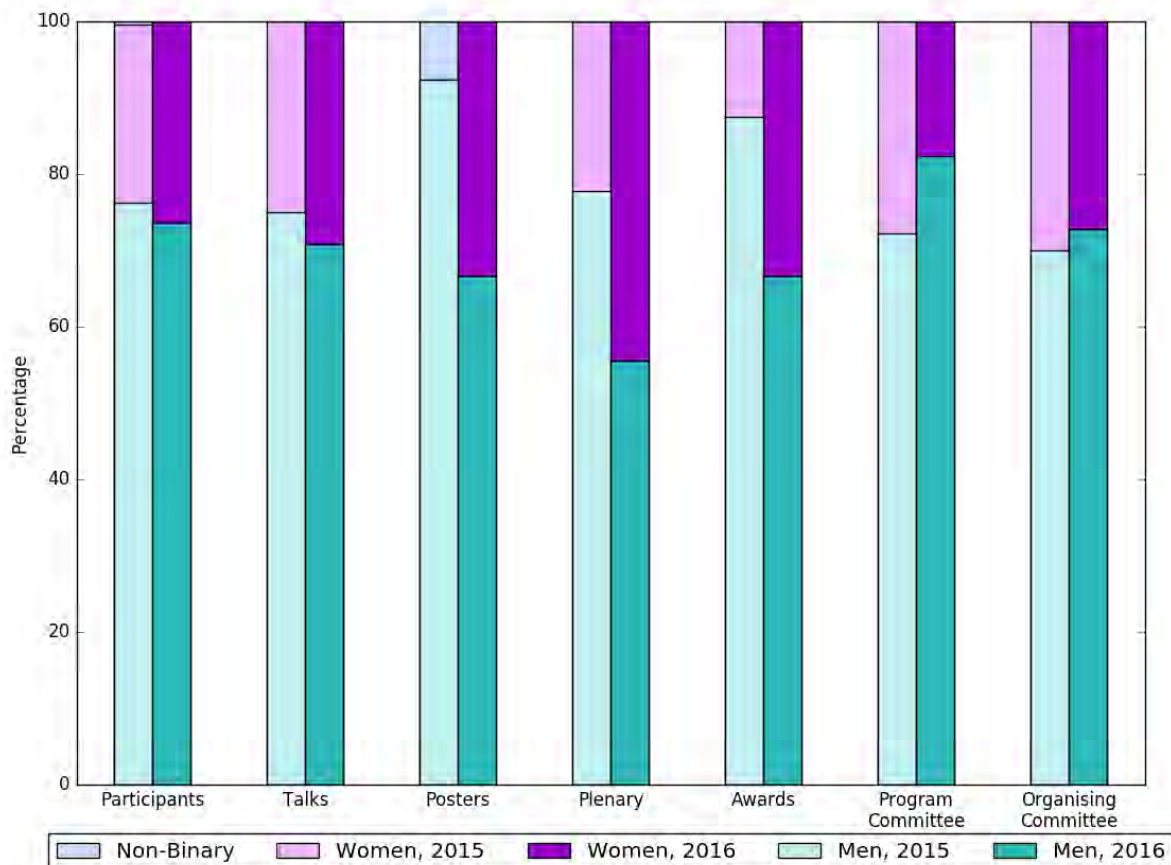


Figure 1: The gender balance of the 15th and 16th Australian Space Research Conferences. For each category, the left-hand column shows the data from the 2015 meeting, whilst the right-hand column shows the balance for the most recent conference. It is apparent that the overall gender balance of the meeting improved in 2016 over the previous year – although we note that the program and organising committees became slightly more male-dominated.

The Women in Space Research Lunch

At the previous two Australian Space Research Conferences, we have held lunchtime discussion meetings in order to examine questions of equity in our community, to provide an environment where researchers can seek advice and mentoring, and to seek feedback on how the conference and our community can be made more equitable. Those meetings have been very well received, and have helped to raise awareness of issues of equity in the wider community. This series of lunchtime meetings continued at this year’s ASRC, which hosted the third annual Women in Space Research Lunch.

The third annual Women in Space Research lunchtime event was once again well attended, with over forty delegates (both female and male) sitting down to discuss equity within our community. One of the key points of that lunch is that it should be a safe space⁸ – and so it would be unreasonable to report specifics of the discussion in this work. We do, however, note some of the initiatives that were discussed therein, and that might be applied to our

⁸ In other words, the lunch is intended to foster a discussion environment that is supportive and positive, and as much as possible, free from bias or criticism. The goal is that delegates should be able to freely discuss issues that they might not otherwise feel comfortable raising.

community in order to help facilitate equity, and also to benefit early- and mid-career researchers of all backgrounds.

The importance of mentoring was raised, and the Astronomical Society of Australia's 'Speed Meet-A-Mentor' events (held at the Annual General Meetings of that society) was suggested as a great mechanism to help early- and mid-career researchers to connect with potential mentors from other institution, as well as building a sense of community amongst the E/MCRs themselves. It was suggested that a similar event would be welcomed as part of the 17th Australian Space Research Conference, to test the waters and see whether it could have a similarly beneficial impact on our community. Such an event could even be extended to be a 'Junior Scientists Workshop', similar to that held at the Division for Planetary Sciences meeting at Pasadena in October 2016 – perhaps taking place the afternoon before the conference, or the day after the meeting concludes.

Once again, the role of implicit bias was raised – with the 'Project Implicit' Implicit Bias tests⁹ being flagged up as an excellent means by which all researchers can make themselves aware of their own inherent biases. This is particularly useful in advance of assessing grant applications, and also as part of the job-hiring process. In a similar vein, the practice of agreeing a suite of very specific assessment criteria for any given advertised position before any applications are received was recommended as both best practice as a means to avoid the impact of implicit bias, but also as a mechanism to make the whole recruitment process proceed more smoothly.

It was also suggested that there may be a number of graduate students in the community who were unable to attend the meeting, for a variety of reasons. Given that networking and meeting potential mentors are vitally important for graduate students, it was suggested that the organising committees of future meetings look at ways to make a limited number of graduate bursaries available, to try to facilitate attendance from those who would otherwise not be able.

Progress from 2015

In [7], we described several potential initiatives that had been put forward as mechanisms by which our community could be made more equitable, with a particular focus on the annual conference itself. These recommendations were well received, and attempts were made to act upon most of them. We repeat them, below, to maintain their visibility, and follow each with an update as to the steps taken to address the initiative:

- The provision of childcare at the conference for delegates

As part of the planning of the conference, we obtained quotes for the cost of offering childcare at the conference. We were advised that at least two carers would be required, one to take care of children under the age of three, and the other to look after those who were older. We approached a number of potential sponsors to see whether it was possible to cover the costs of childcare for the meeting, but were unfortunately unsuccessful in our search. Having discussed the potential need for childcare again at the Women in Space Research lunch, it was felt that this was a relatively low priority for many of the delegates, and that our focus and funds would be better spent elsewhere (e.g. bursaries to help early-career researchers to attend).

⁹ <https://implicit.harvard.edu/implicit/selectatest.html>

- The option to attend the conference remotely (i.e. via streaming) for those who can't attend in person

To test the feasibility of streaming conference sessions, this year we ran live streaming for the plenary talks each day, through Zoom. The audience was limited, but we received good feedback on the quality of the streams. This remains a priority, and we will look to expand the availability of streaming at future meetings following this successful trial.

- The organisation of networking sessions during the daytime, for those who can't attend evening events

As detailed above, we again held a 'Women in Space Research' lunchtime event, which resulted in very helpful discussions, as well as offering an opportunity for networking. In future years, we intend to build upon this by running some form of 'meet-a-mentor' type event, in addition to the lunchtime meeting, to help students and early-career researchers to connect with potential mentors, and to network in a friendly and supportive environment. Mentoring is a critical activity that contributes to career success, and at least one study shows that it is routinely offered more to male students than female students [2].

- Aiming to increase the fraction of female plenary speakers above parity with the current demographic distribution of attendees

The gender balance of plenary speakers at this year's meeting was markedly improved over that at 2015 conference – with four of the nine speakers being female. This is partly the result of members of the Program Committee making deliberate choices to identify and approach women for this role. This trend will hopefully be continued at future meetings.

In the last couple of years, the phenomenon of the 'manel' – a conference session, keynote speaker line-up, or panel with no women participants – has come under increasing scrutiny in social media. It is no longer considered acceptable to have a 100% male composition of such events. This means, frequently, casting a wider net to locate women with the appropriate expertise and accepting that sometimes these women may come from outside the community.

- Inviting a plenary speaker to talk on the topic of equity in space science

Whilst none of the plenary speakers spoke on this topic, we did invite one of the plenary speakers (Professor Fran Bagenal) to speak about equity at the Women in Space Research lunch. In addition, we invited the current president of the Astronomical Society of Australia, Professor Virginia Kilborn, to talk at that meeting, discussing the efforts being made in the Astronomical community to address issues of equity, and to relate her experience in leading the push for a more equitable environment at Swinburne University. This proved a great success, and we hope that, in future, other plenary speakers with experience in this area will be willing to contribute to the lunchtime discussion meetings.

- Increasing the visibility of female space scientists online by creating Wikipedia and Scimex profiles; and creating a repository of information on women working in space science (such as pictures, CVs and biographies) to provide a teaching resource

To date, no progress has been made on these excellent suggestions. More widely, however, there is a push to address the lack of such profiles online, with events such as Hackathons and 'Wikithons' being carried out to increase the number of excellent female scientists being

profiled in this manner. One such resource has been created for women in the ‘trowel-wielding’ professions – archaeology, geology and palaeontology, by a collective of female scholars. Their Trowelblazers website features profiles of famous and forgotten women both living and dead (<http://trowelblazers.com/>). The increased visibility afforded to the featured women allows others to locate them, cite their publications, and incorporate their work into teaching examples.

Conclusions and Discussion

As part of the ongoing push to ensure that the Australian Space Research Community is as equitable as possible, we have carried out an analysis of the gender balance of the 16th Australian Space Research Conference, following on from our previous study of the demographics of the 15th such meeting, in 2015.

In 2016, there was a small improvement in the gender balance of the meeting, with an increase in the representation of women in the total pool of conference delegates (2016 was 26.4% female, as opposed to 23.6% female in 2015). This increase was mirrored by an increase in the percentage of oral presentations given by women (28.9% vs. 25.2% in 2015). The most marked improvement came in the balance of plenary presentations (4 out of 9 female in 2016, vs. 2 out of 9 in 2015), whilst the distribution of poster presentations (7 out of 22 female in 2016) and student prizes (2 of 6 female) were also improved over the distribution in 2015. Whilst these three areas all involve small numbers of participants, and so therefore are naturally subject to significant noise, it will be interesting to see whether these trends continue in future years.

Whilst the gender balance across the conference itself was closer to parity than in 2015, we note that the make-up of the organising and program committees were more male-dominated in 2016 than in 2015.

Our data support our findings from 2015 that, within the Australian Space Research community, when attending the Australian Space Research Conference, women participate as actively in presenting their research as do male delegates. The on-going problem, therefore, lies in increasing the number of women attending the conference (and addressing issues that limit female participation in the wider community).

The Australian Space Research Conference currently solicits papers in a general call out, several months before the meeting, resulting in the audience for the conference to a great extent being self-selecting. It is potentially at this stage where the current gender imbalance might be usefully addressed through schemes that enable those who feel that (for whatever reason) they are unable to attend the coming conference to have access to the meeting. For this reason, we intend to investigate further the possibility of streaming sessions (and even, potentially, allowing delegates to present remotely), as well as looking into the possibility for small travel grants being made available to those who cannot afford to otherwise attend.

It is worth noting, here, that the Australian Space Research Conference covers a wide range of sub-disciplines, within which gender disparities may be markedly different to those for the conference as a whole. To date, we have not carried out an analysis of how the gender distribution of delegates varies from discipline to discipline. Given the large number of conference sessions across the three days of the meeting, and the relatively small number of delegates who present in a given session, such an analysis may not be illuminating. Having

said that, considering of the impact of the disciplines covered by the conference on its overall gender balance is clearly important.

Until fairly recently, the Australian Space Research Conference was known as the Australian Space Science Conference. The name change was adopted by the Programme Committee to attract greater participation from scholars who may not identify as STEM scientists and to reflect the existing inclusion of sessions focusing on social and cultural aspects of space science and exploration. One referee of this work suggested that this change in name may might be contributing to the small observed change in the conference's gender balance. If the gender balance of the conference is truly improving, then that should be reflected across all the disciplines covered. In future years, it would therefore be interesting to examine whether the gender balance the larger sub-disciplines (for which sufficient data can be obtained) has changed with time.

Of the 46 female and 128 male delegates at the 2016 meeting, 14 women and 43 men also attended the 2015 conference. Of the 114 delegates who attended in 2016 who did not attend the 2015 meeting, 31 were female and 83 were male. The gender balance amongst these 'new' delegates was 72.8% male: 27.2% female, reflecting the overall gender proportions at the two conferences. These figures can be used as a baseline against which to assess future retention of female conference delegates.

A number of recommendations were made in 2015 that were acted on in the organisation of the 16th Australian Space Research Conference, and it is promising that the gender balance of that meeting did improve somewhat over the previous year. However, it is important to follow these actions through for a number of years, and to monitor the demographics as a function of time, to ensure that any short-term improvements are not merely the result of noise, and to make certain that positive change in the community is propagated for future years.

Acknowledgements

JH and BN are supported by USQ's Strategic Research Fund: the STARWINDS project, and BN is also in receipt of an Australian Postgraduate Award. The authors wish to thank the two anonymous referees of this paper for their helpful and positive feedback.

References

1. Larivière, Vincent, Ni, Chaoqun, Gingras, Yves, Cronin, Blaise and Sugimoto, Cassidy R., "Global gender disparities in science", *Nature*, 2013, 504 (7479), 211 - 213
2. Moss-Racusin, Corinne A., John F. Dovidio, Victori L. Brescoll, Mark J. Graham and Jo Handelsman, "Science Faculty's subtle gender biases favour male students", *Proceedings of the National Academy of Sciences of the United States of America*, 2012, 109(41):16474-16479
3. Quote sourced from <http://www.ecu.ac.uk/equality-charters/athena-swan/>, accessed on 14th December 2016.

4. Quote sourced from <https://www.sciencegenderequity.org.au/about/what-is-sage/>, accessed on 14th December 2016.
5. Davenport, J. R. A., Fouesneau, M., Grand, E., Hagen, A., Poppenhaeger, K. and Watkins, L., “Studying Gender In Conference Talks - Data From The 223rd Meeting Of The American Astronomical Society”, 2014, arXiv:1403.3091; paper available on the arXiv website at <http://arxiv.org/pdf/1403.3091v1.pdf>
6. Pritchard, J., Masters, K., Allen, J., Contenta, F., Huckvale, L., Wilkins, S. and Zocchi, A., “Asking gender questions: Results from a survey of gender and question asking among UK Astronomers at NAM2014”, *Astronomy and Geophysics*, 2014, 55, 6.8 – 6.12
7. Horner, J., Gorman, A., Cairns, A. and Short, W., “The Gender Balance of the Australian Space Research Community: A Snapshot From The 15th ASRC, 2015”, 2016, *peer-reviewed proceedings of the 15th Australian Space Research Conference*; paper available on the arXiv website at <https://arxiv.org/abs/1605.01498>

Additional Resources

The Women in Astronomy blogspot contains a collection of excellent posts by a number of academics on a variety of topics to do with equity and gender bias. <http://womeninastronomy.blogspot.com.au/>

The Astronomical Society of Australia’s Inclusion, Diversity and Equity in Astronomy chapter (formerly the Women In Astronomy chapter) maintains a website at <https://asa-idea.org/>. Of particular interest are the details of the annual Diversity Workshops, which can be found here: <https://asa-idea.org/meetings/>. Many of the materials from those meetings are hosted on the relevant webpages and can be freely downloaded. The IDEA chapter also hosts statistical information on the makeup of the Australian Astronomical Community, and runs the Pleiades awards, intended to recognise those astronomy departments that make a commitment to fostering an equitable environment for their staff and students.

The ‘Project Implicit’ Implicit Bias tests are a fascinating tool that highlights our implicit associations. These cover a wide variety of topics, from broad fields such as age, sexuality and religion, to more specifically focussed topics such as Gender-Science. They can be found here: <https://implicit.harvard.edu/implicit/selectatest.html>

More information on the Athena SWAN Charter can be found at <http://www.ecu.ac.uk/equality-charters/athena-swan>. The Science in Australia Gender Equity initiative (SAGE), which is based on the Athena SWAN charter, is detailed at <https://www.sciencegenderequity.org.au/>.

The Conference Diversity Distribution Calculator, <http://aanandprasad.com/diversity-calculator/>, is a useful tool, which allows one to quickly visualise how many women would be expected to be included in a random sample of a given size, assuming that they constitute a given percentage of the available population.

Emerald & Mount Burnett Observatories, New Opportunities for Earth Situational Awareness, Research, Education and Tourism

Lachlan Thompson, FIEAust
CEO, Emerald Observatory
lachlan.thompson@gmail.com.

Dr James Murray
President, Mount Burnett Observatory
James.R.Murray@nab.com.au

Anne Brumfitt
Deputy CEO, Emerald Observatory
Anne.brumfit@gmail.com

Abstract

This paper presents opportunities for research and community astronomy with Mount Burnett Observatory (MBO) and the new Emerald Observatory situated in rural Victoria, Australia. Although there are already online observatory programs such as the iTelescope and the Faulkes Telescope South, there exists enormous scope for additional new southern hemisphere [Australian] facilities to satisfy an expanding interest in astronomy. This includes a space situational awareness and research observatory privately commissioned and funded for Emerald, Victoria. In strategic partnership with MBO, the new observatory facilitates both fully remote operation and in-situ research observations. Enclosed in a fully automated 3m ScopeDome, in a 5.5m high tower observatory, the 45cm Optical Tube Assembly Schmidt-Cassegrain Telescope (SCT) is a research grade telescope tool for University and community use. This telescope provides international remote access with strategic partnerships for education and research, and links with United Kingdom institutions.

Introduction

The Observatory at Mount Burnett was established in 1972 by Monash University. Research focused on active chromosphere stars in the southern sky. Superseded technology lead to the site's decommissioning in the late 1990s. The 45cm telescope lay unused until in 2011 MBO formed as an astronomical society to preserve the facility. MBO now hosts the fastest-growing astronomy community (ASV membership list 2014-16) in Victoria with over 280 members. Upgrades at the MBO site include a Sirius dome to house a 33cm go-to SCT for visitor and member use. The MBO will be the host of the 2017 Victorian Astronomical Convention.

Emerald Observatory

The Emerald observatory is a newly commissioned Observatory build to facilitate both hands on and full autonomous astronomy research. The facility is located 70 km from Melbourne in the picturesque forested Dandenong Ranges of Cardinia Shire. In service the facility will be available online to researchers facilitating low entry cost to support earth situational awareness research and the detection and tracking of space debris (space junk). The exponential increase in space debris from the accumulated launching of satellites over 50 years has resulted in a realistic hazard to new space missions. It is estimated that there are over 5000,000 items of sizable space junk in orbit with 17,000

items currently identified (Molotov, 2011) and being tracked by ESA and NASA. Space debris has an orbital velocity of 11,000 to 25,000kph. To address this concern a global program (Molotov, 2011) to detect, identify and track space debris. The Emerald facility has been installed to specifically address the need for southern hemisphere observation sites.

The observatory is located on the property *Fernglade on Menzies* a large Federation style new homestead dating from 1903, Figure 1. The observatory building consists of a 5.5metre tall tower observatory with a fully automated ScopeDome 3metre diameter cupola housing a 45cm OTA f10 4000mm computer controlled go to Schmidt-Cassegrain telescope. The entire observatory can be autonomously or remotely operated using ASCOM Platform 6.2 (ASCOM Standards, 2016) compliant software. Facilities are provided for resident researchers and the observatory is fitted with reverse cycle split system air conditioning for manual observations.

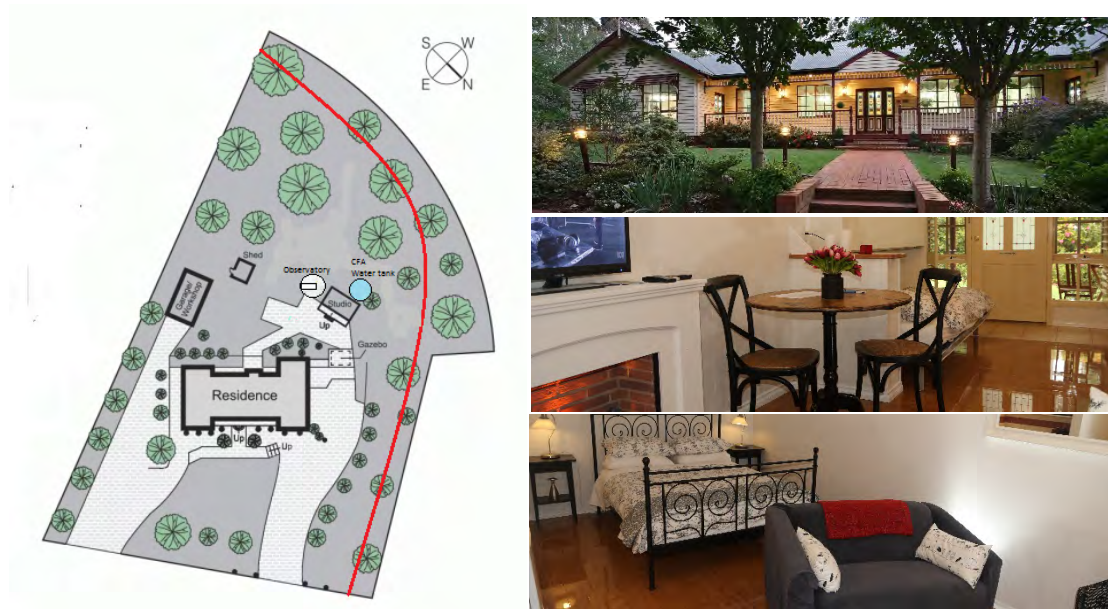


Figure 1, The Emerald Observatory site plan showing the Observatory, CFA water tank and Homestead. Photos show the Homestead and the residential researcher accommodation suite. (Lachlan Thompson).

Designing for bushfire

Technical design hurdles unique to Australia needing to be overcome were not those for astronomical observing. Instead the difficulties focused entirely on the research station design to comply with Victoria's new CFA Bushfire Planning requirements (CFA, 2012).

The site is located in a green wedge overlay with adjacent State and National Parks of temperate mountain ash eucalypt forest. The area is classified as a Bushfire Attack Level of BAL29, that is, a bushfire attack level of 4 on a scale of 1 to 6. Historically

the effect of bushfire on observatories located in forest areas has been devastating, Figure 2, as was the case at Mt Stromlo in the 2003 ACT bushfires. For the Emerald Observatory the bushfire resistance design was contracted to Brumfitt, Thompson & Thompson (Thompson, 2016) with the brief to adapt an original astronomy tower observatory design by architect Aleksandra Narkowicz-Pala (Narkowicz-Pala & Wojcik, 2009) to comply with the CFA Bushfire Attack Level (CFA, 2012) requirements.

The Narkowicz-Pala tower observatory design was a proven design with a number of examples being constructed in locations across Europe. One of particular note is the excellent Sternwarte Rotheul Private Observatory of Henry Bolgehn in Germany, Figure 3. The Sternwarte Rotheul design is driven by meeting the opposite extreme of climate to that of bushfire, instead an environment of long periods of snow and ice. The Sternwarte Rotheul design had to endure an average outside winter daytime temperature of -10 degrees Celsius requiring thermal insulation and building protection. The exterior of the Sternwarte Rotheul Observatory (Narkowicz-Pala & Wojcik, 2009) is clad with moisture proof 50mm closed cell Blue-Styrofoam over which a thin acrylic and cement rendering is applied for UV protection.



Figure 2, The remains of the 50 inch Great Melbourne Telescope. One of the Mount Stromlo telescopes destroyed in the 2003 Bushfires ACT. (Lachlan Thompson 2007)



Figure 3, The Sternwarte Rotheul Observatory by Henry Bolgehn, in Germany, the cupola is a 3 metre ScopeDome with tower design based on drawings by Narkowicz-Pala. (*Henry Bolgehn 2011*).

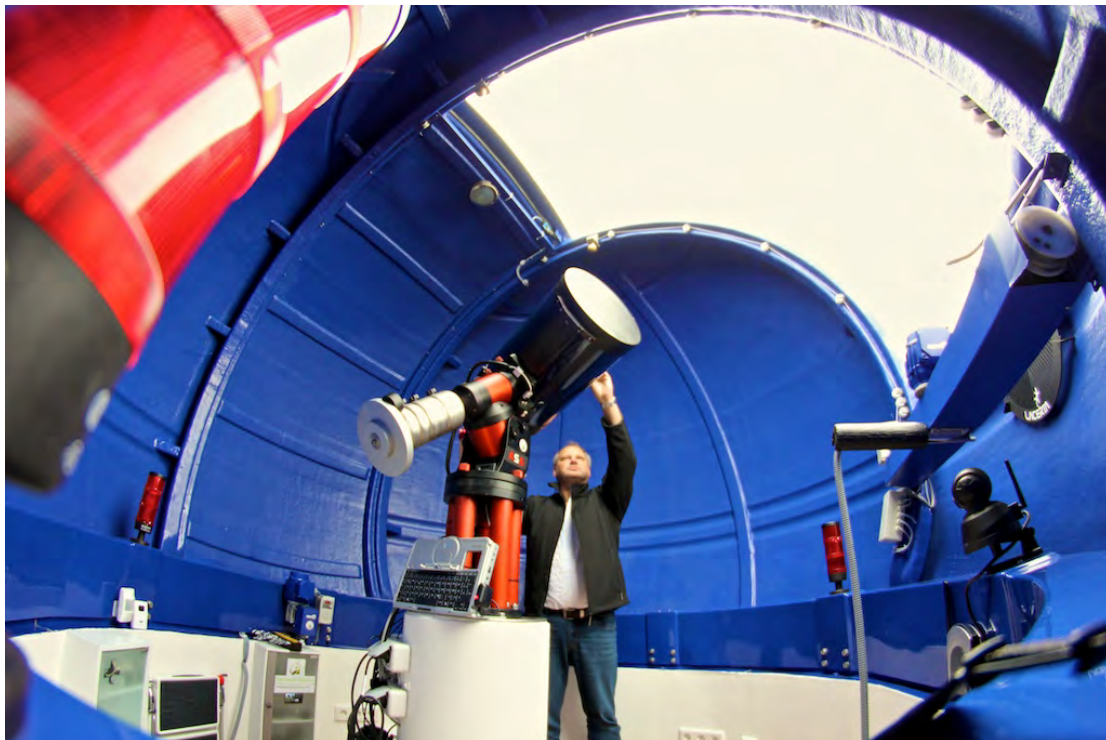
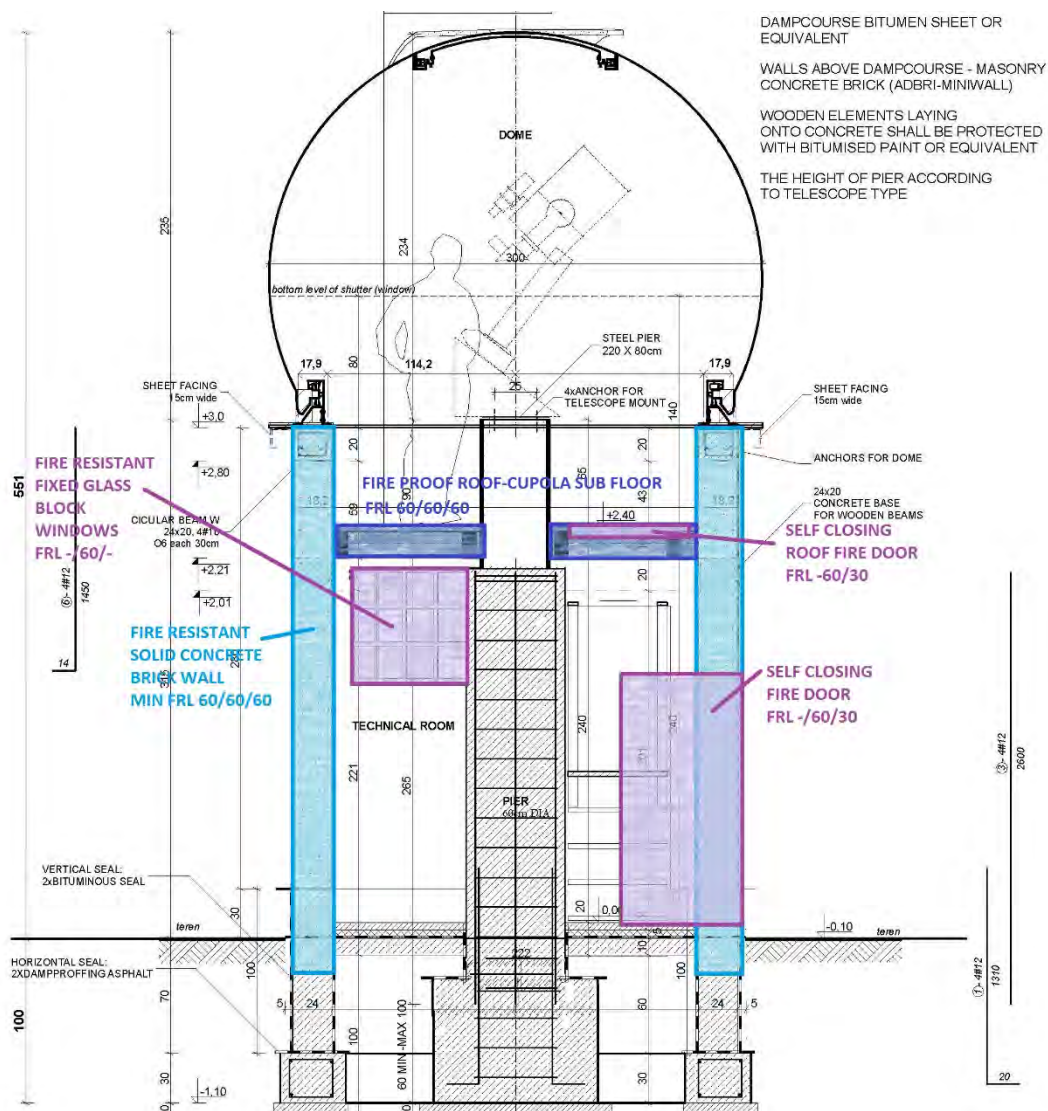


Figure 4, Sternwarte Rotheul Observatory, Germany ScopeDome 3metre cupola, with a 33cm OTA SCT installed by Henry Bolgehn, (*Henry Bolgehn 2012*).

The Emerald Observatory is classified under the Australian Building Code (Australian Building Codes, 2016) as a Class 10a structure - a non-habitable building being a

private garage, carport, shed or the like. The CFA requirements for a building of this classification sited in a BAL29 overlay is that the walls must have a Fire Resistance Level of 60/60/60, self-closing fire doors, fire resistant windows (if fitted), a fireproof roof and not intrude on the 10metre defensible space of nearby inhabited buildings.

Observatory as originally designed features a fully automated ScopeDome 3m V3 cupola, Figures 4 and 5. The cupola is a cast fiberglass structure of just over 3metres in diameter. The cupola by nature of its materials offering little resistance to bushfire attack. The decision was taken to make the cupola and telescope expendable in the event of a bushfire and to secure the primary part of the building against fire attack. The logic being to minimize combustible installations near dwelling and habitable buildings.



The telescope pier is a 3metre reinforced concrete column of 60cm diameter that is cast with an integral 1metre³ reinforced concrete footing foundation that acts as a counter weight that is vibration isolated from the observatory building. The fireproof roof (cupola floor) is vibration and mechanically isolated from the pier and from the tower.

The bushfire regulations require BAL29 sited buildings to have a fireproof roof structure and a roof that can withstand wind speeds of up to 12.5m/s (45kph). Wind tunnel tests on the cupola (Flaga, Bosak, Flaga, Kimbar, & Florek, 2011) have demonstrated that the cupola is structurally able to withstand wind speeds up to 50m/s.

A summary comparing the original Narkowicz-Pala design and the critical Bushfire design changes are presented in Table 1. One of the most significant design changes (Thompson, 2016) was to replace the cupola floor with a fireproof sub roof which doubles as the cupola floor and the building roof.

Building Component	Original Design (Narkowicz-Pala & Wojcik, 2009)	Redesign for CFA BAL29 (Thompson, 2016)
Cupola sub floor	Plywood or particle board FRL 0/0/0	Fireproof roof (cupola floor) Fibre cement/sarking/plywood FRL60/60/60
Tower Cladding	50mm Styrofoam	None
Tower Wall	250mm Foamed Brick FRL 0/0/0	182mm Solid cement brick FRL60/60/60 to FRL180/180/180
Side Door	Timber	Self-closing Fire door FRL-/60/30
Roof door	Plywood FRL 0/0/0	Self-closing fibre cement/sarking/plywood FRL-/60/30
Windows	Double or triple glazed glass	Non opening Glass blocks (CSIRO, 2010) FRL-/60/-
Site of building	unrestricted	Minimum of 10metre separation from nearest habitable building
Other	None specified	10,000litre steel or concrete water tank dedicated to CFA use
Wind speed limit	50m/s	no change to original design

Table 1, Changes (Thompson, 2016) implemented to the original design (Narkowicz-Pala & Wojcik, 2009) to order to comply with CFA Bushfire Planning Victoria (CFA, 2012).

Equipment and capability

The 45cm OTA Schmidt-Casegrain telescope is fork mounted on an equatorial wedge and pier mount. The SCT tracking computer and drive has an accuracy of tracking periodic error of observatory standard that is of less than 5 arc seconds. Providing observers an uninterrupted 45 degree arc cone window of the Southern sky.

Precision tracking is complimented by a CCD star lock off axis guider employing a Meade 105mm, focal length 700 mm f/7.0 ED5000 3-element Apochromatic Refractor (APO) guiding telescope fitted with an Starlight Xpress Ultrastar C, CCD real time imaging and guiding software offering a of tracking periodic error of less than 3 arc seconds. Both the 45cm OTA SCT and the 105mm APO are fitted with MoonLite (MoonLite Telescope Accessories, 2016) CSL 62mm and 50mm respectively large format Crayford SCT/RC focusers with MoonLite mini-V2 controller for High res stepper motors and software as standard. Researchers and schools requiring remote operation the telescope interface uses MoonLite 32/64 bit universal ASCOM driver that requires ASCOM Platform 6.0 or later (fully compatible with ASCOM Platform 6.2).

The telescope has supporting imaging equipment ranging from a Central DS Canon 5D Mark III Astrophotography Cooled -40 degrees Celsius Colour CCD System to dedicated spectroscopy. Our Spectroscopy capability ranges from a Paton Hawksley SA100 spectroscopy grating for International Baccalaureate Astrophysics students to professional equipment for undergraduate university and post graduate research. The facility is fully equipped for robotic remote operation using ASCOM Platform 6.2 (ASCOM Standards, 2016) compliant software.

What will it do?

The ever increasing swarm of orbiting space debris (United Nations, 1999) presents the Emerald Observatory with a clear capability role. The optical detection and tracking of space debris using small telescopes has been validated (Hampf, Riede, Stöckle, & Buske, 2013). These experiments have shown that computer guided optical telescopes of less than 40cm are able to detect and track space debris as small as 0.5m^2 . The optical viewing of precision of the order of 1.1 to 1.8 arcseconds, was more than satisfactory to detect low 19 magnitude objects. Low earth orbit (LEO) targets of altitudes between 160km to 200km included the successful acquisition and tracking of the German Aerospace Center (DLR) Tubesat of $0.6 \times 0.4 \times 0.4$ metre cube sat. Geostationary earth orbit (GEO) space debris of 18 magnitude (which corresponds to 30-40 cm size and larger, assuming standard reflectivity characteristics) and situated at altitudes 20,000km to 40,000km, assuming standard reflectivity characteristics) exist (Molotov, 2011) are detectable. The absence of space debris optical tracking facilities in the Southern hemisphere is clearly seen in Figure 6. (Molotov, 2011). Further the figure shows the extensive reliance on small optical telescopes of the 20cm to 40cm size. The role that committed observatories in the small telescope category is significant.

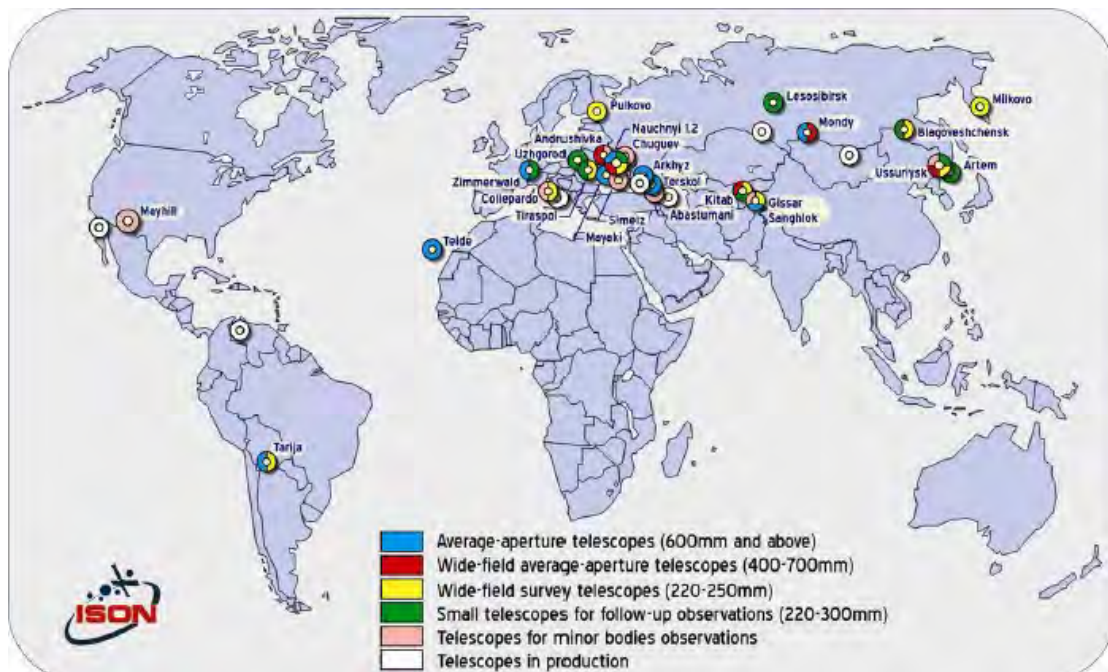


Figure 6. (Molotov, 2011). Shows the extensive reliance on small optical telescopes of the 20cm to 40cm size to optically detect and track space debris.

Mount Burnett Observatory

The Emerald Observatory operates in collaboration with the Mount Burnett Observatory with each observatory having distinctly different roles. The Observatory at Mount Burnett was established, Figure 7, in 1972 by Monash University. Research focused on active chromosphere stars in the southern sky. Superseded technology led to the site's decommissioning in the late 1990s. The 45cm telescope lay unused until in 2011 MBO formed as an astronomical society to preserve the facility. MBO is now the fastest growing astronomy group in Victoria with over 280 members. Additions to the MBO site include a Sirius dome to house a 33cm go-to SCT for guided visitor and member use.

The two observatories work together where the MBO facility brings public outreach and member use and the Emerald Observatory brings a research capability to the collaboration. In September 2017 the MBO will host the 2017 Victorian Astronomical Convention. The opening of the Emerald Observatory is planned to coincide with the convention.



Figure 7, Mount Burnett Observatory. (*Courtesy of MBO*)

Research opportunity

The Emerald Observatory 45cm OTA SCT will come on line in September 2017. The location 70 km from Melbourne facilitates hands on observing and access to set up and calibrate equipment. The site offers high quality accommodation and support facilities that facilitate observing stays. The Observatory executive board is openly seeking research collaboration with researchers in Australia, Europe and Russia. The facility is also available for training programs. Research enquiries should be directed to the authors.

References

- ASCOM Standards. (2016, September 24). *ASCOM Standards for Automated Astronomy*. Retrieved from ASCOM Standards: <http://ascom-standards.org/index.htm>
- Australian Building Codes. (2016). *NCC 2016 Building Code of Australia - Volume Two*. Canberra: Commonwealth of Australia.
- Australian Space Research Institute SSRP. (2007, October 4). *Scout Australia payload 1*. Retrieved from ASRI SSRP Campaigns: <http://www.asri.org.au/SSRP/Campaigns>
- Brumfitt, A., Thompson, L., & Raitt, D. (2006). The Art of Space Mission Patches and their Origins in Society. *Astra Astonautica*, IAC-06 E5 3 4913.
- CFA. (2012). *Planning for Bushfire Victoria Ver 2*. Victorian Government, Country Fire Authority. Melbourne: Vic gov. Retrieved from http://www.cfa.vic.gov.au/fm_files/attachments/plan_and_prepare/planning-for-bushfire-web.pdf
- CSIRO. (2010). *Fire Performance of Glass Block Wall When Tested to AS 1530.4*. CSIRO, Fire Testing and Assessments. CSIRO.
- Department of Environment. Land, Water and Planning. (2016, September 21). Planning Property Report. Melbourne, Victoria, Australia.
- Flaga, A., Bosak, G., Flaga, L., Kimbar, G., & Florek, M. (2011). *Wind action on small sky observatory ScopeDome*. Lublin University of Technology, Department of Architecture. Lublin: Lublin University of Technology.
- Hampf, D., Riede, W., Stöckle, G., & Buske, I. (2013). Ground-based Optical Position Measurements. *Deutscher Luft- und Raumfahrtkongress* (pp. 1-10). Stuttgart: Deutscher Luft- und Raumfahrtkongress.
- Haverling School UK. (2008, September 15). *bettshow.com*. Retrieved from Bett show: <https://haverlingict.edublogs.org/2008/03/13/haverling-cleans-up-at-the-igfl-bees-in-space-competition/>
- International Astronautical Federation. (2016, September 24). *FRANK J. MALINA ASTRONAUTICS MEDAL*. Retrieved from International Astronautics Federation: <http://www.iafastro.org/activities/honours-awards/frank-j-malina-astronautics-medal/>
- Molotov, I. (2011). Optical Tracking of Space Debris. *Beijing Space Sustainability Conference* (pp. 1-12). Beijing: Beijing Space Sustainability Conference.
- MoonLite Telescope Accessories. (2016, September 24). *MoonLite CSL 2.5 inch Large Format Crayford SCT/RC Focusers*. Retrieved from MoonLite Telescope : <https://focuser.com/products.php>
- Narkowicz-Pala, A., & Wojcik, Z. (2009, January 30). *Astronomical Observatory Tower Type*. Słupsk: Obserwatoria Astronomiczne.
- Thompson, L. (2016). *Emerald Observatory Construction Design*. Melbourne: Brumfitt, Thompson & Thompson.
- United Nations. (1999). *Technical Report on Space Debris*. United Nations, Science and Technical Sub Committee on the Peaceful use of Outer Space. New York: United Nations.

The Ethics of Working with Robots

Gabi Hobbs - University of New South Wales, Canberra

Abstract

Since our human nature is prone to take shortcuts rather than go the long ethical way in finding solutions to urgent problems, our behaviour around artificial intelligence depends upon each individual's ability to act morally when alone with robots or during interaction with other human beings. Unlike robotic patterns – due to set and sometimes inflexible programs, man is adaptive and has multiple ways of dealing with ethical dilemmas. Ethics may be entering a golden age: the space robotic age, when men will work together ethically with robots due to improved focus on human rights, environmental considerations and ethical research. This will be possible through human ethical behaviour and also through sophisticated robotic technology shaped by ethical behaviour trends inserted in future software. In the near future, robots will be programmed to pick up unethical human actions due to ethical principles inserted into their programs. Human and robotic behaviour in space has to be based on universal moral principles in order to evolve and constantly re-shape our space industries. The future of industries, such as asteroid mining, depends not only on the peaceful space commercialization or the ethical software, but also on humanity's ethical interaction with robots (i.e. sending cubesats or small spacecraft with an ability to cause no space debris or have zero pollution).

At Arkaroola, in the South Australian desert, researchers' work testifies that great minds focus on high values such as freedom and kindness even if we are far from creating 'the ethical' software. Robot designers' behaviour was ethical most of the time and most robots were capable of performing tasks correctly. Nor did extreme tests make people behave unethically despite some small accidents. Having a noble purpose in mind like space exploration made people ponder more on their acts and thus, act highly unselfishly and more ethically they would normally do to save face.

Introduction

There are many instances which humans don't want to accept given rules and the fact that our time on Earth is limited is one of them. It is important to understand that, similar to our taking for granted this planet and its resources, the advanced technology, if not used correctly, could also make impossible human life in outer space, where the key for survival will entail living ethically around robots despite our many customs and various faiths (1).

The main purpose of this Arkaroola research is to understand how humans interact with each other while building robots and conducting robotic experiments, including the causes and the consequences of such behaviour. Robotic discoveries reaching unprecedented levels with innovations go beyond scientific challenges due to their unimaginable potential. Examples include the search for alien life, an opportunity which will determine the future progress of morality.

I will start this paper by introducing the Arkaroola Expedition and then present the concept of '*robot ethics*' in order to propose some behaviour trends for robots and people. A key argument will be the need for ethical behaviour while working with robots, based on the scientific teams' behaviour during the July 2016 Arkaroola expedition (Fig. 1). Ethical considerations drawn from personal conclusions in regards to human and robot interaction will also be discussed, thus stating the importance of robot ethics and offering some recommendations for future research.



Fig. 1 Robotic testing at Arkaroola, 2016

1. Arkaroola - A diverse region for analogue research

Arkaroola's peaceful beauty is due not only to its great variety of geological structures, but also to its people who promote great values such as space exploration and friendship between nations. While the interaction between nations and group of people is very important for space research, the amazing and breathtaking images of outer space received from unmanned vehicles such as Mariner, Viking and Voyager have completely changed humanity's perception of the universe. In this sense, the robotic spaceflight is certainly compelling and part of international news because they are the only one that go into 'the depth' of outer space, where people can only dream of (2).

a) Location and Short History

Australia has numerous landforms with unique features that provide a useful reference for interpreting the results of spacecraft orbiting outer space bodies and exploring alien regolith surfaces. Examples of desert landforms, impact structures, relief inversion, long-term landscape evolution and hydrothermal systems that are relevant to outer space have been outlined and reviewed for many years now (3).

Arkaroola is such a landscape and is commonly known as the Arkaroola Wilderness Sanctuary - a desert area situated on 610 square kilometers, in South Australia (4). This wilderness sanctuary is located 700 kilometers north of Adelaide, in the Northern Flinders Ranges, and is bordered, in the south, by the sinuous, ordered ranges of the Vulkathunha-Gammon Ranges National Park and the Mawson Plateau (5). Its spectacular, jumbled rocky chaos of massive granite and volcanic rocks, deeply incised with gorges and creeks, were occupied for thousands of years by the Adnyamathanha Aboriginal people (6). Later, in the 1850s, the early European settlers originally called this country 'Mount Painter' due to its dry and rugged terrain, and has been difficult to farm due to devastating droughts (7).

b) Large Scientific Interest

The distinctive characteristics of the Arkaroola Region have been assessed for almost one hundred years and its benefits for education and science are very well documented (8,9,10). More recently, since late 1990s, the Arkaroola scientific research focused on this land as a Mars Analogue and, thus, is greatly linked to future industry work opportunities and other outer space advantages (11). The Arkaroola Mars Analogue Region research is currently

outlined by Australian researchers specialised in robotics and human-machine interactions, such as Jonathan D. Clarke, Graham Mann, Annalea Beattie, Guy Murphy, James Waldie and Steven Hobbs. Mars Society of Australia (MSA) uses Arkaroola's acid lakes, hypersaline embayments and mound spring complexes as analogue to life on Mars.

The waters of Paralana geothermal springs issue from geological faults dating back one billion years and are heated by uranium rich granites which enrich the waters in radon (12). Despite the high radioactivity of these waters, an extremophile algae survives on the floor of these springs at a warm temperatures of 62 °C, which is of a great interest due to the possibility of life on outer space bodies.

However, the main scientific benefits of the Arkaroola expeditions regard the education of future generations and the development of artificial intelligence, with both software and hardware configuration management, and the understanding of how human interact around and with robots or, in other words, the ethics of artificial intelligence. Human psychological and character traits whilst wearing space suits and challenging attitudes about outer space is another new trend in space research (13).

While NASA's statistics regard the success of the Mars automated space equipment and technology, an integral part of its Martian space research is focused on major ethical questions such as 'Should life be replicated in outer space?' or 'How exactly will future colonists be able to live and work side by side with highly independent robots, which will be able to adapt their programming and perhaps gain human behavioural traits?' (14).

c) Present and Future Developments

Over the past decades, MSA has contributed to a large body of literature through its workshops, the Australian Mars Exploration Conference series that ran from 2001 to 2012 (subsequently incorporated into the Australian Space Research Conference Mars Society Australia's contribution has included focused on planetary science (15, 16, 17), scientific and engineering analogue research (18, 19) site selection (20), psychological (21) and ethical studies (22).

2. Robot Ethics

Ethics have evolved greatly since the initial use of simple telescopes or the days of Giuseppe Piazzi (1801- discovery of asteroid Ceres), Harding (Juno, 1804) or Olbers (1802, Pallas and 1807, Vesta). As technology continues to revolutionise our daily life with autonomous robots and modern sophisticated equipment and instruments, the intrigue of how humanity should behave in regards to artificial intelligence retains its pull while working on Earth or in the cosmos. The sphere of ethics is inherently applied in all areas of life and of profound interest to most people since it regards humans' behaviour and their interaction with each other and all objects around them. There is a growing body of research around 'robot ethics', with multiple conferences organized by multidisciplinary research groups in the last few years (23,24). With all its phenomenal outer bodies, space could be regarded as an object that humanity could interact with daily.

The international community has many reasons to continue to encourage ethical behaviour for both government and private companies who enter the space industry (25). At present, we can talk of a *space ethics*, with numerous supporters in all nations, and of research into the new field of robot ethics which emerges through ethical experiments into human-robot interaction to defuse public confusion (26,27).

Despite the fact that people might think morality amidst space robots is being studied by the engineering ethics (28,29) which primarily refers to chemical, physical, astronomical and geological factors, robot ethics, as a branch of space ethics, is in fact a symbiosis of both scientific and moral dimensions. Thus, it includes psychological (30,31,32), sociological (33), cultural (34,35,36), and even historical (37) elements of observation. Although it mainly deals with the study of the behaviour of astronauts and their candidates during astronaut programs or deployment in outer space (38,39), it also includes assessments on various groups of population performing complex tasks in isolated confined environments like Antarctica (40,41), the Polar Regions (42,43,44) and deserts such the Utah Desert (45) and the Australian outback (46), where people and robots interact on a daily basis since life without machines is impossible.

Additionally, robot ethics deals with the transhumanism movement (47) and the long-term visions regarding the status of robots (48), which carry immense potential for beneficial space developments. However, if misused, new technologies, such as genetic engineering and nanotechnology, could cause enormous harm, such as ecological annihilation, destruction of meaningful human relationship or even the extinction of human race (49,50). Although risks need to be taken seriously, the root of evil is not technology, but human nature. Improving physical/biological and emotional qualities won't fix immorality; only education and cultural refinement are proven traditional means for radical changes in our human character development and in society, in general. It is also incorrect to assume that applied ethics often reflect a reactionary attitude towards new technologies (51,52) since ethics are not reactionary to progress or to new moral views (e.g. slavery assimilated into our ever-changing law) (53,54).

The suggestion that evolving into a post-human with the opportunity to live for hundreds or thousands of years with full bodily and psychic vigour will help us rediscover new values and greater capacities is probably incorrect. If being post-human means to be perfect (55), humanity will lose both its capacity to create or strike higher or even desire to try if failure would be seen to be human and thus not genuine for a post-human. Similar to asteroid mining, enhancement's purposes are extremely important due to the fact that reason is vital for all mankind's choices. Thus, we should choose to enhance ourselves, but not because it gives us better active lifespans, better memory or greater intellectual and emotive capacities. In a similar method to vaccination, mankind has to discover the enhancement's benefits before declaring it safe and prosperous. A forged character can't ever be formed through genetics (despite the removal of genes like anger or lust) since without failure both humans and post-humans can't appreciate the true taste of success (56).

3. Behaviour Trends in Arkaroola Researchers

Developing mechanical navigation systems and software programs to operate robots on rough terrain represents only a small part of the robotic space challenge (57). The main issue in our modern '*era of flagships*' is setting *unrealistic dreams* (58,59) such as the future objective of asteroid mining despite the problems in the legal arena (60). New entrants in this fierce competition for space supremacy are set 'to steal' the robotic show from a 'financially strapped' United States and a 'technically limited' Russia (e.g. Japan and European Union cooperative programs) (61,62). India and China also have the capability to join in deep-space missions (63).

Despite the greatest tragedies outer space exploration brings (64,65), there will always be advancements in robotics, in order to make space robots cheaper and smarter (66) – for

example, practical new inventions seen today in the Mars Exploration Rovers, the cubesats or the robotic human organs. In order to help with urgent cosmic tasks such as maintaining the International Space Station or less stringent and repetitive terrestrial jobs such as digging tunnels or collection of rubbish, space robots will surely change the ethics of human survival. Most of the difficult aspects of robot operation such as alignment of wheels, tracking and guiding radio signals require the collaboration of a minimum of two people whose behaviours can be predicted at times, but which could get very tense when things go wrong.

a) A growing fascination with Mars which fosters human love for advanced technology such as cubesats and mining rovers: Human society has been concerned with space ethics since pre-history, although erratic and unclear at times when stars were thought to possess souls and comets, eclipses or meteor storms were signs of doom. Universe special events such as rotations of planets are still seen as favourable conjunctions in people's lives. However, there are still many people who still believe space and space exploration in particular is 'a lot noise for nothing' - mainly because of their focus on terrestrial concerns and consumption needs.

Mining concepts on another world like Mars have already been tested through Opportunity (2004), Curiosity (2012) and will again be verified during the Exo-Mars rover this year, when it lands on the Red Planet. However, the latest NASA missions carry already cubesats for scientific experiments and give an opportunity to people to test their own research ideas. It won't be long and space mining rovers might become a reality to foster a Mars culture on this planet, not only from terrestrial hubs.

b) A compelling need for new modern technology: Over the last decades, nations all around the globe have recorded the greatest number of 1.7 million robots in 2015 (67) for industrial purposes. The average annual growth rate will be 12 per cent between 2015 and 2018 (68). That is a lot of robots for lesser number of people! In other words, taking into account that we are around 7,324,645,000 billion living at present on Earth (69), this corresponds to a global year-on-year growth of 8 per cent (70). The greatest demand of robots is registered by the automotive industry (71) and defence which has unclear robot statistics due to internal or external fluctuating threats, and, of course, national budget provision (72).

So, why so many? An answer is the cheap cost for production, the great benefit for the average person and the safety that comes with developing more efficient robots. While a percentage of consumers are unhappy with automatic work, it is fair to assume that most of us regard robots as the next step in our colonising of the planet Mars.

During Arkaroola 2014 robotic trials, the understanding of how the Australian outback and human care affect electronics was greatly enhanced since all robots had to cope with different variations of climate, such as electrically conductive dust, humidity and precipitation. It was both a scientific opportunity and a financial challenge to prepare them for various testings. Everyone stepped outside their comfort zone and pushed their instruments to the limits of endurance in a competition of brains and adaptability. The Arkaroola researchers' topic was to conduct standardised engineering testing on custom built robots.

c) Increased focus on social ethics - due to millions of advocates for ethical commerce of robots (web-based sales): Dealers are selling more and more robot parts via the internet. It is usually cheaper and more convenient because researchers know most of the time what they are looking for. Unfortunately, fewer and fewer electronic retailers exist in Australia where robot programmers can walk in and rapidly select robotic equipment for their needs. In this sense, the internet is an option for most Australians or other nations, despite the long wait for

the post to arrive from overseas. Thus, to keep things into perspective, robot engineers have to foresee difficulties and implement solutions until parts reach their destination.

Could the local community help? Yes, by promoting local space technology so that one day our Australian social astronomy clubs, public schools and outreach organisations can enjoy local manufactured robots. Time will tell if our government is interested in subsidising future space technology.

d) Increased connectivity between ordinary people – the corner stone for great interaction between present and future space faring nations: Robots and their accessories like robot arms, batteries, wheels, Arduino program are going to get better and more affordable as the computational power gets cheaper and more integrated in devices like cameras and spectrometric pieces (however the holy grail for robots remains the internet where information travels fast). With greater robot designs on the market, competition is tough for each robotic element. While building their own robot, it is very tempting for universities to overspend and also very hard to predict the lifetime of such robot due to numerous testings, done in a limited time, on a very hazardous terrain.

Arkaroola research teams this year comprised nine individuals. From present and past expeditions there is no doubt in the minds of all participants that the start of international collaboration between universities and organisations like the Mars Society Australia (MSA) is worth all the effort of organising visas, special diets and language translations. Mixed ideas are the key for future space mining and it has been seen so far at its best in the robotic partnership between the Japanese Aerospace Exploration Agency (JAXA) and National Aeronautics and Space Administration (NASA) during their planned asteroid return sample missions (NASA sharing its three-dimensional models of asteroids to assist Hayabusa2 in its navigation and the Japanese first landing's data available for NASA) (73). Predicting how robots react on a non-gravitational outer space body is crucial and thus, one can never have enough experts.

e) Smart ways of learning - robots as perfect tools for learning about the cosmos: New peripherals like the Mars Rovers help people set foot in pristine places and also learn new things about themselves such as the creation of universal moral standards for the international community which was a dream before space exploration). Additionally, the exploration journey made by robots takes scientists, such as the physicist Richard Hawking, to reach for new resources and ways to cope with daily life (74).

Robot drones or unmanned vehicles (aerial – UAVs, undersea UUV, and surface USV) have existed in unsophisticated shape for hundreds of years, with the first documented use by the Austrian army which used balloon bombs to attack Venice in 1849. In the 20th century, research led to an increased number of Global Positioning Systems and assisted by the use of the internet. Thus, this modern technology led to the development of pre-programmed drones that can fly any path and survey unexplored territories like Gale Crater, on Mars.

Both ethics and science may combine to play a pivotal role on our understanding of asteroids through robotic missions since recent advances in electronic miniaturisation, laser technology, fabrication of extremely thin and light materials and nanotechnology make asteroid mining missions realistic to plan even by private companies.

f) New direction towards engineering cooperation and common solutions: With many robotic researchers and space amateurs purchasing robots of any sort, there is a dimension of active interest in having a robotic presence on Mars which will lead to a desire to possibly mine its

moons for a human presence on Mars. Many desire to see plenty of nations mining asteroids so that humanity's curiosity can be satisfied and enjoy the benefits of such endeavour while colonizing other planets. The robotic presence on Phobos or Deimos will make humans ponder beyond the technical, instrumental meaning of machines: it will make us all marvel at this new relationship humans will have with robots.

During the 2016 Arkaroola expedition researchers have treated their inventions with great care. Naming robots has greatly contributed to the attachment people felt for their machines, in the sense that all scratches and computer failures were sadly felt. There was also the birth of great friendship being built between opposed personalities, due to a common focus on productivity and correct gathering of scientific data.

4. Behaviour Trends in Robots

a) The overwhelming difference between humans and robots: What robots and people have in common? When viewed through human eyes, robots have nothing in common with people since it is believed that emotions and needs are irrelevant when describing machines. As odd as it might seem, robots have nevertheless essential requirements (75) and thus, similar to us, people, they come in different shapes and sizes. They start to resemble people more than we think because, like living organisms, they can adapt and also learn new skills - i.e. the need for human recognition while dealing with passwords or the cute Japanese robot companion, Kirobo, on the International Space Station (ISS) (76). However, robots possess rather inflexible computer programs with inexistent moral behaviour (despite cognitive processing of instructions) and lacking team loyalty, unlike humanity rich in reciprocal, adaptive thinking, sophisticated moral trends and great team building skills.

At present, we have advanced our understanding of ethics, which make humans unique. It takes more than human physic and intellect capacity to be really human. Thus, robots are not ethical or unethical since they lack moral principles. However, the robotic revolution - another famous step in our evolution, such as Darwin's famous 'Origin of Species' (1859), the publishing of Mendeleev's Periodic Table (1869) or Shoemaker NEAR mission of (2001 the study of asteroid Mathilde and the soft-landing on asteroid 433 Eros) could be an unethical step since it will uncover new ethical dilemmas. Nevertheless, it is beneficial for humankind to have robots because the ethical decrypting of programs will give us a better chance of being able to conduct ourselves in outer space and in solving ethical problems such as aged care or performing demeaning/boring/repetitive and dangerous jobs.

In the future, space ethics will have to study the socio-physiological link between humans and robots. Ethics will look at how robots change the way we relax, play or work or even at their potential of inspiring us - better than other human beings. Advanced technology will not only make our lives easier, healthier and more fun, but it will teach us to be versatile in our behaviour and think more ethically than ever. In this sense, well-resources organisations (such as the U.S. and the Australian defences) or tech giants (e.g. Google, IBM and Qualcomm) use robots in search of survivors during dangerous missions such as nature disasters (77).

There are no research ethical studies on how people will interact with other robots during social activities such as playing games, enjoying a drink or booking into a hotel. The clues we have so far suggest people will adapt and even welcome a robotic presence during any stage of human life, especially when our mobility and intellect are highly reduced (78). However, this might not be true because video games already dismiss the benefits social skills have in the developing of a child. Will we gladly choose to board a train or a car run by a robot? It

might be safer than hitchhiking with a stranger, but vandals are not going to disappear soon and the presence of robots will not likely make ethical dilemmas disappear; on the contrary, they will increase due to the increase number of robot-man interactions. Thus, the mixed attitude towards robots doesn't change the fact that their presence is a must in our modern society. They will probably never replace the heart-warming kindness or smile people get from helping strangers, but nor will we ever be able to uncover the mysteries of asteroids without them.

b) The powerful growth of computers in modern times: Without a doubt, computers capture the imagination of all ordinary people due to its increased applications throughout the modern world. Even if the construction of computers has started long ago with the ancient worlds (79), it hasn't got easier for the space capability to cut edges in innovation. Space exploration still involves extra amount of time and computer ingenuity to solve problems like zero gravity or radiation which overheats sensors and most electronics if not encased in special boards.

The rise of computers is well underway with the Raspberry Pi designed to work on distant planets using terrestrial controllers. This inevitable revolution of computers and the befriending of robots by people is a choice humanity makes daily in own backyard or in scientific labs of various mechanical, chemical or health criteria. Robot advancement helps us with practical discoveries such as ice on Mars (80,81) and benefits us indirectly by understanding how unique human brain is, for instance or what great self-healing power it has compared to a computer programme. In this sense, another example is the future home which might very well depend on building a strong robot to deflect a killer-asteroid or start the gruelling challenge of colonising a different planet if Earth becomes inhabitable one day.

The huge amount of information utilised by computers these days begs a re-evaluation of the question: how much are we willing to depend on computers? Is there a limit for people to allow machines to be trusted, especially when venturing into the unknown of outer space?

c) Better robots (huge or tiny) require flexible, recyclable hardware and advanced, unfailing software if a Mars experience is to take place: Robots are going to get bigger and also smaller. They have already been tested in isolated, confined and extreme environments such as Antarctica and the Artic. Serious asteroid mining observations already plan to push the limit toward larger 'potable' drillers and spinning distilleries.

A current example of a large robot is a 3,500-tonne coal dragline featuring automated loading and unloading (82), while the tiniest measures only 60-250 micrometres and is a wormlike robot, called 'nano-bot' since it can just be seen with the use of a microscope (83). Such is the nature of extracting minerals and the high competition of this industry that new inventions appear each year on the international trade: e.g. the Artic drills used by the Russians and the big robotic instruments of Origins, Spectral Interpretation, Resource Identification, Security-Regolith Explorer [OSIRIS-REx - NASA's spacecraft about to intercept the target asteroid 101955 Bennu in 2018 - with return samples to Earth in 2023, in the Utah desert (84)]. If we consider Hayabusa2 of Japan, we see a plethora of small mining robots waiting to drill into the 162173 Ryugu in the same year 2018 - with return samples in 2020, in the Australian outback (85).

Depending on the size of asteroid planned for mining, small robots are definitively the way to go for the first mining expeditions because of a compact, lightweight design which requires smaller spacecrafts and less operational power.

d) Oversaturation of academia talks and enough robotic experiments like Arkaroola:

The future of the Australian robotic industry and space exploration depends greatly on how engaged the government and academia are in developing apolitical experiments and also by encouraging future generations in inventing robotic products. The topic of space is hardly discussed in the media and the prediction for an Australian Space Agency looks doomed despite the enthusiasm of many citizens, as seen through during the Arkaroola expedition, where enthusiastic four volunteers assisted, one aged even eight.

However, the robotic interest in Australia will continue to rise although the current pace is not a fast one and growing mostly due to mining industry experts desiring to profit from mining asteroids and private companies entering the space industry like Planetary Resources, Deep Space Industries, Global Space Organization, Infinite Space Dynamics, Exo-Moon and Stott Space (86). Robots will continue to foster the children's fascination with space and maybe with free publicity and proper funding, Australia will be the leader in space robotic e-commerce.

More research on robot ethics is necessary because people and robots are designed differently, and, unlike robots, humankind is not easy to predict and much vulnerable than robots in space. Unless we understand our behaviour around passive robotic behaviour, on Earth, as in outer space, it will be hard, if nor impossible, to have an effective communication between us – earthlings and advanced machines which could one day recognise or have built-in ethical traits. Contrary to a robotic system, human behaviour is based on intuition blended with hope and reacts often due to inhibition and suppression of negative feelings, thus, with great consequences when working with machines.

5. Robots' Characteristics

At Arkaroola, researchers experienced increased connectivity between man and machine, in different environments (like wet slopes, grassy patches and desert dunes). Two Australian universities (UNSW and ANU) worked together closely with MSA in robot testing three rovers which served many roles (e.g. carrying loads, examining rocks, gathering data). As robotics technology advances each year, the ethical concern of Arkaroola participants also increases, partly due to the pressing interaction with international partners. Additionally, the risk of forming emotional bonds between team members is higher than those links between owners and robots due to human reciprocity element.

All participants had various personalities ranging from extraversion, openness, to agreeableness and conscientiousness (87). My method used personality inventory and personal functioning. The predominant behaviour was the agreeable character with main traits including: persistence, consistency, frantic observation of nature elements like wind and rain. My experiment also considered the peaks of tension between some researchers. This included a degree of cowardice experienced by some during demonstrations or tests, in the sense that high precaution was taken in order not to damage the rovers or terrestrial desert layers. I found no verbal aggression towards each other (e.g. when set schedule hadn't been followed), since kindness and appreciation marked all experiments and because all team members were ready to help each other if not busy with their own machines. As a consequence, human behaviour involved no hacking or debugging since all experiments were friendly and most procedures and data were shared amicably.

a) Little Blue (88) - The robot called 'Little Blue' was differentiated by other robots in terms of size and instrumentation carried. Little Blue possessed a multispectral camera, a webcam

for macroscopic analysis of regolith, a video camera for driving, and weather and temperature instruments. It has achieved all goals through its high manoeuvrability and has been considered the most reliable rover.

b) Burra (89) - Being the most ‘stubborn’ machine at Arkaroola, this rover performed well in finding particular objects due to its complex sensors and motors taking into account that it has been built a week before the trials. Although it was always moving the safest during experiments, it had the worst time at completing tests. Of medium size, its characteristics included loss of mobility and of reception at times. This robot was differentiated from the other ones mainly due to the extra materials from which it was made: tough plastic hardware. The way they joined together the motor and the transmission also varied because the on board computer system was set lower than the others.

c) Crab (90) - The physical structure of this robot is unique: it was made entirely of aluminium and used motors from the same company that supplied them to the NASA Mars rovers. It was very animated due to its special grinding sound and original hollowed wheels which were designed to get rid of soil if stuck onto the ground. Its ability to move in a coordinated way was fantastic since it covered all sorts of soil and different inclinations of slopes. It successfully navigated in complex desert environment using rocker bogie suspension and high torque motors.

Although the planning of this rover was carefully conducted with multilateral input from all members of this expedition, which included geometric models of accurate distances and measurements of rover components, this rover was slower than the other two rovers, lurching behind others about five meters for every ten to fifteen minutes (Fig. 2 & Fig. 3).



Fig. 2 Present horizon for humanity and robots



Fig. 3 Future robotic perspective

6. Ethical Considerations on the work of Arkaroola robot experiments

a) Global Behaviour Patterns: Planning for such a ground-breaking project is ongoing; but the Australian team has demonstrated that they already have the advanced technology to simulate a Mars expedition in Arkaroola using their precision and portable instruments (e.g. thermal/atmospheric, chemical and radio payloads). Most of the time, there was a combination of various robot packages to suit various needs of mobility and of data accuracy. The difference in robot sizes and programme competences raised questions about funding and personnel problems – similar to the collaboration between the Japanese Aerospace Exploration Agency (JAXA) and the U.S. National Aeronautics and Space Administration (NASA) during their planned asteroid missions.

Some researchers argue that robotic missions reveal the ethical problem of space power imbalance between nations (91,92), or universities' influence in our case, which is untrue because for the exploring of heavenly bodies to be effective, more than one nation is needed and for the future of Australia in space to take place, various actors need to be involved. Although competition is important at both national and international levels, ethical behaviour in robotic research always equals cooperation and teamwork between engaged university groups and organisations like MSA. In Arkaroola, these characteristics of transparency greatly prevailed despite independent data being collected from all sites and various degrees of technical skills. Additionally, there were no relevant cultural differences like between space-faring nations of America and Asia (93) and no business conflicts between the Australian space volunteers and academia. The coordinator, Dr J. D. A. Clarke (the president of MSA) kept everyone busy with animated talks, media interviews, robotic missions and geological project updates. Much of the MSA's outreach took place on its website and Facebook page, both run in English, by the members of this non-profit organisation. All rovers were equipped with multiple technologies, but there was a limit as to how much one could put on top of a metal case and how remotely a robot could operate before losing reception. One major step was that all teams had the necessary equipment required to identify rocks samples, including digital imaging software and infrared light sometimes used to select minerals based on colour and texture. No drilling equipment was needed to access stromatalites and no decontaminated containers was used since there was no alien threat or possible terrestrial seals needed before, during and after the collection and analysis of soils and while performing endurance robotic tests.

Yet, despite the Australian enthusiasm, there were mismatches in hard work and recognition. While I cannot name 'the best team', in the sense of gathering and recording scientific data, nor 'the most ethical one', in the sense of consistency in displaying moral integrity, I can conclude that there is a lot to learn about human behaviour around robots since efficiency and morality vary while performing complex tasks in harsh environment such as the Australian Outback. I have also noticed that uploading pictures on the internet and sharing new scientific data with the public or the academia are not always in the best interest of researchers due to the lack of time, especially when controversies arise. Explanations take more than one exchange of emails, and, most of the time, researchers don't have all the answers until after months of processing their data. While we typically divide these results into team effort and not personal hardship, the best way to differentiate the work done at Arkaroola from other previous Australian or overseas experiments is to describe the renewed passion for Mars with the new theory that, by using Indian collaboration (94,95), Australia may have its own rover on our neighbouring planet. This view is definitively going to be tested during the Australian robotic experiments scheduled for August 2016, in the Himalayan Indian territory.

b) Individual Behaviour Patterns: Apart from valuable robotic resources used at Arkaroola, invaluable social capital also contributed to the reputation of the involved universities and participant organisation. Additionally, extreme loyalty and commitment to particular groups were evident due to individuals' affiliation to others through fairness and respect. Group size, cultural differences and gender distribution mattered less than personality and leadership styles which were crucial in coordinating all projects. However, for a realistic ethical research I believe only time and environment are the correct measuring scales.

It is true that group and individual profiles provide insight into predicting the interaction preferences which impacted each group and the entire mission performance. Although individual discipline and stress were relevant at times, they were no reliable issues to be considered measuring tools for this environment, maybe due to the short period of

experiment. The predominant results were evident at individual level: the positive profile for being conducive to group performance and the negative, self-focused cluster formed by our two young volunteer members - focused on personal needs regardless of testing type. The researchers' profile had personal attributes like being instrumental at completing tasks, high interpersonal expressiveness/openness and agreeableness. No one has experienced any sort of hostility, verbal aggressiveness, neuroticism or consciousness leading to a negative behaviour for all tasks.

Instead of using past simple ethical descriptors such as: *right stuff* (for high in all areas of competitiveness, performance standard), *wrong stuff* (for the observation of some negative traits of character like hostility, impatience and irritability during independent or group tasking.) and *no stuff* (for low in all dimension or disinterest in most tasks) (96), I have looked in detail at ethical traits like achievement striving and motivation using my own ethical questionnaire.

Past Arkaroola robot technology testing and demonstrations were dedicated to gathering rock samples and improving rover collection, with very little study on ethical performance of organisers and participants. This year, Arkaroola expedition fostered improved care for ethical behaviour and more realistic expectations for the future of this space program which would be impossible without the support from community. Nevertheless, future governmental help is expected if Australia is to educate future generations on space ethics.

7. Conclusion

Arkaroola amazing robotic research solidifies the scientific relationship between Australian scientists. However, regarding human behaviour around robots, more ethical studies are needed since we hardly know how inventors and helpers react when robots stop working and what unethical strategies they are willing to use to compete during failure times. Nor do we know enough on how greatly they rejoice, nor on their reasons of being kind while helping or sharing scientific data with their competitors.

At Arkaroola, while all teams easily helped each other with ideas on how to fix robots, the information sharing process was less volunteered and only happened on a reciprocal basis. I have seen that when things go according to research schedule, people tend to be friendly and helpful, unlike under stress or time pressure. Innovative robotic ideas such as asteroid mining will open the gate for a new relationship between man and machine; the robot will be more than a tool, more than a hobby, more than a product of the human brain: it will be an interdependent evolution link between humanity and its future.

Through the asteroid mining industry alone, a variety of robots will be born and our life will be forever changed; the buzz of plastic and metallic sounds will be like the singing of birds on Earth – both pleasure to the ear and environmental block stone.

Acknowledgments: Thank you very much to my supervisor **Dr Ned Dobos of U.N.S.W. Canberra** for his kind support and to **MSA** for inspiring and allowing me to participate in the 2016 Arkaroola Mars Bound Expedition. Additionally, a sincere debt of gratitude to **Dr. Jonathan D. Clarke** and to **my anonymous reviewer** who helped me describe the Arkaroola Expedition which greatly improved this research.

References

1. Atkinson, Nancy, *Incredible Stories from Space: A Behind-the-Scenes Look at the Missions Changing Our View of the Cosmos*, Page Street Publishing, pp. 8, 2016.
2. Supra Note 1.

3. www.nasa.gov as read in 17 Mar 2017.
4. www.Arkaroola.com.au as read in 17 Mar 2017.
5. www.environment.sa.gov.au/files/sharedassets/consultation/arkaroola_plan/arkaroola-protection-area-draft-management-plan-2015.pdf as read in 7 Jun 2016.
6. One of their dreamtime stories says that Arkaroo, a mythical monster, drank the nearby Lake Frome dry.
7. <http://history.flindersranges.com.au/places/arkaroola/> as read in 22 Jul 2016.
8. Read more about the Sprigg family (and especially Dr Regg Sprigg AO, a student of Sir Douglas Mawson) and the Arkaroola Education and Research Foundation Sprigg, Reg C. 1984. Arkaroola-Mount Painter in the Northern Flinders Ranges, S.A.: The Last Billion Years. Arkaroola: Arkaroola Pty. Ltd.
9. Clarke, J. D. A., Thomas, M. & Norman, M., The Arkaroola Mars analog region, South Australia, Abstracts of the 35th Lunar and Planetary Science Conference, Abstract #1029, 2004.
10. Thomas, M., Clarke, J. D. A., Gostin, V. A. & Williams, G. E., The Flinders ranges and surrounds, South Australia: a window into astrobiology and planetary geology, *Episodes*, Vol. 35, No.1, pp. 226-235, 2012.
11. www.themarslab.org as read in 17 Mar 2017.
12. Brugger, J., Long, N., McPhail, D. and Plimer, I., An active amagmatic hydrothermal system: The Paralana hot springs, Northern Flinders Ranges, South Australia: *Chemical Geology*, Vol. 222, pp. 35–64, 2005.
13. www.australianscience.com.au as read in 26 Feb 2017.
14. Supra Note 17, pp. 100-114.
15. Pain, C. F., Clarke, J.D., Thomas, M., Inversion of relief on Mars, *Icarus* No. 190, pp. 478-491, 2007.
16. Hobbs, S. W., Pain, C. F., and Clarke, J. D. A., Slope Morphology of Hills at the Mars Pathfinder Landing Site, *Icarus*, No. 214, pp. 258-264, 2011.
17. West, M. D., Clarke, J.D., Potential Martian mineral resources: Mechanisms and terrestrial analogues, *Planetary and Space Science*, Vol. 58, No. 4, pp. 574-582, 2010.
18. West, M. D., Clarke, J.D., Laing, J.H., Willson, D., Waldie, J.M.A., Murphy, G.M., Thomas, M. & Mann, G.A., Testing technologies and strategies for exploration in Australian Mars analogues: A review, *Planetary and Space*, Vol. 58, No. 4, pp. 658-670, 2010.
19. West, M. D., Clarke, J.D., Thomas, M., Pain, C.F. & Walter, M.R., The geology of Australian Mars analogue sites, *Planetary and Space Science*, Vol. 58, No. 4, pp. 447-458, 2010.
20. Clarke, J. D. A., Willson, D., Smith, H., Hobbs, S. W., and Jones, E., Southern Meridiani Planum - A candidate landing site for the first crewed mission to Mars, *Acta Astronautica*, No. 33, pp. 195-220, 2017.
21. Krins, P. W., Beyond “the right stuff”: the role of group processes in isolated confined extreme environments, Australian National University (ANU), PhD thesis (unpublished), 2009.
22. Hobbs, G., The Case for Asteroid Mining, *ARSC*, Oct 2015.
23. www.robots.law.miami.edu as read in 24 Mar 2017.
24. www.conferences.au/dk/robo-philosophy as read in 19 Mar 2017.
25. www.openroboticethics.org as read in 21 Mar 2017.
26. Kahn, P.H.; Friedman, B.; Pérez-Granados, D. & Freier, N.G., Robotic Pets in the Lives of Preschool Children, *Interaction Studies*, Vol. 7, Issue 3, pp. 405-436, 2006. They clarify blurring concepts like robots are dysfunctional, by discussing the positive impact robots have on children’s moral and social development.
27. Wallach, Wendell, Killer robots are coming next: The next military-industrial complex will involve real-life Terminators, *Salon*, 2015.
28. Read more about this false hypothesis in Fleddermann, Charles B., *Engineering Ethics*, Prentice-Hall Inc., New Jersey, U.S., 1999.
29. Pinkus, Rosa Lynn B.; Shuman, Larry J.; Hummon, Norman P.; Wolfe, Harvey, *Engineering Ethics: Balancing Cost, Schedule, and Risk – Lessons Learned from the Space Shuttle*, Cambridge University Press, 1997.
30. Lin, Patrick; Aloney, Keith & Beckey, George A., Robot Ethics: The Ethical and Social Implications of Robotics, Massachusetts Institute of Technology (MIT), pp. 333-345, Dec. 2011 on risky emotional bonds with robots and on robotic threat of nihilism for mankind.
31. Kaplan, Frederic, Who is Afraid of the Humanoid? Investigating Cultural Differences in the Acceptance of Robots, *The International Journal of Humanoid Robotics*, Vol. 1, No. 3, World Scientific Publishing Co., pp. 1–16, 2004. on examples of Japanese traditions of encouraging the artificial reproduction of nature and incorporation of an aesthetic dimension to the quest for recreating life-like creatures.
32. Arkin, Ronald C., Behaviour-Based Robotics, *MIT Journal*, London, pp. 45-47, 1998.
33. Fong, Terrence; Nourbakhsh, Illah & Dautenbahn, Kerstin, A Survey of Socially Interactive robots, *Robotics and Autonomous Systems Magazine*, Vol. 42, Issues 3-4, pp. 143-166, Mar. 2003.
34. Culture affects the way robots are perceived by humans and, reciprocally, technology shapes culture in particular ways. Supra Note 6.
35. Additional research investigates the space exploration’s impact on human culture in Gorman, Alice, Culture of the Moon: Bodies in time and Space, Jan 2016 on doi://10.1007/s11759-9286-7 as read in 01/05/16.

36. Anker, Peder, The Ecological Colonisation of Space, *Environmental History*, No.10, pp. 239-268, 2000 as read on 22/04/16.
37. There are no studies on the progress of man's morality around robots despite accurate research on the recent history of unmanned aerial, ground and undersea vehicles (UAV, UGV and UUV) and modern robots depicted as anthropomorphic creatures (fashioned in the image of man, with 2 arms, 2 legs, a torso and a head). Maybe the reason for this is the market unavailability of uncommon, autonomous insect-like (i.e. the geckoes used by NASA) or humanlike robots (i.e. the Japanese Kirobo as well on ISS). Read more on the effects of the robot industry such as growing human needs and developmental aspects in Tyokumbur, Emmanuel Tryila, Review of Potential Ecological Impacts of Peaceful Robotic Drone Use and Policy Implications for Developing Countries, *American Journal of Environmental Policy and Management*, Vol. 1, Issue 4, pp. 67-71, 2015.
38. Helmerich, R.L., Culture and Error in Space: Implications from Analogue environments, *Aviation, Space and Environmental Medicine*, Spring, Special Issue, 2001.
39. Rose, R.M.; Helmreich, R.L.; Fogg, L.F. & McFadden, T. Psychological Predictors of Astronaut Effectiveness, *Aviation, Space and Environmental Medicine*, No. 64, pp. 910-915, 1994.
40. Costa, P.T. & McCrae, R.R., NEO Five-Factor Inventory, 1978, 1985, 1989, Psychological Assessment Resources, Inc., U.S., 1989.
41. Spielberg, C.D., State-Trait Anxiety Inventory, Form Y, Mind Garden, Redwood City, U.S., 1983 & Spielberg, C.D., Professional manual for the State- Trait Anger Expression Inventory-2 (STAXI-2), Psychological Assessment Resources, Odessa, Florida, 1999 & Harrison, Albert A.; Clearwater, Yvonne A. & McKay, Christopher P., From Antarctica to Outer Space: Life in Isolation and Confinement Springer Science & Business Media, 2012.
42. Helmreich, R.L. & Merritt, A.C., Culture at Work in Aviation and Medicine: National, Organizational and Professional Influences, Brookfield VT, Ashgate, 1998.
43. Bishop, Sheryl L. & Primeau, L., Assessment of Group Dynamics, Psychological and Physiological Parameters during Polar Winter-Over, *Proceedings for Human Systems Conference*, Nassau Bay, Texas, 2001
44. Bishop, Sheryl L.; Grobler, L.C. & Schjølt, O., Relationship of Psychological and Physiological Parameters during a 350 km Arctic Ski Expedition: A Case Study, *Acta Astronautica*, No 49, Issue 3-10, pp. 261-270, 2001.
45. McPhee, Jancy C. & Charles, John B., Human Health and Performance Risks of Space Exploration Missions: Evidence Reviewed by the NASA Human Research Program, U.S., National Aeronautics and Space Administration Government Printing Office, 2009.
46. Clarke, Jonathan D. A. (ed.), Mars Analog Research, *Science and Technology Series*, Vol. 111, American Astronautical Society, 2006.
47. Bostrom, Nick, Human Genetic Enhancement: A Transhumanist Perspective, *The Journal of Value Inquiry*, No. 37, pp. 493-506, 2003. He defines human enhancement as 'radical extension of human health-span, eradication of disease, elimination of unnecessary suffering, and augmentation of human intellectual, physical, and emotional capacities (...) is not limited to gadgets and medicine, but encompasses also economic, social, institutional designs, cultural development, and psychological skills and techniques'.
48. The robot seen as a slave, caretaker, equal fellow being or even human friend, Van der Plas, Arjanna; Smith, Martijntje, & Whermann, Caroline, Beyond Speculative Robot Ethics: A Vision Assessment Study on the Future of the Robotic Caretaker, *Accountability in Research: Policies and Quality Assurance*, Taylor & Francis Group, pp. 308, 2010. They talk about metaphors like 'the robot – the patient as king of his castle' or assumptions like 'the robot is the rival colleague'.
49. Hawkins, Richard, Artificial Intelligence Could End Human Race, Dec 2014, as read on www.livescience.com in May 2015.
50. Sparrow, Robert, Robotic Weapons and the Future of War, in Wolfendale & Tripodi (ed), *New Wars and New Soldiers: Military Ethics in the Contemporary World*, Surrey, UK & Burlington, VA: Ashgate, pp. 117-133, 2011; Sparrow, Robert, Twenty Seconds to Comply: Autonomous Weapon Systems and the Recognition of Surrender, *International Law Studies*, No. 91, 2015 & Wallach, Wendell, Terminating the Terminator: What to do About Autonomous Weapons, *ScienceProgress.org*, Jan 2013 on campaign against lethal force by autonomous robots
51. Supra Note 22, pp. 493 & Supra Note 36, pp. 311 & 313. Read more in Matthew H. Nitecki, Doris V. Nitecki, *Evolutionary Ethic*, Sunny Press, 1993 & Lawrence C. Becker & Charlotte B. Becker, *Encyclopaedia of Ethics*, Routledge, 2013.
52. Smits, M., Taming Monsters: The Cultural Domestication of New Technology, *Technology in Society*, No. 52, pp. 489-504. He calls this moral evaluation 'the utopia-dystopia syndrome', which often leaves the public with 'two worn-out grooves'.
53. Singer, Peter, *Wired for War*, The Penguin Press, New York, pp. 67, 2009 He calls ethical discussion on robots: 'sense-think chain', which is an appropriate definition.

54. Nordmann, A., & Rip, A., Mind the Gap Revisited, *Nature Nanotechnology*, No. 4, pp. 273-274, 2009. They justly declare ethical debates on human-robot interactions as 'reality checks'.
55. Supra Note 22, pp. 495 Bostrom offers the similarity with chimpanzees- men to suggest that an unenhanced man is less evolved and thus with diminished ideals and lesser values. However, I agree with his supposition that a post-man will discover new ways of living, feeling and thinking, which I argue that they will not necessarily be a result of new genetics as much as due to the adaptability to live in new environments. I also disagree with his idea that new inequalities between enhanced people and normal humans will rise and thus need to be addressed in time, due to universal application of human rights principles. Time shows resistance to moral reforms, and not technology as such, is futile: i.e. mobile phones are widely spread due to human connection they bring, and not because man desires to be technologically advanced.
56. Cernan, Eugene, Last Man on the Moon, *Public Talk at the Canberra Theatre*, 09 June 2016, regarding the importance of lives sacrificed on the space exploration's altar. He talked about Neil Armstrong - the perfect man selected for the greatest task in history: the first Moon walk, due to Neil's exceptional morality, of which humility in the face of international fame was probably the most relevant feature.
57. Ulivi, Paolo & Harland, David M., *Robotic Exploration of the Solar System, Part 2 Hiatus and Renewal 1983-1996*, Springer - Praxis Publishing Ltd., Chichester, U.K., pp. 340-342, 2009.
58. Space exploration needs to go beyond the international *kizuna* or international government & scientific collaboration, because goodwill is not enough within space industry, but legal channels to deter unethical robotic behaviour. Read more on t the Japanese '*kizuna*' – social networks and personal contacts forming the core of the recovery process in the aftermath of disasters and on how people in crisis become extremely resilient due to bonds formed during unfortunate times – like those made during the 11th of Mar 2011, during the nuclear Fukushima accident. Read more in Kitazawa, Kay, Five Years on, Japan's Crisis Response Infrastructure is Still Lacking, *East Asia Forum, Economics Quarterly: Politics and Public Policy in East Asia and the Pacific*, Vol. 8, No.1, pp. 13-14, Jan-Mar 2016.
59. Henderson, B.W., NASA Scientists Hope Mars Rover Will Be Precursor to Manned Flight, *Aviation Week & Space Technology*, pp. 85-94, Oct 1989.
60. Tingkang, Andrew, These Aren't the Asteroids You Are Looking for: Classifying Asteroids in Space as Chattels, Not Land, 2009, as read on <http://digitalcommons.law.seattleu.edu/> on 02 Mar 2016.
61. Brunier, Serge, *Space Odyssey: The First Forty Years of Space Exploration*, Cambridge University Press, p.140-149, 2002.
62. www.cnes.fr as read in Aug 2016.
63. Liang, Xiaodon, India's Space Program: Challenges, Opportunities, and Strategic Concerns, Feb. 2016, as read on <http://www.nbr.org/research/activity.aspx?id=651>
64. Lewis, Richard S., *Challenger: The Final Voyage*, Columbia University Press, 1988.
65. Evans, Ben, *Space Shuttle Columbia: Her Missions and Her Crews*, Springer Science & Business Media, 2007.
66. <https://solarsystem.nasa.gov/> as read in 03 Jan. 2014.
67. <http://www.ifr.org/industrial-robots/statistics/> regarding robot supplies in the Americas will increase by 11% and in Asia/Australia by 21%, while robot sales in Europe will rise by 9%.
68. Supra Note 34.
69. As read on <http://www.livepopulation.com/> on 04 Jun 2016
70. <http://www.worldrobotics.org/> as read in May 2016.
71. i.e. two robots used as police officers to direct traffic in Kinshasa, Democratic Republic of Congo, O'Neill, Tom, Obey the Robot, *National Geographic*, Vol. 226, Issue 2, Aug 2014.
72. Detsch, Jack, The Rise of Military Robot R&D: A Global Phenomenon, May 2015. <http://thediplomat.com/2015/05/the-rise-of-military-robot-rd-a-global-phenomenon/> (in both China & U.S.A.)
73. www.astronomy.com as read on the 18th of Apr 2016.
74. www.dailytelegraph.com.au pp. 17, 14 Apr 2016 read more about the 'human nature to fly' according to Hawking while talking about the \$130 million project 'Breakthrough Starshot'. Travelling at a speed of 60,000 km per second, this swarm of tiny spacecrafts weighing about 20g each is to reach the Alpha Centauri star system in 20 years in search for alien life in outer space.
75. Requirements and not 'needs' as this term has a strong human connotation, in my opinion.
76. www.space.com & www.nasa.gov/mission_pages/station/main/robotnaut.html as read in 01/08/2016.
77. Sharkey, N., The Ethical Frontiers of Robotics, *Science*, Issue 19, Vol. 322. No. 5909, pp. 1800 – 1801, as read on doi: 10.1126/science.1164582 He is keen in seeing international ethical guidelines for the use of robots, similar to the U.N. Convention on the Rights of Children. In my opinion, an international unified code of ethics for robots is not only unrealistic, but also impractical due to nations' cultural differences. For instance, human beliefs and practices place a different value on the development of independence in children (toddlers especially).

78. Guo, Shesden & Zhang, Ganzhou, Robot Rights & Hurtley, Stella, Unconventional Attraction, two articles in *Science*, Vol. 323, pp. 851 & 876, Feb 2009.
79. Antikythera Mechanism was created in 205 BC and is a device tracked the movements of Mercury, Venus, Mars, Jupiter and Saturn - the only planets known at the time, the position of the Sun, and the location and phases of the Moon Read more: <http://www.dailymail.co.uk/sciencetech/article-2853082/World-s-oldest-computer-ancient-thought-Antikythera-Mechanism-created-205-BC-study-claims.html> However, the first design of a modern computer is considered to be analytical engine, made in 1834, by Babbage as read on <http://www.thocp.net/timeline/1830.htm>
80. Taylor Redd, Nora Water on Mars: Exploration & Evidence, 2015 on <http://www.space.com/17048-water-on-mars.html> as read in Jul 2016.
81. Jones, Eriita, Shallow transient liquid water on Mars and its implications for Life: Lessons from the Phoenix Lander and Curiosity Rover, <http://www.nssa.com.au/15asrc/papers/> as read in Aug 2016.
82. M.K. Jha, M.K., Natural and Anthropogenic Disasters: Vulnerability, Preparedness and Mitigation Springer Science & Business Media, pp. 347, 2010.
83. Mishra, Krishna B., Handbook of Performability Engineering, Springer Science & Business Media, pp. 1267, 2008. Nano-bot was invented by Naiman Seeman's team of New York University.
84. Tasker, Elizabeth, New Missions Mine Asteroid Secrets, in *Astronomy Magazine*, Vol. 44, No. 4, Kalmbach Publishing Co., Waukesha, WI, U.S.A. and Canada, pp. 28-33, Apr. 2016.
85. Supra Note 59, pp.32-33.
86. www.gso-space.org; <http://team-hakuto.jp/en/history/>; www.deepspaceindustries.com & www.planetaryresources.com, as read in 20/05/16.
87. Bishop, S.L.; Dawson, Steve; Rawat, Nish; Rhynolds, Kate; Eggs, Rachael; Bunzelek, Kelly, Assessing Teams in Mars Simulation Habitats: Lessons Learned from 2002-2004, pp. 172-196, in Supra Note 34.
88. Little Blue took his name from its bright blue colour.
89. named after Mr Andrew Wheeler's little companion Kookaburra
90. name suggested by Mrs Anna Clark due to its potential to perform extremely well in desert sands
91. Launius, Roger D., *Frontiers of Space Exploration*, Greenwood Publishing Group, pp. 120, 2004.
92. Lambright, W. Henry, *Space Policy in the Twenty-First Century*, JHU Press, pp. 107-109, 2003 & Sputnik International, *Rise of the Machines: Robots, Cyborgs to Play First Fiddle in War of 2050*, *Sputnik News*, 2015.
93. See the perception of space designers in Japan: the shaking of Shogo Tachibana's hands while kneeling by a bartender according to Connolly, a scientist working with NASA. Supra Note 59.
94. Partnership with India looks bright since India has the world's third largest economy measured in purchasing power (with the greatest growth rate of 7 percent per year) and also the youngest population on Earth (some 260 million people below the age of 25!) which could explain the rise of its economy in the next century.
95. Shah, Shekhar & Chadha, Rajesh, Why India's Policy Makers Need to Fire on All Cylinders, pp. 27-28, Supra Note 33. India will definitively get richer due to the future less restrictive laws & great investments into a Mars robotic presence & probably future involvement into space mining.
96. Helmrich, Robert L.; Rose, R.M., McFadden, T.J; Childester, T.R.; Gregorich, S.E.; Geis, C. E.; Pred R. S.; Spence, J.T., Stapp, J., Sawin, L. L. & Carsrud, A.L. - 1978-2000 Studies (on individual behaviour studies in ICE, unlike interpersonal research done by researchers like John Paul, F.U.; Ramachandran, K. & Panwar, M.R., *Interpersonal Behaviour in an ICE*), Jul 2009, doi:10.1177/0013916509336889 as read in Apr 2016.

Educational and Scientific Benefits of Extreme Environments

Gabi Hobbs – University of New South Wales, Canberra

Abstract Australian studies regarding land forms have been carried out in the Kangiara disused mine, in Yass region since the beginning of 19th Century. The ethical dilemma of rehabilitating damaged land systems into educational or scientific zones has never been explored in Australia despite the fact that they have the potential to be linked both to safety and economic prosperity. Extreme landscapes with adverse land conditions and unique geochemistry could hold the key to future invaluable space education. Based on deontological reasons and possible legal implications of possible mining accidents, an answer is needed for the owners of such degraded land and perhaps also for the communities of last-century mines. This paper assesses the educational and scientific benefit of such environment. The Kangiara closed mine in Yass NSW has the potential to become an invaluable science hub, or space analog unit in particular, due to its Mars-like terrain and harsh environment conditions and close proximity to Canberra. A field examination during the Mars Society of Australia's scientific testing in May 2016 has demonstrated that extreme environments can be used for testing outer-space equipment and that foreign investment might become a reality for those governments or private companies desiring to conduct space simulations in Australia.

1. Introduction

Access to land and other natural resources is an important basis for the livelihood of Australian farmers. Access must be stable and secure if it is to provide economic growth and incentives for others to invest in our land (1). The use of farms in Yass region must be appropriately planned to ensure sustainable development and also pay respect to finite resources, similar to past Aboriginal ownership, which promoted good land and water governance (2,3,4,5,6,7).

The object of this paper is to give a broad description of an ethical dilemma facing Australian farmers with hazardous and noxious land (Fig1.). This common problem characterising all abandoned mines in Australia is an old one and will continue to persist without efficient, well planned local and/or federal government help. A mixture of local community initiatives and official response is needed for safety purposes, current revegetation needs, and also topography aspects of Kangiara's non-aesthetic landscape.



Fig1. Robotic experiments at Kangiara Closed Mine

Landform Australian studies have been carried out in the Yass region since the beginning of 19th century. While the first works of Taylor (1907) (8) and Susmilch (1909) (9) referred to erosion surfaces, later papers such as Craft's (1932 and 1933) (10) and Lewis (1967) (11) speculated on the landscape's early geologic history and the economic benefits. Van Dijk (1959) (12) and his collaborator Woodyer (1961) (13) gave further details of the nature, texture and distribution of the mantles within the Yass catchment in the North-West of New South Wales (NSW). However, the first official study of this area was a cooperative one, since it had been carried out by the NSW Department of Agriculture and CSIRO, during the period 1957-1962 (14) and its sole objective was the assessment of agricultural land use in the valley. Over the years, these results have been recorded in a series of reports issued by the Joint Planning Committee of the local Northern Victorian government (15) and still remain the best available account relating past and present geology of this fairly weathered and unpreserved land.

Reconnaissance surveys of large areas in mainland Australia have been carried out throughout the past century (16). These surveys were carried out by the Division of Land Research of CSIRO at the request of the States and Territories to define the major types of country and assessing natural resources mainly in sparsely populated areas such as Yass Valley. They are based generally on the use of conventional medium to small scale (of 1:40,000-85,000), black and white aerial photography, the recognition of distinctive photographic patterns, and the examination of representative sites on the ground.

More recently, colour and false-colour photography and other remote sensing techniques used by satellites have become available through the usage of Geographical Information System (GIS) and are being tested in many parts of NSW. Similarly, computers are currently used for processing, storing, and retrieving the mass of field data collected during land surveys. Being in close proximity to our capital, Yass Valley was selected by CSIRO primarily to test the application of these new modern techniques in land research such as satellite measurement and processing of data on various land parameters.

2. Location of Yass surveyed area and purpose of this ethical study

The survey area for this ethical study covers ninety-seven hectares, recently administrated by the Eden-Monaro Federal Electorate in the NSW, of which around 50 hectares belong to Richard McGuirk and the rest to his sister's family who also owns the farm house on top of the hill (see below Fig1). This past mining land lies near the main highway between Cowra and Yass, near the picturesque Tallanganda Creek. It has been in the possession of McGuirk family since 1960, when after several land transactions made by Richard's father, the farm's ownership included small pockets of land neighbouring big Kangiara farm properties. The area also includes a small lake, a drainage area, a hill, and numerous gullies and channels.

Recently, this land has been designated as 'Wildlife Sanctuary', with the main objective of revegetating the desolate mining landscape and of providing shelter for exotic birds, native Australian bees, rare reptiles and marsupials. As a consequence of its current owner's kind agreement to allow the Mars Society of Australia to run robotic testings on the 13th of May 2016, I had the opportunity to witness this land's major ecological features and look at the ethical dilemmas surrounding this land.

My quest in this paper is to determine whether it is ethical to use the land for further scientific experiments since this terrain is analogous to the Martian and asteroidal regolith and presents researchers with a variety of hazards which man surely will encounter in further space

exploration. Could this area be used for a future Mars hub such as that of the USA's Utah desert or the Russian Arctic? And, if so, what kind of benefits would this scenario bring to the farmer and his local community?



Fig. 1 The McGuirks' farm – May 2016

3. History of the Local Kangiara Area

Gold has always been important in Australia's history. It was discovered in Yass region before 1850, but colonial governors suppressed news of the finds in the belief that the lure of instant wealth would encourage convicts and free settlers to desert cities and their jobs (17). Cities such as Sydney owed their rapid growth between 1850 and 1890 to the wealth that gold brought to the colonies. Whole regions were saved from bankruptcy and population increased by 300%, thus ensuring the Australian progress from dumping grounds for convicts to prosperous homes and businesses. Paul de Strzelecki found small amounts of gold in Yass area, as well as in the Mount Kosciusko's area (18).

The utilisation of land in the Yass surveyed area has proceeded in stages corresponding with those in other mining regions of Australia. Prior to settlement into the Lanyon Plain, the land and vegetation were in equilibrium, with scattered marsupial fauna and a small Indigenous Aboriginal population. The Aboriginal Ngunnawal and Wiradjuri tribes have traditionally inhabited in the Yass Shire (19). While the Ngunnawal people, consisting of many tribes (20), covered a very large area in the NSW, which is present day Canberra and extends into the majority of Yass Valley area, the Wiradjuri clan were spread only in a small part within the Western edge of the present-day Yass Valley.

The Aboriginal society had strict boundaries for each family and language group, which was an efficient way of owning a land. The McGuirk, similar to others (21), has Aboriginal cultural significance due to language and cultural heritage, despite the fact that it poses a significant threat for contamination and many public safety risks.

Following exploration of the area about 1820, stockmen moved their herds of sheep and cattle into the Yass plains and other parts of the Molonglo River drainage areas. By 1830 practically all the accessible land was occupied by large holdings under a pastoral grazing system characterised by movement of herds to fresh pastures (22,23).

The farming industry was interrupted by a severe national drought in the period of 1838 and 1839, and by a depression in the wool market in 1843, when a local severe drought again occurred. These market and climate uncertainties together with an increased local demand for

agricultural produce prompted wheat-growing in the Yass region – industry which led to production of dairy products, bacon, fruit and vegetables (maize, potatoes, apples, apricots and peaches) in the following years. This increase was sharply followed in 1852 by the discovery of many rock chip samples with significant gold indicators in the Kangiara area, which later prompted extensive drillings in this NSW Palaeozoic terrain (24).

By 1850 land ownership became established and holdings were gradually fenced, water supplies were created and the clearing of timber extended the area of pastures. For the next 80 years grazing of natural pastures have continued in the common area of this farm, alongside with the mining of the gold, copper, zinc, silver and lead deposits, which are still extremely important to the economy of NSW.

Intermittent mining activity and over-grazing resulted in soil degradation and land erosion in this area - features exacerbated by the massive cutting of trees as firewood for the mining town of around 500 people, according to this closed mine landowner.

4. Current Legislation regarding the Australian Abandoned Mines

Abandoned mines are not positive legacies of the past mining industry. Additionally, it is important to state that the Australian Constitution does not list minerals as an area over which the Federal Parliament has jurisdiction (25), even though the Crown owns all underground resources.

As early as the 16th Century, the common law regulated the Crown's ownership over all Australian underground resources (like gold, silver, copper, zinc, platinum group metals), whether situated on public or private land (26). Nevertheless, Australia has a national mine legislation, including regulations and policies for abandoned, closed mines (27) even if these are yet to be implemented by each state government (28). At present, only the Government of Western Australia requires mining companies to provide a financial bond as a security to ensure their environmental obligations are fulfilled (29), thus finding adequate solutions even if the returns are not as high as expected (30).

The current legislation doesn't solve incoming new environmental challenges of this millennium (31) and, at times, it doesn't answer the safety issues for both people and animals (32,33) because it lacks in long-term planning (34) for most official administrations. Cleaning up mining sites is no simple matter. The problem has been acknowledged by past governments who tried to fix it (35). However, the implementation of strategic remediation measures is still to come in Kangiara.

At present, the Native Vegetation Act 2003 and the Native Vegetation Regulation 2013 provide the legislative framework for the management of abandoned mine's flora and fauna in NSW. In fact, these acts do not override the requirement to obtain consent from a local council where an approval for the clearing of abandoned mine vegetation is required under an environmental planning instrument under the Environmental Planning and Assessment Act 1979 (36). Thus, sometimes, all that is required for land innovation is a different perspective (37).

5. Major Current Features of the McGuirk Farm Landscape

The Yass area has a long history of mining for non-ferrous metals. Active exploration and development began in 1850 and lasted for about one hundred years, time enough for materials

to be eroded and transported away from their original site due to weathering and mining erosion. As a landscape develops, both transported and residual regolith form (38).

At present, the farm of Richard McGuirk's family of Kangiara is almost completely depleted of native trees and of many species of birds and insects such as native species of Australian bees. Despite the fact that the Government invests heavily in climate change projects, small places like this farm are often forgotten. However, efficient farming requests all areas to be treated equally and, thus, have proportional access to state benefits. Additionally, while most farms deal with pest and weed infestations, and mounting rabbit populations started at the beginning of last century (39), areas like this are much unpredictable due to instable land shapes and the main problem of toxic chemicals used during mining excavations up to 1950.

Arsenic (As) and mercury (Hg) contaminations are present in Kangiara due to fine airborne particles of As which can be accumulated into the human respiratory system and impacts especially communities residing in the downwind direction mine waste deposits. However, coarse particles were also 'lost' many times during mining activities (40). Apart from these health conditions, systematic epidemiological investigation and genetic mutations in new born babies in Yass have also identified how vulnerable and at risk this local population is and how contaminated the land is because the common mining method was to amalgamate Hg to small particles of gold (Au) to improve the rate recovery. This was used when chlorination and treatment with cyanide failed in quartz reefs, in late 20th century (41). However, in Yass, gold was buried deep and thus, only small quantities of pure Hg were used, which, instead, increased the usage of As (42). Due to the global aspirational stop on pollutants, new methods like carbon-in-pulp (using carbon to capture the gold) and oxidation (Au exposed to water and oxygen) are well regulated, and, thus, many environmental issues caused by acid and metalliferous drainage – known as acid mine drainage – are controlled in Australia.

At present, despite the fact that there are no active mine workings, environmental issues still persist in the area and are clearly visible with the naked eye: especially in the greenish, noxious lake at the edge of the property.

The NSW Government's past and present diligent attempts to reduce the soil acidity by covering the soil with organic material have had a minor impact of reactivating the growth of native vegetation. A deep weathering profile has for years developed and unfolds each time heavy rains fall onto the muddy sediments the farm is covered in. Thus, acid volcanic rocks and sandstones collapse down into the mining channels reaching two hundred-meter deep (43).

The family's efforts to rehabilitate the land has never ceased since it keeps its hope despite all adversities and decades of own futile experiments. For example, each year the tiny citric trees they try to grow dry out because as soon as these newly plants get to have deeper roots, the sulphate salts containing elevated metal contaminants, released from the waste materials located in the below tunnels, kill them (44,45,46,47).

Currently, Kangiara Village has recorded only eight inhabitants (48) - a number which is in great decline (49) and doesn't lobby at all for intense environmental action to eradicate the toxicity problems known to exist near the Lavelan River.

6. Ethical Discussion

This farm is unsuited for the pursuit of economic benefits from livestock, cultivation of crops, eucalyptus oil production (50) or timber export. One might think it could be used for outdoor

recreation purposes as Canberra population continues to grow. However, this area cannot be used for camping, fishing, bush walking or swimming (51,52,53,54), which are becoming increasingly important relaxation activities for town people. The rationale for assigning capability values such as wildlife or educational and scientific uses (Fig. 2 & Fig. 3) is firstly based on the argument that this land has a very limited agricultural use, and secondly, a Martian-analogue exploration will not conflict with future major land purposes, in case one day this land will become fertile.

In addition to acidity, seasonal cycles of hydration-dehydration are responsible for morphological variations in the instability/rolling of layers. Yearly rainfall causes the crystallisation of minerals and the degradation of clay elements supporting life (55). Thus, it is not a productivity rating the farmer is after, but a degree of limiting hazards and wildlife incidents like trapped kangaroos.

Tractors and machinery are impracticable here unless great improvements are made to the road leading into the farm. The lack of funding and the adverse climate such as severe droughts or excess of flooding, drying winds, deficient moisture and frost hazard prevent the farm proper usage despite the regular conservation practices led by the farmer and his family (i.e. the early-spring planting of native savannah with small roots, chosen due to restricted rooting depth). In my opinion, the major problem is the soil toxicity and layer erosion. Plant fertility has also been linked to bee polarisation. But a relocation of insects is costly and it doesn't necessarily improve an environment because bee habits like aerial coordination form during several generations. Poor soil drainage and occasional inundation also contribute to faster water evaporation - much higher in summer than in winter. This effect results in soil moisture deficits which then lead to layers of salt covering the entire area, and thus killing all newly planted trees and the insects or young birds trapped inside the farm.



Fig. 2 Robotic testing on the alluvial plain



Fig. 3 Robotic Testing on a slope

6.1. Benefits of Rehabilitating the Area into a Wild Life Sanctuary

Large areas of natural eucalyptus forest don't exist near Kangiara anymore and thus, the protection to the catchments of the main streams in the area is gone. As the development of water catchments continues each year, local watershed management with its protective measures to minimize erosion and floods forgets to take into account the toxic underground flowing of farms like this one. Other problems such as grazing, cultural treatments and fertilising used in the nearby farms also pose a serious threat to water supplies and wildlife (56) and are very difficult to assess.

The edges on the eastern side of this farm hill was once used as a common for the original town and the lack of grazing control shows up in two ways: a patch and ragged appearance of what used to be a green pasture once and a heavy trampling of the soil. Drainage lines made

by the stock are noticeable from the top of the hill, but are not the main damage if we take into account the pioneer species introduced with multiple negative effects upon the native savannah.

The combined effects of chemical contamination and selective deforestation (57) disturbed the native habitat, which is at present invaded by seedling trees or the presence of stumps. It is not a coincidence that this former eucalyptus territory is currently characterised by a completely disturbed fauna and flora.

Mr McGuirk's past dealings with the Ngunnawal people, the Australian Farming Group and Local Government Officials have all proved unsuccessful despite the fact that implementing new methods are scientifically available (58). Nevertheless, small help into environmental research is often offered by climate workshops around the country because they give some coping strategies like fencing the area and proper signing.

6.2. Educational and Scientific Advantages of Abandoned Mines

Why is the McGuirk farm such a great analog to Mars and a great investment for future prospectors? Dr Jonathan Clarke of the Mars Society asserts it would be an over-simplification to think this land could be properly rehabilitated for a wildlife sanctuary or agricultural purposes due to multiple and rising difficulties Mr McGuirk faces such as: soil degradation, unpredictable climate (such as heatwaves, extreme storms or floods), insufficient machinery, lack of conservation methods, limited funds, shortage of both skilled employees and environmental professional advisers, etc. Thus, Dr Clarke has proposed the solution of developing the old mine into an educational and scientific hub for the Australian students and researchers.

The benefits of rehabilitating this land into a scientific-educational complex are multiple, various, with higher returns and for a longer period and for a much diverse population than a wildlife sanctuary.

Mars Analog Station – scientific benefits

Australia has numerous landscapes and features that resemble the Red Planet. This farm is one of them due to its unique desert regolith impact structures, mineral composition, relief inversions of soils, long-term landscape evolution and hydrothermal systems that are relevant to Mars (59). It could also provide a very useful reference for interpreting the results of space robot mobility while exploring the Martian surface and also review some of well-known about deep water contamination, land erosion, soil toxicity and human resistance to microbes (Fig. 4 Mars Society Robot Testing – May 2016).

The Mars analog value was explained in detail by Dr Clarke while describing its acid lake, its hypersaline embayment and its complex of channels that is similar to some space craters. These distinctive characteristics could guide our understanding on human and robot manoeuvres in alien territory and also help Australia develop future space robotic missions. The study of fossils is also another scientific possibility. Additionally, a future Mars Hub with a possible cargo vehicle and a Mars Transfer vehicle could teach students the importance of proper space sheltering against radiation caused by solar flares or cosmic rays.

The rehabilitation of this farm towards a Mars hub is an exciting opportunity to achieve a better environmental and community outcome at a lower cost because it will make this farm safer and perhaps bring new value to the region. It would also be a great initial infrastructure

step for Australia in setting outer-space short and long term goals since building up a permanent, flexible architecture is vital for Australia's future space program.

Inspiring progress is a powerful key ethical argument for any scientific cause. The best moral choice for this land would be to allow young generations to 'terraform' it into an innovative 'Space Island'. Similar to: Flashline Mars Analog Research Station (F.M.A.R.S.) in Devon Island, Mars Analog Research Station (M.A.R.S.) in Utah desert, and the Arctic and the Antarctica science facilities, this land could soon be used by both Australians and their partners in a quest for a human presence on Mars. Although red and inhospitable at present, with proper care, this farm could become green and blue as a terraformed Mars, very well symbolised by its unofficial flag of red, green and blue vertical bands (Fig. 5). This official Mars flag was approved by the Mars Society and Planetary Society. NASA's engineer Pascal Lee proposed it to Dr Robert Zubrin in 1993, during the 1998 Haughton-Mars Project Arctic Expedition to Devon Island, Canada. Since then Mars' tricoloured flag designates the future evolution of this planet: red, green and blue, as described by Kim Standley Robinson's popular trilogy: Red Mars, Green Mars and Blue Mars.



Fig. 4 Some Robot Testing participants include the farm owner Richard McGuirk, the 4th person standing from the left, followed by Dr Jonathan Clarke, Richard's sister Jessica, Anna Clarke and Savannah McGuirk, the farm owner's daughter

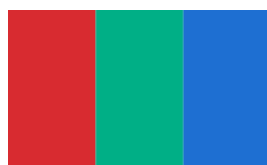


Fig. 5 The Unofficial Flag of Mars

6.3. Legal and Financial Obstacles

The Mike Baird N.S.W. state government chose to undermine native vegetation and biodiversity (60,61,62) by implementing new legislation that will remove land restrictions on land clearance and threaten the benefits of a wide land biodiversity in a quest for a new market-based approach. This legislation could have devastating effects - similar to the

Queensland past legal changes, mainly due to incorrect checks on farmers' activities and improper climate balances. The reason is that future environmental recommendations and juridical approvals regarding increased land clearing will not halt land erosion, decrease salinity and toxicity caused by fertilisers; nor will they solve the problem of pest resistance (63,64,65). For wind breaks and natural pollination to occur, trees need to be preserved and their protection should follow the international conservation standards (66).

This draft legislation makes incorrect economic assumptions like approved forest clearing will improve environmental conditions of other areas on properties, will facilitate economic development and protect the environment (67). By giving farmers the freedom, the legislators believe that the native vegetation will be preserved. However, I believe that if we put our trust in the farmers, the environment of most farms will not be conserved since some of them might prioritise short-term financial goals which will have a negative impact on fauna and flora mainly. Additionally, not all farmers and land developers have environmental training or high standards of responsible land management (68).

Although the current Native Vegetation Act (adopted in 2003 and implemented in 2005) restricts land clearance on farms, it doesn't cover the demands of closed mines. The present legal tendency favours the ethical decisions concerning the large agricultural business firms and not the management of small, unproductive farms (69,70,71,72).

However, if Australia values its environment protection and the future generations' prosperity, it is also ethical to discuss the interests of small landowners and the need for proper legislation because only through laws and policies, viable financial measures can be implemented (73). The reason for this is that Mr McGuirk doesn't lack freedom, since the new act claims to facilitate it. On the contrary, funding is his major concern for becoming a responsible farmer (74) and unless provided with financial assistance, his farm cannot be correctly managed to facilitate scientific development.

7. Conclusion

Disturbed communities like this farm are both a good lesson on previous incorrect agricultural or pasture practices and also a reflection on past unreliable mining operations carried out with total disregard for native wildlife at the end of 19th century and at the beginning of last century. One must examine the anaesthetic landscape to find out the negative impact humans could have on their surroundings, outer space included. No allowances should be made for any devastation and though this community looks stable, only the future can tell us how past mines will influence the life of the future local community and beyond (i.e. Australian mentality, legal preventive measures, international relief mining programs). The unstable red and brown soil of this area makes it a hazard for locals, possible wondering tourists visiting the Kangiara mine and wild life such as kangaroos trapped into the farm's shafts and channels. The proximity of the land to the highway concerns the owner in relation to public safety. Currently, Mr McGuirk is keen to raise funds for the construction of Mars Hub on his natural private preserve in order to promote both land conversation and science within Australia.

In conclusion, the opportunity exists for this farm to be used for a highly educational objective such as outer space exploration since the McGuirk land is ideal for scientific experiments. The potential exists for the land to become an invaluable science hub - a space analog unit in particular, due to its Mars-like terrain and harsh environment conditions. Additionally, its close proximity to Canberra makes this location a perfect set-up for outer-

space equipment testing by Mars experts and space enthusiasts (Fig. 6 & Fig. 7). Such an enclosed environment led by a responsible farmer and space enthusiasts could provide a future for Australian space robotic missions, astronaut training and medical research. The best alternative is not necessarily an environmental commitment, but an educational one.



Fig. 6 Current Marsobot's testing on McGuirk mine



Fig. 7 Future educational programs on this farm

Acknowledgments

Many thanks to my professor **Dr Ned Dobos of University of New South Wales, Canberra**, for his constant great support with ideas, accurate and detailed review and for invaluable cross-references regarding environmental issues. I would also like to thank **Mr McGuirk and his entire family** for their great kindness and patience during this investigation and to **Dr Jonathan Clarke** for the opportunity to participate in the Mars Society Australia's robot testing and also for the usage of this paper's pictures.

I also express my deep gratitude for the efficient review and great insights on writing research papers to **Dr Carol Oliver, the Deputy Director of the Australian Centre for Astrobiology, University of New South Wales, Sydney**.

References

1. Spatial Initiatives for Sustainable Land Management, Global Magazine for Geometrics, Issue 4, Vol. 30, pp. 16-24, Apr 2016.
2. Howitt, A., The Native Tribes of South-East Australia, Facsimile Ed. Canberra: Aboriginal Studies Press, 1996.
3. Young, M., The Aboriginal People of Monaro, 2nd ed., N.S.W. Department of Environment and Conservation, Sydney, 2005.
4. Hancock, K., Discovering Monaro. A Study of Man's Impact on His Environment, Cambridge University Press, New York, 1972.
5. Tindale, N., Aboriginal Tribes of Australia, University of California Press, Berkeley, 1974.
7. Bowdler, Hunters in the Highlands, Aboriginal Adaptations in the Eastern Australia Uplands, Archaeology in Oceania, Vol. 16, Issue 2, pp. 99-111, 1981.
8. Taylor, T.G., The Lake George Senkungsfeld. A Study of the evolution of Lakes George and Bathurst, the 32th Proceedings of Linn Society, N.S.W., pp. 325-345, 1907.
9. Sussmilch, C.A., Notes on the Physiography of the Southern Tablelands of N.S.W., *Journal of Regional Society N.S.W.* No. 43, pp. 331-354, 1909.
10. Craft, F. A., Notes on Erosional Processes and Stream Gravels, 57th Proceedings of Linn Society, N.S.W., pp. 280-290, 1932 and Craft, F.A., The Surface of Monaro, N.S.W., 58th Proceedings of Linn Society, N.S.W., pp. 229-244, 1933.

11. Lewis, M.B., Economic Aspects of Agriculture and Afforestation on Comparable Lands, Australian Forest No. 321, pp. 3-9, 1967.
12. Van Dijk, D.C., Soil Features in Relation to Erosional History in the Vicinity of Canberra, *CSIRO, Australian Soil Publication*, No. 13, 1933.
13. Van Dijk, D.C. & Woodyer, K.D., Soils of the Yass River Valley, *Regional Resource Study of Southern Tablelands of N.S.W.*, No. 6, 1961.
14. Gunn, R.H.; Story, R.; Galloway, R.W.; Duffy, P.J.B.; Yapp, G.A. and McAlpine, J.R., Lands of the Queanbeyan-Shoalhaven Area A.C.T. and N.S.W., *Land Research Series No. 24*, Commonwealth Scientific and Industrial Research Organisation, Melbourne, Australia, pp. 9-10, 1969.
15. Ibidem.
16. Division of Land Research- CSIRO studies as on www.csiro.au/en/Publications from early 1960s until May 2016. Read more in CSIRO's publications like: Science Magazine, Commonwealth Industrial Research, Wildlife, Soil Resources, Crop and Pasture Sciences, Helix, Australian Journal of Botany, Australian Journal of Chemistry or Australian Journal of Zoology.
17. Thomas, Jordan, Gold Rushes, Australian Knowledge & Trocadera Publishing, Sydney, pp. 2-5, 2066. He talks about James McBrien, the first government surveyor who first mentioned the yellow metal in the Fish River, Bathurst, which opened the western region for Blaxland, Lawson and Wentworth explorers, and later George Gipps, the governor of N.S.W. who stopped the reports of gold near Cox's River and Wollondilly River.
18. Supra Note 16, pp. 14, 2006 & Blainey, Geoffrey, The Peaks of Lyell, Melbourne University Press, Carlton, Victoria, 1967 regarding the role of precious metals in politics and in the drafting of the Australian Constitution in 01 Jan 1900 when Western Australia joined the Australian federation, as part of the Commonwealth.
19. Cultural deposits of Namadgi Indigenous people in this region dating to Holocene period (9,000-6,000B.C.) Theden-Ringl, Fenja, Aboriginal Presence in the High Country: New Dates from the Namadgi Ranges in the Australian Capital territory, pp. 25-42 doi:10.1080/03122417.2016.1163955; Wesson, S., An Historical Atlas of the Aborigines of eastern Victoria and Far South-East N.S.W., Monash University, Melbourne, 2000; www.yassvalley.nsw.gov.au & <http://www.ngunawal.com.au/>
20. Supra Notes 16. Some tribes included the Wallabaloa clan who lived particularly in the area near Burrinjuck Dam, the Pajong tribe in the Tallaganda Valley and the Kamberri in the Canberra region.
21. Oak Hill, Hollywood and Hatton's Creek
22. Land Research Series No. 24, Commonwealth Scientific and Industrial Research Organization Australia, Melbourne, 1969.
23. For centuries, in Australia, the grazing was incorrectly thought to improve the grasses and to introduce or foster new species of plants, based on the effects of manuring and of stamping the soil by sheep's feet, in particular. Read more of incorrect land improvements sought by colonists and dismissed at present, in The Cornhill Magazine, Vol. V, Smith, Elder and Co., London, pp. 354-358, 1862.
24. Slayter, R.O., Agricultural Climatology of the Yass Valley, CSIRO Australian Division - Land Resources, Regional Survey, Technical Paper, 1966.
25. However, if in conflict with Commonwealth law, federal law overrides state legislation.
26. This royal prerogative, applied by common law and legislation in Australia, is a universal rule in all Commonwealth and is based on Crown ownership of minerals. Even if the Roman law principle doesn't apply ('*Cujus est solum, ejus est usque ad coelum et usque ad inferos*' – whoever owns the soil, also owns the sky above and its depths/the hell), the Crown may grant various leases or licences to others to enter the mining land and take minerals.
27. www.industry.gov.au as read in 01 Jun 2016.
28. In 2012, the NSW Auditor General declared that derelict mines represent the largest category of contamination liability for the state. Read more on www.conversation.com as read in May 16 & www.industry.gov.au as read in May 16.
29. Government of Australia, Mine Closure and Completion, from the leading Practice Sustainable Development Program for the Mining Industry Publication Series, 2006.
30. This new approach is called 'The Mining Rehabilitation Fund'. Read more in Davis, Chris, Environmental Rehabilitation and Mine Closure, *AusIMM Bulletin Magazine*, pp. 44-46, Feb 2015.
31. Mining Act 1971 for SA and TAS, 1980 NT, 1991 A.C.T. – Land and Environmental Planning Act, 1992 QLD, 1992 N.S.W. & 1978 WA; Mineral Resources Development Act 1990 & 1995; Corporation Act 2001 and the Australian Stock Exchange Listing Rules with special provisions governing the conduct and reporting requirements for mining companies. Supra Note 15.
32. Fitzgerald, Anne M., Mining Agreements: Negotiated Frameworks in the Australian Minerals Sector, Chatswood Prospect Media, 2002. Read more on how owners can financially default and thus renounce ownership in favour of the Australian government. However, this solution is not an easy road for most owners who highly mistrust state structures to rehabilitate their beloved land, owned at times for entire generations.

33. Thrun, Sebastian; Hähnel, Dirk; Ferguson, David; Montemerlo, Michael; Triebel, Rudolph; Burgard, Wolfram; Baker, Christopher; Omohundro, Zachary; Thayer, Scott & Whittaker, William, A System for Volumetric Robotic Mapping of Abandoned Mines, in Proceedings of ICRA, 2003, as read on www.cs.cmu.edu on Jul 2016. These authors propose the usage of robots for 3D-mapping closed mines of hundreds of meters in diameter.
34. Old Australian mines are a huge, unacceptable legacy for local communities, the environment and mining companies in question mainly due to lack of legislation, but also factors like: incorrect mining company's perception of its place in the community, unwillingness to invest in environmental outcomes, particular conditions of mining, government and community expectations, environmental groups' applied pressure for environmental outcomes, insufficient technologies or unavailability of skilled people to lead rehabilitation works.
35. Around 300 abandoned coal-drilling sites promised to be correctly managed by Tony Abbott's government haven't been cleaned yet in N.S.W. I believe the main reason is the private ownership excuse. Mines owned by individuals or businesses are not considered the Crown's or the community's responsibility despite the fact that present owners haven't contributed to the damage.
36. <http://www.environment.nsw.gov.au/vegetation/localgovt.htm> since mines are not in the excluded legal provisions.
37. CSIRO's developed tool CRATER – Climate Related Adaptation from Terrain Evaluation Results has the ability to identify flooding vulnerabilities using detailed GIS data to support decision making. Supra Note 30, pp. 32.
38. The weathering of rocks may also happen below the land surface Scott, Keith M. & Pain, Colin F., *Regolith Science*, Springer, CSIRO Publishing, Collingwood, Australia, pp. 32-102, 2008. Read more on the process of water saturation of the rock in open and closed mines especially when mines are closed using flooding, in Bukowski, Przemyslaw; Augustyniak, Iwona & Niedbalska, Katarzyna, Some Methods of Hydrogeological Properties Evaluation and Their Use in Mine Flooding Forecasts, *International Multidisciplinary Scientific GeoConference Surveys Geology and Mining Ecology Management (SGEM)*, No. 2, Sofia, 2015.
39. Molnar, I. (ed.), *A Manual of Australian Agriculture*, Heinemann, Melbourne, pp. 767-777, 1961. Pest infestation continued until eradication methods had some success in the 1950s.
40. e.g. 121 tonnes of mercury discharged in Victoria alone according to contemporary sources like Mineral Statistics of Victoria and Mining Surveyors Reports from 1668-1888 & Davies, Peter; Lawrence, Susan & Turnbull, Jodi, Mercury Use and Loss from Gold Mining in Nineteenth-Century Victoria, *The Royal Society of Victoria*, No. 127, pp. 44-54, 2015.
41. Canavan, F., Deep Lead Gold Deposits of Victoria, Geological Survey, Bulletin No. 62, Melbourne, 1988. If sulphur and arsenic can't be driven off the gold ores by crushing and oxidation, artisanal gold miners still use this method today.
42. McQueen, K., Mercury Mining: A Quick History of Quicksilver in Australia, *Journal of Australasian Mining History*, No. 9, pp. 74-93, 2011 about frequent past conflicts between European and Chinese miners using Hg underground as well; not limited to alluvial-easy-access gold nuggets.
43. Mr Richard McGuirk's personal communication in 14/05/2016.
44. Dr Jonathan Clarke, president of Mars Society Australia Organisation – personal geological communication, May 2016.
45. Bigham, J.M. & Nordstrom, D.K., Iron and Aluminium Hydrosulphates from Acid Sulphate Waters, doi:10.2138/rmg.2000.40.7, 2000.
46. Grover, B.P.C.; Johnson, R.H.; Billing, D.G.; Weiersbye, I.M.G. & Tutu, H., Mineralogy and Geochemistry of Efflorescent Minerals on Mine Tailings and Their Potential Impact on Water Chemistry, doi:10.1007/s11356-015-5870-z, Dec 2015 regarding different colours of crust due to Al, Fe, Mg, etc.
47. Read more on how the oxidation of remnant sulphides, mainly efflorescent sulphate salts and pyrite, negatively impacts soil and ground and surface water chemistry in Nordstrom, D.K., *Hydrogeochemical Processes Governing the Origin, Transport and Fate of Major and Trace Elements from Mine Wastes and Mineralized Rock to Surface Waters*, doi: 10.1016/j.ageochem.2011.06.002, 2011.
48. http://en.infodesti.com/AU/Farm/Tallagandra_Hill as read in 16 Jun 2016.
49. <https://www.propertyvalue.com.au> as read in 16 Jun 2016.
50. The local area produces broad-leaved peppermint (*Eucalyptus dives*) oil used for the manufacture of soaps, detergents and disinfectants. *Eucalyptus Dives* plants offer three times more oil than normal *Eucalyptus Robertsonii*, mainly for export and also to cover a small local demand. Supra Note 14, pp. 138-139.
51. De Lacerda, L.D., Updating global Hg emissions from small-scale gold mining and assessing its environmental impacts, *Environmental Geology*, No. 43, pp. 308-314, 2003.
52. Casina, J.; Field, J.; Taylor, M.P.; Gao, S.; Landazuri, A.; Bettertn, E. & Saez, A.E., A Review on the Importance of Metals and Metalloids in Atmospheric Dust and Aerosol from Mining Operations, *Science of the Total Environment*, No. 433, pp. 58-73, 2012.

53. Kelly, F.J.; Miller, S.; Rosales, R.A.; Sugihara, E.S. & Akau, J., Microspectroscopic Analyses of Particles Size dependence on Arsenic Distribution and Speciation in Mine Wastes, *Environmental Science and Technology*, Vol. 45, Issue 15, pp. 8164-8171, 2013
54. Martin, R.; Dowling, K.; Pearce D.C.; Florentine S.; McKnight, S., Stelcer, E.; Cohen, D.D. Stopic, A. & Bennett, J.W., Trace Metal Content in Inhalable Particulate Matter (PM_{2.5-10} and PM_{2.5}) collected from Historical Mine Waste Deposits Using a Laboratory-Based Approach, *Environmental Geochemistry and Health*, Springer, pp. 1-15, May 2016, as read on doi.10.10007/s10653-016-9833-1
55. Gold mines are characterised by profound transformations which make the iron oxyhydroxides and hydrosulphates the most visible materials in such areas. Read more on soil contamination in Murad, E. & Rojik, P., Iron-Rich Precipitates in a Mine Drainage Environment: Influence of pH on Mineralogy, *American Mineralogy*, No. 88, pp. 1915-1918, 2003.
56. i.e. the Poa grass is steadily on the increase and the high grass Themeda is slowly disappearing in the area and with it many native species of insects. Damaged Themeda pastures don't recover quickly even rested due to successive and consistent mixture of toxic elements carried by rain drops and wind beyond the farm. In addition, elements like Mg, Ca, K, which help the rooting of plants are wasted away and the most abundant minerals left are the waste dump minerals: Fe, As, S and Na. Read more in Valente, T.; Gomes, P.; Sequiera Braga, M.A.; Dionisio, A.; Pamplona, J. & Grande J.A., Iron and Arsenic-Rich Nanoprecipitates Associated with Clay Minerals in Sulphide-Rich Waste Dumps, *Catena*, No 131, Elsevier, pp.1-13, 2015.
57. The original tree cover as displaced due to local pioneer practices of massive cutting of straight trees and of leaving the entire area, not only this farm, with very little – if only patches of native plants.
58. e.g. The GeoFlow method is a recent software package developed by James Cook University to monitor network of mining channels. This algorithm is capable in determining acid concentration and underground system of wells. Datta, B.; Durand, F.; Laforge, S.; Prakash, O.; Esfahani, H.K.; Chadalavada, S. & Naidu, R., Preliminary Hydrogeologic Modelling and Optimal Monitoring Network Design for a Contaminated Mine Site Area: Application of Developed Monitoring Network Design Software, *Journal of Water Resource and Protection*, No. 8, pp. 48-64, 2016.
59. Jonathan D. A. Clarke, Wilson, David & Murphy, Guy, Mars Analog Research, American Astronautical Society, Univelt, 2006 & Levine, David D. (ed.), The Mars Diaries: The Story of the Crew 88 of the Mars Desert Research Station in their own words, Bento Press, 2010.
60. Perry, Neil, The N.S.W. Government is Choosing to Undermine Vegetation and Biodiversity, May 2016, as read on 18/05/16, on www.theconversation.com
61. Read more on official incorrect assessments on cleared vegetation trees and grasslands as of being of low conservation value and of low-risk to climate change in Kauffman, Jobriath S. & Prisley, Stephen P., Automated Estimation of Forest Stand Age Using Vegetation Change Tracker and Machine Learning, in *Mathematical and Computational Forestry & Natural Resource Sciences*, Vol. 8, Issue 1, pp. 4-13, Mar 2016.
62. Hunter, John T., Validation of the Greater Hunter Native Vegetation Mapping as it pertains to the Upper Hunter Region of N.S.W., *Ecological Management & Restoration*, Vol. 17, Issue 1, pp. 40–46, Jan. 2016.
63. Mutze, Greg A.D.; Cooke, Brian B & Scott Jennings, Scott C., Estimating density-dependent impacts of European rabbits on Australian tree and shrub populations, as read in May 16, on www.publish.csiro.au/?paper=BT15208
64. Macris, Chris; Macnamara, James; Freame, Evan, The Gritty Fight against Feral Rabbits: Testing the Effectiveness of A Browsing Deterrent (Sen-Tree) on Native Grassy-Groundcovers, *Australasian Plant Conservation: Journal of the Australian Network for Plant Conservation*, Vol. 24, Issue 2, pp. 5-7, Sep/Oct/Nov 2015.
65. Kasper, Wolfgang & Kelly, Paul, Australia's Future in the Balance, *Policy: A Journal of Public Policy and Ideas*, Vol. 31, Issue 2, pp. 15-23, Winter 2015.
66. Ugner, Corine, Abandoned Mines, as read on May 16 on www.conversation.com
67. Supra Note 60.
68. Some farmers view the repetition of animal or agricultural plants and modification of certain shared blueprints more important than the responsible development of an area. Read more on naturphilosophy in Honderich, Ted (ed.), *The Oxford Companion to Philosophy*, Oxford University Press, Oxford & New York, 1995.
69. Stoeckle, N.; Chaiechi, T.; Farr M.; Jarvis D.; Álvarez-Romero, J.G.; Kennard, M.J.; Hermoso, V. & Pressey, R.L., Co-benefits and trade-offs between agriculture and conservation: A case study in Northern Australia as read in May 2016, on <http://dx.doi.org/10.1016/j.biocon.2015.07.032>
70. Tamásy, Christine & Diez, Javier Revilla, Regional Resilience, Economy and Society: Globalising Rural Places, Routledge, 2016 Read more on the conspiracy of 'corporate control'.
71. Goss, David, Small Business and Society, Routledge, 2015.
72. Nedles, Wayne, The Right to Organic/Ecological Agriculture and Small-Holder Family Farming for Food Security as an Ethical Concern, *The 1st International Conference of the Asia-Pacific Society for Food and*

Agricultural Ethics (APSAFE 2013: Food Safety and Security for the 21st century, Nov. 2013, pp. 141-150 or doi: 10.1007/978-981-287-417-7_13, as read in May 2016.

73. Gardner, Gary T., *Inspiring Progress*, W.W. Norton & Company, New York & London, 2006.

74. The reasons vary from funds given to communities rather than directly to small individual farms to large agricultural activities having negative effects such as pollution. Market forces alone are also not able to ensure safe environmental levels since government interventions can also be problematic due to costly and inefficient policies. Read more on this in *Multifunctionality in Agriculture What Role for Private Initiatives? What Role for Private Initiatives?* *OECD Publishing*, 2005.

Antarctic Psychological Health as a Space Analogue

Kimberley Norris ¹

¹ *School of Medicine (Psychology), University of Tasmania, Private Bag 30, Hobart, Tasmania, 7001, Australia*

Summary: Antarctica is one of the most extreme environments on Earth. The physical, psychological, social and technological parameters associated with this environment parallel those found in space. For this reason, Antarctica is well-recognised as a space analogue. By extension, research investigating psychological health in Antarctica has applications for supporting human wellbeing during both short and long-duration manned space missions. However, to date such research has largely overlooked the impacts on relationship dynamics with those left behind, including the family unit. Consideration of these issues is vital, as it can influence astronaut health, wellbeing and performance far beyond the confines of the family unit into the spaceflight experience itself.

Keywords: Psychology of extreme environments, Psychological health, Space analogue, Extreme environments, Relationship dynamics, Psychological interventions.

Extreme and unusual environments (EUEs) are those which pose extraordinary challenges for individuals who inhabit them and require significant, complex, and deliberate action for successful adaptation and performance [1]. Antarctica is one of the most extreme and unusual environments on Earth, posing physical, psychological, social, and technological challenges that are unlikely to be encountered anywhere else. The nature of these challenges are such that they arguably parallel those experienced during manned-space missions, and for this reason Antarctica has long been considered a space analogue [2, 3, 4]. As evidence of the similarities between Antarctic and space experiences, parallels have been noted between expeditioner and astronaut reports of the impacts of separation from home, the challenging social environment, and interactions with the home organization [6]. By extension, research investigating the influences and interventions for psychological health in Antarctica can be, and have been, used to model, manage, and potentially mitigate those experienced in both long and short-duration manned space missions [5]. Ongoing research collaborations between NASA and Antarctic research programs, including those undertaken by Australia, are further testament to the acceptance of Antarctica as an example of a space analogue [5]. Such research is vital considering the increasingly long duration manned missions that are occurring. Thus, the aim of the current article is to review current understanding of Antarctica as a space analogue, and the impact of these environments on psychological health.

Researchers have consistently demonstrated that within EUEs psychological parameters have a disproportionately larger impact on human adaptation and functioning than all other parameters. Psychological parameters associated with EUEs, such as Antarctica and space, that pose challenges to human performance and wellbeing relate more to individual perceptions and responses to the environment, as opposed to the environment itself. Although people are likely to find Antarctic and space environments intrinsically challenging, the specific experience within EUEs can differ between individuals residing within the same environment [6] and may relate to differences in self-perception, preparedness for the experience, personality characteristics, and motivation [5]. Therefore, it has been argued that these differences are not directly influenced by the environment itself, but the meaning the individual attributes to their experience [7]. Individual perceptions and responses may also be influenced by

social/interactive parameters including group cohesiveness, leadership, and structure [5] as well as the availability of, and satisfaction with, social support [8].

The psychological impacts of EUEs on individual health and wellbeing are well documented, with both positive and negative consequences acknowledged. Positive psychological consequences documented to result from exposure to Antarctica include increased self-reliance [9], self-efficacy [10], self-growth [11], cooperativeness, and increased striving towards important or challenging goals [12]. Antarctic expeditioners also make frequent reference to the positive effects engendered by the grandeur of the physical environment, the experiences of camaraderie and support amongst station members, and the sense of achievement in overcoming the inherent challenges of the physical environment [13], with many considering their Antarctic residence as one of the best experiences of their life [14]. These results indicate that the challenges associated with Antarctic, and by extension space, employment are not inherently detrimental to human functioning and performance. Furthermore, positive consequences appear to persist beyond return home. Negative psychological consequences associated with Antarctic employment include symptoms of depression, insomnia, anxiety [15], aggressive behaviour, difficulty in concentration and memory [16], and the occurrence of mild fugue states – however, the incidents of clinically diagnosable psychological conditions is rare (approximately 4-5 percent of expeditioners) [17]. It also appears that conditions associated with employment – such as organisational practices [18] and leadership styles [19], have a greater impact on human performance than more stable, person-level characteristics [20]. Of note, the majority of psychological declines are temporary and largely resolve upon return home or shortly thereafter [9]. Importantly for the context of the current argument, similar positive and negative psychological sequelae are not only postulated to be relevant for manned space missions, but have been demonstrated as occurring [9].

Numerous studies have identified that the primary psychological challenges associated with extended Antarctic residence involve individual adjustment to the physical and social environment; the lack of physical, psychological, and social novelty for extended periods; and the absence of social support from family and friends throughout the expeditioner's time 'on the ice' [5]. In particular, the effects of separation from family and friends, especially intimate partners, have been reported as a major stressor for expeditioners [21] and are a common reason for seeking counselling from the station medical officer [22]. Furthermore, researchers have indicated that prolonged isolation from family and friends may precipitate mood or adjustment disorders in expeditioners [23], and may also exacerbate pre-existing conditions including personality or substance use disorders [24] that were not previously identified. However, despite the recognised interrelationship between work and family roles on human performance and wellbeing in EUEs, there remains a dearth of research in this regard. Notable exceptions are the works by Taylor and McCormick [25] and Norris [26].

Taylor and McCormick [25] were the first researchers focusing on Antarctic psychology to publish an empirical study in which both the expeditioner and their partner's psychological health and wellbeing were simultaneously considered. Their investigation found that even prior to deployment, there were differences in the psychological profiles of expeditioners and partners with partners less anxious about the risk of illness or injury occurring during the expedition than expeditioners, although more anxious about the risk of death in this regard. Expeditioners were more anxious about their ability to cope with the expedition prior to departure, whilst partners were more anxious during the expedition itself. Post-return, there were similarities in the experiences of expeditioners and partners as they related to pleasure, arousal and relationship distress although only expeditioners reported excitement during this time. Overall, Taylor and McCormick concluded there was little evidence that couples were

anxious about family matters to the extent that they severely impacted work-related duties whilst on the expedition.

Leveraging from this seminal work, Norris [26] extended the research paradigm to a sample of over 400 expeditioner-partner dyads. Employing a mixed-methods design, Norris replicated Taylor and McCormick's finding that there were recognisable differences in the experiences and expectations of expeditioners and partners prior to and during Antarctic deployment, as well as post-return. Whilst this finding is important in and of itself, Norris further demonstrated that these differences were influenced by factors outside the relationship unit, including organisational climate and the degree of communication between expeditioner, partner, and the organisation. In turn, the degree of communication shaped perceptions of social support, trust, empowerment, and ultimately adaptation to the employment experience (Fig 1). When well adapted, expeditioner performance and wellbeing was optimised which facilitated increased likelihood of achieving work-related goals and also increased the likelihood of employee retention and subsequent deployments. Experienced expeditioners represent an important resource for the organisation in that they are already trained, better equipped to successfully adapt to Antarctic conditions, are more aware of difficulties associated with Antarctic employment, better suited to undertake positions of leadership, and represent an important resource for new expeditioners in that they can share their knowledge and coping strategies in order to assist adaptation once in Antarctica [26]. In light of the parallels that arguably exist between Antarctica and space, these are all important considerations when considering long-duration manned space missions and should be used to inform strategies to maximise human health and performance in such environs.

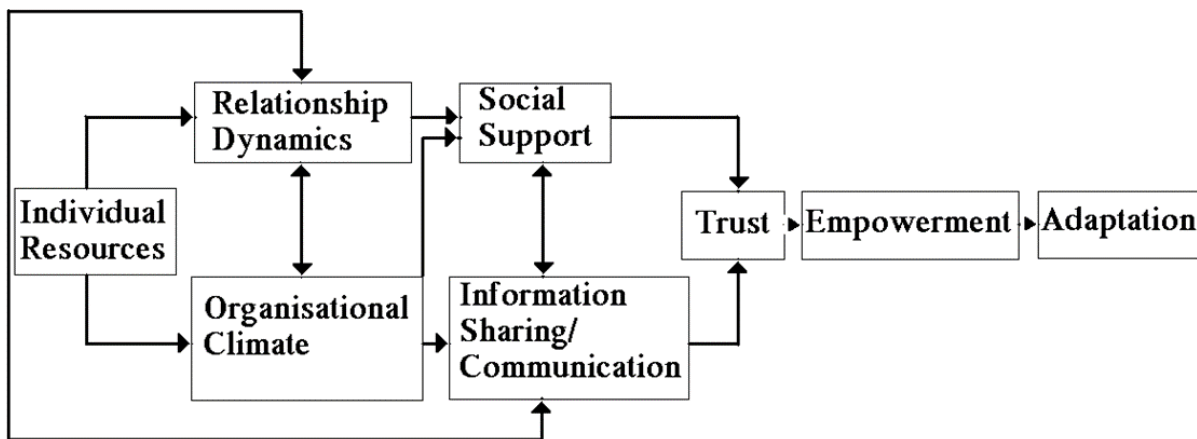


Fig 1. Model of adaptation to an EUE

As demonstrated in Fig 1, adaptation (which in this context indicates effective functioning in an EUE such as Antarctica and space) results from interplay between person, relationship, and organisational-level factors which feed into trust and empowerment. A particularly encouraging outcome of this model is that it identifies psychological factors across person, organisational, and relationship-level factors which are malleable for change, and therefore important targets for both proactive prevention and intervention. The importance of this model in influencing intervention planning was further emphasised by recent results published by Moulton, Norris, Paton and Ayton [27]. Their findings not only reinforced the interplay between partner and expeditioner experiences through evidence of reciprocal relationships between expeditioner and partner wellbeing, but also identified that post-return adaptation was influenced by experiences

within preceding phases of the employment cycle, for example, wellbeing post-return to Australia was predicted by factors including pre-departure wellbeing. This suggests that by implementing proactive prevention and intervention strategies for both personnel and their families throughout the deployment experience, overall health and wellbeing can be maximised.

Traditionally, formal psychological interventions are underutilised by Antarctic expeditioners, as in many other populations. Reasons for this include a perceived risk to ongoing and future employment in the EUE due to perceptions of 'not coping' or not having 'the right stuff', threats to identity as a capable and high-performing individual, and a reliance on telehealth or e-interventions that may require a higher degree of motivation and reliable and ready access to the internet for improvements to be made [34]. Furthermore, few individuals selected to work in EUEs such as Antarctica or space would regularly engage in formal psychological interventions outside the work context, therefore it is not surprising that they similarly eschew such interventions within the work context. Of concern however, is that individuals in such environments are subject to more extreme challenges that may tax their pre-existing resources and limit the opportunity for the development of alternative coping strategies, thereby resulting in stress or distress. In such environments, stress should be considered a normal and necessary reaction to the situation [28] that can facilitate engagement with adaptive coping strategies, whereas distress is more akin to pathology and is more likely to result in the use of maladaptive coping strategies potentially leading to a cycle of distress.

To overcome the identified barriers in engaging with preventative psychological programs, it is suggested that they be embedded into organisational training programs. Not only do such approaches ensure access to and encourage better engagement with the program, but they simultaneously work to reshape the organisational culture and belief systems regarding the role of psychology and interventions in the workplace. Furthermore, such an approach facilitates proactive prevention and intervention across the employee lifecycle. For example, pre-departure foci could include psychoeducation about common challenges experienced within the context of their employment, interpersonal skills including conflict management and communication, and the development of flexible coping strategies including a focus on self-care; during the deployment period, a series of 'just in time' interventions could be implemented based on research identifying key triggers and challenges experienced during this period, including those related to tempo; and post-return, psychoeducation and interventions to facilitate adaptive reintegration into more routine life.

In consideration of the increasingly recognised interplay between work and non-work performance and experiences insofar as EUE populations, it is also important to ensure that families are included in this proactive approach to psychological health management, whether it be through dissemination of information to integration in specific intervention components. Such processes would facilitate enhanced communication, which according to the model in Fig. 1, leads to enhanced trust, empowerment, and positive adaptation within EUE populations. Further supporting this argument are findings from non-EUE populations in which researchers have identified that positive experiences associated with interactions between work and family roles often outweigh the experience of negative interactions [29]. Specific positive outcomes associated with interrelationships between work and family roles include increased role flexibility [30], positive psychological spill over [31], enhanced self-esteem and self-efficacy [32], and increased perceptions of social support [33]. Furthermore, it has been demonstrated that employees working within organisations in which support services were made readily available to both the employed individual as well as their partner, and in which institutional norms facilitated use of such services, reported more positive benefits associated with both work and family roles [34].

The overarching message to consider is that even in space analogues, and space itself, ‘no man is an island’. Consideration of issues beyond the individual to include relationship and organisational factors is vital, as it can influence astronaut health, wellbeing and performance far beyond the confines of the family unit into the spaceflight experience itself. These influences can persist beyond the duration of the mission itself and impact successful reintegration experiences, and potentially impact the likelihood of sustained engagement with the profession representing a loss of knowledge and expertise.

Conclusions

Previous research has demonstrated that individuals in EUEs and space analogues such as Antarctica are impacted by individual, interpersonal, and organisational factors that shape their behaviour during pre-departure, whilst in Antarctica, and post-return. As Antarctica is a well-recognised space analogue, it is arguable that similar experiences and outcomes will be reported by those who undertake manned space missions. For this reason, it is imperative that a comprehensive and robust human research program to complement space endeavours is developed and implemented that ensures *all* aspects of the employment experience are simultaneously assessed to understand and address the mechanisms that underpin the known impacts of working in EUEs. Such programs must consider person, relationship and organisational-level factors when implementing proactive prevention and intervention strategies.

Acknowledgements

I wish to acknowledge the ongoing generosity of Antarctic expeditioners, especially those within the Australian Antarctic program with whom I have had the pleasure of working, who willingly and voluntarily support research into behavioural health in extreme environments by participating in research projects in this regard. I would also like to acknowledge the support and assistance of the Australian Antarctic Division staff who facilitate recruitment of participants for such endeavours, including Polar Medicine Staff and Doctors.

References

1. Barnett, J., and Kring, J.P. (2003). “Human performance in extreme environments: A preliminary taxonomy of shared factors”. *Proceedings of the Human Factors and Ergonomics Society 47th Annual Meeting* (pp. 961-964). Santa Monica, CA: Human Factors and Ergonomics Society.
2. Rivolier, J. and Bachelard, C. (1988). “Study of analogies between living conditions at an Antarctic scientific base and on a space station”. *European Space Agency Report*, Paris, pp. 1-158.
3. Harrison, A.A., Clearwater, Y.A., and McKay, C. (Eds). (1991). *From Antarctica to outer space – life in isolation and confinement*. Springer, Berlin. pp. 1-410.
4. Lugg, D., and Shepanek, M. (1999). “Space analogue studies in Antarctica”. *Acta Astronautica*, Vol. 44., pp. 693-699.
5. Suedfeld, P. (1991). “Polar psychology: An overview”. *Environment and Behavior*, Vol. 23, pp. 653-665.

6. Sandal, G.M., Leon, G.R., and Palinkas, L.A. (2006). "Human challenges in polar and space environments". *Reviews in Environmental Science and Biotechnology*, Vol. 5, pp. 281-296.
7. Levine, S. and Ursin, H. (1991). "What is stress?" In M.R. Brown, G.F. Koob, & C. Rivolier (Eds.), *Stress – neurobiology and neuroendocrinology* (pp.3-21). New York: Marcel Dekker.
8. Lugg, D.J. (2004). "International collaboration in Antarctic medical research". *Antarctic Science*, Vol. 2, pp. 187-187.
9. Palinkas, L.A. (1991). "Effects of physical and social environments on the health and well-being of Antarctic winter-over personnel". *Environment and Behavior*, Vol. 23, pp. 782-799.
10. Kahn, P.M., and Leon, G.R. (1994). "Group climate and individual functioning in an all-women's Antarctic expedition team". *Environment and Behavior*, Vol. 26, pp. 669-697.
11. Mocellin, J.S.P., and Suedfeld, P. (1991). "Voices from the ice: Diaries of polar explorers". *Environment and Behaviour*, Vol. 23, pp. 704-722.
12. Suedfeld, P. (2002). "Applying positive psychology in the study of extreme Environments". *Human Performance in Extreme Environments*, Vol. 6, pp. 21-25.
13. Mocellin, J.S.P., and Suedfeld, P. (1991). "Voices from the ice: Diaries of polar explorers". *Environment and Behaviour*, Vol. 23, pp. 704-722.
14. Oliver, D. (1991). "Psychological effects of isolation and confinement of a winter-over group at McMurdo Station, Antarctica". In A.A. Harrison, Y.A. Clearwater, and C.P. McKay (Eds.), *From Antarctica to outer space: Life in isolation and confinement*. New York: Springer-Verlag.
15. Natani, K., and Shurley, J.T. (1974). "Sociopsychological aspects of a winter vigil at South Pole station". In E.K.E. Gunderson (Ed.), *Human adaptability to Antarctic conditions* (pp. 89-114). Washington, DC: American Geophysical Union.
16. Palinkas, L.A., Glogower, F.G., Dembert, M., Hansen, K., and Smullen, R. (2004). "Incidence of psychiatric disorders after extended residence in Antarctica". *International Journal of Circumpolar Health*, Vol. 63, pp. 157-68.
17. Lugg, D.J. (2005). "Behavioural health in Antarctica: Behavioural implications for long-duration space missions". *Aviation, Space, and Environmental Medicine*, Vol. 76, pp. 74-77.
18. Sarris, A. (2006). "Personality, culture fit, and job outcomes on Australian Antarctic Stations". *Environment and Behavior*, Vol. 38, pp. 356-372.
19. Schmidt, L.L, Wood, J., and Lugg, D. J. (2004). "Team climate at Antarctic research stations 1996-2000: Leadership matters". *Aviation, Space, and Environmental Medicine*, Vol. 75, pp. 681-687.

20. Carver, C.S., and Scheier, M.F. (1994). "Situational coping and coping dispositions in a stressful transaction". *Journal of Personality and Social Psychology*, Vol. 66, pp. 184-195.
21. Godwin, J.R. (1991). "A preliminary investigation into stress in Australian Antarctic expeditioners". *SPRIO Polar Symposia*, Vol. 1, pp. 9-22.
22. Palmai, G. (1963). "Psychological observations on an isolated group in Antarctica". *British Journal of Psychiatry*, Vol. 109, pp. 364-370.
23. Palinkas, L.A., Gunderson, E.K.E., Holland, A.W., Miller, C., and Johnson, J.C. (2000). "Predictors of behavior and performance in extreme environments: The Antarctic Space Analogue Program". *Aviation, Space, and Environmental Medicine*, Vol. 71, pp. 619-25.
24. Strange, R.E., and Youngman, S.A. (1971). "Emotional aspects of wintering over". *Antarctic Journal of the United States*, Vol. 6, pp. 255-257.
25. Taylor, A.J.W., and McCormick, I.A. (1987). "Reactions of family partners of Antarctic Expeditioners". *Polar Record*, Vol. 23, No. 147, pp. 691-700.
26. Norris, K. (2010). "Breaking the ice: Expeditioner and partner adaptation to Antarctic employment". *Unpublished Doctoral Thesis*, University of Tasmania.
27. Moulton, C., Norris, K., Paton, D., & Ayton, J. (2010). Predicting positive and negative change in expeditioners at 2-months and 12-months post Antarctic employment. *The Polar Journal*, Vol. 5, No. 1, pp. 128-145.
28. Norris, K. and Jones, J. (2016). "Behavioural Health in Extreme Environments: Normal Reactions in Abnormal Environments". *Scientific Committee for Antarctic Research 34th Open Science Conference, Malaysia*, August 20-26.
29. Bernas, K.H., and Major, D.A. (2000). "Contributors to stress resistance: Testing a model of women's work-family conflict". *Psychology of Women Quarterly*, Vol. 24, pp. 170-178.
30. Hughes, D., Galinsky, E., and Morris, A. (1992). "The effects of job characteristics on marital quality: Specifying linking mechanisms". *Journal of Marriage and Family*, Vol. 54, pp. 31-42.
31. Larson, R.W., and Almeida, D.M. (1999). "Emotional transmission in the daily lives of families: A new paradigm for studying family process". *Journal of Marriage and the Family*, Vol. 61, pp. 5-20.
32. Barnett, R.C. (1999). "A new work-life model for the twenty-first century". *The Annals of the American Academy of Political and Social Sciences*, Vol. 562, pp. 143-158.
33. Carlson, D.S. and Perrewé, D.L. (1999). "The role of social support in the stressor-strain relationship: An examination of work-family conflict". *Journal of Management*, Vol. 25, pp. 513-540.

34. Vinokur, A.D., Pierce, P.F., and Buck, C.L. (1999). "Work-family conflict of women in the Air Force: Their influence on mental health and functioning". *Journal of Organisational Behaviour*, Vol. 20, pp. 865-878.

Mobility Trials of a Small Planetary Science Rover for Mars Surface Exploration

Steven Hobbs^{1,2}, David J. Paull¹, Jonathan Clarke², Siddharth Pandey^{1,2}

¹UNSW Canberra ²Mars Society Australia.

Summary: No nano-rover (2 kg) class vehicle has ever landed on Mars. Such a small vehicle would make it an ideal secondary payload with its own independent mission in a similar manner to Cubesat missions. Two nano size rovers (29 X 28 cm), approximating the size of an A4 sheet of paper (29.5 X 21 cm) were constructed to characterise and evaluate the application of novel skid steer drive system for a Mars rover. A combination of hand made and machined hardware and open source electronics were used for the two rovers and subjected the hand-built version to a series of mobility tests on surfaces expected to be found on Mars. A series of metrics from these tests were generated that were able to identify mobility limitations and potential catastrophic failures for the vehicle. The tests were used to improve the design of the A4 Rover project, as well as provide informed decisions on generating engineering constraints for Martian landing site selection.

Introduction

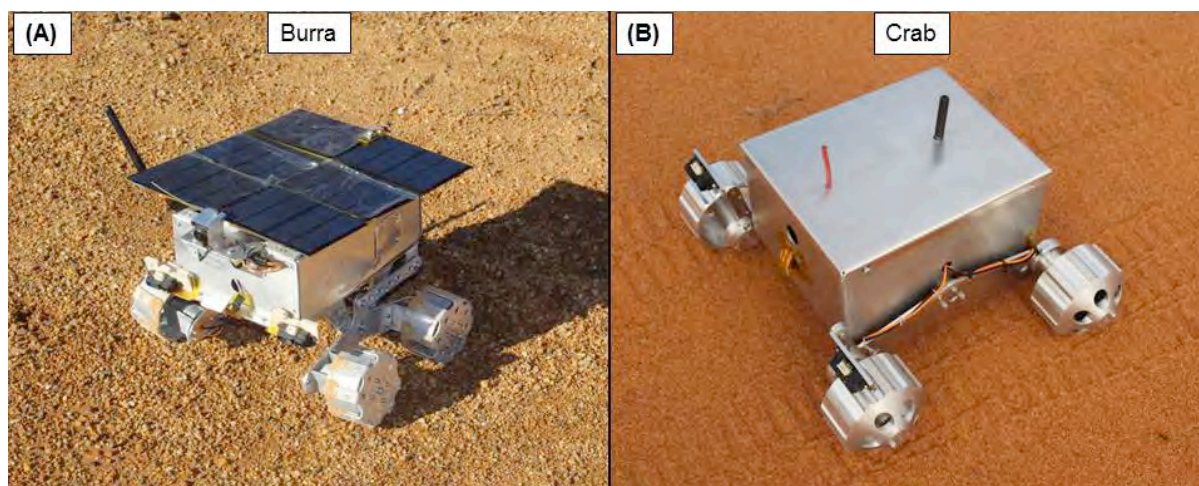


Figure 1. (A) Hand-built version of the A4 Rover, “Burra”. (B) Machined version of the A4 Rover, “The Crab”. Note solar panels for the Crab had not yet been fitted.

In 2015 we proposed the design of an A4 sized rover, smaller than the Sojourner rover that went to Mars [1] that could be flown as a secondary payload and increase the data returned from a robotic Mars lander mission [2]. The small size, weight and power requirements of such a vehicle would make it an affordable payload [3, 4], while the proliferation of miniaturised, open source sensors would still allow it to carry a useful payload of scientific instruments [5]. In this work the mobility of the hand-built rover is tested on a variety of surfaces and slope angles in order to characterise its performance on potential Martian surfaces it may encounter [6, 7, 8]. Traversing on the Martian surface has had significant advantages compared to a fixed lander mission [9, 10, 11, 12], though the diversity of the terrain has also presented significant challenges to robotic mobility [13, 14]. Testing the mobility characteristics of terrestrial versions of a planetary rover is thus crucial in the design process, and has implications for selecting suitable landing sites for the mission [15, 16, 17].

Understanding of peak loads and deflections the surface would impart on the vehicle has been considered as paramount in previous flight rover testing [7, 12, 18]. The mobility testing conducted for Sojourner and the MER Rovers were used to determine engineering constraints that helped determine suitable landing sites for operations of these rovers [7, 12, 18]. Additionally, characterising the power requirements of the rover while traversing differing slopes will provide essential information for power management, and the length of time the rover is able to drive prior to having to stop and recharge its batteries.

Wheel sinkage and slip on surfaces where vehicle tracks were able to be clearly identified and measure were measured. This information is important as wheel slippage can lead to errors in dead reckoning navigation, particularly where wheel revolution counts provide an indication of distance travelled [19, 20, 21, 22]. Terrestrial trials of the Mars Exploration Rover designs have shown substantial amounts of slippage during driving on Mars like terrain, degrading accuracies in navigation as well as increasing the power required for traversal [22, 23, 24]. Additionally wheel slippage and sink have led to situations where Mars rovers have become bogged in loose sand [8, 25]. Additionally, wheel sinkage and slip can be used to infer the strength and composition of the surface, once wheel and drive characteristics are known [14, 26]. This has important implications to understanding the local geology of the exploration area [14].

Slip was determined by physically measuring the distance between eight cleat imprints, equating to the circumference of the rover wheel. We then used the following formula to estimate average wheel slip [14]:

$$\{S\} = 1 - (d/2\pi\{r\}) \quad (1)$$

Where $\{S\}$ is the wheel slip, d is the distance between eight cleat imprints and $\{r\}$ is the wheel radius. The wheel sinkage was measured by counting the number of sand covered wheel cleats for each wheel and taking the average as the final result.

Rover Design

Two rovers were built based on the specifications outlined in our 2015 rover proposal, which outlined the design for a 2-3 kg nanorover design [2]. The first rover, called “Burra”, was built as a first-draft prototype using hand tools and commercial off-the shelf (COTS) electronics (Fig. 1A). Burra was built as a lower cost, reusable rover in order to conduct initial trials of components and suspension designs. The lower cost of Burra allowed for large scale changes to the design and electronics if required. The chassis was made from aluminium with a four wheel, rocker bogie design. For ease of construction, both bogies were connected using an under-chassis torque arm, allowing for passive suspension control at the expense of a higher centre of gravity. The second rover, called “Crab”, was machined by the University of New South Wales (Fig. 1B) and incorporated refinements of the design of Burra following field testing of this earlier rover. The Crab predominantly used identical electronic components to Burra, two main exceptions included the replacement of the 70 RPM, 4mm shaft motors with Maxon 16S Gb 24 motors with GPX19A gearheads with a turn rate of 45 RPM and replacing the 12 volt Lipo battery with three Sony 18650 batteries for power.

The main components are shown in Fig. 2 with the primary processor being an Arduino Mega, while motor control was performed using an Arduino Uno with Polulu VNH5019 motor controller [27]. Two electronics configurations were considered for Burra: during mobility trials which are the focus of this paper, currents drawn from motor pairs on each

side of the vehicle were transmitted via serial modem live to a receiving laptop. Additional engineering data were measured and included battery voltage measurements and temperature measurements sampled directly above the motor controller and also from the front of the rover. These results, as well as science measurements obtained from a Melexis non-contact thermometer [28] and a UVM-30A UVA/UVB sensor [29], were recorded by the Arduino Mega and saved onto an SD card for later analysis. The scientific payloads were designed to provide useful data from a diversity of Martian landing sites [9, 11]. An alternative mode was trialled where the Arduino Mega was reprogrammed to transmit images and scientific data on command from the ground laptop. In this configuration the serial modem was removed from the motor controller/Arduino Uno combination and connected to the Arduino Mega (red circle, Fig. 2).

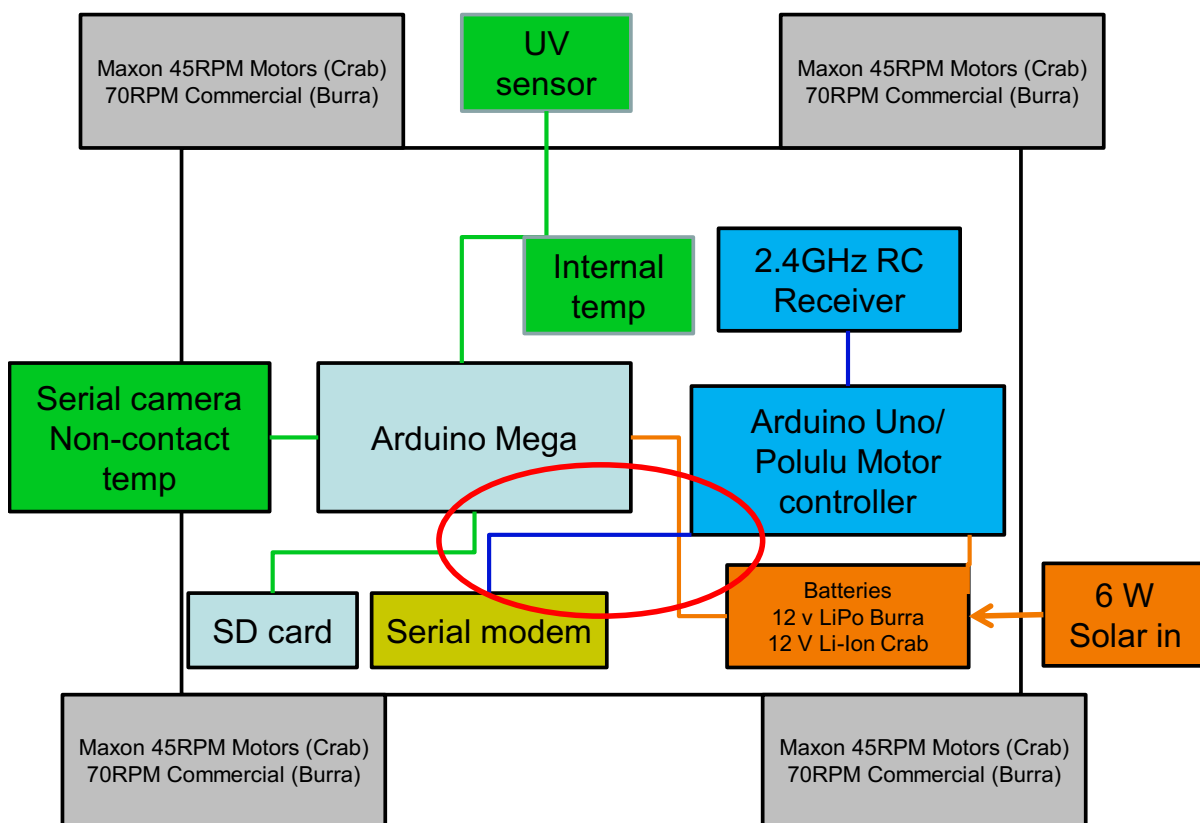


Figure 2. Block diagram of rover electronic design. Red circle denotes area of modem wire changeover when switching from engineering to science mode.

Mobility Trial Methods

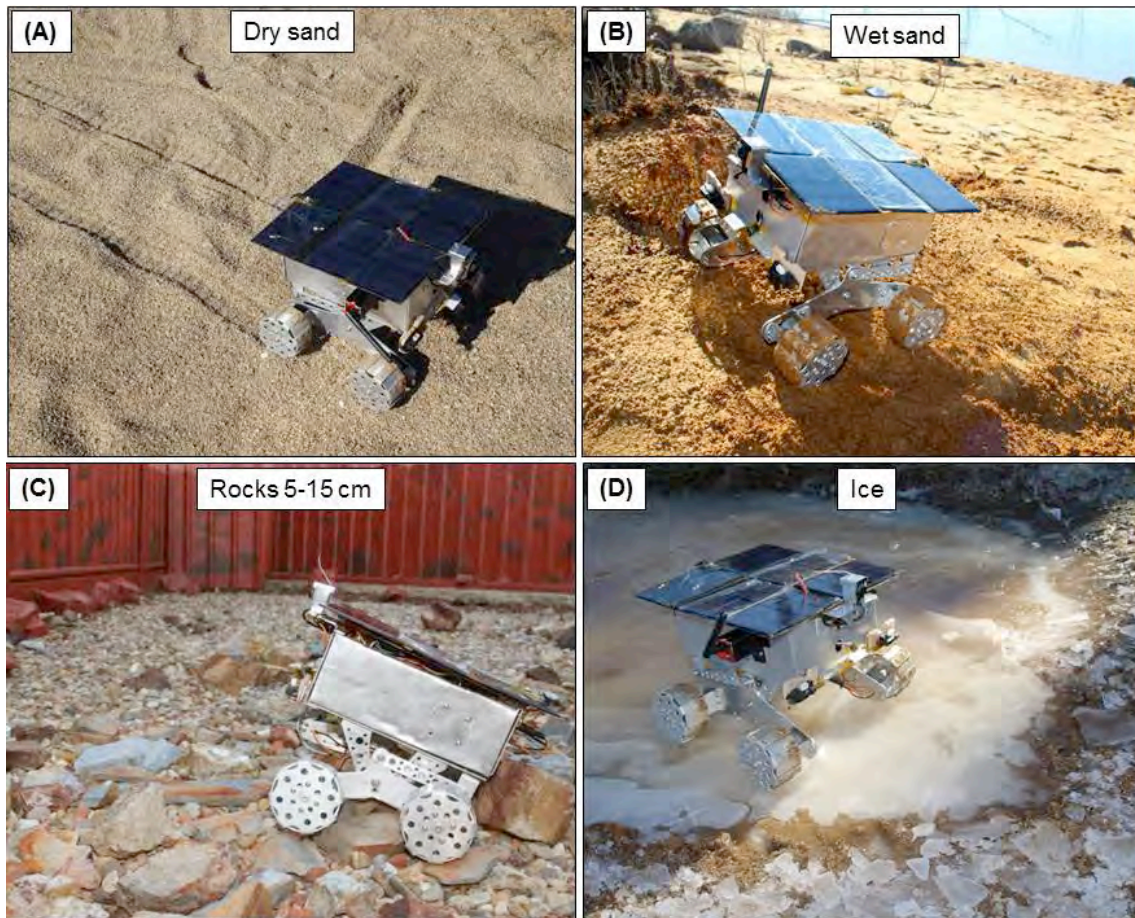


Figure 3. Example trial surfaces for Burra Rover testing. (A) Dry sand. (B) Wet sand. (C) Rough surface consisting of 5-15 cm rocks. (D) Icy surface.

Burra's mobility was trialled on a variety of surfaces and slopes in order to characterise performance and power requirements of the rover's wheels, suspension and motors. Initial trials were performed on a high grip surface on a custom-made wooden ramp that could be positioned at angles ranging from zero to 20° . Trials on this high-grip surface were used as a "best case" scenario representing optimal, no-slip conditions [7]. Other surfaces trialled included dry sand (Fig. 3A), wet sand (Fig. 3B), a rough surface consisting of 5-15 cm rocks (Fig. 3C), and ice (Fig. 3D). Surfaces and angles trialled are shown in Table 1.

The rover was driven forward on the surfaces and angles shown in Table 1. Burra transmitted motor current data from each motor pair 50 times per second, which we received and recorded on a receiving laptop. Voltages were also measured and logged five times per second on an sd card on board the rover. Power draw was thus able to be calculated from the rover for each traverse. We also timed the duration of the traverse and measured distance travelled; from which we could calculate rover speed. The traverses were conducted three times for each surface and slope and the average was used for analysis. The rover was initially driven down each slope in order to determine velocities and power draw while Burra traversed downhill. While undertaking this task the rover motors were found to generate dangerous amounts of feedback current which began interfering with operations and resetting the Arduino microcontroller. In light of these findings downhill traverses were restricted to the dry and wet sand surfaces where the increased friction encountered by the rover would help mitigate the power feedback issue.

Surface	Slope (degrees)
High grip	0, 5, 10, 15, 20
Dry sand	0, 5, 10
Wet sand	0, 5, 10, 15, 20
Ice	0
Rocks 5-15 cm	0

Table 1. Surface types and angles trialled during mobility testing.

Results

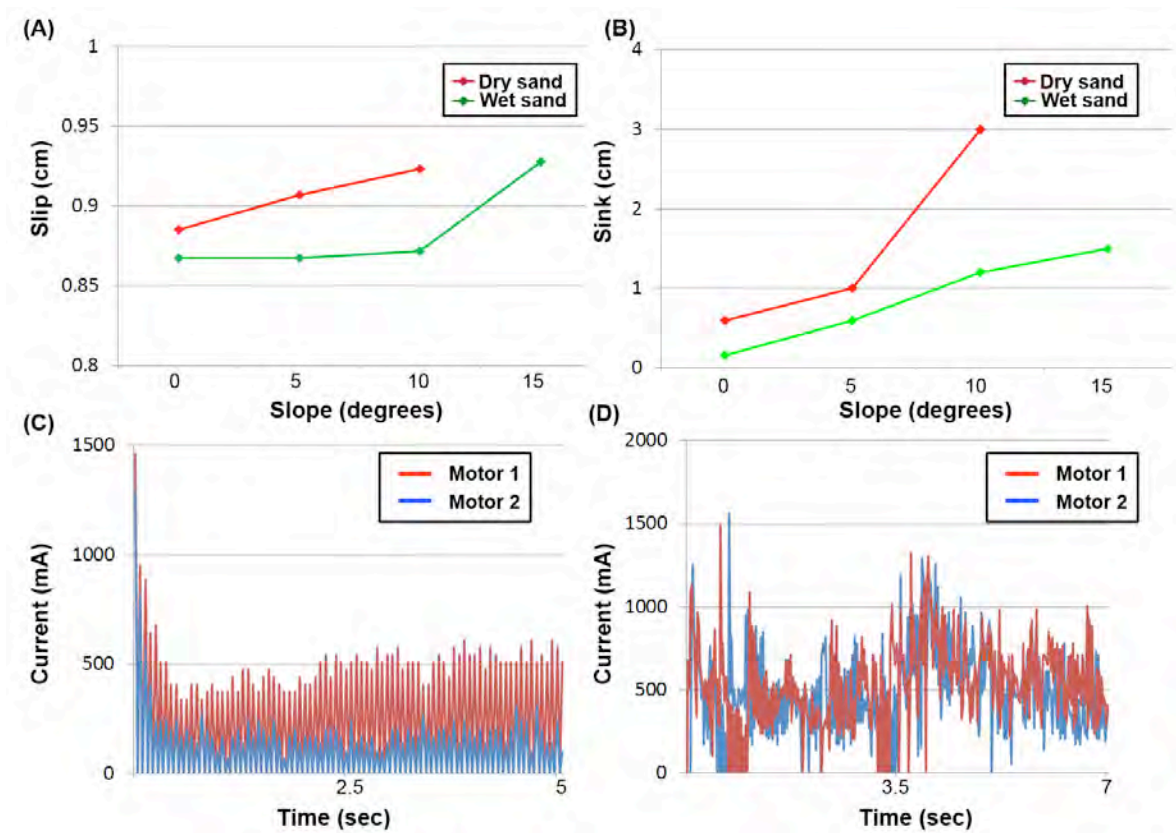


Figure 4. (A) Vehicle slip on wet sand and dry sand slopes. (B) Measured wheel sink on dry and wet sand slopes. (C) Raw current measurements on flat high-grip surface. (D) Raw current readings during traverse over rough (3-10 cm rocks) surface.

Wheel slip and sink was only able to be measured on dry and wet sand surfaces where the rover tracks were visible and could be measured. Burra's wheel slip on wet sand was found to show slight increases for slopes up to 10 degrees (~0.85, Fig. 3A), before sharply increasing for 15 degree slopes (0.93, Fig. 3A). Wheel slip on dry sand increased to a maximum slip of 0.92 (Fig. 3A). Wheel sinkage was highest in dry sand, increasing dramatically between 5-10 degrees (Fig. 3B) where Burra had sunk to its wheel hubs. Wheel sinkage increased to ~1 cm between 0-10 degrees (Fig. 3B), though the increase in wheel sinkage was less between 10-15 degrees (Fig. 3B). Raw motor measurements were also found to be noisy (Fig. 3C and D). Raw motor current measurements during a flat forward traverse on a high stick surface

showed an initial spike in current draw on motor startup prior to levelling off at ~500mA for Motor 1 and 250 mA for Motor 2. Current draw across a rough surface of the Mars Yard test site showed greater variation as the rover negotiated rocks between 5-10 cm in size (Fig. 3D). We also noted variations in current draw as Burra negotiated a 15 cm wide by 9 cm high gully in wet sand (Fig. 4A). Motor current draw decreased while Burra traversed downward into the gully while increasing for the climb out (arrows, Fig. 4B).

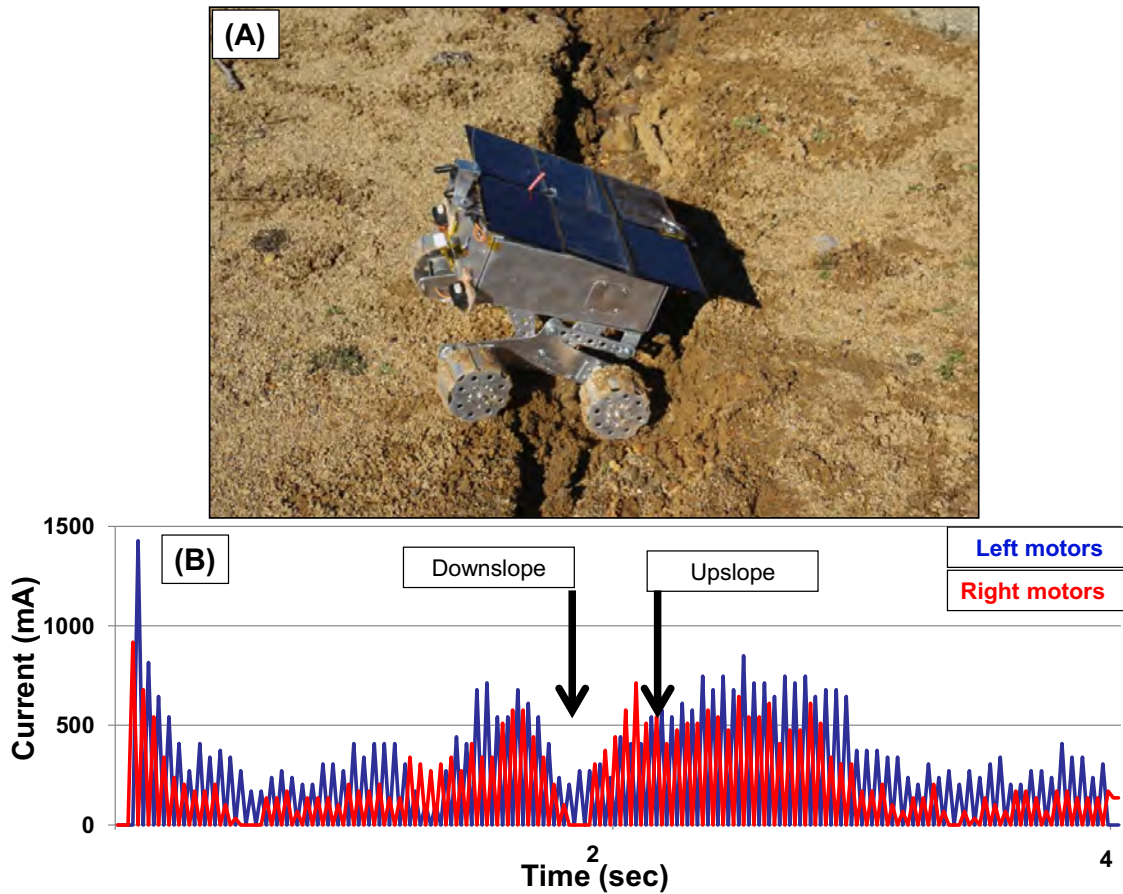


Figure 5. (A) View of Burra crossing a small gully. (B) Raw current measurements from each motor pair with downslope and upslope portions marked.

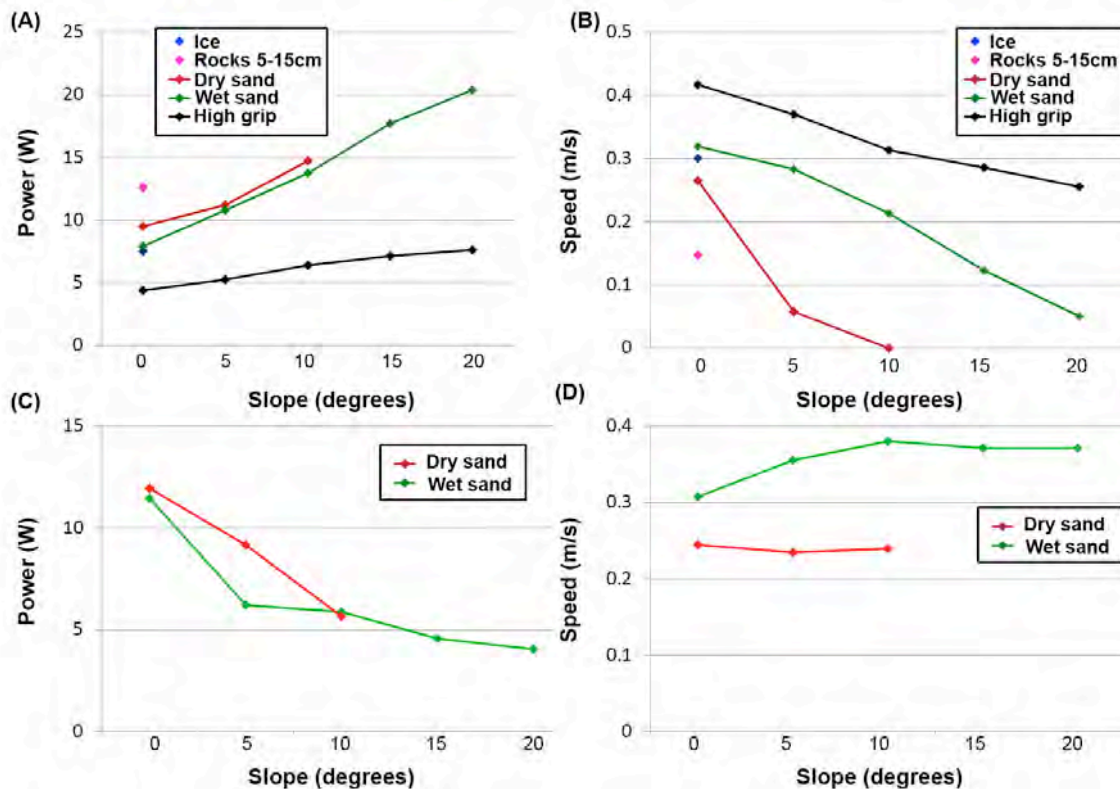


Figure 6. (A) Measured motor power usage for Burra traversing up different slope types at different angles. (B) Measured speeds for Burra traversing up different slope types at different angles. (C) Measured motor power usage for Burra traversing down different slope types at different angles. (D) Measured speeds for Burra traversing down different slope types at different angles.

Rover Power Draw and Speed:

Figure 5A shows power usage derived from total motor current draw of Burra traversing upslope on five different terrain types. Burra was able to be successfully driven up slopes of 20° on indurated wet sand and high stick surfaces and on slopes up to 10° on the dry sand test surface (Fig. 5A). Power draw for Burra on the wet and dry sand surfaces were similar for slopes up to 10° , while power draw for the 20° slope (~ 20 W, Fig. 5A) was almost three times higher on the wet sand surface than that of the high stick surface (~ 7.5 W, Fig. 5A). We noted driving forwards on the flat non-stick surface drew the lowest power (4.3 W, Fig. 5A). Traverses on flat terrain showed increases from 4.3 W to 12.5 W in power usage for ice, wet sand, dry sand and rough terrain respectively (Fig. 5A). Rover traverse speed was highest on the high grip surface on all slope angles (Fig. 5B). Measured speed decreased as slope angle increased, and Burra consistently became bogged on the 10° slope of dry sand. Flat traverse speeds on ice were lower than for the high stick and wet sand runs, while speeds on the rough terrain was the lowest of all flat terrain traverses at 0.15 m/s (Fig. 5B). Downhill slope power draw and speed was only able to be measured on the wet and dry sand surfaces as damaging feedback current was being generated on the high grip downhill traverses. Power usage decreased approximately in linear fashion for the downhill dry sand traverse while usage for the wet sand traverse showed lower decrease at slopes greater than 5° (Fig. 5C). Burra speeds leveled off past 10° on wet sand surfaces while traverse speeds were relatively constant for increasing angles downslope for dry sand (Fig. 5D).

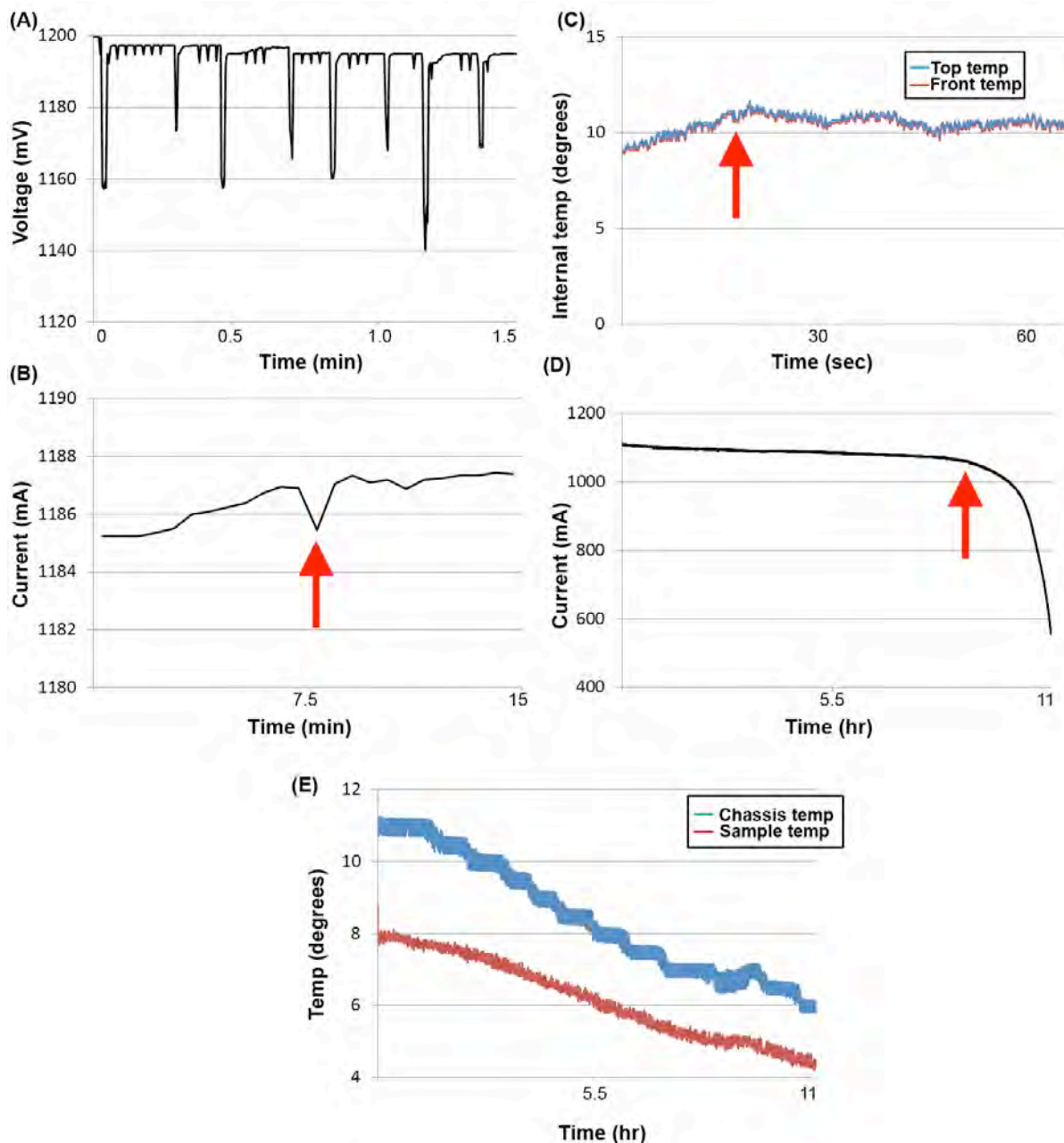


Figure 7. (A) Voltage measurements during upslope traverses for Burra. (B) Voltage accumulation during solar charging. Red arrow marks voltage drop. (C) Internal temperature measurements during rover operations. Red arrow denotes voltage level off. (D) Voltage measurements during static endurance test. Red arrow denotes sharp dropoff of voltage. (E) Internal and sample temperature measurements during endurance trial shown in Part D.

Figure 6A shows measurements of battery voltage during traverses by Burra with the solar panel unplugged over a 1.5 min period. Battery voltages decreased from 12 volts to 11.94 volts during eight traverses on five degree slopes. Battery voltages sharply dropped to as low as 11.4 volts during brief periods when the motors were initially engaged, before recovering to a relatively constant value. These voltage drops equated to the high current draw exhibited to the motors as shown in Fig. 3C. Periodic voltage drops of ~ 5 mV also occurred during the traverses, likely due to small scale variations in motor draw (Fig. 6A).

The results of solar recharging test over a 15 minute period is shown in Fig. 6B. In this test, Burra was left in a powered on, stationary state, with a 0.5 sec forward traverse conducted at 7.5 min into the test. This configuration minimized current draw on the battery as the motor controller was able to isolate the high power draw of the rover motors when not running. The 0.5 sec motor run was designed to test the voltage drop and recovery of the rover during a short-duration, high power drain event. The 6 W solar panel was able to increase battery voltage by 0.02 volts during the test. A 0.02 V drop occurred approximately half way through the test, marking the location of the .05 sec motor run (Red arrow, Fig. 6B). Battery voltage recovered almost immediately after the event and steadily increased to the end of the testing period (Fig. 6B).

Internal temperature measurements over a one minute period for Burra are shown in Fig. 6C. During this time Burra performed eight upslope traverses on wet sand slopes of 0-5 degrees. Pauses between traverses as the rover was physically repositioned were between 5-10 sec. Burra's chassis temperature was 8.9°C, 6.7° higher than the ground temperature of 2.3°C. Internal temperatures rose to a high 11.5°C as measured above the motor controller of the vehicle, before levelling off for the remainder of the measurement period. Rover chassis temperatures at the front and top of the vehicle were noted to be very closely related, with 0.2 degrees difference. The rover temperatures indicate temperature equilibrium was probably reached within the first 20 seconds of the rovers operation.

A night-time battery endurance test of Burra was performed over increasing time periods of 4, 10 and 12 hours at ambient temperatures as low as 2.3°C. The rover was powered on with the non-contact thermometer pointed at a 2 kg piece of basalt. Temperature measurements of the basalt over time, used to provide an indication of ground temperature, internal temperatures and remaining battery voltage measurements were logged and saved to the rover's SD card at 0.5 sec intervals. We found that while Burra was able to maintain power during the 4 and 10 hour endurance tests, it suffered a critical voltage drop at the 11 hour mark of the 12 hour test (red arrow, Fig. 6D). At this point battery voltage sharply dropped below the minimum 5 V required to operate the rover electronics and all readings ceased. The LiPo battery, sensitive to permanent damage if individual cell voltages becomes too low, suffered permanent cell damage and had to be replaced. Temperature measurements over this period indicated a steady drop in chassis temperatures that followed the drop in ground temperature (Fig. 6E). At the start of the test, chassis temperature was ~2° higher than the ground temperature, though this difference declined to ~1.5°.

Discussion

The Burra Rover was trialed on four different surfaces in field conditions in order to gain metrics on rover power usage, wheel slippage and sink. We used similar tests to these conducted on previous Mars rovers, such as MER that included mobility and obstacle clearance tests [7]. We found that Burra was able to climb slopes up to 20° on high grip and wet sand surfaces, while suffering substantial slippage on dry sand. The rover became bogged on slopes exceeding 10° on dry sand, and required corrections to maintain course on 10° slopes. Wheel sink was found to be non-linear for both the dry sand and wet sand trials. The reduction of wheel sink increase between 10-15 degrees (Fig. 3B) may be caused by the indurated property of the wet sand. Induration of a surface has been an important consideration in Martian geomorphology as it affects the stability of a given surface [30, 31]. We found the surface tended to be firmer below the drier top 1 cm of the sandy surface. The marked increase in wheel sink between 5-10° on dry sand slopes is likely to be caused by the rover wheels becoming ineffective at remaining above the sandy surface at this slope. The

vehicle tended to push mounds of sand in front of its wheels and bog down to the hubs after traverses of ~1 m.

Our analysis of rover power usage while traversing surfaces analogous to those found on Mars showed ranges from 4.3-20 W (Fig. 6A, C). Apart from downhill or flat traversal on firm surfaces we found these power requirements to exceed the 7 W power generation capability of Burra's solar panels. Indeed our solar recharging trial showed sensitivities to voltage drops whilst recharging (Fig. 7B). We will use these findings to develop a power management plan for Burra that would balance driving and collection of science with time to recharge. We also noted power usage became non-linear as a function of uphill and downhill slope traverses (Fig. 5C and D). The size of Burra probably makes the rover more sensitive to small scale effects in the local environment. This has likely caused variations in the graphical plots for rover power and speeds. The extra friction caused partial burial of the rover wheels in dry sands was likely the cause of Burra maintaining its speed at various angles downslope. This also occurred to a lesser extent on the wet sand slopes, where rover speed leveled off at slopes greater than 10° .

Power generation and endurance testing of Burra showed that the vehicle was able to supply adequate voltage for the duration of the mobility testing (Fig. 7A) and generate sufficient charging voltage in bright sunlight in excess of power demands (Fig. 7B). Owing to the critical battery failure that occurred during the 12 hour endurance test (Fig. 7D); it was not possible to determine how much lower the chassis temperature would have fallen prior to reaching temperature equilibrium. Endurance testing indicates that Burra would be able to remain functioning over a 10.5 hour night before failing. This would be insufficient to survive overnight in a Martian environment, except during equatorial summer periods where the hours of darkness are at a minimum [8]. A future aim to incorporate a low voltage protection circuit for the Crab, along with the Sony 18650 batteries in order to mitigate against similar catastrophic battery failures. At idle Burra's internal temperatures remained at least 1.5 degrees above the surroundings (Fig. 7E). This indicates that the rover chassis is able to provide a degree of insulation against the cold; however additional temperature testing is required for more detailed characterisation.

The testing program explained in this manuscript has allowed us to develop a good understanding of the performance of our vehicle's mobility limits, as well as potential catastrophic situations (vehicle becoming bogged or tipping over). We now have a series of metrics regarding Burra's performance on surfaces likely to be encountered on Mars and these can be used to generate a series of engineering constraints that can inform potential landing site selection [15, 16, 17]. An understanding of the power generation and endurance capability for Burra has also developed, and these results will be used to refine the design of The Crab, currently under testing. Results obtained indicated that Burra was less mobile than Sojourner, only able to climb obstacles 5 cm in height as opposed to 10 cm [6, 10]. Additionally, power generation was only 30% that provided by Sojourner, though we note we were using commercial grade panels.

Conclusion

The A4 Rover project is designed to develop and field test a 2 kg nano-rover in Mars-like conditions in order to develop a space qualified vehicle for planetary science. Two rovers were built and mobility and power endurance testing was conducted on Burra, the hand-built version, in order to characterise the suspension design and return critical data on power generation and limits of the vehicle. It was found that Burra was able to negotiate rough

terrain consisting of rocks up to 15 cm in size, negotiate a 9 cm deep gully, and traverse slopes up to 20° on firm surfaces. Burra's performance degraded on soft, dry sand surfaces, where the vehicle became bogged on slopes greater than 10°. Limitations were also found with the power generation and management system used in Burra. This work has generated key metrics that will be used to refine the design and electronics of the Crab, the machined rover, as progress is made towards building a space ready vehicle.

Acknowledgements

The authors would like to thank Mr Andrew Wheeler for his assistance in undertaking rover testing. The authors would also like to thank Mr Rhys Aitken for his assistance in developing electronics for the Burra rover.

References

1. Hayati, S., Volpe, R., Backes, P., Balaram, J., Welch, R., et al., "The Rocky 7 Rover: a Mars sciencecraft prototype". *Proceedings of the 1997 IEEE International Conference on Robotics and Automation*, 1997, pp. 2458-2464.
2. Hobbs, S.W., Clarke, J.D.A., Coleman-Jennings, C., Pandey, S., Van Kranendonk, M., and Willson, D. "A4 Rover proposal: a small planetary science rover for geologic and astronomy investigations for Mars surface exploration." *15th ASRC Conference Proceedings*, 2015.
3. Wilcox, B.H., and Jones, R.M. "The Muses-CN nanorover and related technology." *IEEE Proceedings*, pp. 2000, 7803-5846.
4. Post, M.A., "Planetary micro-rovers with Bayesian autonomy", *PhD Thesis*, York University, Toronto, 2014.
5. Sipos, A., and Vizi, P.G., "Simulated Mars model competition", *Proceedings of the 42nd Annual Lunar and Planetary Science Conference, 2011, The Woodlands, Texas. Lunar and Planetary Institute, Houston, TX*, abst 2014, 2011.
6. Bickler, D., "Roving over Mars", *Mechanical Engineering Magazine*. American Society of Mechanical Engineers, 1998.
7. Lindemann, R., "Dynamic testing and simulation of the Mars Exploration Rovers", *Proceedings of the ASME International Design Engineering Technical Conferences & Computers and Information in Engineering Conference*, Long Beach, Ca, USA, 2005.
8. Barlow, N.G., "Mars: An Introduction to its Interior, Surface and Atmosphere", *Cambridge University Press*, Cambridge, 264 pp, 2008.
9. Soffen, G.A., "The Viking Project", *J. Geophys. Res.* 82, pp. 3959-3970, 1977.
10. Mishkin, A., "Sojourner: an insider's view of the mars Pathfinder Mission", *Berkley Books*, 2003.
11. Grotzinger, S J., and 25 colleagues, "Mars Science Laboratory mission and science investigation", *Space Sci. Rev.* 170, 2012, pp. 5-26.

12. Arvidson, R., et al. "Localization and physical properties experiments conducted by Spirit at Gusev Crater", *Science* 305, 2004, pp. 821-824.
13. Arvidson, R., Bell III, J., Bellutta, P., Cabrol, N., Catalano, J., Cohen, J., et al., "Spirit Mars Rover mission: overview and selected results from the northern Home Plate winter haven to the side of Salamander Crater", *J. Geophys. Res.* 115, 2010, doi:10.109/2010E003633.
14. Zhou, F., Arvidson, R.E., Bennett, K., Trease, B., Lindemann, R., Bellutta, P., Iagemma, K., and Senatore, G. "Simulations of Mars Rover traverses", *Journal of Field Robotics* 31, 2014, doi: 10.1002/rob.21483.
15. Young, A., "Lunar and planetary rovers: the wheels of Apollo and the quest for Mars", *Praxis Publishing Ltd*, 2007.
16. Soderblom, L.A., and Bell III, J.F., "Exploration of the Martian surface 1992-2007", in: *The Martian Surface: Composition, Mineralogy and Physical Properties*, J.F. Bell III, Ed., *Cambridge University Press*, New York, 2008.
17. Baker, B., "Reconfigurable wheels: re-inventing the wheel for the next generation of planetary rovers", *Msc Thesis*, Massachusetts Institute of Technology, 2012.
18. Lindemann, R., et al., "Mobility sub-systems for the Exploration Technology Rover", *Proceedings of the 33rd Aerospace Mechanisms Symposium*, Pasadena, Ca, NASA/CP-1999-209259, 1999.
19. Musser, G., "The spirit of exploration", *Scientific American* 290, 2004, pp. 52-57.
20. Roman, M.J., "Design and analysis of a four wheeled planetary rover", *Msc Thesis*, University of Oklahoma, 2005.
21. Cheng, Y., Maimine, M.W., and Matthies, L., "Visual odometry on the Mars Exploration Rovers", *IEEE Robotics & Automation Magazine*, 2006, pp. 54-62.
22. Reina, G., Ojeda, L., Milella, and Borenstein, A., "Wheel slippage and sinkage detection for planetary rovers". *IEEE/ASME Transactions on Mechatronics* 11, 2006, pp. 185-195.
23. T. Huntsberger et al., "Rover autonomy for long range navigation and science data acquisition on planetary surfaces", *presented at the IEEE ICRA*, Washington, DC, 2002.
24. Ojeda, L., Reina, G., and Borenstein, A., "Experimental results from FLEXnav: An expert rule-based dead-reckoning system for mars rovers", in *Proc. IEEE Aerospace Conf.*, Big Sky, MT, pp. 816-825, 2004.
25. Kerr, R.A., "Mars rover trapped in sand, but what can end a mission?", *Science* 324, 2009, doi: 10.1126/science.324_998.
26. Ding, L., Gao, H., Deng, Z., K., Yoshida, and Nagatani, K., "Slip ratio for lugged wheel of planetary rover in deformable soil: definition and estimation", *The 2009 IEEE/RSJ International Conference on Intelligent Robots and Systems*, St Louis, USA, 2009.

27. Polulu., “Pololu VNH5019 Motor Driver Shield User’s Guide”, <http://www.polulu.com/docs/0J49/all>, website accessed 6 September 2016.
28. Adafruit., “Using Melexis MLX90614 Non-Contact sensors”, Adafruit Learning System, <http://learn.adafruit.com/using-melexis-mlx90614-non-contact-sensors.com>, website accessed 19 may 2015.
29. DFRobot., “UVM-30A UVA/UVB Sensor”, [http://www.dfrobot.com/wiki/index.php/UV_Sensor_\(SKU:TOY0044\)](http://www.dfrobot.com/wiki/index.php/UV_Sensor_(SKU:TOY0044)), website accessed 28 March 2016.
30. Fenton, L. K., and M. T. Mellon., “Thermal properties of sand from Thermal Emission Spectrometer (TES) and Thermal Emission Imaging System (THEMIS): Spatial variations within the Proctor Crater dune field on Mars”, *J. Geophys. Res.*, 111, 2006, doi:10.1029/2004JE002363.
31. Schatz, V., Tsoar, H., Edgett, K. S., Parteli, E. J. R., and Herrmann, H. J., “Evidence for indurated sand dunes in the Martian north polar region”, *J. Geophys. Res.*, 111, 2006, doi:10.1029/2005JE002514.

Hands Off Field Work: Comparison of Human and Robotic Methods for Gathering Terrain Data using Structure From Motion.

Steven Hobbs^{1,2}, David J. Paull¹, Jonathan Clarke², Siddharth Pandey^{1,2}

¹UNSW Canberra ²Mars Society Australia.

Abstract

Robotic performance of performing Structure from Motion (SfM) mapping surveys was conducted using an object of known dimensions, and on a small gully in New South Wales, Australia, using two rovers of different sizes that each captured photographic images from cameras of differing resolutions. Results from these trials were compared with a simulated Unmanned Aerial Vehicle (UAV) SfM survey of the same gully feature using a high resolution handheld camera. Accuracy of the resulting point clouds and time taken to complete the surveys were used as the key metrics to assess the performance of the respective methods. The high resolution camera surveys produced digital elevation models (DEMs) that were the most accurate, though the robotic surveys took an order of magnitude longer to complete. Additionally, camera resolution and height above ground were critical factors in determining the success of generating SfM data.

Introduction

Structure from Motion (SfM) allows for the creation of detailed 3D models or elevation data using overlapping images [1, 2]. The advantage of SfM over traditional photogrammetry methods has been that the process is relatively automated, and complicated camera models are not required as these are automatically calculated by the software [1, 3]. The simplicity of SfM has allowed it to be used in diverse applications in environmental modelling [2, 3, 4].

Obtaining accurate elevation data has proved essential for planetary science and modelling processes in geomorphology where direct field measurements are either extremely difficult or impossible [5, 6, 7]. The only methods available for conducting surface work on planetary bodies, such as the Moon or Mars, are through the use of robotic lander missions [8]. Recently, robotic rovers have been employed for Martian exploration as their mobility has allowed them to explore far more terrain than static landers, though they are far less efficient than equivalent human-based surveys [9, 10]. In this work small, ground based robot rovers were used to capture SfM-derived elevation data of a small erosional feature in New South Wales, Australia and compared the results with direct field measurements and a capture run using handheld photography. We aimed to characterise the effect that rover mobility, camera height above the ground and camera resolution had on the quality of the resulting SfM models.

Methodology

Rover Design

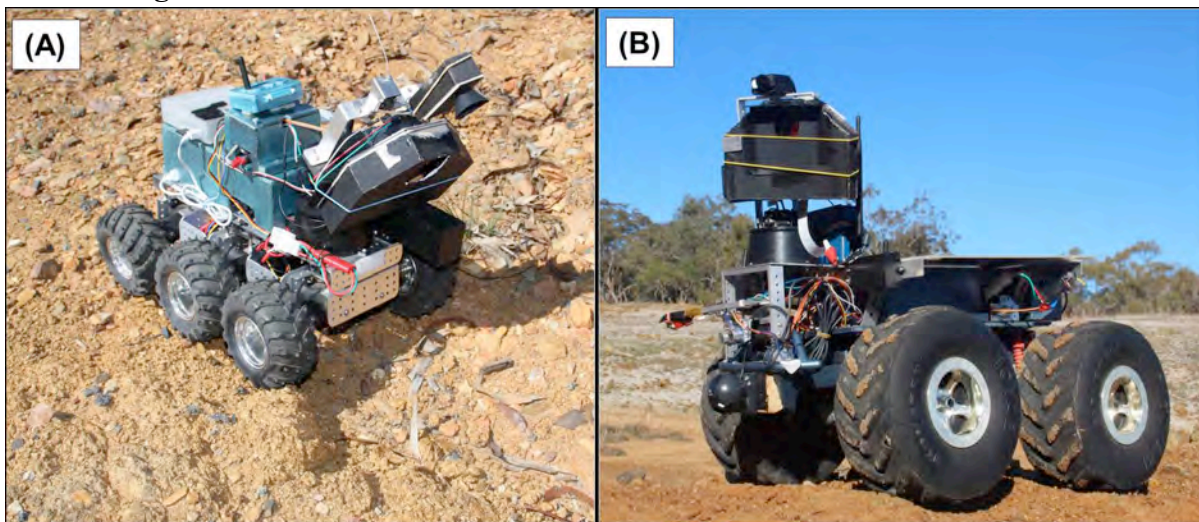


Fig. 1. Marsbot rovers trialled for SfM. (A) Junior Rover. (B) Little Blue.

Fig. 1A and B show the two rovers that participated in the SfM trial. Both rovers were teleoperated by links to a ground station. Table 1 lists the key attributes of the rovers. Both rovers have been used in our previous research. Little Blue was trialled in Arkaroola, South Australia, where engineering data obtained from standardised testing were obtained [11]. Little Blue was built to approximate the size of the 11.5 kg Sojourner Mars rover deployed in 1997 [12] with control provided by an Arduino microcontroller connected to Dagu 1:131 motors coupled to each of its four wheels [11]. The chassis of Little Blue is derived from a monster truck design, but has been heavily modified and ruggedized to support greater mobility and a scientific payload. The 5.4 GHz first person video (FPV) camera is able to transmit video images to a range of at least 200 m [11]. Although the video signal is analogue, an open source video capture program on a remote laptop was able to digitize Junior's incoming stream at 25 frames/sec, equating to a usable bandwidth of approximately 1.4 Mbits/sec. The video files were saved at full resolution while post-processing of the video allowed for selection of suitable images for subsequent SfM exploitation. The images were captured using maximum size JPG format (the only format acceptable to the chosen SfM software) in order to minimize lossy image compression artefacts. During this process, it was found that video noise became an issue during the trial, particularly where Little Blue's video antenna was obscured by terrain or other parts of the rover. Instances of this noise were immediately visible to the operator; allowing Little Blue to be repositioned for a re-shoot of the traverse affected by the noise, or affected frames discarded from further analysis.

Table 1. Attributes of trial rovers.

Rover	Junior	Little Blue
Chassis dimensions (L, W, H)	6-wheeled, 45 x 28 x 18 cm	4-wheeled 62 x 45 x 30 cm
Rover speed (no slope, m/sec)	0.3	0.47
Control	RC control, Raspberry Pi Wi-Fi	RC control, Arduino serial modem
Camera resolution (pixels)	Webcam, 1024 x 768	720 x 576
Camera height (cm)	28	33
Video transmission	Raspberry Pi Wi-Fi stills transmission	Video transmission

Junior is based on a commercially available Dagu 6 wheeled Wild Thumper chassis and employs 1:75 electric motors coupled to each of its wheels for mobility. As with Little Blue the rover is controlled using RC and employs an Arduino microcontroller for its main processing. Although a small video transmitter setup is used on the rover for navigation, the primary imaging is derived from a 1024 x 768 pixel webcam connected to a Raspberry Pi Model B. Junior was used in astrobiological trials in New Zealand where its webcam was employed to identify photosynthetic life forms living in extreme environments [13]. Imagery from the webcam was captured in a different manner to that of Little Blue. The webcam was commanded to capture still images, which were saved to the Raspberry Pi SD card and then subsequently transferred via Wi-Fi ftp to the remote laptop. The webcam natively saved stills as a minimum loss JPG image. Although bandwidth for the Wi-Fi was approximately 1.5 mBit/sec, more time was lost during the manual process of acquiring and transferring the images.

The camera used in the handheld survey was a Canon EOS 450D with a 10 megapixel resolution. As the camera was handheld, the height above ground ranged from 1.66–1.7 m, being approximately 5–6 times higher than the camera height of Little Blue and Junior, respectively.

Controlled Survey of House Brick

In our first SfM trial we used a house brick of known dimensions (8 x 11 x 23 cm), and commanded our rovers to drive 360° around the brick to take photographs (Fig. 2). We chose times of day where the lighting on the brick was constant, avoiding shadows that may have changed during the survey and affected the results.

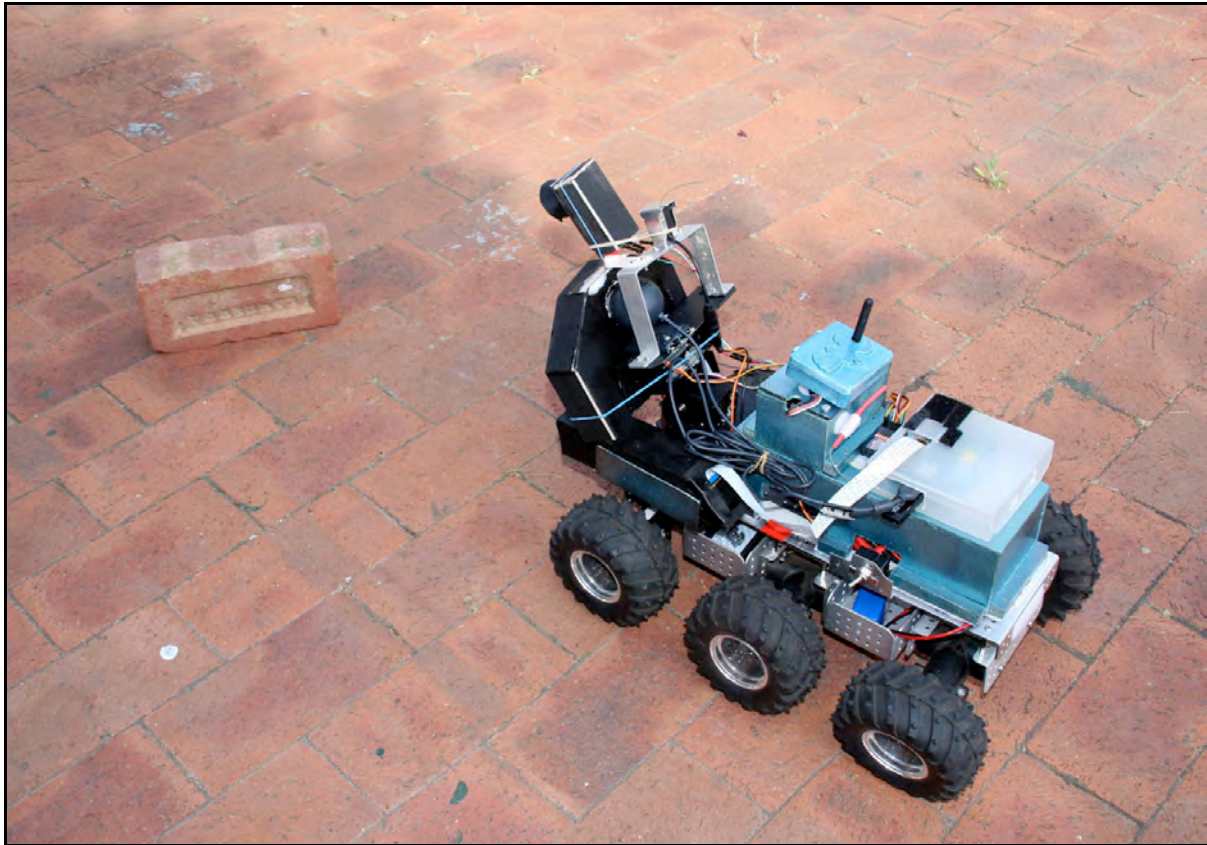


Fig. 2. First SfM trial using a house brick of known dimensions to compare model accuracies. Junior is shown imaging the brick.

We also photographed the brick using handheld photography in order to compare results obtained from robotic methods with those from a human-based survey. We used the time taken to complete the survey, number of images taken and model points generated as metrics for comparison of the different methods. Additionally we measured the brick dimensions from each of the models and compared these with the actual dimensions as physically measured to generate an error rating for each of the models. The SfM software used for all of the trials was Photosynth, which is an open source online program offered by Microsoft (www.photosynth.com). The process employed by this software entailed resampling all captured images to 2000 pixels on their longest side and uploading them to the Photosynth online server. The limitations of Photosynth required us to ensure all images possessed the same dimensions prior to being able to ingest into the software. Once uploaded point clouds were generated within 1–2 hours and meshes were exploited in Meshlab, an open source 3D mesh editing application.

Field Survey of Gully

The field trials were conducted on a small ~1 m wide x ~8 m long, gully at a locality known as ‘The Scar’ (lat -35.369150°, long 149.218819°, elev 662 m) in New South Wales, Australia. This local drainage feature was incised into material consisting of loosely bound stones ~1–5 cm in size. The main gully channel was adjoined by a shallower tributary, and a ~1 m diameter boulder was situated at the downslope, northern end of the main area of interest (Fig. 3A). We chose this site as it was relatively devoid of vegetation and was

analogous to small-scale features found on Mars [12, 14]. The surface enabled a degree of traversal of small, wheeled vehicles and the variety of slopes allowed for testing the impact of mobility restrictions on the accuracy of the resulting SfM model.

We set up a series of five stones at 1 m intervals on the western side of the gully (blue arrows, Fig. 3B). We used these as markers that would be identifiable on the resulting SfM models in order to tie distances in the models to those physically measured in the gully. We used the average difference between the point cloud and physical distance measurements to generate a percentage error. We conducted handheld photography on the gully to simulate and aerial image capture and also operated the Junior and Little Blue rovers over the study area. As with the house brick trials we used differences between these to generate error measurements between our models. As with the house brick trial we used the time taken to complete the survey, number of images taken and model points generated as metrics for comparison of the different methods.

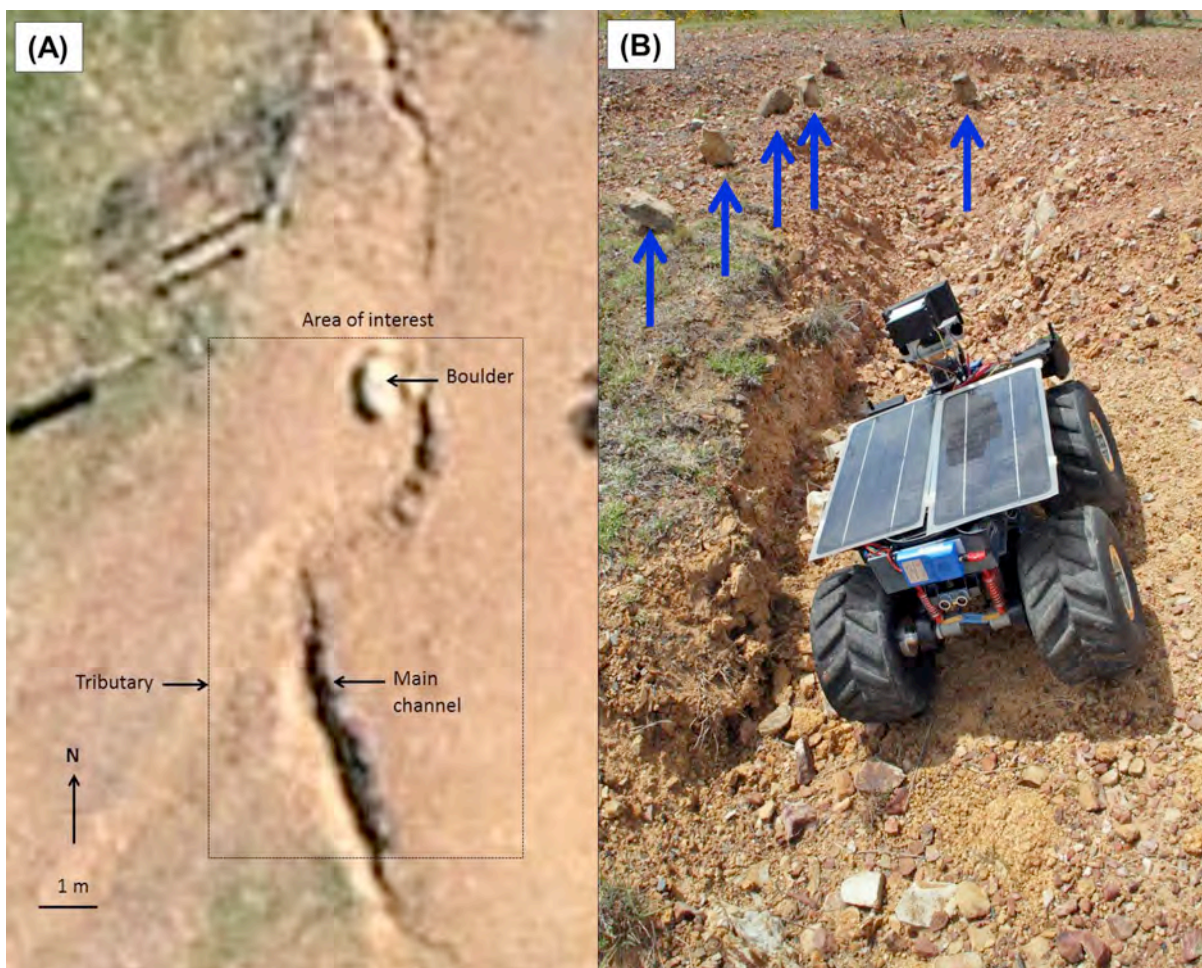


Fig. 3. (A) Overview of surveyed gully site (Nearmap Ltd imagery, 17 March 2014). (B) Little Blue about to commence a survey on the gully. Blue arrows highlight stones emplaced for gully measurements.

We exploited the point clouds within ArcGIS. We also noted terrain visibility issues may be prominent in the undulating gully terrain versus the static house brick test. We thus

measured the total surface area covered by each of the SfM models and expressed the amount of area occluded by the rover's inability to see parts of the terrain as a percentage of this area.

We also calculated surface roughness of each of the DEMs by employing a 10 x 10 cell minimum value DEM obtained, a 10 x 10 cell maximum value DEM using focal statistics in ArcGIS with a 10 x 10 cell smoothed DEM and using the following formula [15]:

$$(10 \times 10 - \text{minDEM})/(\text{maxDEM} - \text{minDEM}) \quad (1)$$

where 10 x 10 is the smoothed DEM, minDEM is the minimum value DEM, maxDEM is the maximum value DEM.

This provided an index that indicated a degree of complexity of the DEM. Indices between 0–0.45 and 0.55–1 indicate roughness within the DEM, whereas values between 0.45–0.55 indicate little or no surface variation is present. We measured the 0–0.45 and 0.55–1 values within each DEM and expressed them as a percentage of the total DEM to provide a roughness metric.

Results

House Brick

Fig. 4 A and B show handheld-derived point clouds of the house brick. The point cloud generated using this method possessed the most number of points (86460, Table 2) and proved to be the most accurate (0.71%, Table 2). This is despite the method producing the least amount of photos and taking an order of magnitude less time (0.4 min, Table 2) than using the two rovers.

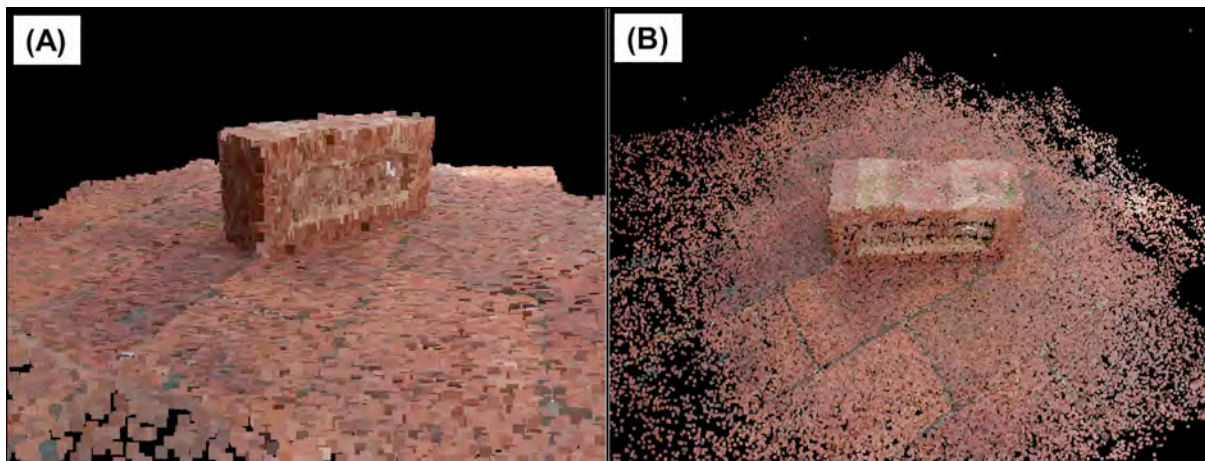


Fig. 4. (A) SfM model of the house brick as captured by handheld photography. (B) Overhead view of the modelled brick. Note the patterned ground below the brick.

Table 2. Results from the house brick trials.

Capture	Error (%)	Photos	Points	Time (min)
Little Blue	2.3	29	12369	11
Junior	2.6	38	54322	12
Handheld	0.71	21	86460	0.4

Results from the two rovers were comparable in time taken (11 min, Little Blue; 12 mins, Junior, Table 2) and generated error (2.3%, Little Blue, 2.6%, Junior, Table 2). We were able to capture nine more images using Junior than for Little Blue, though the measurement error by using Junior was higher (Table 2).

Gully

Fig. 5A shows an overhead view of the study site as well as the routes taken by the handheld, Little Blue and Junior surveys. As shown by the green ring representing the handheld track, we were able to completely traverse the study site in the human-led survey. The terrain presented little hindrance for mobility and a 360° coverage was obtained of the gully.

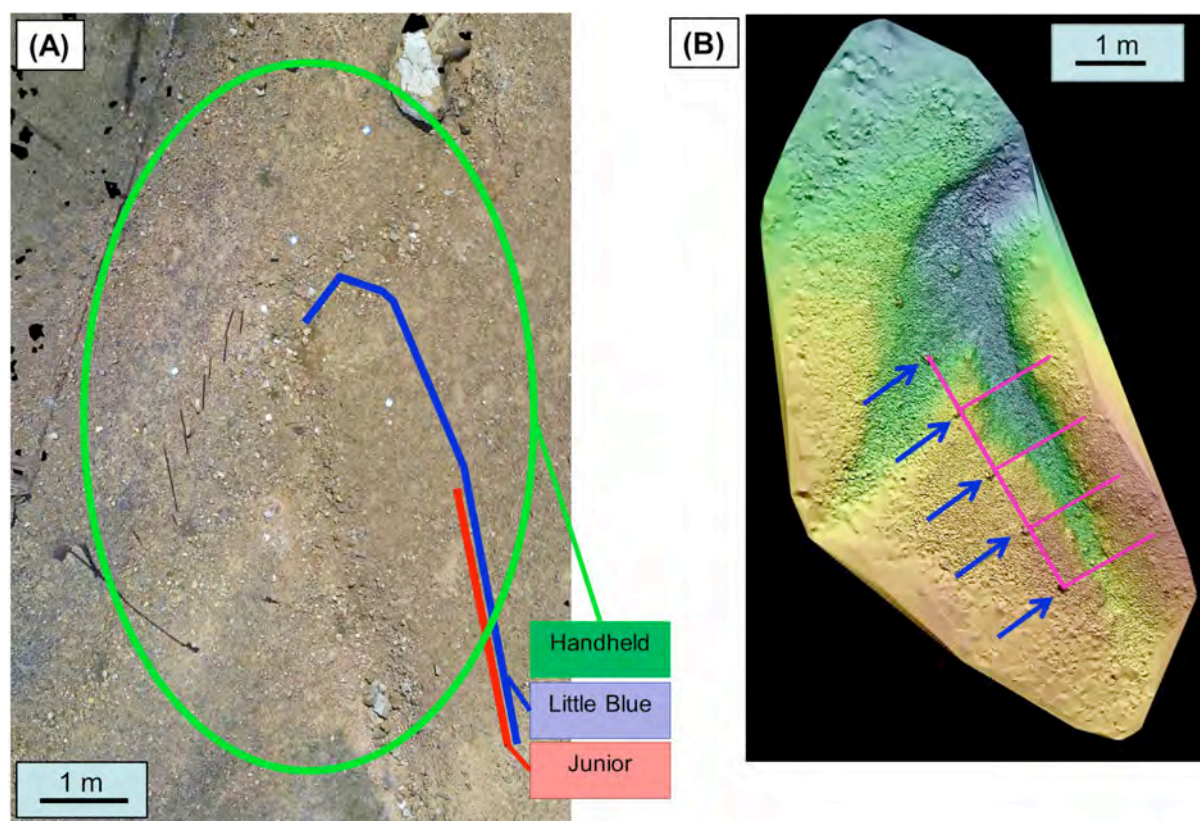


Fig. 5. (A) Overhead view of the studied gully showing paths of the handheld, Little Blue and Junior traverses. (B) Elevation image showing the locations of the five stones used for measurements (arrowed). The pink lines show the measurement samples taken, along with four cross-sectional profiles.

The result of this unrestricted traverse, as well as an average camera height of 1.6–1.7 m, enabled all portions of the gully to be imaged. The Little Blue Rover possessed sufficient mobility to traverse approximately 7 m along the eastern wall of the gully and into the channel at the gully confluence (blue line, Fig. 5A). In contrast the smaller size of Junior restricted its safe operating area to an approximately 3 m traverse on the eastern side of the gully from its starting point. Range issues were experienced with the rover’s Wi-Fi connection, increasing the time taken to operate this rover. Fig. 5B shows an elevation model of the gully, where stones used for the distance measurements are highlighted. Pink lines represent locations of measurements and cross profiles, respectively.

Table 3 shows the measured metrics for each of the methods used to survey the gully. As with the house brick test, the handheld survey took the least amount of time and produced the densest point cloud (Table 1). Errors generated by the handheld survey were the lowest of all survey methods (0.26, Table 3).

Table 3. Results from the gully trials.

Capture	Error (%)	Area (m ²)	Points	Time (min)	Void (%)
Little Blue	6.0	60	39103	28	31
Junior	1.4	46	73096	23	28
Handheld	0.26	42	267568	3	0

Survey times of the two rovers were an order of magnitude higher than for the handheld survey (Table 3), despite the smaller distances covered (Fig. 5A). The point cloud models covered a greater area than for the handheld survey (46–60 m², Junior and Little Blue cf 42 m², handheld; Table 3), though the number of points within the clouds was fewer (Table 3). The point cloud generated by Little Blue contained the fewest points (39103, Table 3), being a little over half of those generated by Junior (73096, Table 3) and only 15 % of those generated by the handheld survey (267568, Table 3). Additionally, point clouds generated by the two rovers possessed data voids (28%, Junior; 31% Little Blue, Table 3) that were not present for the handheld survey. Figure 6 shows perspective views of the surfaces generated by the point cloud models, with overlaid longitudinal and cross-sectional profile lines shown in Fig. 5.

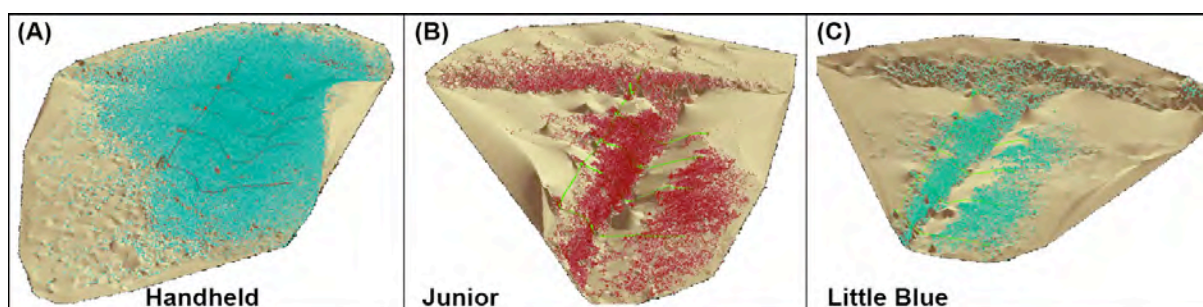


Fig. 6. Elevation models derived from the (A) handheld, (B) Junior and (C) Little Blue point clouds.

The denser point cloud generated by the handheld survey is clearly visible (Fig. 6A), while the Junior (Fig. 6B) and Little Blue (Fig. 6C) models possessed progressively fewer points. Voids observed in the rover point clouds coincided with areas of high slope, or where landscape was obscured by other landscape features (Fig. 6B and C).

Analysis of roughness of the point cloud data revealed that handheld photography generated the most detailed model (57%, Fig. 7A). Roughness measurements dropped substantially with the two rover surveys (13%, Junior; Fig. 7B; 9% Little Blue, Fig. 7C). Regions beyond the immediate gully area were particularly poor in detail, equating to low roughness scores in these areas (Fig. 7B and C).

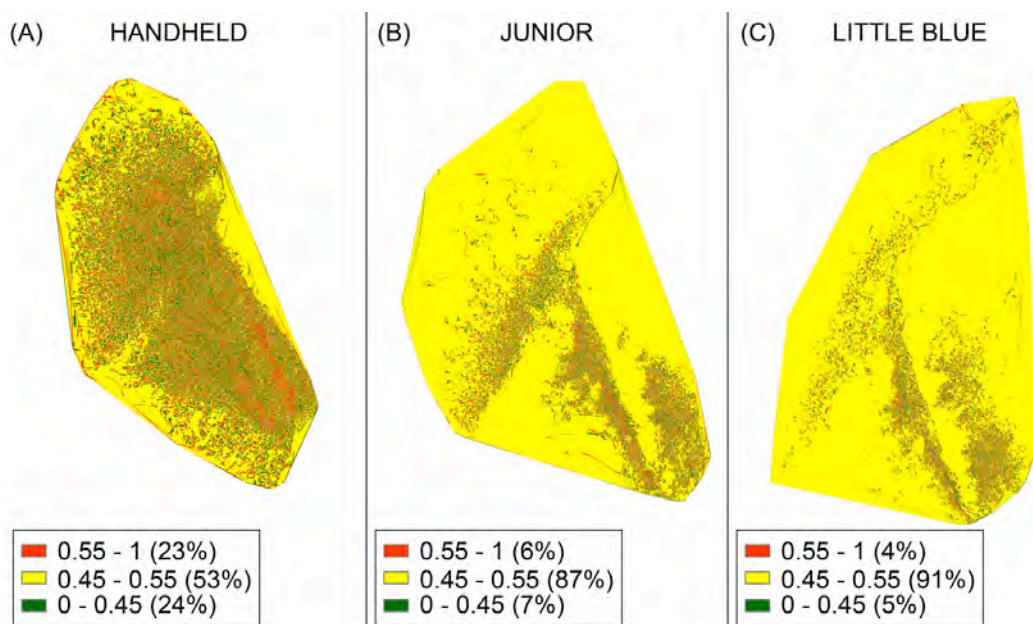


Fig. 7. Roughness measurements derived from the (A) handheld, (B) Junior and (C) Little Blue point clouds.

Discussion

Our SfM trials using small rovers and handheld photography indicated a relationship between camera resolution, the number of images captured and the camera height above the ground. Operating the rovers consistently took far longer than the human-based survey. Lengthy delays were incurred in positioning the rovers and commanding the capture, transmission and receiving of images. In the case of Junior, Wi-Fi dropouts exacerbated this time as image transfer commands needed to be continually resent. The rover surveys revealed issues with rover mobility. Prior to the survey, it was initially considered that the low maximum speeds and turn rates of the rovers would be limiting factors for the survey. Instead lower speeds and turns resulted in higher torque and an increased ability to negotiate steeper slopes. Instead it was found that the small sizes of the rovers to have constrained their mobility. The small size and wheel base of Junior, and to a lesser extent Little Blue, restricted their ability to negotiate

the steeper slopes of the gullies, and the larger (~10 cm) rocks found within the feature. The monocular nature of the video feeds from the navigation cameras also hampered safe rover operations. The limited field of view from the video feed constrained the operator to closely scrutinize the path ahead for safety, before moving the rover to its next position. Even in the case of the more benign environment of the house brick survey, operation and positioning of the rovers took far longer than for a human-based survey (Table 2). This was again due to the limited field of view of the video feed and lack of stereo information, making location estimation of the target more difficult than for the handheld survey. It was noted that the rovers were able to capture larger SfM models than for the handheld run on the gully (Table 3). The increased area covered by the rovers compared to the handheld survey was probably due to more horizontal position of the rover cameras, allowing them to capture more distant elements of the study area. In contrast, the near-vertical orientation of the handheld survey excluded all background except the primary study area. We noted that the detail of these more-distant regions surveyed by the rovers to be very poor (Fig. 7B, C).

Effects of camera height above the ground were found to be another critical factor in successful terrain generation. This was observed by the portions of terrain that were not covered by the rover surveys. The eastern side of the gully was not visible to the rovers as its steep slope caused it to be hidden from view of the rover cameras, as manifested by a lack of points in this area (Fig. 6B and C). Parts of the western bank, and northern areas of the gully were also obscured, leading to the high void values in the resulting point cloud, as compared to the handheld survey (Table 3). We were also unable to drive the rovers on steeper portions of the gully for risk of the vehicles tipping over, further excluding these areas of the gully from surveying. The handheld survey, as with previous research undertaken with UAVs was unencumbered by these restrictions [2, 4, 16].

Camera resolution also adversely affected the quality of the resulting point clouds. This was highlighted by the consistently more detailed point clouds for the handheld trial of the house brick, where rover mobility and safety was less of an issue (Table 2), and the gully survey (Table 3). We noted that Little Blue, using the lowest resolution camera (720 X 576 pixels, Table 1) of the three survey methods, produced point clouds with the lowest point count for both trials, as well as the lowest elevation roughness values (9%, Fig. 7C). Junior, possessing a higher resolution camera (1024 X 768 pixels, Table 1), was able to produce more detailed point clouds, despite being a smaller and less manoeuvrable rover than Little Blue. The handheld survey point clouds were consistently higher in the number of points, accuracy (Table 2 and 3) and roughness (Fig. 7A) than for the two rovers, suggesting that the higher resolution of this camera sensor allowed for more accurate image matching [17, 18]. Subject to additional funding, future versions of the rovers will be equipped with additional sensors, such as inertial navigation units, to assist with position estimation. Roll and turn rates could be measured, and position estimation could be further enhanced by the use of wheel encoders. These measurements would then be used to enhance the accuracy of the resulting terrain model by providing more accurate camera locations.

Implications for Planetary Rovers

This survey was conducted using teleoperation. This is impractical for rovers on Mars where communications delays are prominent [8, 19]. Thus, all surface rover missions have required a degree of autonomy [20, 21, 22, 23, 24, 25]. Additionally, bandwidth limitations place constraints on the number and resolution of images that can be returned [26]. This work highlighted the importance of producing sufficient overlapping images to cover an area of interest, and at high enough resolution, to create a successful SfM model. The rover camera would also need to be mounted high enough to avoid issues with foreground objects obscuring parts of the target. This will remain an issue for smaller rovers, such as Sojourner [12]. In this case possibly joint rover/lander missions may be planned, where a stationary lander would be able to provide greater camera elevation and better view of the terrain, which can then be used to assist the rover. Additionally, a larger lander would have extra space for more powerful processors to enable on-board SfM generation; something not possible with the processors used in this work. Conversely the missions of smaller rovers may be constrained to only produce SfM of their immediate area. This would entail placing engineering constraints on only exploring terrain the rover was able to safely negotiate, assisting in minimising mobility and line of sight limitations.

Future Mars mission may benefit from development of UAV technology, which has been a popular method for SfM capture on Earth [1, 4]. Ongoing developments in computer processing power will also lead to the ability to process SfM point clouds on board a rover, thus reducing the bandwidth requirement for returning multiple images to a ground station. Creation of on board SfM would also open up the possibility of using the point clouds for more accurate obstacle avoidance and route planning, without the requirement of having to carry on board additional range finding sensors. Elimination of these sensors would reduce the power and size requirements of the rovers, lowering the overall cost. In a future mission, the rover would image its surroundings during a traverse. These images would be used to process a point cloud on-board that would be appended with new imagery as the rover progressed. The result would be a map of the surrounding environment that would increase in detail, providing navigational and also geomorphological information for the mission. A version of this process was conducted using the internet to control spatially separated rovers where compression algorithms facilitated transmission of 3D mapping data [27]. Although no internet protocols currently exist for spacecraft operating beyond Earth orbit, a future data sharing and bandwidth protocol may facilitate transmission of SfM point clouds accurate enough to infer small-scale geological features. We note that initial trials of SfM have commenced for imagery of the Curiosity Rover on Mars [28].

Conclusion

SfM has become a widely used method for generating high resolution elevation data, with capture by UAV being the most popular method. We compared the performance of two small rovers using cameras of differing resolution with handheld photography to determine how mobility, camera height above ground and camera resolution impacted on the accuracy of generated point clouds. We found that mobility restrictions and requirements to position the rovers caused lengthy delays in the time taken to complete the surveys using these methods.

The height of the cameras above the ground was the most limiting factor, with parts of the gully being invisible to the sub-30 cm elevation of the rovers compared to the ~1.5 m height of the handheld imagery run. Thus, although SfM surfaces were able to be constructed using our small ground vehicles, limiting factors of camera resolution, mobility, time lag and height above ground need to be factored into collecting data in this way.

References

1. M.J. Westoby, J. Brasington, N.F. Glasser, M.J. Hambrey, and J.M. Reynolds. 'Structure-from-Motion' photogrammetry: A low-cost, effective tool for geoscience applications. *Geomorphology* 179, pages 300-314, 2012.
2. N. Micheletti, J.H. Chandler, and S.N. Lane. Investigating the geomorphological potential of freely available and accessible structure-from-motion photogrammetry using a smartphone. *Earth Surface Processes and Landforms* 40, 473-486, 2014.
3. F. Clapuyt, V. Vanacker, and K. Van Oost. Reproducibility of UAV-based earth topography reconstructions based on Structure-from-Motion algorithms. *Geomorphology* 260, 4-15, doi:10.1016/j.geomorph.2015.05.011, 2016.
4. T.N. Tonkin, N.G. Midgley, D.J. Graham, and J.C. Labadz. The potential of small unmanned aircraft systems and structure-from-motion for topographic surveys: a test of emerging integrated approaches at Cwm Idwal, North Wales. *Geomorphology* 226, 35-43, doi:10.1016/j.geomorph.2014.07.021, 2014.
5. J.R. Jensen. *Introductory Digital Image Processing: A Remote Sensing Perspective*, 2nd edn, Prentice Hall, Upper Saddle River, N.J., 316 pp, 1996.
6. A.L. Albee, R.E. Arvidson, F. Palluconi, and T Thorpe. Overview of the Mars Global Surveyor mission, *Journal of Geophysical Research-Planets*, 106(E10), 23291-23316, doi: 10.1029/2000je001306, 2001.
7. G. Neukum, R. Jaumann, & the HRSC Co-Investigator and Experiment Team. HRSC: The high resolution stereo camera of Mars express, in: *Mars Express: The Scientific Payload*, A. Wilson (ed.), ESA, Noordwijk, The Netherlands, pages. 17-35, 2004.
8. R. Greeley. *Introduction to planetary geomorphology*, Cambridge University Press, New York, 2013.
9. E.G. Cowart. Lunar roving vehicle: spacecraft on wheels. *Proceedings of the Institution of Mechanical Engineers June 1973*, pages 463-491, 1973.
10. B. Glass, G. Briggs, J. Jasper, and K Snook. Evaluation of human vs teleoperated robotic performance in field geology tasks at a Mars analog site. *iSAIRAS 2003*, Nara, Japan, 2003.

11. S.W. Hobbs, J.D.A. Clarke, and G.A. Mann. Field testing Marsobot, A Mars Society Australia robotics project. *Proceedings of the 14th Australian Space Research Conference*, 2014.
12. N.G. Barlow. Mars: An Introduction to its Interior, Surface and Atmosphere, *Cambridge University Press*, Cambridge, 264 pp, 2008.
13. Hobbs, S.W., Clarke, J.D.A., Campbell, K.A., Astrobiology with Mars'Obot: Identifying Microbial Life Forms Using Ground-based Remote Sensing. Astrobiology with Mars'Obot: Identifying Microbial Life Forms Using Ground-based Remote Sensing. *Proceedings from the 15th Australian Space Research Conference*, 2015.
14. J.P. Grotzinger, and 25 colleagues, 2012. Mars Science Laboratory mission and science investigation. *Space Science Reviews* 170, 5-56, 2012.
15. Riley, S.J., DeGloria, S.D., and Elliot, R. A terrain ruggedness index that quantifies topographic heterogeneity. *Intermountain Journal of Sciences* 5, 23-27, 1999.
16. J.C. Ryan, A.L. Hubbard, J.E. Box, J.Todd, P. Chrostoffersen, J.R. Carr, T.O. Holt, and N. Snooke. UAV photogrammetry and structure from motion to assess calving dynamics at Store Glacier, a large outlet draining the Greenland ice sheet. *The Cryosphere* 9, doi: 10.519/tc-9-1-2015, 2015.
17. M.E. Spetsakis, and Y. Aloimonos. A multi-frame approach to visual motion perception. *International Journal of Computer Vision* 6, 245-255, 1991.
18. N. Snavely, S.N. Seitz, and R. Szeliski, R. Modeling the world from internet photo collections. *International Journal of Computer Vision* 80, 189-210, 2008.
19. C. Culbert et al. Activities of the NASA Exploration Team Human Robotics Working Group. *Proceedings of the American Institute of Aeronautics and Astronautics Space 2003 Conference*, Long Beach, Calif, 2003.
20. J.F. Bell III, and 24 colleagues. Mars Exploration Rover Athena Panoramic Camera (Pancam) Investigation. *Journal of Geophysical Research*, DOI: 10.1029/2003JE002070 2003.
21. R. Li, K. Di, A.B. Howard, L. Matthies, J. Wang, and S. Agarwal. Rock modelling and matching for autonomous long-range Mars Rover localization. *Journal of Field Robotics* 24, 187-203, 2007.
22. P.S. Schenker, T.L. Huntsberger, P. Pirjanian, E.T. Baumgartner, and E. Tunstel. Planetary rover developments supporting Mars exploration, sample return and future human-robotic colonization. *Autonomous Robots* 14, 103-126, 2014.
23. J.J. Biesiadecki, E.T. Baumgartner, R.G. Bonitz, B.K. Cooper, F.R. Hartman, P.C. Leger, M.W. Maimone, S.A. Maxwell, A. Trebi-Ollenu, E.W. Tunstel, and J.R. Wright. Mars Exploration Rover surface operations: Driving Opportunity at Meridiani

- Planum. In *IEEE Conference on Systems, Man and Cybernetics*, The Big Island, Hawaii, USA, 2005.
24. R.C. Anderson, A.F.C Haldermann, J. Dohm, and T. Huntsberger. A Dress Rehearsal for the 2003 Mars Exploration Rovers, *Mars Analog Research*, San Diego, California, 2006.
 25. J.J. Biesiadecki, P.C. Leger, and M.W. Maimone. Tradeoffs between directed and autonomous driving on the Mars Exploration Rovers. *The International Journal of Robotics Research*, doi: 10.1177/0278364907073777, 2007.
 26. S. Li, and D.T.H. Kao, D.T.H. Rover-to-orbiter communications on Mars: taking advantage of the varying topology. *IEEE Proceedings*, doi: arXiv:1504.04797v3, 2015.
 27. Guivant, J., Cossell, S., Whitty, M. and Katupitiya, J. Internet-based operation of autonomous robots: The role of data replication, compression, bandwidth allocation and visualization. *J. Field Robotics*, 29: 793–818. doi:10.1002/rob.21432, 2012.
 28. Ostwald, A.M., Hurtado Jr, J.M., 2017. 3D models from structure-from-motion photogrammetry using Mars Science Laboratory images: methods and applications. *Proceedings of the 48th Annual Lunar and Planetary Science Conference*, The Woodlands, Texas. Lunar and Planetary Institute, Houston, TX, abst 1787.

The Little Blue Rover: Robotic Characterisation of Mars Analogue Sites in Arkaroola.

S.W. Hobbs^{a,b*}, D.J. Paull^a and J. D. A. Clarke^b

^a School of Physical, Environmental and Mathematical Sciences, University of New South Wales Canberra, Australian Defence Force Academy, Northcott Drive, Canberra, Australian Capital Territory 2600, Australia.

^bMarsSociety Australia, P.O. Box 327, Clifton Hill, VIC 3068, Australia

*Corresponding author. Tel.: +6126268 8455; E-mail: swhobbs2000@hotmail.com.

Summary

The Mars'O Bot project proposes to develop affordable rover platforms suitable for undertaking scientific exploration in terrestrial environments analogous to Mars. We conducted science trials of a small Sojourner size rover, "Little Blue", in the Arkaroola region, South Australia, between 2 and 10 July this year. The Arkaroola site contains extremophiles inhabiting thermal environments, which are adapted for living in areas hostile to regular life forms. Evidence of past thermal environments have been found in different areas of Mars (eg Gypsum deposits, Gusev Crater) and our aim is to determine how well analogous environments at Arkaroola can be characterised using open source robotics and instrumentation. Our work assists in providing a baseline for what an early Martian environment might have been like, as well as provides guidance on unmanned field survey techniques, and performance of commercial grade instruments.

Keywords: Astrobiology, robotics, remote sensing, Mars analogue research, South Australia.

Introduction

The Mars'O Bot project proposes to develop affordable rover platforms suitable for undertaking scientific exploration in terrestrial environments analogous to Mars. Previous research with Marsobot has included engineering trials in Arkaroola, South Australia [1], in characterising extreme life forms within hot spring environments in the Rotorua area, Taupo Volcanic Zone, New Zealand [2]. Table 1 lists the rovers built as part of the Marsobot project to date, key instruments and deployed locations. In this contribution we conducted science trials of a small, teleoperated rover, "Little Blue", in the Arkaroola region, South Australia, between 2 and 10 July 2016. The Arkaroola site contains extremophiles inhabiting thermal environments, which are adapted for living in areas hostile to regular life forms. Evidence of past thermal environments has been found in different areas of Mars (eg Gypsum deposits, Gusev Crater, [3]). Other extremophiles, such as hypoliths, are also present at Arkaroola. Hypoliths are photosynthetic, bacteria-based life forms that are typically found on the underside of quartzite rocks in arid environments [4, 5, 6]. The translucent nature of quartzite rocks allow them to transmit enough sunlight that allow hypoliths to photosynthesis, while also condensing sufficient

moisture to allow their survival [7]. Hypoliths use the light filtered by the quartzite rock as well as water condensed around it to survive [4, 5]. Our aim is to determine how well analogous environments at Arkaroola can be characterised using commercially available robotics and instrumentation as compared to human-based surveys using commercial equipment.

Table 1. Previous Marsobot rovers, deployments and instrumentation.

Robot	Main instruments	Deployed locations	Year
Junior	Multispectral camera, IR and weather	ACT, New Zealand	2012, 2015
Little Blue	Multispectral camera, IR and weather	ACT, Arkaroola	2014, 2015, 2016
Miner	Navigation camera, GPS, weather	ACT, Arkaroola	2014, 2016
A4 Rover	Multispectral camera, IR and weather	ACT, NSW, Arkaroola	2015, 2016

Methods



Fig. 1 Overview of Main instruments carried on Little Blue: (1) FPV navigation camera, (2) MMC, (3) Non-contact thermometer swing arm bay (4) Webcam for macroscopic

Little Blue (Fig. 1), measuring 62 cm x 45 cm and weighing 7.5 kg, was built to approximate the size of Sojourner, a microrover deployed to Mars in 1997 [8]. The Little Blue chassis was based on a heavily modified Toyabi Monster truck with the original motors being replaced with four Dagu 1:131 12 V motors coupled to the hub of each wheel and driven by a Sabretooth 2 x 24 A motor controller to provide four wheel drive capability.

Little Blue was equipped with range finding ultrasonic sensors and a first person video (FPV) camera for navigation. The rover was developed with independent power supplies for the operation of the mobility system and the science system to provide redundancy allowing for useful science to be conducted in case of mobility failure, and vice versa. A 14.6 V 5 Ah Lithium Polymer (LiPo) battery has been used to power the mobility system, while an 11.2 V 2.4 Ah LiPo battery has provided power to the wireless camera and Arduino. Power has been supplied through two solar panels to a maximum of 16 W. The solar panels were connected via a LiPo charger wired into the 11.2 V battery. A rear facing ultrasonic sensor has been placed aft of the solar panels, providing some degree of hazard detection while reversing the rover. The ultrasonic sensor was rear facing as the cameras on Little Blue were unable to see behind the rover. Readings from the sensor facilitated detection of potentially hazardous objects the rover might otherwise have reversed into. In the case of positioning the rover we were less concerned with position accuracy than with safety of the vehicle when it came to reversing as all of our scientific instruments were forward facing.

Little Blue was designed to be manoeuvred using skid steering in a similar manner to the Soviet Lunokhod rover [9]. Skid steering (tank steering) operates by varying the speed of motors on either side of the vehicle. The rover platform was characterised in a Mars Analogue environment using standardised US National Institute of Standards and Technology (DHS-NIST-ASTM for response robots; [10, 11] engineering trials conducted at Arkaroola, South Australia [1]. The results of those tests demonstrated that Little Blue was able to operate in outdoor environments possessing geology that would be expected to be found on Mars [1].

We have upgraded the science payload carried by Little Blue. Figure 1 shows an overview of the current configuration of the rover, with key instruments numbered. Along with a navigation camera (1, Fig. 1) the primary science instrument carried on the rover is a custom made multispectral camera (MMC), (2, Fig. 1) which used a Raspberry Pi NoIR camera (pixel resolution of 2592 x 1944) and a filter wheel consisting of visible pass, #25A red, and long pass NIR filters with wavelength ranges listed in Table 1. The standard sensitivity curve for CMOS cameras indicate usable sensitivities between 400-900 nm [12, 13, 14]. Although CMOS sensors are capable of detecting NIR wavelengths between 900-1000nm [12, 13, 14], we considered the sensitivity falloff in this portion of the spectrum to be too noisy to produce meaningful results. We thus considered 400-900nm to be the useful sensitivity range of our instrument to reduce noise effects. The filters were mounted on a filter wheel controlled via serial commands from an open source Arduino Uno 8-bit microcontroller. This microcontroller was well supported and

has been used in many robotics applications [15, 16]. Little Blue captured multispectral images by sequentially photographing through one visible, one red and one near infrared (NIR) filters. These separate images were transmitted to a ground station where they are exploited further. This type of camera was also used on the Mars Pathfinder mission [17].

We incorporated a Melexis non-contact thermometer on a swing arm in order to sample ground temperature measurements (3, Fig. 1). Temperature was found to be an important factor in the determining the types of extremophiles that exist in ecosystems [18, 19]. We trialled the use of the Melexis non-contact thermometer examining extremophiles in New Zealand in 2015 [2]. We found that the setup of the Melexis on Junior restricted its freedom of movement, rendering it difficult to point downwards enough to sample temperatures immediately in front of the rover. To mitigate this issue, we mounted a Melexis to face directly downwards on a swing arm on Little Blue. On receiving a serial command, the swing arm would rotate 90° from its stowed position to sample a 10 X 10 cm area immediately in front of the rover. This design would enable Little Blue to sample extremophiles living within hot spring environments.

The NIR sensitive webcam originally used on Marsobot Junior [2] was used as an additional imaging experiment on Little Blue (4, Fig. 1). The webcam was fitted with a #25A red filter, similar to that used in the MMC, in order to generate visible/NIR pair single filter images useful for identifying the presence of photosynthetic life [20].

A BMP085 temperature and pressure sensor (Bosch Sensortec 2015) and a DHT 11 temperature and humidity sensor [21] provided Little Blue with the ability to sense weather information. Fig. 1 shows the location of the power and controller systems for Little Blue. We based control of the sensor and science suite of this rover on the Arduino 8-bit microcontroller. This microcontroller is well supported and has been used in many robotics applications [15, 16]. The Arduino Uno can be programmed using the open source Arduino environment and possesses 14 digital input/output pins and six analogue input pins. We used these pins on Little Blue to interface with the ultrasonic sensor (Fig. 1A), operate a relay to power the camera (Fig. 1B), control the camera filter wheel servo (Fig. 1B) and read data from the two weather sensors (Fig. 1E).

Table 1. Wavelength ranges for filters used in custom multispectral camera.

Filter	Bandpass
Visible	400–700 nm
720 nm NIR short and long pass filter	720–1000+ nm

In order to achieve this we compared the performance of Little Blue’s suite of sensors with those of commercially available instruments and human-based surveys. The instruments carried by Little Blue include a multispectral camera (MMC), non-contact IR thermometer; ambient temperature sensors, a webcam for macroscopic imaging and proximity distance sensors for obstacle avoidance. We used a commercially available multispectral camera, the Tetracam as a comparative instrument. We used time taken and data collected as metrics for performance, and also compared the spectral response of the Tetracam with the MMC of Little Blue.

We corrected our MMC images by using dark current offset [22, 23], vignetting correction [24, 25, 26] and empirical linear regression to radiometrically correct images from our camera. This method assumes a linear relationship exists between values measured by the multispectral camera and surface reflectance methods gathered by a laboratory spectrometer [27, 28, 29, 30] or similar instrument. The generated calibration equation takes the form [31]:

$$DN = K \times R + F \tag{1}$$

where DN is the digital number, where K is the slope, R is the reflectance and F is the offset. The offset and slope of the calibration equation are typically known as calibration coefficients [31].

We conducted field trials of Little Blue on basaltic plains approximately 20 km from the Arkaroola Village and observed to possess hypolith-bearing quartzite pebbles. We also conducted tests at Ochre Wall, approximately 15 km from Arkaroola Village. The 780 Ma Ochre wall site consists of siltstone layers that have been strongly oxidised by hydrothermal fluids and deeply penetrating groundwater. Although this site did not contain hypoliths, we aimed to test the performance of the MMC and Tetracam in distinguishing between different rock types site as well as identifying the oxidisation present at the Ochre Wall site.

Results

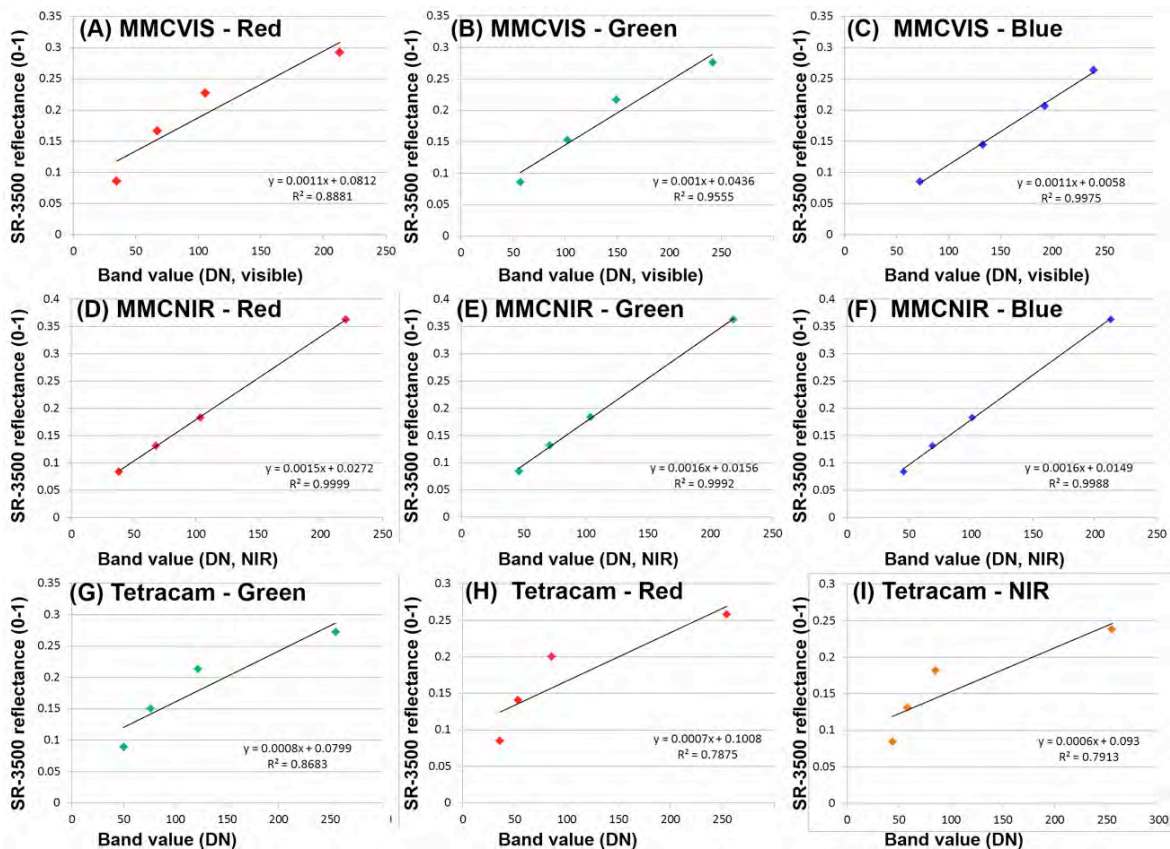


Fig. 2. Linear regression of custom multispectral camera, Tetracam and SR -3500 based

on four level calibration targets. SR/SM-3500 reflectance units vary between 0 and 1 while the Tetracam and MMC units are in DN.

Fig. 2 shows the empirical regression results from the MMC and Tetracam compared to the SR-3500 reflectance values. The strength of each relationship is shown as R-squared values for each of the trend-lines in Fig. 2. As seen in Fig. 2 the R-squared values were consistently higher for the MMC visible/NIR filters (0.8881–0.9999, Fig. 3A–F) than the Tetracam (R-squared: 0.7875–0.8683, Fig. 3G–I). The red band of the MMC NIR wavelengths was highly related to the SR-3500 (R-squared: 0.99999, Fig. 3D), while the green band provided the best relationship with the Tetracam NIR wavelengths (R-squared: 0.8683, Fig. 3G).

Table 2. Comparison of performance between Little Blue.

Survey type	No. of hypoliths	Time	Distance travelled	Performance factor
Site 1				
Little Blue	3	12	25	0.25
Human	8	0.6	3	13.3
Ochre Wall	Sites visited	Time	Distance travelled	Performance factor
Little Blue	5	21.88	17	.23
Human	5	0.4	25	12.5

Table 2 shows metrics for the sites visited and times taken to conduct human and robotic surveys with Little Blue. At our first field site we conducted analysis on radioactive hot springs in Arkaroola with Little Blue’s multispectral camera and IR thermometer (Fig. 3A). Initial qualitative results using near-infrared (NIR) false colour analysis indicate the MMC was capable of identifying the photosynthetic life forms living within the hot spring, though the NIR reflectance of the subsurface biota was partially absorbed by the overlying water (Fig. 3B). Temperature readings of the hot spring indicated a surface water temperature of 29–30°C, with an ambient temperature and humidity of 14–15°C and 48.6%. Fig. 3C shows the Arkaroola basaltic plains where the hypolith trials were conducted. A white quartzite pebble is immediately in front of Little Blue. A false colour view from the MMC is shown in Fig. 3D. Results from the macroscopic webcam of the rover of the underlying regolith and hypolith containing quartzite pebbles are shown in Fig. 3E and F respectively. As shown in Fig. 3F the presence of hypoliths were difficult to determine using this camera due to the red filter being unable to clearly separate visible and NIR wavelengths.



Fig. 3. (A) Little Blue at the hot spring. (B) False-colour view of the hot spring from the MMC. Photosynthetic algal mats are revealed as red in NIR. (C) Little Blue undertaking tests to identify hypoliths at Arkaroola, one of which is immediately right of the rover. (D) False-colour image from MMC of hypolith shown in part A. (E and F) Images of ground and hypoliths from the Little Blue webcam

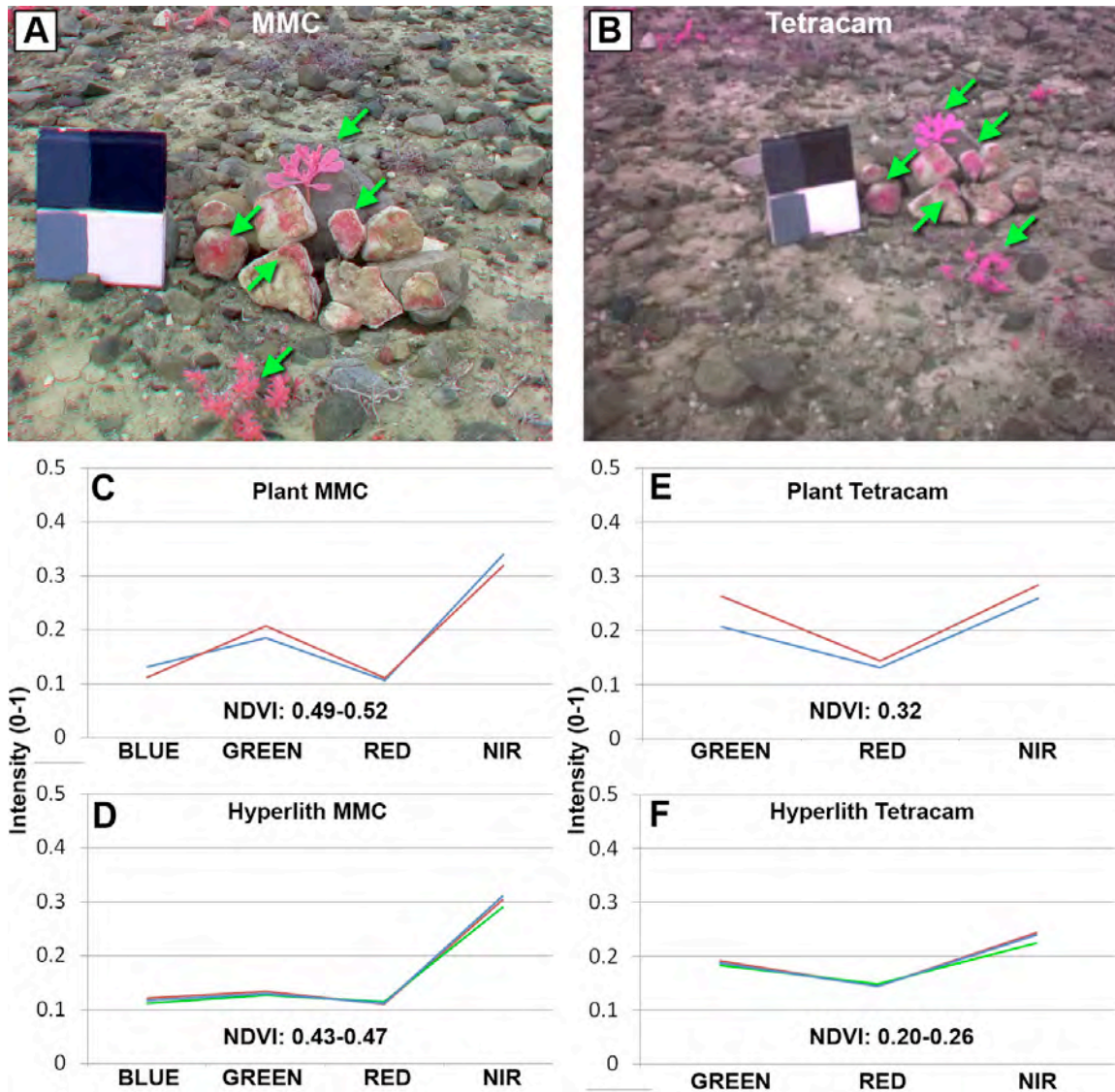


Fig. 4 (A) False-colour view of hypoliths and calibration panel from the MMC. Arrows highlight locations of samples for spectra. (B) False-colour view of hypoliths and calibration panel from the Tetracam. Arrows highlight locations of samples for spectra. (C) Spectra of two plant samples from MMC with NDVI range shown. (D) Spectra of three hypolith samples from MMC with NDVI range shown. (E) Spectra of two plant samples from Tetracam with NDVI range shown. (F) Spectra of three hypolith samples from Tetracam with NDVI range shown.

Our second field experiment compared the performance differences between robotic and human exploration of hypoliths, photosynthetic life forms living underneath quartzite pebbles on stony plains in Arkaroola (Fig. 3C). We found that even with teleoperation, identification of hypoliths with Little Blue took up to 65 times longer than using a human (Table 2). Additionally, Little Blue was not equipped to extract the hypoliths, which was easily achieved during the human-based survey. Multispectral analysis of hypoliths and plant material was conducted using Little Blue's MMC and the Tetracam (Fig. 4A and B). False colour analysis showed both the MMC and Tetracam were able to easily

distinguish photosynthetic biota from the surrounding material. Green arrows (Fig. 4A-B) show the location of pixels sampled for spectral analysis (Fig. 4C-F). Spectral analysis of plant material and hypoliths of the Tetracam and MMC (Fig. 4C-F), showed larger differences between the two plant samples (Fig. 4C, E), than with the three hypolith samples (Fig. 4D, F).

NDVI values for the hypolith and plant samples derived from the MMC were higher (0.43-0.47 Hyerlith; 0.49-0.52, plant, Fig. 3C and D) than for the Tetracam (0.2-0.26 Hyerlith; 0.32, plant, Fig. 4E and F).

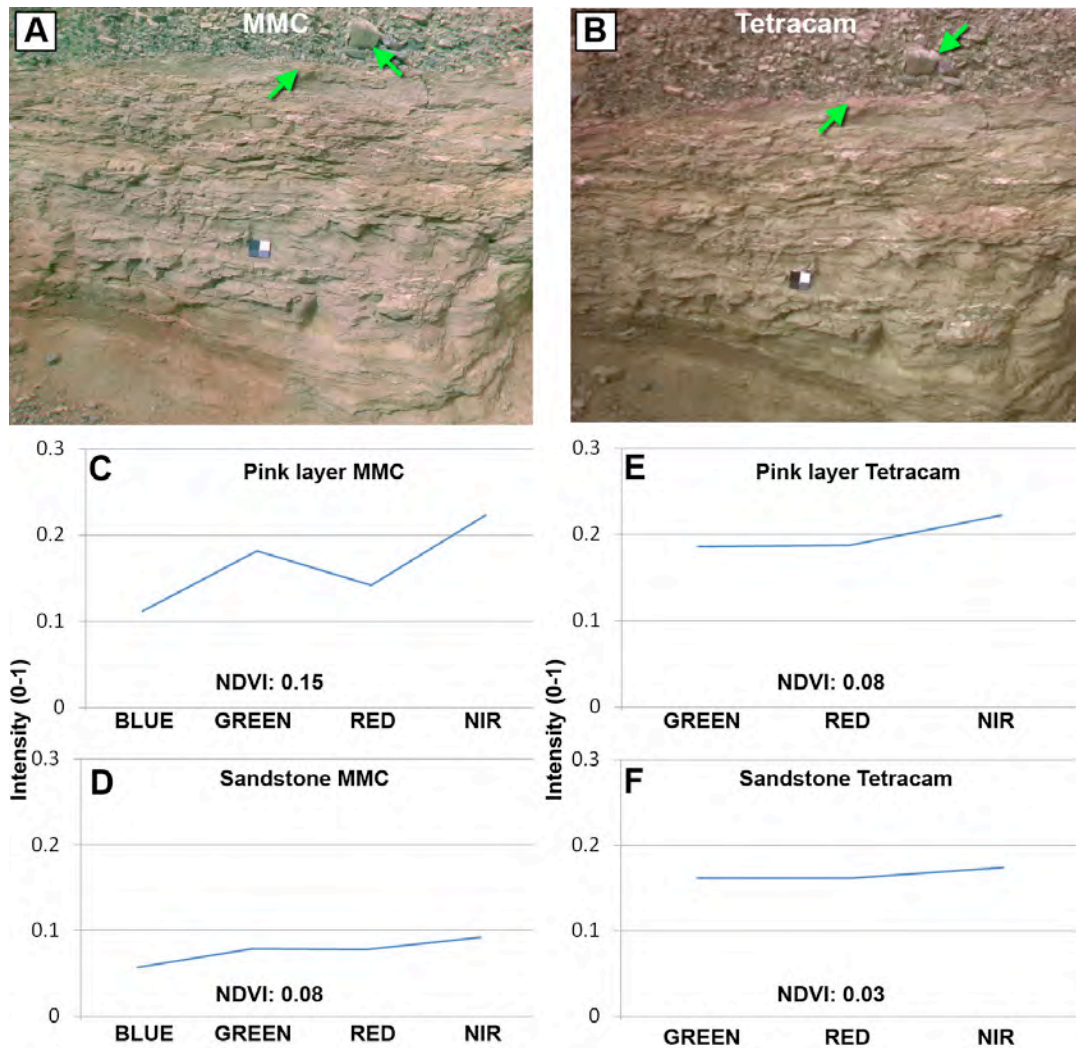


Fig. 5 (A) False-colour view of ochre wall and calibration panel from the MMC. Arrows highlight locations of samples for spectra. (B) False-colour view of ochre wall and calibration panel from the Tetracam. Arrows highlight locations of samples for spectra. (C) Spectra of a pink rocky layer sample from MMC with NDVI range shown. (D) Spectra of a sandstone sample from MMC with NDVI range shown. (E) Spectra of a pink rocky layer sample from Tetracam with NDVI range shown. (F) Spectra of a sandstone sample from Tetracam with NDVI range shown.

We conducted an analysis of the Ochre Wall site in Arkaroola. The Ochre Wall formed

an eastern embankment of a perennial stream, the bed of which consisted of rounded stones 5-15 cm in diameter embedded within a sandy matrix. Although the overall surface was rough, we were able to operate Little Blue at the site and traverse the rover 17 m along the stream bed, sampling five different sites. As with the hypolith trial we also conducted a human survey of the Ochre Wall area, sampling multispectral images with the Tetracam for comparison. Fig. 5A and B show false colour images of the Ochre Wall captured by the Little Blue MMC and Tetracam respectively. The top 50 cm of the wall contains an overlying matrix of stones ranging from 2-20 cm. We chose the largest of these, a ~20 cm sized rounded sandstone, to conduct spectral analysis on for the two cameras (green arrow, Fig. 5A, B). We also observed a ~10 cm thick layer immediately below this rocky matrix that appeared red toned in false colour imagery, with which we also conducted spectral analysis (middle green arrows, Fig. 5A, B).

Fig. 5 C-F shows the results for spectral analysis of the sandstone and pink layer in the Ochre Wall site. Both the MMC and Tetracam revealed a higher NIR than visible reflectance in the pink layer, equating to positive NDVI for this region (Fig. 5C and E). The sandstone spectrum showed less variation between bands, and NDVI values were lower overall (Fig. 5 D and E).

Discussion

We investigated the utility of operating Little Blue in field environments in Arkaroola and were able to characterise the open source MMC against a professional multispectral camera, the Tetracam. We found that analysis of variance for the Tetracam produced lower values of reflectance to reflectance values acquired by a laboratory spectrometer, compared to the MMC (Fig. 2). We noted during capture of the hypoliths and vegetation the NIR channel would frequently saturate, possibly skewing regression results. We found that the MMC did not tend to saturate, possibly allowing for stronger relationships to occur between DN and reflectance values (Fig. 2).

We found that human-based surveys conducted at our test sites were up to 55 times faster than those performed by Little Blue (Table 2), indicating that even for teleoperated robots, times required to perform tasks will be much slower. Apart from the moon, where two Lunakhod rovers were directly controlled from Earth [30], teleoperation is impractical for any planetary science mission, given the communications delay imposed by the vast distances involved [32, 33]. Thus, all surface rover missions have required a degree of autonomy [24, 34, 35, 36]. The vastly increased risk to missions, as well as the slow nature of autonomous operation exacerbates the time required to undertake scientific analysis, including photography, on a planetary surface. Future Mars missions may employ robotic rovers controlled from orbit or a nearby base in a mission similar to that proposed by [37]. Although this would increase operation time, our experiments show that human operated surveys provide a much faster method for acquiring data.

Ground robotic surveys could also be applied in terrestrial environments where human access would be difficult due to dangerous conditions, or where the fragility of the region would preclude such activity. An example of this is within the Antarctic Dry Valleys where extreme forms of life living in this region are highly sensitive to damage caused by human field excursions [38, 39, 40]. The Little Blue Rover in particular was designed to minimize the environmental impact of sampling in fragile areas, with its large

wheels allowing for a maximum weight on the surface of each wheel of 1.75 kg, versus ~70+ kg for a human survey. In contrast, the NASA Mars Exploration Rovers and Curiosity Rover exerted 11.4 kg per wheel and 57 kg per wheel on the Martian surface respectively [36, 41].

The instruments carried on Little Blue were able to successfully return useful data on the local environment. The MMC and Tetracam were both able to produce multispectral images capable of distinguishing between photosynthetic biota and surrounding material. NDVI values for the MMC were higher than for the Tetracam (Fig. 4C-F). These findings possibly indicate that the MMC possesses a higher radiometric resolution than for the Tetracam sensor, and is better able to distinguish between different NIR wavelengths. Results were comparable for the Ochre Wall test site, where spectra were obtained (Fig. 5). Although a layer was found where NIR reflectance was greater than for visible wavelengths, NDVI values were much lower than for the sampled photosynthetic specimens (Fig. 4). We thus found that both the MMC and Tetracam were able to return useful information. The inclusion of a spectrometer sensitive to shortwave infra-red wavelengths would assist in further characterising mineralogy, though these instruments are well beyond the budget of the Marsobot project [42]. Our testing of open source instruments within an environment analogous to those extant on early Mars provide useful benchmarks for designing future robotic astrobiological missions targeting such features.

Conclusion

We compared the performance of a custom made multispectral camera, the MMC, and robotic rover, Little Blue, using off the shelf parts and open source electronics with a commercial grade multispectral camera and a human conducted survey in Mars analog environments in Arkaroola. It was found that the results from the MMC were comparable with, and in some cases, outperformed the commercial camera and provided sufficient spectral resolution to readily distinguish vegetation from other samples. Little Blue would be useful for operation in fragile environments on Earth where direct human-lead surveys would be hazardous or impractical, though rover operations proved to be consistently slower than for human-based surveys. Time taken to complete tasking, as well as the number of instruments able to be carried on board, remain limiting factors for conducting robotic surveys of this type, even for teleoperated vehicles.

Acknowledgements

The authors would like to gratefully acknowledge the assistance of Mr Andrew Wheeler, Sabina and Nadia Hobbs, and Mars Society Australia.

References

1. Hobbs, S.W., Clarke, J.D.A., Mann, G.A. "Field testing Marsobot: a Mars Society Australia robotics project". *Proceedings of the 14th ASRC Conference*, 2014.

2. Hobbs, S.W., Clarke, J.D.A., and Campbell, K.A. Astrobiology with Mars'Obot: identifying microbial life forms using ground based remote sensing. *Proceedings of the 15th ASRC Conference*, 2015.
3. Ruff, S.W., Farmer, J.D., Calvin, W.M., Herkenhoff, K.E., Johnson, J.R., Morris, R.V., Rice, M.S., Arvidson, R.E., Bell III, J.F., Christensen, P.R., and Squyres, S.W., Characteristics, distribution, origin and significance of opaline silica observed by Spirit rover in Gusev Crater, Mars. *J. Geophys. Res.* 116, E00F23, 2011.
4. Budel, B., and Wessels D.C.J. Rock inhabiting blue-green algae from hot arid regions. *Archiv fur Hydrobiology* 92:385–398, 1991.
5. Cockell, C.S., Rettberg, P., Horneck, G., Scherer, K., and Stokes, D.M. Measurements of microbial protection from ultraviolet radiation in polar terrestrial microhabitats. *Polar Biol* 26:62–69, 2003.
6. Cockell, C.S., and Stokes, M.D. Widespread colonization by polar hypoliths. *Nature* 431:414ADS, 2004.
7. Berner, T, and Evenari, M. The influence of temperature and light penetration on the abundance of the hypolithic algae in the Negev Desert of Israel. *Oecologia* 33:255–260, 1978.
8. Hayati, S., Volpe, R., Backes, P., Balaram, J., Welch, R., et al., “The Rocky 7 Rover: a Mars sciencecraft prototype”. *Proceedings of the 1997 IEEE International Conference on Robotics and Automation*, 2458-2464, 1997.
9. NASA National Space Science Data Center. Luna 17/lunokhod, 2005. Accessed online on 15/5/05 <http://nssdc.gsfc.nasa.gov/database/MasterCatalog?sc=1973-001A>.
10. Jacoff, A., Messina, E., and Evans, J., “Experiences in Deploying Test Arenas for Autonomous Mobile Robots”. *Intelligent Robots and Systems Proceedings*, 2003.
11. Jacoff, A., Wavering, A., Messina, E., Virts, A., Huang, H., and Downs, A., “Response Robots – DHS/NIST sponsored evaluation exercises”. *NIST Technology Administration, US Department of Defence* 90, pp231, 2010.

12. Lelong, C.C.D., Burger, P., Jubelin, G., Roux, B., Labbe, S., and Baret, F. Assessment of unmanned aerial vehicles for quantitative monitoring of wheat crop in small plots. *Sensors* 8, 3557-3585, 2008.
13. Hunt, E., Hively, D.W., Fujikawa, S., Linden, D., Daughtry, C., and McCarthy, G., 2010. Acquisition of NIR-green-blue digital photographs from unmanned aircraft for crop monitoring. *Remote Sens.* 2, 290-305, 2010.
14. Geipel, J., Link, J., Wirwahn, J.A., and Claupein, W. A programmable aerial multispectral camera system for in-season crop biomass and nitrogen content estimation. *Agriculture*, doi:10.3390/agriculture6010004, 2016.
15. Shue, S., Hargrove, C., and Conrad, J., Low Cost Semi-Autonomous Sentry Robot. *IEEE Proceedings*, 2012.
16. Gonullu, M.K., Development of a Mobile Robot Platform to be used in Mobile Robot Research, *Masters thesis*, Middle East technical University, 2013.
17. Farrand, W.H., Bell III, J.F., Johnson, J.R., Bishop, J.L., and Morris, R.V. Multispectral imaging from Mars Pathfinder, in: *The Martian Surface: Composition, Mineralogy and Physical Properties*, ed. J.F. Bell III, *Cambridge University Press*, New York, 2008.
18. Barnes, S.M., Delwiche, C.F.D., Palmer, J.D., Dawson, S.C., Hershberger, K.L., and Pace, N.R., Phylogenic perspective on microbial life in hydrothermal ecosystems, past and present, In Bock, G.R., Goode, J.A., (Eds), *Evolution of Hydrothermal Ecosystems on Earth (and Mars?)*, Ciba Foundation Symposium 202, John Wiley and Sons, Chichester, 1996.
19. Capece, M.C., Clark, E., Saleh, J.K., Halford, D., Heintz, N., Hoskins, S., and Rothschild, L.J. Polyextremophiles and the constraints for terrestrial habitability. J. Seckbach et al. (eds.), *Polyextremophiles: Life Under Multiple Forms of Stress*. Cellular Origin, Life in Extreme Habitats and Astrobiology 27, 3–59, DOI 10.1007/978-94-007-6488-0_1. 2013
20. Rabatel, G., Gorretta, N., and Labbe, S. Getting simultaneous red and near infrared bands from a single digital camera for plant monitoring applications, in: *Proceedings of the International Conference of Agricultural Engineering (CIGR-AgEng)*, Valencia, Spain, 6 pp, 2012.
21. Nguyen, T., Slonaker, J., and Kadous, M., “Semi-autonomous wireless controlled robot.” *Capstone Senior Design Project*, Indiana University, 2012.
22. Mullikin, J.C. Methods of CCD camera characterization. *Proceedings of SPIE* 2173, 73-84, 1994.

23. Mansouri, A., Marzani, F., and Gouton, P. Development of a protocol for CCD calibration: application to multispectral imaging system. *International Journal of Robotics and Automation*, 20, DOI: 10.2316/Journal.206.2005.2.206-2784, 2005.
24. Bell III, J.J., and 24 colleagues. Mars Exploration Rover Athena panoramic camera (Pancam) investigation. *J. Geophys. Res.* 108, doi: 10.1029/2003JE002070, 2003.
25. Goldmann, D.B. Vignette and exposure calibration and compensation. *IEEE transactions on pattern analysis and machine intelligence* 32, 2276-88, 2010.
26. Kelcey, J., and Lucieer, A. Sensor correction and radiometric calibration of a 6-band multispectral imaging sensor for UAV remote sensing. *International Archives of the Photogrammetry, Remote Sensing and Spatial Information Sciences*, XXXIX-B1, Melbourne, Australia, 2012.
27. Smith, G.M., and Milton, E.J. The use of empirical line method to calibrate remotely sensed data into reflectance. *Int. J. Remote Sens.*, 20, 2653-2622, 1999.
28. Edirisinghe, A., Chapman, G.E., and Louis, J.P. A simplified method for retrieval of ground level reflectance of targets from airborne video imagery. *Int. J. Remote Sensing* 22, 1127-1141, 2001.
29. Karpouzli, E., and Malthus, T. The empirical line method for the atmospheric correction of IKONOS imagery. *Int. J. Remote Sensing* 24, 1143-1150, 2003.
30. Wang, C., and Myint, S.W., 2014. A simplified empirical line method of radiometric calibration for small unmanned aircraft systems-based remote sensing. *IEEE Journal of Selected Topics in Applied Earth Observations and Remote Sensing*, 8, 1876-1885.
31. Edirisinghe, A., Louis, J.P., and Chapman, G.E. Radiometric calibration of multispectral airborne video systems. *Int. J. Remote Sensing* 20, 2855-2870, 1999.
32. Greeley, R. Introduction to planetary geomorphology, *Cambridge University Press*, New York, 2013.
33. Culbert, C. et al. Activities of the NASA Exploration Team Human Robotics Working Group. *Proceedings of the American Institute of Aeronautics and Astronautics Space 2003 Conference*, Long Beach, Calif, 2003.
34. Biesiadecki, J.J., Baumgartner, E.T., Bonitz, R.G., Cooper, B.K., Hartman, F.R., Leger, P.C., Maimone, M.W., Maxwell, S.A., Trebi-Ollenu, A., Tunstel, E.W., and Wright, J.R. Mars Exploration Rover surface operations: Driving Opportunity at Meridiani Planum. In *IEEE Conference on Systems, Man and Cybernetics*, The Big Island, Hawaii, USA, 2005.

35. Li, R., Di, K., Howard, A.B., Matthies, L., Wang, J., and Agarwal, S.. Rock modelling and matching for autonomous long-range Mars Rover localization. *Journal of Field Robotics* 24, 187-203, 2007.
36. J.P. Grotzinger, and 25 colleagues. Mars Science Laboratory mission and science investigation. *Space Science Reviews* 170, 5-56, 2012.
37. Aldrin, B. Mission to Mars. *National Geographic Society*, Washington, USA, 258pp, 2013.
38. Tangley L. Who's polluting Antarctica? *Bioscience* 38, 1988.
39. Ronayne, J., and Boag, C. Science and technology in Australasia, Antarctica and the Pacific Islands, *Longman*, pp. 287-306, 1989.
40. Noble, N. Robots and their place in Antarctica. Literature Review, *University of Canterbury*,
www.anta.canterbury.ac.nz/documents/GCAS_1/Noble_Nicola_Lit.Review.pdf,
website accessed 21 June 2016.
41. Lindemann, Randel A., and Chris J. Voorhees. "Mars Exploration Rover mobility assembly design, test and performance." *Systems, Man and Cybernetics, IEEE International Conference*. Vol. 1. IEEE, 2005.
42. Brown, Adrian J., T.J. Cudahy, and M.R. Walter. "Short Wave Infrared Reflectance Investigation of Sites of Palaeobiological Interest: Applications for Mars Exploration." *Astrobiology* 4, no. 3 (2004): 359–76.
doi:10.1089/ast.2004.4.359, 2004.

Designing an Experiment to Improve the Understanding of Thermal Convection to aid Gas Gap Design of Mars Rovers

Siddharth Pandey¹, Sean Tuttle², John Young³

¹PhD Student, ²Senior Lecturer, ³Associate Professor at the School of Engineering and Information Technology, University of New South Wales, Canberra, Australia

Summary: Solid thermal insulation such as thermoplastics and silica aerogel material have been used in Mars surface spacecraft designs to protect internal electronics and instrumentation of the rovers/landers from harsh Martian temperatures. However, several critical factors, such as fear of contamination of instrument collected samples, difficulty during spacecraft assembly and testing and extra volume and mass occupation tend to lead us to look at other alternative thermal insulation techniques for Mars surface-bound spacecraft design. Gas gaps are carefully designed hollow spaces around the protected volumes within the rover that fill with Martian atmosphere, primarily CO₂ to provide insulation. Several spacecraft thermal design groups have presented this technique as a viable technique but further analysis and characterization of these gas gaps is required to better understand and predict the onset of thermal convection within the trapped atmosphere that might diminish the benefits of this thermal insulation technique. Natural convection within horizontal enclosures is modeled using CFD for 2D geometries and the onset of convection is compared from calculated temperature distributions with that from analytical calculations based on empirical data and that published by other groups. The experimental setup is presented for future tests to validate the same.

Introduction

Mars has a cold environment and machines operating on its surface require efficient thermal insulation to keep critical payload and subsystems (e.g. batteries, camera parts) within desired operable temperature ranges[1]. Standard spacecraft thermal insulation solutions (e.g. Kapton sheets and Multilayer insulation (MLI)) are effective while spacecraft is transiting through space but cannot protect flight hardware against dynamic thermal and structural loads during entry, descent, landing and operations in Mars atmosphere[1]. To this end, previous surface missions have used special low mass density and low thermal conductivity options such as thermoplastics and Silica based foam material to considerable effectivity[1, 2]. Thermal insulations take up valuable mass and volume allocations within the rover therefore priority is given to materials with the lowest heat transfer coefficient value per occupied volume and mass. Other important selection criteria are availability of insulation material, structural rigidity, convenience during rover assembly integration and testing and non-interference with instruments onboard the rover[2]. These rule out the available solutions mentioned above; Si based foam is hard to procure[2], is also delicate and require supports to hold them in place which create complications during assembly [3] and testing and increases mass allocation. An alternative is using gas gaps as a thermal insulation technique. It utilises the Mars surface atmosphere (with average pressure of

6-11mbar and low thermal conductivity, (96% CO₂ with average $k_{\text{CO}_2_{\text{mars}}}$ = 0.01 W/m-K)) to fill narrow cavities around sensitive hardware to protect against heat loss. [3-6]. This reduces the overall system mass and volume required by conventional insulants, which is a tremendous advantage for an interplanetary mission in bringing down cost and development time. Therefore, bulky solid thermal insulation is replaced by designing gas gaps to vent in ambient Mars atmosphere and protect warm electronic enclosures. However, natural thermal convection can set in if the gas gaps are designed to be too wide, also the effectiveness of the system diminishes beyond critical gap sizes, eating into precious volume allocations within the rover[4]. To create design guidelines that help estimate the contribution of heat loss via convection, an understanding of the impact of several relevant gap configurations on the onset and stabilization of convective heat transfer within them is required.

Review of Current State of the Art

Fundamentally, natural convection in enclosures has been reported to be a complex, chaotic phenomenon. There is strong thermal-fluid coupling, with sensitive dependency of the heat transfer on the enclosure geometry, fluid properties, enclosure orientation, etc. The phenomenon has been historically studied for various fluid pressure and temperatures and extensively reported for a diverse range of terrestrial applications. For our fluid regime, low gravitational acceleration-low temperature-low pressure case within gaps of sizes ranging from anywhere between 0.5 mm to 200 mm lead to scenarios where anything from pure conduction to laminar steady convection phenomena can set in. To help accurately estimate the heat transfer characteristics in such cases, we reviewed previous published literature on the fundamental flow physics, an introductory collection of which is referenced in most standard heat transfer textbooks [7]. The results of these studies indicate sets of empirical relations between the heat transfer parameter, 'Nusselt number' and the flow descriptive parameter, 'Rayleigh Number' for several gap configurations. Generic trends are reported by all, indicating an increase in Nusselt number for increasing Rayleigh numbers, with the flow going from stable (no movement), to development of convection cells, to steady laminar flow rotations and eventually turbulent unsteady flow movement. Critical parameters that affect the Rayleigh number are discussed in most papers, with characteristic length scales, temperature differences and fluid viscosities being the most sensitive[8]. However, it is very soon realized that beyond that, there is extensive disagreement in the Nusselt Number correlations for Rayleigh numbers for different configurations. Also, most of the correlations presented are only applicable to simplistic two dimensional gaps. Gap profiles, as can be seen from Figure 1 are quite complex due to the presence of edge or corner effects, which have not been accounted for in the conducted studies. [7]. Jet Propulsion Laboratory (JPL) Mars thermal group has conducted some CFD-experimental testing for simplistic horizontal gaps to arrive at a set of finite gap size information relevant to their Mars Science Laboratory (MSL) Rover. There is a clear need to normalize the characteristic length scale to make these findings relevant to rover designs with a range of gap length/area ratios. Other rover teams [2, 3, 5, 6] have avoided CFD modelling aided experiments and have used node based thermal models to estimate thermal convection contribution. Work published as recently as in 2016 by one of these teams reports high modelling error resulting from these single and multiple node models for parallel plane and free space convection assumptions[6]. Overall, the teams have reported strategies to work around the fluid modelling aspect of thermal convection and towards estimating 'worst case' assumptions to get final heat transfer balances.

This can easily lead to over-estimation of thermal convection loss which affects the efficiency of the on-board thermal power compensation system in place. This could be more of an issue for smaller, low power solar-electric rovers than with the larger nuclear powered ones (which have larger heat reserves). Even for the MSL currently operating under thermal stresses due to regular temperature cycling, the automated heating system performance efficiency has been reported lower than expected. Its mission life, if not determined by the life of its wheels shall be determined by the power efficiency of the radioisotope unit, which has been dropping steadily over the last four years of its operation. Thus, there is a strong need to design experiments to improve the understanding of thermal convection in gas gaps for more realistic (complex) geometries than the simplistic ones that have been investigated until date.

Research Aim and Methodology

Our overall aim is to normalize some of the reported length scales to produce heat transfer characteristics for Mars atmosphere fluid enclosures at low temperatures that could be widely applied to a range of gap configurations. Special cases of gap configurations, relevant to most enclosure configurations involving corners are being studied to characterize their effect on the overall heat transfer.

We first derive material and physical property variations (thermal conductivity, viscosity, etc.) with temperature and pressure. To understand the impact of geometry, the next step is to use commercially available CFD solver (ANSYS FLUENT) to model enclosure driven thermal convection for Mars environment, first in 2D and then in 3D environment. Based on the findings from the CFD, a set of experimental campaigns would be designed and conducted to help validate the findings.

As a start to that, the aim of this paper is to present some initial CFD results in support of previously reported heat transfer characteristics for simple gap scales in literature and discuss the experimental setup for the upcoming planned experiments.

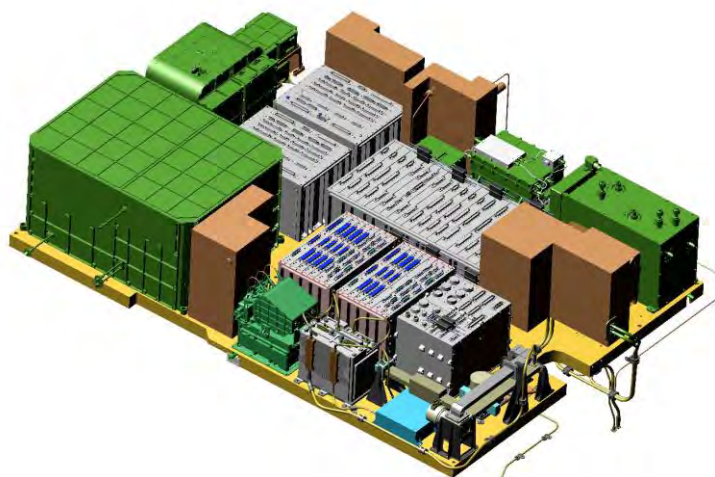


Figure 1: Mars Science Laboratory Curiosity Avionics Platform. It is enclosed within a chassis that creates narrow cavities, vented with Mars air, around the on-board temperature sensitive

electronics. Gap profiles around the components are complex with several corners requiring detailed analysis. [4]

Enclosure-bound convection theory

Two surfaces separated by a certain minimum distance, enclosed by a surrounding wall at different temperatures can cause the fluid within to move due to the density driven thermal convection from the warmer surface to the colder surface. This condition requires the warmer surface to be lower than the colder in order for the fluid to rise driven by buoyant forces. This is the classic Rayleigh Benard convection phenomenon that is has been well studied over the last century for several applications in various industries.

The critical parameters that govern this onset and stabilization of thermal convection are defined by the play between buoyant and viscous forces within the flow. This is non-dimensionalized and presented as the Grashoff number. The Prandtl number gives us the contribution of the viscous forces as compared to the thermal forces on the flow. A product of the Grashoff and the Prandtl number gives us the critical Rayleigh number for the flow regime.

These numbers and relations are described below or the flow:

$$Gr_L = \frac{g \beta (T_s - T_\infty) L_c^3}{\nu^2}$$

$$Nu = \frac{h L_c}{k} = C (Gr_L Pr)^n = C Ra_L^n$$

$$Ra_L = Gr_L Pr = \frac{h L_c}{k} = \frac{g \beta (T_s - T_\infty) L_c^3}{\nu^2} Pr$$

$$\dot{Q}_{cond} = k A_s \frac{(T_1 - T_2)}{L_c}$$

$$\dot{Q} = h A_s (T_1 - T_2) = k Nu A_s \frac{(T_1 - T_2)}{L_c}$$

$$k_{eff} = k Nu$$

For horizontal enclosures that contain air, Jakob recommends [7]

$$Nu = 0.195 Ra_L^{1/4} \quad 10^4 < Ra_L < 4 \times 10^5$$

$$Nu = 0.068 Ra_L^{1/3} \quad 4 \times 10^5 < Ra_L < 10^7$$

Can also be used for other gases with $0.5 < Pr < 2$.

Where g is the gravitational acceleration of the region, $T_s - T_\infty$ is the temperature difference between the surfaces, L_c is the characteristic length, in this case the gap between the surfaces, β is the coefficient of thermal expansion, ν is the kinematic viscosity, k is the thermal conductivity of the fluid, h is the heat transfer coefficient and k_{eff} is the effective thermal conductivity due to the convection.

CFD Model

For simple horizontal gap geometries, effective thermal empirical data is well reported in literature (both published journals and standard textbooks). Our first efforts were to validate these results by reproducing the CFD qualitative and quantitative data. Towards this, a simplistic two-dimensional rectangular control volume domain was chosen to study the thermal convection onset and stabilization studies to be performed.

The flow domain was discretized using a structured mesh with quadrilateral mesh scheme. K-ε turbulence model was chosen to provide closure to the open-ended turbulence equations, given the well-documented effectiveness of this model for such flow conditions. [9]

Fixed heater power at hot end, fixed cold plate temperature setup was replicated, as is done for most Rayleigh Benard case studies, also done by a previous Mars rover team[4] The boundary conditions are a bottom surface fixed with a fixed heat temperature input of 240 K and a top cold plate with a fixed temperature input of 190 K. The gas within was CO₂ at 1100 Pa.

Several gap lengths were tested between the surfaces and the temperature contours and profiles were compared to gauge the onset of thermal convection.

Grid Independence Analysis for Presented CFD result cases

For each case, three grids with varying refinements were run and line averaged vertical centre line temperature were sought for comparison to check if the solutions were affected by the mesh.

Grid Independence Study (6 cm gap plate)

Grid	Normalized Grid Spacing	Line Averaged Vertical Centre-line Temperature
Coarse	4	221.2
Medium	2	222.321
Fine	1	223.22

Grid Independence Study (12 cm gap plate)

Grid	Normalized Grid Spacing	Line Averaged Vertical Centre-line Temperature
Coarse	4	220.689
Medium	2	221.820
Fine	1	222.733

Grid Convergence Index (GCI) was reported for the cases to assess the convergence quality of the solutions.

$$GCI = \frac{F_s |e|}{r^p - 1}$$

Where F_s (Safety factor) of 1.25 was selected, r is the order of grid refinement, 2

p is the order of convergence, $p = \frac{\ln(f_3 - f_2)}{\frac{\ln(f_2 - f_1)}{\ln r}}$

To check whether we are within the asymptotic range of convergence, we calculated GCI_r

$$GCI_r = \frac{GCI_{2,3}}{GCI_{1,2} * r^p} \cong 1$$

GCI_r values close to 1 are achieved, i.e. 1.0229 and 1.0461 were attained for the 6 cm gap and 12 cm gap cases respectively, reflecting our solution for the two gap cases are grid independent.

Setup for the first experiments

A small thermal vacuum chamber is being set up for convection experiments to validate the results from the CFD model. After completing chamber commissioning tests which involved temperature and pressure logging while the turbo and backing pump were running along with Helium leak detection tests, the first campaign shall be set up to benchmark plate heat input stabilization and surface heat transfer measurement.

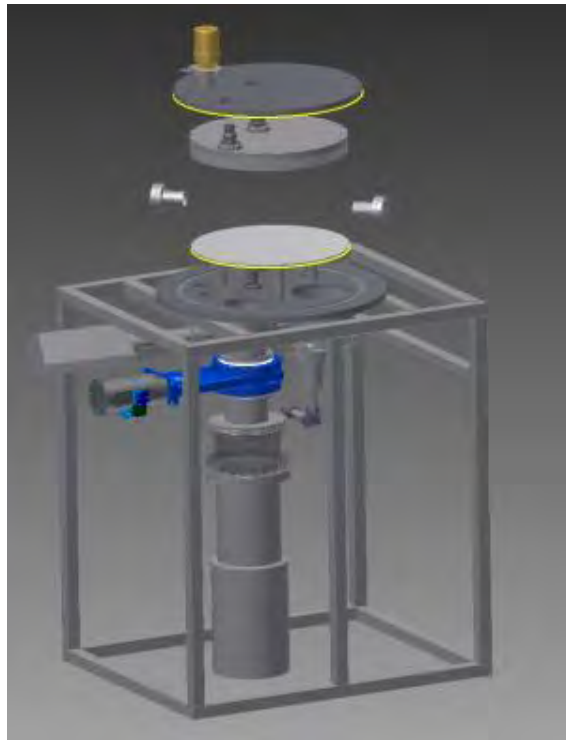


Figure 2: Assembly CAD rendering, exploded view of the small vacuum chamber

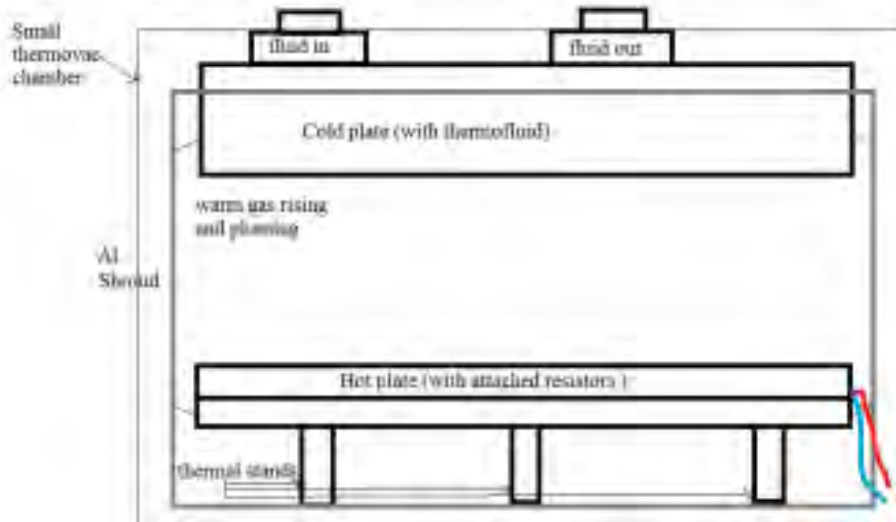


Figure 3: Schematic of horizontal gap enclosure setup within the thermal vacuum chamber



Figure 4: Thermal Vacuum Chamber Lab at UNSW Canberra

Since the lab and the chamber are still in the stage of being set up, it allows several insights into the challenges of setting up an ideal low pressure or vacuum environment for carrying out the experiments. Given the closed and isolated control volume under investigation, there are limited measurement technique options that can be used to study the convection driven flow. The benchmarking tests shall reveal if surface temperature measurements are an efficient technique to gauge heat transfers across the plates and predict the onset of thermal convection within the control volume.

A 3 mm thin Aluminum 5051 material shroud is placed around the two plates to create a classic horizontal gap. Several thermal stand lengths are used to simulate a set of gap lengths between the plates.

Results

Thermal Conductance is an efficient quantity that is used to predict the onset from pure conduction to conduction-convection to pure convection within the gas gaps. This quantity is represented by G (W/k) and equals the product of the heat transfer coefficient and the surface area of the heated surface.

As seen in Figure 5, in the absence of thermal convection, pure conduction causes the overall conductance to drop asymptotically with gap thickness. With convection setting in, one sees a rise in thermal conductance at a critical gap thickness. This value is governed by the Rayleigh number that indicates a higher contribution of buoyant forces as compared to viscous forces within the fluid. (Rise in the Grashoff number). Thus, the critical Rayleigh number is related to the change in thermal conductance and therefore the heat transfer contribution due to convection, reflected in the Nusselt number. Our numerical model predicts a critical gap thickness of 7.3 cm, which leads to the rise in thermal conductance from 0.023 W/K to 0.025 W/K and then subsequently slowly drops below 0.02 W/K as seen in Figure 6. This is in close agreement with that indicated by an earlier published work by JPL Thermal team[4] which predicts a value of 6.5 cm for the same conditions. Figure 6 shows us two starkly different thermal contours for a narrow (6cm) and a wider (12cm) gap between the plates. We also see that the thermal perturbations over the hot plate for the latter case are uniformly spaced based on the length of the two-dimensional domain. The numbers of plumes were found to be dependent on the length of the domain. A transient run of the problem showed the perturbations rose to create plumes over the flat hot surface. Earlier works on horizontal gap thermal convection studies have documented the same. Higher gap thicknesses result in stabilized convection plumes with parabolic temperature profiles across plate boundaries. The assumptions within this simple 2D flow CFD were that there was no fluid motion in the third axis, sidewalls were adiabatic and periodic heat transfer was enforced. Holman's compilation and corrective methods were used to create the analytical data set[7].

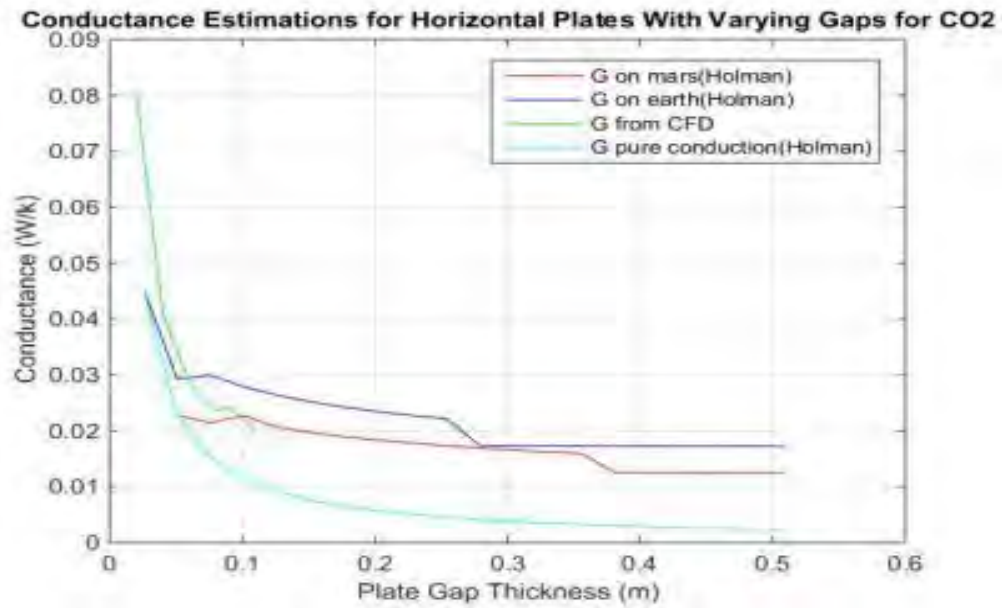


Figure 5: Thermal conductance plots from JP Holman's compilation of correlations for horizontal gas gaps and from our numerical model (shown in green) [7]

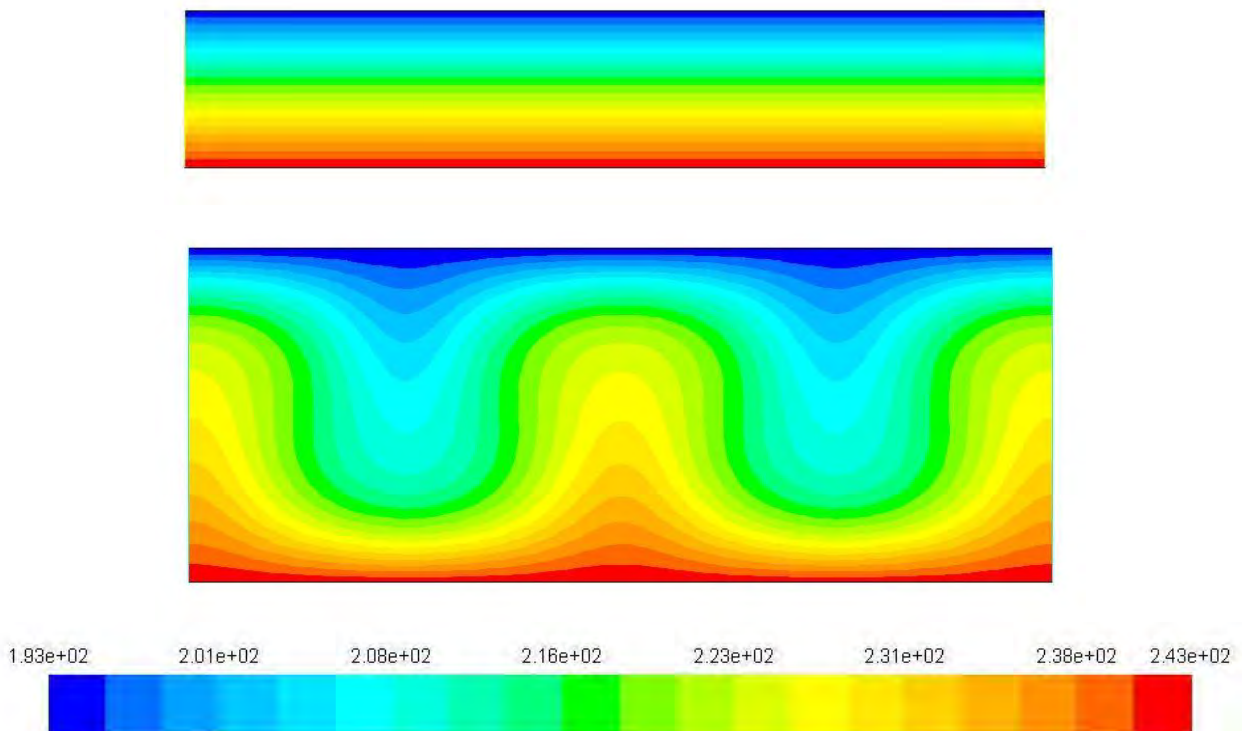


Figure 6: Temperature contours from the CFD study for 6cm gap between plates (above) and 12 cm gap between plates (below)

Conclusions

The first steps towards designing an experiment to improve the understanding of thermal convection in gas gaps with more complex geometries have been undertaken. In addition, quantitative estimation of thermal conductance G (W/K) and Nusselt number correlations for relevant temperature and pressure are compared from numerical estimation with literature.

The two-dimensional analytical and numerical model horizontal gap solutions give comparable surface heat transfer conductance values. The planned experimental setup is presented and critical benchmark tests to be conducted are mentioned along with expected challenges.

Future Work

The two-dimensional work is to be conducted within three-dimensional control volume to encapsulate the effect of fluid motion in all the directions and establish if the flow is symmetric radially. Experimental validation of the computationally simulated cases is to be carried out. Efforts shall be made to non-dimensionalize the characteristic length effect on overall Rayleigh number by studying the effect of Gap aspect ratios on change in heat transfer (Nu values). In addition, the effect of non-uniformly heated surfaces is to be studied. The eventual outcome of the study of aspect ratios and heating ratios on the heat transfer development within gaps shall enable thermal designers understand thermal convection impacts on thermal performance for Mars surface spacecraft.

References

1. Manvi, R., *Thermal Challenges of Mars Exploration*, in *International Conference on Environmental Systems*. 1998.
2. Quinn, A., Jacobs, A., Jones, G., *Testing of the Gas Gap Insulation Concept for the ExoMars Rover Vehicle*, in *International Conference on Environmental Systems*. 2010.
3. Ryuta Hatakenaka, K.F., Taku Nonomura, Moto Takai, Hiroyuki Toyota, Takehiko Satoh, Hiroyuki Sugita, *Preliminary Thermal Design of the Japanese Mars Rover Mission*, in *International Conference on Environmental Systems*. 2015.
4. Pradeep Bhandari, P.K., Kevin Anderson, Keith Novak, *CO₂ Insulation for Thermal Control of the Mars Science Laboratory*, in *AIAA*. 2011.
5. Edward Nelson, H.M., Luke Tamkin, *Characterization of the insulation provided by a carbon dioxide gap for the ExoMars 2018* 2015.
6. Tamkin, L., Nelson, E., McQuail, H., *Evaluation of Modelling Techniques for a Carbon Dioxide Gas Gap for the ExoMars Rover and Surface Platform Mission*, in *International Conference on Environmental Systems* 2016.
7. Holman, J.P., *Heat Transfer* 1964.
8. Talukdar, P., *Natural Thermal Convection*. 2001, Indian Institute of Technology Bombay, India
9. *ANSYS FLUENT MANUAL* 2015.

Evaluation of the Performance of Field Science in an Analogue EVA suit II

Jonathan D. A. Clarke¹, Anna M. Clarke², Gabi Hobbs², Steve Hobbs², Richard McGuirk², Savannah McGuirk², James Waldie^{2,3}, and Andrew Wheeler^{2,4}

¹ Mars Society Australia, 43 Michell St, Monash, ACT 2904, Australia

jon.clarke@bigpond.com

² Mars Society Australia, P.O. Box P.O. Box 327 Clifton Hill, VIC 3068, Australia

³ School of Aerospace, Mechanical & Manufacturing Engineering, RMIT University, GPO Box 2476, Melbourne VIC 3001, Australia

⁴ QGESS Pty Ltd, PO Box 368, Mt Ommaney Qld, 4074 Australia

Summary: Understanding the constraints of field work while in a space suit is critical when planning crewed exploration strategies for the surface of the Moon, Mars, and other accessible Solar System bodies. Mars Society Australia has undertaken a number of studies into the effect of simulated or prototype space suits on field work performance, in the Pilbara in 2011 and at Arkaroola in 2014 and 2016 (this study). Performance was assessed using accuracy in identification of stromatolites. Unexpected results from the 2014 study were that participants, both geologists and non geologists, performed better suited than unsuited. These results are contrary to initial expectations that participants would perform less well whilst in the suits. One possible explanation for this was that the suited trails were performed first with more engaged participants. We tested this possibility in 2016 by suiting the unsuited trials first, with the same result. We are therefore confident that this trend is valid, given the other constraints of the experiment. Other results of the 2011 and 2014 trials were confirmed, including the value of trained scientists in the performance of science tasks under simulated EVA conditions of trained geologists in performing specific field observations while non-geologists made more observations than geologists, but with less accuracy. In future we hope to possible explanations for this trend, including the possibility of greater participant focus while enclosed, the role of terrain difficulty on field performance and assessing the role suit familiarity.

Keywords: Mars analogue research, EVA suits, geology, astrobiology, human factors research, stromatolites, Arkaroola.

Introduction

Detailed, complex, and sophisticated field science investigations are essential to crewed missions to the Moon and Mars and elsewhere (Refs. 1, 2). Quantifying the capabilities of scientists and non-scientists to do such investigations while wearing EVA suits is important for designing mission goals, setting expectations, refining suit and field tools or instrument design, and mission architecture. This is required because of the difficulties of intense and sustained field operations in EVA suits such as those developed for Apollo (Ref. 3).

This paper describes a small, low-cost trial that examines one particular aspect of the performance of science tasks, the ability to identify stromatolites by geologists and non-

geologists under analogue EVA conditions. It builds on previous research at Arkaroola (Ref. 4) and before that in the Pilbara (Ref 5.) and reports on tests specific hypotheses arising from that work. In particular, we test the observations in the previous Arkaroola study, contra the predictions in Ref. 4, the analogue EVA suits used did not appear to degrade observational performance, but enhance it (Ref. 4).

If valid, these results are significant for the design and interpretation of human factors investigations that compare the performance of tasks while using specific analogue technology that mediates between the user and/or operator.

Experiment Aim

The principle results of the 2014 of results from the 2014 trial (Ref. 4). These were:

1. That both geologists and non-geologists were able to recognise specific scientific features, e.g. stromatolites.
2. Geologists performed better than non-geologists, as shown by accuracy of observations.
3. Non-geologists made more observations than geologists, but with less accuracy.
4. Participants overall made more observations with greater accuracy while wearing the EVA suit than when they were not wearing it.

Result four was unexpected as it was contrary to predictions that the suit would impede observational ability. Several hypotheses were generated to explain these results:

- The participants were less fatigued and more capable of observations in the suited as opposed to the unsuited trials because the suited trials were performed first,
- The actual wearing of the suit may have led to increased observational focus and thought in the participants whilst carrying out the test, and
- The participants did not take the unsuited test as seriously and so were less diligent in their observations (Ref. 4).

The aim of the 2016 trial was to test the validity of result 4 and confirm results 1-3.

Experimental Methods

The trials were run over two days in July 2016. Experiment scenario, location, geological context, observed features, and overall methods were as far as possible identical with those of the 2014 trials (Ref. 4). The scenario was the investigation of a potentially fossiliferous carbonate outcrop on Mars identified by satellite imagery and hyperspectral data and accessed by a sortie from a landing site several tens of km distant. Non geologists and qualified geologists would spend a 20 minutes assessing whether or not the outcrop contained mesoscopic signs of life in the form of stromatolites.

Stromatolites are microbial organo-sedimentary columnar to branching constructs with laminated internal fabrics that grow in shallow subaqueous environments include shallow marine, lacustrine, and hot spring settings (Ref. 5, 6). They occur in some of the oldest known sediments on Earth (Ref. 7, 8), and will potentially be found on Mars where they will potentially be the most readily recognized indicators of past life (Ref. 5, 9). Furthermore,

possible geysers, small stromatolites formed in hot springs, have been observed on Mars in *Spirit* rover imagery (Ref. 10).

The site selected test site was at 30°26'29.47"S and 139°19'45.42"E with an elevation of 204 m above sea level at the foot of slope. It is 14.3 km in a direct line south of Arkaroola, and 18.1 km by road. The outcrop begins 55 m east of the Arkaroola road. The outcrop is west dipping at 25-35°, and is of the Trezona Formation (Ref. 11). The stromatolites at the outcrop are simple columns composed, typically 5-10 cm high and 2-5 cm across. They are exposed largely as circular impressions on the upper surfaces of the bedding planes on massive to slabby dolomitic limestone outcrop and sometimes on loose boulders of the same lithology (Fig. 1). The photograph illustrates the suitability of these features for trials such as this, being easily identified and interpreted, astrobiologically significant, and leading to readily assessed responses from the participants.



Figure 1. Columnar stromatolites exposed on the side and top of a loose cobble of Trezona Formation (Ref. 5) ~15 cm in length at the trial site.



Figure 2. Simulated EVA during in the 2016 trial.

The analogue EVA suit (Fig. 2) was designed and built by MSA and almost identical to the Victorian Space Science Education Centre (VSSEC) suits used in the 2014 trial (Ref. 4). The suit is intended to mimic a future mechanical counter-pressure planetary exploration suit (Ref. 3). Gloves and boots were specified to provide some inhibition to mobility and hand dexterity. Cotton drill coveralls simulate an outer protective garment. The MSA developed pseudo life-support system consisting of a helmet, backpack and ventilation system. The helmet provides a clear upper dome that rests lightly on the shoulders of the wearer. Life support is contained within a Boblbee hard-shell backpack. High ventilation sufficient to meet safety requirements is met by two fans inside the backpack and plumbed to each side of the helmet. A 7Ah 12V lead-acid battery provides approximately 5 hours of ventilation. The primary difference between the VSSEC and MSA suits was that the VSSEC suit was fitted with a UHF radio whereas the MSA suit used in 2016 was not. Verbal instructions used in 2016 without the radio, these proved sufficient.

Participants were first tested unsuited and then suited. This tested the possibility that carrying out the suited observations first resulted in better performance than the unsuited trials in 2014.

Six people took part in the trials, four non-geologists and two geologists, with geologists being defined as those two or more years of formal geological training. The other participants had a range of skills and training, including nursing, remote sensing, environmental management, and law. The reader is referred to Ref. 4 for further details on scenario, location, geological context, observed features.

The participants were required to point out any stromatolites and describe them as probable or possible. Probable stromatolites were features identified as stromatolites with a high degree of confidence. Possible stromatolites were features identified as possibly stromatolitic but with lower confidence. False positives (sites identified as probable or possible stromatolites that were judged as non stromatolitic by the experiment controller) and false negatives (sites

rejected as stromatolites that were considered stromatolitic by the controller), were also noted. These results were communicated immediately to, and recorded by, the experiment controller.

The MSA overall did not fit one participant, so they carried out the trial wearing the boots, gloves, backpack and helmet.

Table 1: Results of 2016 trial: Accuracy while suited and unsuited.

Suit	Participant	Probable	Possible	False Positive	False Negative	Total	Total Valid	Score %
Y	Subject 1 NG	30	10	21	0	61	40	65.6
Y	Subject 2 G	26	18	1	0	45	44	97.8
Y	Subject 3 NG*	23	12	11	0	46	35	76.1
Y	Subject 4 NG	18	17	2	6	43	35	81.4
Y	Subject 5 NG	23	14	9	9	55	37	67.3
Y	Subject 6 G	10	6	4	1	21	16	76.2
N	Subject 1 NG	43	17	22	2	84	60	71.4
N	Subject 2 G	21	9	5	5	40	30	75
N	Subject 3 NG*	23	16	8	0	47	39	83
N	Subject 4 NG	2	9	4	9	24	11	45.8
N	Subject 5 NG	15	20	12	10	57	35	61.4
N	Subject 6 G	19	5	4	2	30	24	80
	TOTAL	253	153	103	44	553	406	73.4

Results

Individual observations made in 2016 are shown in Table 1. Summary data for suited and unsuited geologists and non-geologists in 2014 and 2016 are shown in Table 2. Standard Deviations are not shown because of small sample size when broken down into skills and year.

Table 2: suited and non-suited performance by geologists and non geologists, 2014 (suit test first) and 2016 (unsuited test first)

Year	Suited	Skill	Average accuracy	Increased suit accuracy
2014	Yes	Geologists	97%	1.5%
	No	Geologists	95.2%	
2014	Yes	Non-geologists	83%	3.4%
	No	Non-geologists	79.6%	
2016	Yes	Geologists	87%	9.5%
	No	Geologists	77.5%	
2016	Yes	Non-geologists	72.6%	7.2%
	No	Non-geologists	65.4%	

We conclude from these data that the increased observational accuracy while wearing a suit is real. We therefore consider it reasonable to aggregate the results from the two years to explore the statistical significance of the aggregate results. The aggregated results of the trials from 2014 and 2016 are shown in Tables 3-5. Table 3 shows participant accuracy in stromatolite

identification when suited. Geologists identified them with an accuracy of 93.9% and non-geologists with an accuracy of 75.8%. The combined accuracy was 81.3%

Table 3: Results of the 2014 and 2016 trials: Accuracy while suited.

Skill	Probable	Possible	False Positive	False Negative	Total	Total Valid	Total Errors
Geologists	72	52	6	2	132	124	8
%	54.5	39.4	4.5	1.5	100	93.9	6.1
Non-Geologists	143	89	55	19	306	232	74
%	46.7	29.1	18	6.2	100	75.8	24.2
TOTAL	215	141	61	21	438	356	82
%	49.1	32.2	13.9	4.8	100	81.3	18.7

Table 4 shows the results from the unsuited trials. Geologists scored 85.3% correct identifications but non-geologists did so only 72.1% of the time. The aggregate result was 76.3%. The suited performance is noticeably better with respect to identification than the unsuited performance, despite the handicaps of wearing the suit especially reduced vision.

Table 5 records the numbers of observations made by participants with different skill sets under suited and non-suited conditions, the mean number observations for each group, accuracy in identification, and the standard deviations for number of observations and observation accuracy.

Table 4: Aggregate results of the 2014 and 2016 trials: Accuracy while unsuited

Skill	Probable	Possible	False Positive	False Negative	Total	Total Valid	Total Errors
Geologists	64	46	11	8	129	110	19
%	49.6	35.7	8.5	6.2	100	85.3	14.7
Non-Geologists	110	90	51	29	280	202	78
%	39.3	32.1	18.2	10.4	100	72.1	27.9
Total	174	136	62	37	409	312	97
%	42.5	33.3	15.2	9	100	76.3	23.7

Table 5: Aggregate valid observations of the 2014 and 2016 trials: Means and Standard Deviation

Skill	Suited	Valid observations	# Observers	Observation Mean	SD observations	Accuracy	SD Accuracy
Geologist	Yes	124	5	24.8	11.10	93.9%	10.10
Geologist	No	110	5	22.0	8.12	85.3%	8.12
Non-geologist	Yes	232	8	29.0	10.28	75.3%	
Non-geologist	No	202	8	25.25	18.54	72.1%	19.91

The results in Table 5 show that both geologists and non-geologists made more valid (i.e. correct) observations when suited than when non-suited. However the variance is within the Standard Deviation. Geologists were more accurate in their observations than non-geologists, with the results greater than the Standard Deviation. Despite their greater accuracy, geologists

made fewer observations both suited and non-suited when compared with non-geologists. Once again the variance is within the Standard Deviation.

Qualitative Comments by Participants

Several of the 2016 participants made spontaneous comments about their experience while wearing the suits. Several were to do with lighting conditions on the two days as they had quite different weather conditions. The first day had low cloud and consequently relatively dim and very diffuse lighting conditions (Fig. 2). As a result all participants on that day encountered helmet fogging. However, the diffuse light may have made observations of stromatolites easier, compared to the following day of bright sun, low sun angle, especially and in the morning, and sharp shadows (Fig. 3). The bright sunlight meant that glare was commented on by some as a problem when looking in the up-sun direction, exacerbated by scratches and dust on the helmet. One participant commented on sensations of CO₂ build-up, this may have led to that person stumbling and tripping. No similar difficulties were reported by others.

The experiment observer noticed that the participants used two different search strategies, either picking up small rocks and looking for stromatolites (Fig. 3), or examining whole outcrops (Fig. 2). The first method was useful in examining possible stromatolites on loose rocks close up, but overall the second method was more effective because of the size of the stromatolites. Rocks that were picked up ranged from three to 15 cm across, as the stromatolites columns were 2-5 cm across, the smaller rocks were often too small to allow accurate identification of any stromatolites that may have been present.



Figure 3. Typical conditions of bright sunlight and sharp shadows on second day. Participant is examining small hand held specimen for possible stromatolites.

Three participants showed evolving strategies over the course of the trials, one using a mixture of hand specimen and outcrop examination during the first (unsuited) trial and almost

exclusively outcrop examination during the second (suited) trial. One participant, remembering a scene from a dramatization of Apollo astronaut training (Ref. 12), specifically tried to place the outcrops in a broader context, describing larger scale (five-10 m) scale but poorly expressed features that may be related to clustering of stromatolites into bioherms (clusters of stromatolites that form reef-like features, see Ref. 6).

Discussion

Caveats

As for the 2014 trial, the sample size for this study is small and therefore conclusions drawn from the above statistics are both tentative and provisional. As already noted, since the same trends are visible in both trials, despite the reversed suited vs. unsuited order, we are confident that we can aggregate the data trends. As a result aggregate number of participants is now increased from seven to 13, the number of trial runs from 14 to 26, and the total number of data points from 294 to 715. We therefore have greater generalised confidence in the data trends than we had in the 2014 results presented in Ref. 4.

Trends observed in the data

Prediction 1) of the 2011 Pilbara trial, that useful field science can be performed while wearing analogue EVA suits, continues to be confirmed. This is as expected from the success of Apollo astronauts on the Moon (Ref. 13) and will not be discussed further.

Prediction 2), of the 2011 Pilbara trial (Ref.5) and summarised in Ref. 4, which was the suit would impede performance, continues to be inconsistent with the aggregate data from the 2014 and 2016 Arkaroola trials (Tables 2-5). Overall the suited and unsuited participants scored 81.3% and 86.3.4% correct results respectively.

Prediction 3(a) of the 2011 Pilbara trials, that geologists would make fewer but more accurate observations than non-geologists, was only partly borne out in 2014 trials at Arkaroola (Ref. 4) and is confirmed in the aggregate data from 2014 and 2016. (Tables 2-5). Geologists made an average of 26.4 observations while suited opposed to 38.3 for the non-geologists. When unsuited, geologists again made fewer observations per observer (25.8) than non-geologists (35).

Prediction 3(b) from the Pilbara trials, that geologists would out-perform non-geologists in the accuracy of their observations, is validated in the aggregate data (Table 1-2). This was true in both suited (93.9% compared with 85.3%) and unsuited (75.8% as against 72.1%) trials.

Prediction 4) from the Pilbara, that geologists would be less impeded by the suits than non-geologists, continues to be inconsistent with the Arkaroola data (Tables 2-5). The performance gap, as measured by accuracy of observations, between the geologists and non-geologists was 13.2% without a suit to 18.1% while wearing a suit, and geologists made more observations while not wearing the suit than non-geologists.

Possible explanations

Seven explanations (Ref. 4) were proposed after the 2014 Arkaroola trials for the unexpected increase in performance whilst wearing a the VSSEC suit when compared with the results from the Pilbara and the University of North Dakota's NDX-1 pressurised suit (Ref. 5). These provided hypotheses and problems for further research. This paper has tested, or at least illuminated, four of the seven by extending the data pool, specifically 2, 3, 4, and 7 (numbering as per Ref. 4):

2. Because the unsuited trials were carried out subsequently to the suited trails, the participants may have been more fatigued and less capable of observations than when they were wearing the suits. A priori this appears unlikely as the tests lasted only 20 minutes and the participants were all in good health and of reasonable fitness.

3. It is possible that the actual wearing of the suit may have led to increased observational focus and thought in the participants whilst carrying out the test.

4. It may also be possible that the participants did not take the unsuited test as seriously and so were less diligent in their observations.

7. During the Pilbara trials the weather was very warm, and all participants experienced over-heating leading to fogging and misting to greater or lesser degrees, which significantly hampered the ability to make geological observations. Similar issues were not experienced with the VSSEC suit, due to cooler weather and the different suit design.

Explanation 2, that the order in which the suited and unsuited trials were done was a factor in determining which performed better, was tested by reversing the order. Since the suited participants performed better irrespective of whether they were carried out first or second, we conclude that the trial order had not significant impact. Thus we consider this explanation falsified as a hypothesis.

Explanation 3, that participants may have been more focused, or hyper-aware, when making observations while suited, remains as a possibility, with some, but not all, unsolicited comments suggesting this. Why this should be the case with the Arkaroola trials but not in the early Pilbara trial, remains unclear. The possibility of a role of unconscious behaviour exists, and need further work.

Explanation 7, impairment of observations by fogging, may be at least partly invalidated, albeit by opposite weather conditions. Helmet fogging was a problem during day 1 of the 2016 trial due to conditions being cold and humid. Despite this the difference in suited performance between the two days was small (Table 6), with the caveat that the sample size is also very small, only three participants on each day (one geologist and two non-geologists each). Because of the small sample size geologists and non-geologists are not differentiated. Those who took part on the foggy day showed better suited performance (4.8%) compared to those on the day when fogging was not an issue. This however may be due to individual performance. While glare, light scattering, and outcrop contrast and shadow interference was an issue on the clear day, it is unlikely to have offset the better visibility overall. The Pilbara trials were undertaken in conditions of diffuse light under a mostly overcast sky (see figures in Ref. 5), so that glare, light scattering, and outcrop contrast and shadow are not likely to have been an issue.

Table 6. Comparison of suited observational accuracy during 2016 trials on days with and without helmet fogging.

Subject	Total Obs	Total Valid	%
FOGGY HELMET			
Subject 1	61	40	
Subject 2	45	44	
Subject 3	46	35	
TOTAL FOG	152	119	78.2
CLEAR HELMET			
Subject 4	37	35	
Subject 5	55	37	
Subject 6	21	16	
TOTAL CLEAR	113	88	73.4

The consistency of the results raises a potential research question about the validity of many experiments comparing performance of tasks that compare performance with and without a specific technological item, be it a tool, or a more complex integrated system such as a suit (e.g. Ref.14. While simple biomechanical, visual, and physiological comparisons are likely to remain valid (e.g. Ref. 15), studies into comparisons involving higher cognitive engagement, including data interpretation and participant imagination (e.g. Ref. 16), may need to be more carefully thought out to ensure useful conclusions.

Further Work

These data and our interpretation of them suggest three lines for further enquiry:

1. To investigate of the role of terrain difficulty in reducing suited performance (explanation 6 of Ref 4). This can be carried out using the VSSEC or MSA suits at Arkaroola, providing a suitably rough stromatolite location can be found. While future EVAs on the surface of the Moon or Mars are unlikely for safety reasons to be conducted in extremely rough and difficult terrain, such trials will enable us to explore some boundaries of the test condition.
 2. To further explore the role of participant's focus and awareness. These will be done in comparative trials through testing whether there are differences in results from differing levels of familiarity with the suit, and thus hyper-awareness induced by unfamiliarity, and;
 3. To investigate whether it is the enclosed helmet or simply the reduced peripheral vision that encourages greater focus. We can do this by removing the plastic bubble from the helmet but otherwise performing the suited test as done here.
- 3) *A repeat of the NDX test with experienced wearers who more closely match the size requirements of the suit should be carried out to test hypothesis 5 above; and*

4) Trials at a different, more rugged stromatolite site at Arkaroola with the VSSEC suits (or similar) and a less difficult stromatolite (or equivalent) site with the NDX-1 suit would assess whether rougher terrain impacts significantly on performance.

Conclusions

This study builds upon the results of the 2014 and 2011 simulated EVA trials (Ref. 4, 5).

These included the superior performance of trained scientists, in this case geologists, in performing specific field observations while non-geologists made more observations than geologists, but with less accuracy. The difference was greater than a Standard Deviation

These tests confirmed the 2014 Arkaroola results that while wearing the VSSEC/MSA suits participants overall made more observations with greater accuracy while wearing the EVA suit than when they were not wearing it. This was regardless of whether the participants performed the suited trails before or after the unsuited trials, eliminating the possibility that fatigue or boredom were a factor in these results. The difference small, within a Standard Deviation, but consistent

Our future research will focus on assessing the roles of terrain difficulty on field performance, helmet enclosure, participant engagement, and simulation realism in tests of complex field tasks.

Acknowledgements

We thank the Arkaroola Resort for their assistance and support while we were in the field. David Willson of NASA Ames Research Center also provided much useful commentary on the paper. William Clancey and Sheryl Bishop of the University of Houston Medical School of Stanford University provided valuable discussion. We also acknowledge the comments of two anonymous reviewers of the paper.

References

1. Schmitt, H.H., Snoke, A.W., Helper, M.A., Hurtado, J.M., Hodges, K.V., and Rice Jr., J.W. Motives methods and essential preparation for planetary field geology on the Moon and Mars. *Geological Society of America Special Paper* 483, 2011, 1-15.
2. Beaty, D. Niles. P., Hays, L., Bass, D., Bell, M. S., Bleacher, J., Cabrol, N. A., Conrad, P., Eppler, D., Hamilton, V., Head, J., Kahre, M., Levy, J., Lyons, T., Rafkin, S., Rice, J., and Rice, M. *Scientific Objectives for the Human Exploration of Mars*. MEPAG Science Analysis Group. Web address when accessed 10/9/15 <http://mepag.nasa.gov/reports/HSO%20summary%20presentation%20FINAL.pdf>, 2015
3. Newman, D. and Barrat, M. Life Support and Performance Issues for Extravehicular Activity (EVA). In: Churchill, S and Heinz, O. eds. *Fundamentals of Space Life Sciences*, Chapter 22, Krieger Publishing Company, 1997.

4. Clarke, J. D. A., Cooper, M., George, S., Hobbs, S., Houlahan, S., Murphy, G. M., Silburn, K., Sprigg, D., Sprigg, M., and Waldie, J. Evaluating the Performance of Field Science in an Analogue EVA suit: Stromatolite Identification by Geologists and Non-Geologists. *Proceedings of the 15th Australian Space Research Conference*, 2015. National Space Society Australia, 2016, 159-172.
5. Willson, D., Rask, J. C., George S.C., deLeon, P., Bonaccorsi, R., Blank, J., Slocombe, J., Silburn, K., Steele, H., Gargano, M., and McKay, C. P. The performance of field scientists undertaking observations of early life fossils while in simulated spacesuit. *Acta Astronautica* 93, 2014, 193–206.
6. Walter, M. R. 1976 (ed.). *Stromatolites*. Elsevier, Amsterdam, 790p.
7. Clarke, J. D. A. and Stoker, C. R. Searching for stromatolites: the 3.4 Ga Strelley Pool Formation (Pilbara region, Western Australia) as a Mars analogue. *Icarus* 224, 2013, 413-423.
8. Nutman, A.P., Bennett, V. C., Friend, C. R.L., Van Kranendonk, M.J., and Allan R. Chivas. Rapid emergence of life shown by discovery of 3,700-million-year-old microbial structures. *Nature* 537, 2016, 535–538
9. McKay, C. P. and Stoker, C. R. The early environment and its evolution on Mars: implication for life. *Reviews of Geophysics* 27, 2, 1989,189–214.
10. Ruff, S. W. and Farmer, J. D. Silica deposits on Mars with features resembling hot spring biosignatures at El Tatio in Chile. *Nature Communications* 7, 2016 doi.org/10.1038/ncomms13554.
11. Coats, R. P. *COPLEY, South Australia, sheet SH54-9*. South Australian Geological Survey 1:250,000 series, 1973.
12. Hanks, T.(director). *From the Earth to the Moon* HBO Inc., Episode 10 *Galileo was right*. 1998.
13. Crawford, I. The scientific legacy of Apollo. *Astronomy and Geophysics* 53 2012, (6), 6.24-6.28, doi: 10.1111/j.1468-4004.2012.53624.x.
14. Soucek, A., Ostkamp, L., and Paternesi, R. Suited versus Unsited Analog Astronaut Performance Using the Aouda.X Space Suit Simulator: The DELTA Experiment of MARS2013. *Astrobiology*. 15, 4, 2015: 283-290.
15. Tanaka, K, Waldie, J., Steinbach, G. C., Webb P., Tourbier, D., Knudsen, J., Jarvis, C.W., and Hargens, A.R. Skin microvascular flow during hypobaric exposure with and without a mechanical counter-pressure space suit glove. *Aviation, Space, and Environmental Medicine* 73, 2002, (11), 1074-1078.
16. Glass, B., Briggs, G., Jasper, J., and Snook, K. Evaluation of Human vs. Teleoperated Robotic Performance in Field Geology Tasks at a Mars Analog Site. *Proceedings of the 7th International Symposium on Artificial Intelligence, Robotics and Automation in Space (i-SAIRAS 2003)*; 1-23 May 2003; Nara; Japan

Imagers for Ionospheric Airglow Observations

Anne M. Unewisse and Andrew D. Cool

Defence Science and Technology Group, PO Box 1500 Edinburgh SA, 5111, Australia

Summary:

Airglow imagers are widely used for mapping large-scale density perturbations of atoms, molecules and ions in the Earth's atmosphere. Over the last five years, the Defence Science and Technology Group (DST Group) has assessed three imager configurations for use as airglow measuring tools in support of over-the-horizon radar: a Keo Sentry airglow imager with filter wheel housed in a 20 ft shipping container, two single filter Atik Sentinel cameras installed in a small purpose-built, insulated enclosure and two retail Canon 6D DSLR cameras affixed to the inside of an insulated icebox. This paper summarizes our results. Criteria include cost, portability, ease of use, robustness and imaging performance.

Keywords: Airglow imaging, ionospheric studies, TIDs

Introduction

The Defence Science and Technology Group (DST Group) operates the Jindalee Operational Radar Network (JORN); a network of three High Frequency (HF) over-the-horizon radars located around Australia. Signals from these radars propagate via regions of high electron density in the Earth's atmosphere known as the ionospheric E and F layers, which have peak densities at altitudes of around 110 km and 250 km respectively. Electron density irregularities are prevalent in these layers and have implications for radar co-ordinate registration, frequency selection and signal strength.

DST Group monitors these irregularities using a variety of instruments including ionospheric sounders, GPS receivers and airglow imagers. Airglow is atmospheric electromagnetic radiation, resulting from chemiluminescence processes, and occurs widely across the visible and near IR spectrum from various defined heights in the atmosphere.

The airglow emission wavelength is species dependent with common reactants being oxygen, sodium and hydroxyl ions and molecules. Of particular interest to HF studies are the 557.7 nm (green) and 630.0 nm (red) oxygen airglow emissions which originate from near the ionospheric E and F layers respectively. Airglow brightness is a function of species density and excitation rate so that, for a constant excitation rate, it may be used to map species density. Ionospheric disturbance phenomena affect the density distribution of ions, molecules and electrons alike. Thus measuring the density patterns in airglow originating from E and F layer heights gives an indication of the electron density profile through which the HF radar transmission is propagating.

Airglow imagers consist of sensitive cameras with wide field of view lenses and narrow band filters designed to isolate specific wavelengths of chemiluminescent radiation. Traditionally,

airglow imagers are used to gather large volumes of data at one location. DST Group's work, however, involves sampling the ionosphere at various locations around Australia under extreme temperature conditions and thus a certain amount of imager portability and durability is required. A summary of some portable airglow solutions may be found in Loughmiller [1].

This paper summarizes five years of work undertaken by DST Group to determine the most suitable airglow imager for remote, relocatable airglow experiments to support HF studies using 557.7 nm and 630.0 nm filters. Three imagers are discussed: 1) TRACE: a commonly used shipping container based imager consisting of a Keo Sentry camera with filter wheel, 2) Port-a-TRACE: two Atik Sentinel cameras installed into a small purpose-built, insulated enclosure and 3) CAIN: two Canon 6D Digital Single Lens Reflex (DSLR) cameras affixed to the inside of an insulated icebox.

Equipment Descriptions

TRACE

DST Group has operated the Thermospheric Radar Airglow Correlation Experiment (TRACE) airglow imager since November 2011 in support of atmospheric studies at altitudes of interest to high frequency radar: specifically the ionospheric E and F layers.

The TRACE airglow imager is shown in Figure 1. It consists of a Keo Sentry camera [2], 180° field of view (FOV) 24mm / F4.0, achromatic Mamiya fisheye lens and a temperature controlled filter wheel mounted on a Pier-Tech telescopic pier located inside a 20 ft shipping container. The Sentry uses a 16 Bit Princeton Instruments Acton backlit Pixis 1024B CCD camera and has a pixel size of 13.3 μm x 13.3 μm . The pier is automated so that the camera rises to fit inside an Aquatica 9.25 inch BK7 glass dome at astronomical dusk and lowers at astronomical dawn. Details on the imager may be found in Unewisse, *et al.* [3].

The filter wheel is kept at a constant optimal temperature of 25°C and has six 3 inch slots, one of which is empty to allow baseline light measurements. The Keo scientific filters have a bandwidth of 2 nm and are centred on: 557.7 nm (OI), 589.3 (Na), 630.0 nm (OI), 777.4 nm (OI) and 572.5 nm (background). Filter transmission is about 66% at 557.7 nm and 95% at 630.0 nm. The 777.4 NIR measurements tend to suffer from a fringing interference pattern known as echeloning which may be mitigated during image processing [4].

The dark current measured by the Pixis camera's CCD at -70°C is typically 0.001 e-/pixel/sec [5] although it regularly operates at -80° C. The maximum readout speed is 2 MHz, which equates to a gain of 1.11 e-/ADU and a readout noise of 12.85 e- rms [6]. The CCD quantum efficiency is around 95% at 557.7 nm, 598.3 nm, 630.0 nm and 572.5 nm but falls to approximately 75% at 777.4 nm.

The camera is controlled autonomously from Keo Scientific "Synopticx" software which determines moon and sun position to ensure imaging only occurs under optimal conditions. A dark frame is taken at the beginning and end of each night.



Figure 1: The airglow imager and filter wheel setup in the TRACE container

TRACE's FOV corresponds to image diameters of ~ 400 km at an altitude of 96 km [7, 8] and ~ 1000 km at an altitude of 250 km [9]. The resolution of the inner region of the image is approximately 0.4 km/pixel at an altitude of 96 km and 1 km/pixel at an altitude of 250 km [10].

TRACE is supported by a Unihedron Sky Quality Meter [11] which records calibrated light readings every minute and a Boltwood cloud sensor [12] which monitors environmental conditions such as temperature, cloud coverage, rain, humidity, wind speed and light every 2.06 seconds. As well as monitoring current weather conditions, the cloud sensor output triggers the automated pier to lower the camera during daylight hours to reduce previously experienced UV-induced lens coating degradation.

Port-a-TRACE

In 2015, a portable version of TRACE known as Port-a-TRACE was built to address cost and portability issues in TRACE. Port-a-TRACE, shown in Figure 2, consists of two single filter Keo Sentinel [13] imagers with 150° field of view f/4.0 lenses placed a meter apart in a 800mm wide x 1200mm deep x 1200mm high IP66 rated outdoor enclosure supplied by OverIP [14]. The enclosure was modified in-house to incorporate two Aquatica 9.25 inch BK7 glass domes and supports for the two cameras. The door mounted 600W air conditioner [15, 16] is supplemented by solar/thermal resistant paint. Port-a-TRACE is mounted on a pallet for easy transportation. The Sentinel cameras do not have a mechanical shutter which reduces equipment cost but also negates the ability to collect dark frames during automated runs.

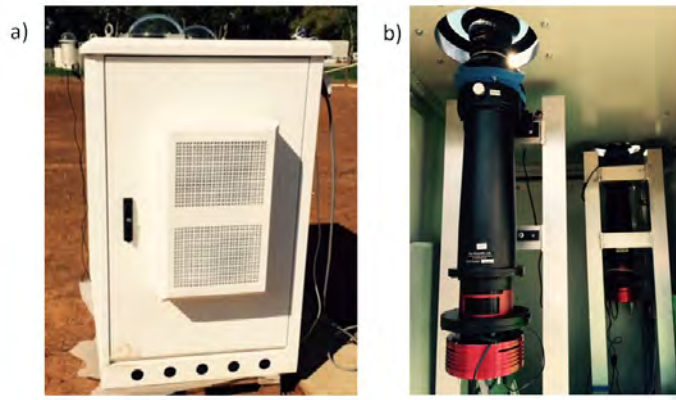


Figure 2 Port-a-TRACE a) external and b) internal

There are four available 3 inch, removable 2 nm bandwidth filters centred on: 557.7 nm O(1S) oxygen emission primarily from an altitude of 96 km, 630.0 nm O(1D) oxygen emission (250 km), 589.3 nm sodium doublet emission (92 km) and 572.4 nm used to measure local non-airglow background conditions (the control image) though only two may be used at any one time – one in each camera – due to the lack of a filter wheel. The filter transmissions are 88% at 557.7 nm and 90% at 630.0 nm.

The imagers cameras may be Peltier cooled down to a maximum of -40°C below ambient but are typically run at -15°C given a pre-set air conditioned ambient temperature of 15°C . Typical dark current noise is 0.01 electrons/pix/sec at -20°C . The Kodak KAI 04022 2048x2048 16 bit CCD has a pixel size $7.4\mu\text{m} \times 7.4\mu\text{m}$ and quantum efficiency (QE) of approximately 50% at 557.7 nm and 35% at 630 nm [13].

The supplied Sentinel software is Atik Artemis which is not designed to run autonomously so an in-house script is run by AstroArt 5 [17] using ASCOM drivers [18] to connect to the cameras. The images are 2048x2048 in GIF or FITS format which may be processed in IDL using the same software as TRACE images.

Port-a-TRACE is supported by an Aurora cloud sensor [19] to determine weather conditions, an internal temperature and humidity sensor and an Oculus all-sky camera [20], both driven by in-house AA5 scripts. The scripts can be configured to use cloud sensor information to avoid imaging during rain and cloud but this has not yet been implemented.

CAIN

Airglow is often photographed by professional and amateur photographers using retail DSLR cameras. Interesting phenomenon such as bores and waves have been published in the open literature [21, 22]. As the retail camera costs are a fraction of the cost of specialised airglow imagers, two 35 mm, full frame Canon 6D cameras and two Sigma 8mm F3.5 180° field of view fisheye lenses were purchased for assessment. All equipment was housed in a 200L icebox modified on site for astronomical use by installing caravan 10A electrical connections, inserting vents and fans for cooling and affixing a metal lid to provide a solid surface to attach domes and cameras.



Figure 3 The CAIN experiment outside and inside.

Camera specifications are available in online reviews [23-25]. The Canon 6D camera has good low-light performance and uses a CMOS sensor. The sensor is similar to that used in a Canon 5D mark II with a quantum efficiency of around 35% in green and 17% in red. It produces 5472 x 3648 14 bit colour images in raw or JPEG. The pixel size is 6.54 μm . This necessitated the purchase of a 5K monitor to view the images with minimal downsizing. The cameras were powered with an AC/DC adapter. The dark current is around 0.2 – 0.3 electrons/pix/sec below 11°C but jumps to 3.023 electrons/pix/sec at 26°C [23].

CAIN suffers from high daytime temperatures which presents a danger to equipment. This could be mitigated with a day time cover, only setting up the equipment at night or employing a DSLR camera cooling system. Insulation tests found that it took approximately 8 hours for the CAIN internal temperature to rise from 15°C to 45°C under 45°C external conditions and 10 hours to return to 15°C.

The Canon 6D camera sensor employs a RGGB Bayer matrix layer to produce separate red, green and blue channels. The Bayer red and green channels are cross-contaminated due to shallow filter cut offs. To alleviate this issue, drop in Clip R and G filters from Astronomik [26] designed to isolate red or green airglow wavelengths were used with one camera designated the red camera and the other green. The Clip filter bandwidths are ~ 80 nm, or 40 times that of the professional filters from Keo Scientific, and so let in extraneous light, but the transmission is good at over 90%. The Canon 6D also comes with an internal UV/IR filter which is similar to the Canon 5D II filter with $\sim 93\%$ transmission in the green but only 45% in red [27]. This filter was removed in the red camera providing 100% transmission across the spectrum, but was not removed in the green camera resulting in a slight overall reduction in the green filtered transmission response to 88%.

Cheap acrylic domes were used in place of the BK7 glass domes used in TRACE and Port-a-TRACE. Dome transmission was measured around 92% at airglow wavelengths. As with Port-a-TRACE, the supplied software is not designed to run autonomously so an in-house script is run by AstroArt 5 [17] using ASCOM drivers [18] to connect to the cameras.

Comparisons

Table 1 is a comparison of some of the properties of these airglow imagers. Note that small pixel sizes are often binned. Night time ambient temperature is assumed to be 11°C for the CAIN though Australian overnight temperatures can be significantly higher.

Table 1 A comparison of some imager properties

Imager	TRACE	Port-a-TRACE	CAIN
Bit depth	16	16	14
FOV	180	150	180
Chip size	1024x1024	2048x2048	5472x3648
Pixel size	13 μm x 13 μm	7.4 μm x 7.4 μm	6.54 μm x 6.54 μm
Operating temp	-80C	-25 below ambient	ambient
Dark current	0.001 e-/pixel/s (-70C)	0.01 e-/pixel/s (-20C)	0.303 e-/pixel/s (11C)
QE	Green 95% Red 95%	Green 50% Red 35%	Green 17% Red 34%
Filter BW (nm)	2	2	80
Filter transmission	Green 66% Red 95%	Green 88% Red 90%	Green 95% x 93% Red 95%

Although the TRACE Pixis Instruments camera has vastly superior dark noise levels and extremely high QE, the Port-a-TRACE Atik cameras have demonstrated comparable performance in terms of detecting airglow features.

Although CAIN failed to detect airglow features on its one dark site field deployment alongside Port-a-TRACE, one of the Canon 6D cameras has detected numerous airglow features at 557.7 nm in an ambient temperature of 20°C without any filters, so the concept of a cheap airglow system using retail DSLR cameras has been demonstrated. CAIN's failure to detect airglow features that were detected by the adjacent Port-a-TRACE may have been due to user error when setting up the CAIN system as much as the less effective filtering.

Cost

A summary of the approximate major costs required for each system are listed in Table 2. Although the costs were born in different years from 2011-2014 the amounts are so disparate that this does not impact on the results. The CAIN camera cost is made up of body (\$1400), sigma 8 lens (\$700) and sD card (\$150). TRACE cooling includes both a Mitsubishi 7kW air conditioner (\$1700) and air conditioner install costs with security cage (\$1800). Port-a-TRACE cooling includes the cost of the air conditioner (\$2000) and the cost of coating with a heat reflecting paint (\$2000).

Table 2 Comparison of major item costs

Item	TRACE	Port-a-TRACE	CAIN
Container	\$50,000	\$5000	\$500
Cameras	\$130,000	\$28,000 x 2	\$2100 x 2 (body)
Filters	\$5000 x 5	\$4300 x 2	\$300 x 2
Domes	\$1700	\$1700 x 2	\$50

Cooling	\$3500	\$4000	\$30
Support	(Pier) \$6000		
Total	\$221,200	\$77,000	\$5380

Additional costing for adaptors, cables and pelican cases to store equipment have not been included. Similarly, computer hardware is not reflected in this table as, in general, stock computers were used. The re-occurring cost of freighting equipment is not included in this section but is covered under transportation.

Portability

DST Group's airglow experiments require a degree of portability. The 20ft TRACE shipping container may be carried on a flatbed truck. It is usually manoeuvred by a crane which can be expensive to send to remote sites. Equipment is packed in Pelican cases and secured using tie-down points for transport. When set up, the empty cases are stored within the container itself.

Port-a-TRACE sits on a pallet and may be transported by commercial freight companies or a utility/pickup vehicle. Upon delivery, it is easily transported by fork lift, readily available on experimental sites. The domes and cameras are stored in Pelican cases but when set up, empty equipment cases must be stored locally to prevent dust intrusion and theft in remote areas.

CAIN is easily transported without issue and may be carried by two people without the need for a forklift. The two Canon cameras, domes, filters and other equipment are contained in one pelican case. A 4WD vehicle is sufficient to carry CAIN and the equipment case.

As an indication, one way freight costs from Edinburgh to Alice Springs are approximately \$8000 for TRACE, \$1600 for Port-a-TRACE and \$200 for CAIN.

Ease of use

TRACE is transported as a sealed container and is reasonably easy to construct with two or three people required to move the pier and the camera safely. Ladders are required to fix the dome and camera in position. The camera and sensor software are programmed to start automatically on boot up and images are saved automatically. Equipment is powered from an Internet addressable power supply unit such that the camera or computer can be re-booted by a 3G mobile phone internet connection. Images can also be downloaded via the 3G link.

Port-a-TRACE can be constructed by a single person though two are used for safety reasons. The enclosure houses a small tool box, two collapsible camping stools and a camping table that allow components to be constructed off the ground. The software is relatively straight forward but requires customised software to achieve automatic start-up.

CAIN can easily be constructed by one person. Default DSLR camera settings are not suitable for astronomical work, and need to be optimised before use. Practical lessons learnt include the need to carefully focus the lens for pinpoint stars, and then securing the focus ring with tape to prevent accidental de-focussing during setup. Similarly the lens cap is supported on a stand-off flange to clear the fisheye lens, and if the user neglects to remove the stand-off flange, then the Field of View is severely compromised.

Robustness

When transporting the TRACE shipping container, items are usually packaged in pelican cases or tied down to points inside the container and transported without issue. Care must be taken to secure the external air-conditioner to ensure that it does not dislodge during transport, especially over rough terrain.

TRACE's Mamiya fisheye lens suffered UV degradation after a two week trial in Alice Springs. Similar degradation has been reported on OMTI [8] and THEMIS Ground Based Observatory [28] imagers. Cost to repair the now obsolete lens was approximately \$300. UV damage has been reduced with the new additions to the pier software to lower the cameras camera during the day but an automated shield to cover the lens in some way is still being considered.

The main issue with port-a-TRACE is lens exposure. There are several 'clam shell' like covers available but at great expense. A sliding cover over the entire box has been designed which would protect the lens from UV and help keep the container cool overnight. Port-a-TRACE's heat resistant paint does not adhere well to the container and easily scrapes off during transport if not well protected. Each recoat costs \$2000. Extra skin protection is required when transporting the container.

Like many inherently light containers, CAIN needs to be anchored down with rope and stakes [1] especially at sites with high wind. The plastic domes tended to degrade so that the flange that holds them onto the icebox disintegrates. They are also easily scratched. The icebox was not well waterproofed, despite extra sealing which leads to water and vermin ingress.

Dome dewing is a common problem in both Port-a-TRACE and CAIN. Moisture absorbing crystals are employed in all three containers to reduce internal humidity. The inside of the Port-a-TRACE container is kept above dew point temperatures throughout the night via the air conditioner. A fan taped to the camera body was used to blow internal container air up around the dome to mitigate dewing but this created a small amount of camera vibration and also posed possible safety concerns if run remotely. Dew straps designed for telescope use wrapped around the camera lens have been successful. A ring of resistors to warm the dome itself has been designed but not yet implemented.

The CAIN domes are very close in diameter to the camera lens and leave little room for air to circulate or for dew straps which has caused significant dewing problems. Widening the space between lens and dome, or heating the domes directly via resistors may be investigated to combat this problem.

Imaging performance

Image processing is detailed in Unewisse, *et al.* [3] and utilizes both in-house code and free astronomical libraries. Processing speed is noticeably slower as the image size increases so that CAIN images are processed in a separate fashion to those from TRACE and Port-a-TRACE. Additionally, CAIN images are in a raw camera format (.CR2) which cannot be read with standard routines and are converted to TIFF format for storage and processing.

Due to the filter wheel system employed in TRACE, the revisit rate for each filter is typically 8 minutes whereas both Port-a-TRACE and CAIN take a series of images with the one filter

so that the revisit time is defined by the exposure time plus download time of approximately 8 second.

A comparison of 2 minutes exposure TRACE and Port-a-TRACE 557.7 nm airglow images taken at DSTO Edinburgh with an SQM light reading of 19.3 mag/arcsec² at the same time with the same processing is shown in Figure 4. Similar airglow ripples features are seen in both images.

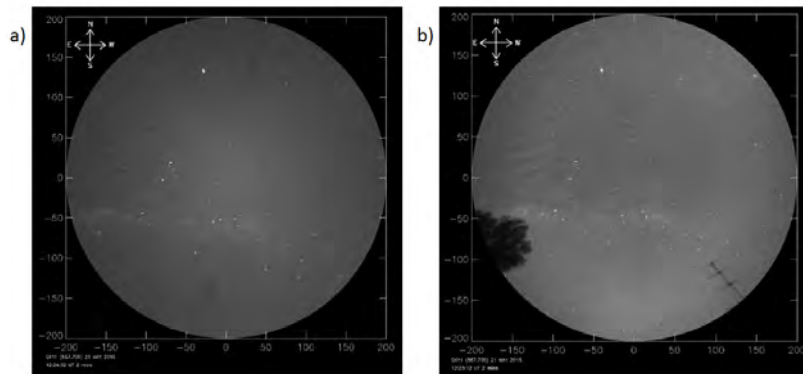


Figure 4 A comparison of 2 minute exposure 557.7nm airglow banding images taken at the same location 12:21 UT on the 21st of May 2015 with an SQM light reading of 19.3 mag/arcsec². a) TRACE and b) Port-a-TRACE

CAIN has not yet been able to detect airglow at the same location as TRACE and Port-a-TRACE in light polluted locations such as DST Edinburgh due to the lack of very narrowband filters needed to exclude urban Light Pollution.

Figure 5 shows a comparison of a 557.7 nm airglow flare imaged on the same night a) two minute exposure TRACE image taken at Edinburgh with an SQM light reading of around 19 mag/arcsec² and b) 45 second exposure, RGB, ISO 3200 CAIN 6D image without filter taken at Sedan, 82km NE of Adelaide with an SQM light reading of around 21.8 mag/arcsec². Banding and bores were also imaged by both detectors on this night.

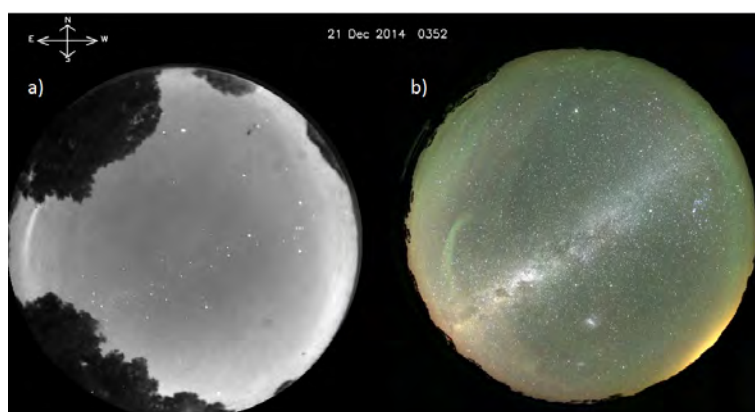


Figure 5 557.7 nm airglow imaged with a) TRACE at Edinburgh (2 minute exposure) with an SQM light reading of ~19 mag/arcsec² and b) CAIN (45 second exposure) at Sedan with an SQM light reading of 21.8 mag/arcsec².

Conclusion

TRACE is a professional airglow imager designed for long-term use in the one location. It is sensitive enough to use even in slightly light affected locations, although sodium observations are precluded in the presence of light pollution from sodium street lighting. Importantly, the CCD and filters allow the results to be calibrated so that absolute airglow intensity may be measured. Apart from damage to the lens from UV exposure, it has performed well over a number of years. Little computer expertise is needed to run the software and the data is amenable to calibration and of publishable quality. It is, however, an expensive investment and best suited as part of a large network or similar instruments such as OMTI [8, 29].

Port-a-TRACE is a good balance between cost and performance. The portability makes it more useful in HF field studies than TRACE and the Sentinel's Atik cameras match the Sentry's Pixis for image quality even in light affected areas. However, due to filter temperature sensitivity and the inability to set the filter temperature, determining exact, calibrated airglow intensities with the Sentinel camera would be difficult. Some programming ability is needed to be run the cameras remotely. Thermal coating of the container is probably too expensive and fragile for experimental benefit.

Canon 6Ds are a viable option for keen photographers in a dark sky location. They have been shown to detect airglow but the data is not suited for quantitative calibration due to the width of the spectral response and the lack of temperature control. An icebox container provided some thermal protection but these cameras are more suited to overnight experiments rather than long term installation and may be better run on just a camera tripod. This could be turned into a relatively cheap school airglow project in a suitably dark location.

Mixing and matching components from the three airglow systems would allow a better compromise. For example, the TRACE camera placed inside a port-a-TRACE container would result in a highly sensitive and portable airglow imager. Additional space requirements for the extra components of the TRACE such as the filter wheel temperature monitor would have to be addressed.

Future work

Due to time and operational considerations, CAIN has been discontinued though the cameras are still available and may be incorporated into the other experiments. Port-a-TRACE and TRACE are destined to be co-located at the Murray Bridge Training Area (MUTA) on a new DST Group experimental site. SQM light readings at this site were 21.3 mag/arcsec², considerably darker than the current Edinburgh location and dark enough for CAIN-type cameras to detect airglow.

Acknowledgements

Thanks to Blair Lade for his time and efforts in testing the CAIN internal temperatures and Kalon Heintze and Jamie Carter for their work in converting the TRACE, Port-a-TRACE and CAIN containers for our use.

References

1. P. J. Loughmiller, "Observational and theoretical studies of mesospheric dynamics and bores using airglow imagers at mid-latitudes," Doctor of Philosophy, Graduate School, Cornell University, 2008.
2. T. S. Trondsen. (2012, March 29). *Low Light Level Imaging Instrumentation for Airglow - Keo Scientific*. Available: <http://www.keoscientific.com/aeronomy-imagers.php>
3. A. Unewisse, *et al.*, "TRACE: A New Relocatable Airglow Imager," in *Proceedings of the 13th Australian Space Science Conference* Sydney., 2014, p. 149.
4. M. Schirmer. (2010). *About superflattening and defringing*. Available: <http://www.astro.uni-bonn.de/theli/gui/aboutsuperflattening.html>
5. "Pixis 1024 review C0," ed: Princeton Instruments, 2011.
6. "Princeton Instruments Certificate of Performance," ed, 2011.
7. S. Suzuki, *et al.*, "Statistical characteristics of gravity waves observed by an all-sky imager at Darwin, Australia," *J. Geophys. Res.-Atmos*, vol. 109, p. D20S07, 2004, doi:10.1029/2003jd004336.
8. K. Shiokawa, Y. Otsuka, and T. Ogawa, "Propagation characteristics of nighttime mesospheric and thermospheric waves observed by optical mesosphere thermosphere imagers at middle and low latitudes," *Earth Planets Space*, vol. 61, pp. 479-491, 2009.
9. T. Ogawa, *et al.*, "Simultaneous ground- and satellite-based airglow observations of geomagnetic conjugate plasma bubbles in the equatorial anomaly," *Earth Planets Space*, vol. 57, pp. 385-392, 2005.
10. F. J. Garcia, M. J. Taylor, and M. C. Kelley, "Two-dimensional spectral analysis of mesospheric airglow image data," *Appl. Optics*, vol. 36, pp. 7374-7385, 1997.
11. "Sky Quality Meter -LU Users manual," Optcorp, Ed., 1.1 ed, 2006.
12. "Cloud Sensor II User's Manual," Boltwood Systems Corporation, V0026 ed, 2009.
13. T. S. Trondsen, "Keo Sentinel Wide-Angle Monochromatic Imager," K. S. Ltd., Ed., ed. Calgary, Alberta, 2016.
14. "Outdoor racks 19 inch mounting IP55, IP65, IP66," OverIPGroupPty.Ltd., Ed., ed. OverIP Group Pty. Ltd., 2014.
15. "Industrial Outdoor Air Conditioners EC Series," ed: OverIP Group Pty. Ltd., 2008.
16. "Cooling for Outdoor Enclosures, Indoor A/C/Heat Exchangers/Hybrids," ed: OverIP Group Pty.Ltd., 2016.
17. *AstroArt*. (2015). Available: <http://www.msb-astroart.com/>
18. *ASCOM: Standard for Astronomy*. (2015). Available: <http://ascom-standards.org/>
19. "Aurora Cloud Sensor User Guide Software version 3.1.0," A. Eurotech, Ed., ed, 2013.
20. M. Hattey, "Handbook for the SX 'Oculus' high resolution all-sky camera," S. X. Ltd., Ed., ed. UK, 2013.
21. T. Ashcroft and W. Lyons. (2014). *Photograph of a mesospheric bore*. Available: http://rammb.cira.colostate.edu/projects/npp/blog/index.php/uncategorized/severe-weather-in-the-mesosphere/attachment/mesospheric_bore/

22. A. Cherney. (2014). *Movie of bore over Heathcote, Victoria, Australia taken with Nikon D700*. Available: <http://vimeo.com/52319627>
23. R. Clark. (2014). *The Canon 6D Digital Camera Review: Sensor Noise, Thermal Noise, Dynamic Range, and Full Well Analysis* Available: <http://clarkvision.com/reviews/evaluation-canon-6d/index.html>
24. Chrisk98. (2014). *Sensor performance, quantum efficiency, sensorgen and DXOMark*. Available: <https://www.dpreview.com/forums/post/53054826>
25. DXOMark. (2013). *Canon EOS 6D*. Available: <https://www.dxomark.com/Cameras/Canon/EOS-6D---Specifications>
26. G. Neumann. (2016). *Clip-Filter system for Canon EOS cameras*. Available: <http://www.gerdneumann.net/english/filter/astronomik-filters/astronomik-clip-filter-system.html>
27. Kolarivision. *Internal Cut Filter Transmission*. Available: <http://kolarivision.com/articles/internal-cut-filter-transmission/>
28. S. E. Harris, *et al.*, "THEMIS Ground Based Observatory System Design," *Space Sci. Rev.*, vol. 141, pp. 213-233, 2008/12/01 2008, doi:10.1007/s11214-007-9294-z.
29. K. Shiokawa, *et al.*, "Development of Optical Mesosphere Thermosphere Imagers (OMTI)," *Earth Planets Space*, vol. 51, pp. 887-896, 1999.

Airglow Observations from ELOISE

Anne M. Unewisse, Manuel A. Cervera, Lenard H. Pederick, Trevor J. Harris and
Andrew D. Cool

Defence Science and Technology Group, PO Box 1500 Edinburgh SA, 5111, Australia

Summary:

In August and September 2015, the Defence Science and Technology Group (DST Group) undertook the Elevation-scanned Oblique Incidence Sounder Experiment (ELOISE): a unique campaign to observe and characterise mid-latitude ionospheric disturbances across Australia using a large number of measurement systems located at 18 sites spanning the Australian mainland. As part of this experiment, two airglow imagers were deployed in the Alice Springs region co-located with a dense Quasi-Vertical Incidence Sounder (QVIS) subnetwork. Airglow images taken over Alice Springs at 630.0 nm and 557.7 nm are discussed and compared to High Frequency soundings from one baseline of the QVIS network. When strong travelling ionospheric disturbances (TIDs) are present, an inverse relationship is seen between airglow intensity and measurements of virtual height at 2.4 MHz and a correlation is seen between the two airglow measurements. The time lag between the two airglow observations and QVIS virtual height time series over a range of HF frequencies is used to derive characteristics of travelling ionospheric disturbances.

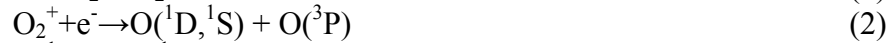
Keywords: Airglow imaging, ionospheric studies, TIDs

Introduction

The Defence Science and Technology Group (DST Group) National Security and Intelligence, Surveillance and Reconnaissance Division (NSID) High Frequency Radar Branch (HFR Branch) is responsible for research into the propagation of High Frequency (3-30 MHz) radar signals in support of Australia's defence. In August and September 2015, it undertook ELOISE (Elevation-scanned Oblique Incidence Sounder Experiment), as reported in Ward, *et al.* [1], one of the largest ionospheric experiments ever conducted in Australia. Designed to observe and characterise mid-latitude ionospheric disturbances across the Australian mainland, ELOISE employed a variety of measurement sensors located at 18 sites including individual HF sounders, 2D HF arrays, a QVIS network, GPS receivers and airglow imagers. Details of this experiment will be reported elsewhere. This paper reports on the airglow and QVIS components of this experiment.

Airglow is atmospheric electromagnetic radiation which results from chemiluminescence. The airglow emission wavelength is species dependent with common reactants being oxygen, sodium or hydroxyl ions and molecules. The brightness of the airglow is proportional to the density of the species which makes it an ideal tool to explore atmospheric density variation. DST Group has studied the Earth's airglow emission originating from altitudes close to the ionospheric E and F layers and its relationship to High Frequency (HF) propagation since 2011 [2].

Although airglow is always present, it is very faint and generally only detectable at night. As night-time HF propagation is primarily via ionospheric F-layer paths, airglow emission originating from altitudes near F-layer altitudes are of the most interest to our studies. F-layer airglow is mainly red 630.0 nm wavelength emission from a ~100 km wide altitude band centred around 250 km but about 30% is green 557.7 nm emission originating from 245 km [3, 4]. The two emissions result from two different metastable states of the dissociative recombination of O_2^+ : $O(^1D)$ which produces 630.0 nm radiation and $O(^1S)$ which is responsible for 557.7 nm emission [5-7]. These reactions are summarised in the following equations:



The $O(^1D)$ state, responsible for red emission, has a radiative lifetime of 110s whereas the $O(^1S)$ state, responsible for the green emission, has a radiative lifetime of 0.91s. Additionally, the $O(^1S)$ reaction leading to 557.7 nm radiation also results in the $O(^1D)$ metastable state required for 630.0 nm emission [7]. Airglow production at this altitude is dependent on the densities of both neutral oxygen atoms and O^+ (the most common ion in the F region) which makes it a sensitive indicator of local density perturbations as well as F-layer height [8] although the peak maximum airglow intensity lies 50 km below the F-layer peak altitude [9].

Under quiescent conditions, only a small fraction of green airglow emission measured on the ground is a result of F-layer dissociative recombination [3, 4, 10]. The greater majority is the result of a two-step atomic oxygen mechanism which occurs in a thin Mesospheric region around 96 km (E-layer) where the atomic oxygen density is highest [7] given by:



where O_2^* is the excited state of molecular oxygen and M is any molecule but usually N_2 .

A common problem in airglow analysis is determining green airglow's altitude of origin. When the ionosphere is benign, about 90% of measured green airglow originates from the bright mesospheric band around 96 km [3, 4, 10]. However, localised density perturbation can enhance or decrease green airglow emission from one altitude over the other [3].

Studies of airglow correlation with HF [11], incoherent scatter radar [5, 12] and TEC measurements [13, 14] have found that falling airglow intensity is associated with increasing virtual heights measured by a Vertical Incidence Sounder (VIS) and rising airglow intensity with decreasing virtual heights. This relationship between airglow intensity and virtual height is also seen in Travelling Ionospheric Disturbances (TIDs) [15], brightness waves [16] and plasma bubbles [17, 18].

This paper discusses 630.0 nm and 557.7 nm airglow emission observed from the 8th to the 13th of September 2015 over Alice Springs, Australia during ELOISE and compares them to each other and to HF observations recorded at the same location and time by a Quasi Vertical Incidence Sounder (QVIS) network.

Experimental overview

The layout of the ELOISE QVIS network [19-21] is shown in Figure 1. The network was composed of two transmitters, located at Alice Springs Airport (AS) and Hart's Range (HR), and three receivers located at Hermannsburg Ranger station (HE), Mount Everard (ME) and Alice Springs airport. Red circles on Figure 1 indicate midpoints from transmitter to receiver and may be regarded as the ionospheric probe point for that path.

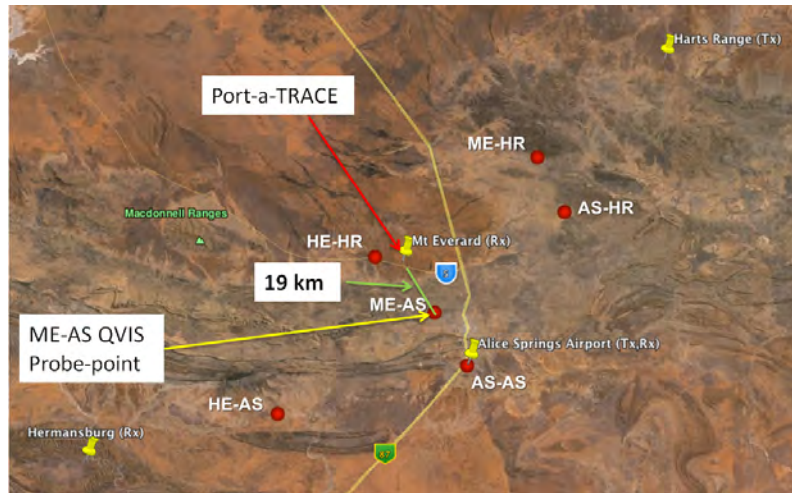


Figure 1 The airglow and QVIS experimental set-up of ELOISE. The notations are: HR: Hart's Range, HE: Hermannsburg, AS: Alice Springs Airport, ME: Mount Everard. Red circles mark QVIS mid points.

The PRIME (Portable Remote Ionospheric Monitoring Equipment) sounders deployed for the QVIS were developed by DST Group [20]. The sounders use a delta transmit antenna with 24 m mast and 21 m arms and a crossed magnetic loop receive antenna. The transmitted waveform is a continuous-wave (CW) signal swept linearly in frequency from 2 to 22 MHz (a chirp) via a solid-state digital waveform generator fed into a 100 W power amplifier, although transmitted power was nominally 50 W. Soundings were taken every 75 seconds.

Airglow emission in the QVIS region was recorded by the Portable Thermospheric Radar Airglow Correlation Experiment (Port-a-TRACE) located at -23.523° , 133.680° , 800 m from the Jindalee Over-the-horizon Radar Network (JORN) receiver site at Mount Everard, Alice Springs (R3). Port-a-TRACE consists of two Keo Sentinel monochrome cameras [22] housed in a purpose built double walled, insulated, air-conditioned OverIP outdoor enclosure [23]. Each imager has a 150° field of view, f/4.0 lens and holds a single 2 nm bandwidth filter. One camera was centred on 557.7 nm and the other on 630.0 nm. Sentinel's Kodak KAI 04022 2048x2048 16 bit CCD has a pixel size $7.4\mu\text{m} \times 7.4\mu\text{m}$ and quantum efficiency of approximately 50% at 557.7 nm and 35% at 630 nm. Two minute exposures were taken continuously through the night on each camera.

Observations

QVIS

QVIS observations reported in this paper were made on the Alice Springs airport to Mount Everard path (ME-AS probe point located at 23.6616°S, 133.7889°E) shown in Figure 1. Although the closest ionospheric probe point to the centre of the Port-a-TRACE FOV lies between Hermannsburg and Harts Range, the Hermannsburg sounder suffered from high noise problems and was not processed further for this work.

Figure 2 shows a typical day time quasi-vertical ionogram collected during ELOISE. The data was processed to determine the Ordinary (O)-mode virtual height of the ionosphere as a function of frequency at the midpoint by range converting the QVI to produce an equivalent vertically incident ionogram.

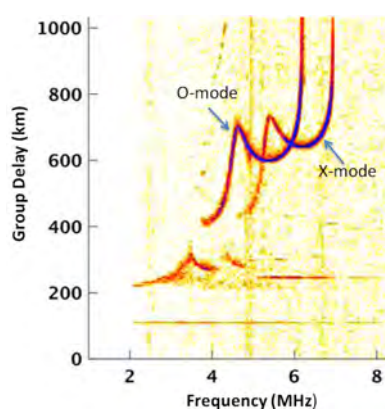


Figure 2 A typical frequency vs group delay ionogram obtained during ELOISE.

Airglow

Airglow intensity was calculated using an 80x80 pixel square centred on the ME-AS probe point covering the region from the transmitter to the receiver for this path as shown in detail in Figure 3a and as an inscribed square on the airglow image in Figure 3b.

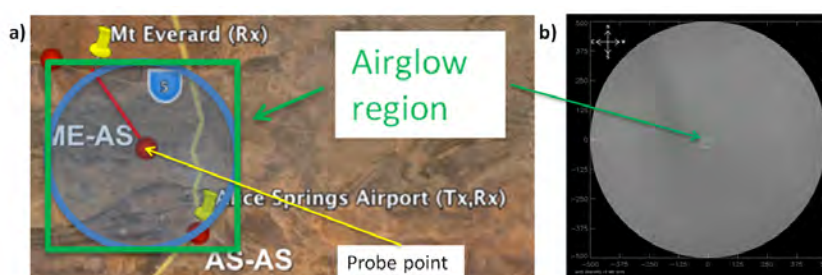


Figure 3 The airglow region used to calculate the median value a) around the ME-AS probe point on a map and b) on the airglow image.

Two minute exposure airglow images were taken at 630.0 nm (red) and 557.7 nm (green) with a gap interval of about 8 seconds. All images were processed using TRACE software [24] to subtract dark frames, correct for atmospheric and van Rhijn effects [25], minimise star interference, correct for fisheye lens distortion and convert from pixels to km.

Figure 4 illustrates the small-scale ripples commonly seen in 557.7 nm (green) airglow emission images during ELOISE. The field of view (FOV) at this altitude has a diameter of approximately 400 km. These ripples appear as short wavelength (<15 km) wavy structures and are usually due to small scale local instabilities (~20 m) in the Mesosphere [26]. Note that, by convention, east and west are reversed on the images.

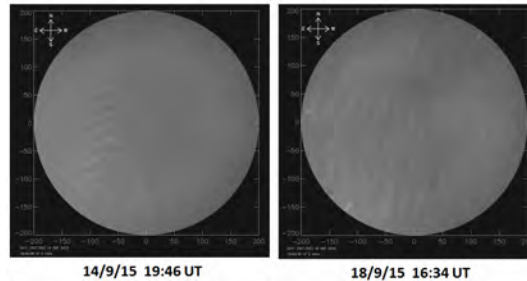


Figure 4 Typical 557.7 nm (green) 2 minute exposure images taken during the trial.

Figure 5 shows typical examples of 630 nm (red) airglow emission images seen during ELOISE. The FOV at this altitude has a diameter of approximately 1000 km. The images consist of large scale bright and dark bands that change over time with a general motion from south-east to north-west.

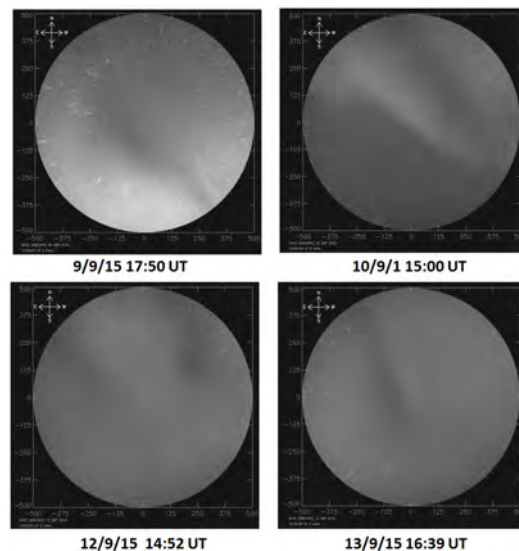


Figure 5 Typical 630.0 nm (red) 2 minute exposure images taken during the trial.

Analysis

Figure 6 compares smoothed median 630.0 nm (red) and 557.7 nm (green) airglow intensity values in arbitrary units to the corresponding QVIS O-mode virtual height at 2.4 MHz in km (black) from the 8th to the 13th of September 2015 over 12.0-17.5 UT around the ME-AS probe point. Also marked on the figure is the maximum cross correlation and corresponding time lag between a) median 630.0 nm airglow and 557.7 nm green airglow intensity and b) median 630.0 nm airglow intensity and QVIS virtual height at 2.4 MHz. The maximum correlation is obtained by applying a series of positive and negative time lags to the red

airglow data and calculating the correlation. QVIS time series were resampled to the airglow sample spacing of 2.13 minutes and corrected for any offset in starting time. A positive time lag represents a red airglow lag with respect to green airglow or QVIS measurements.

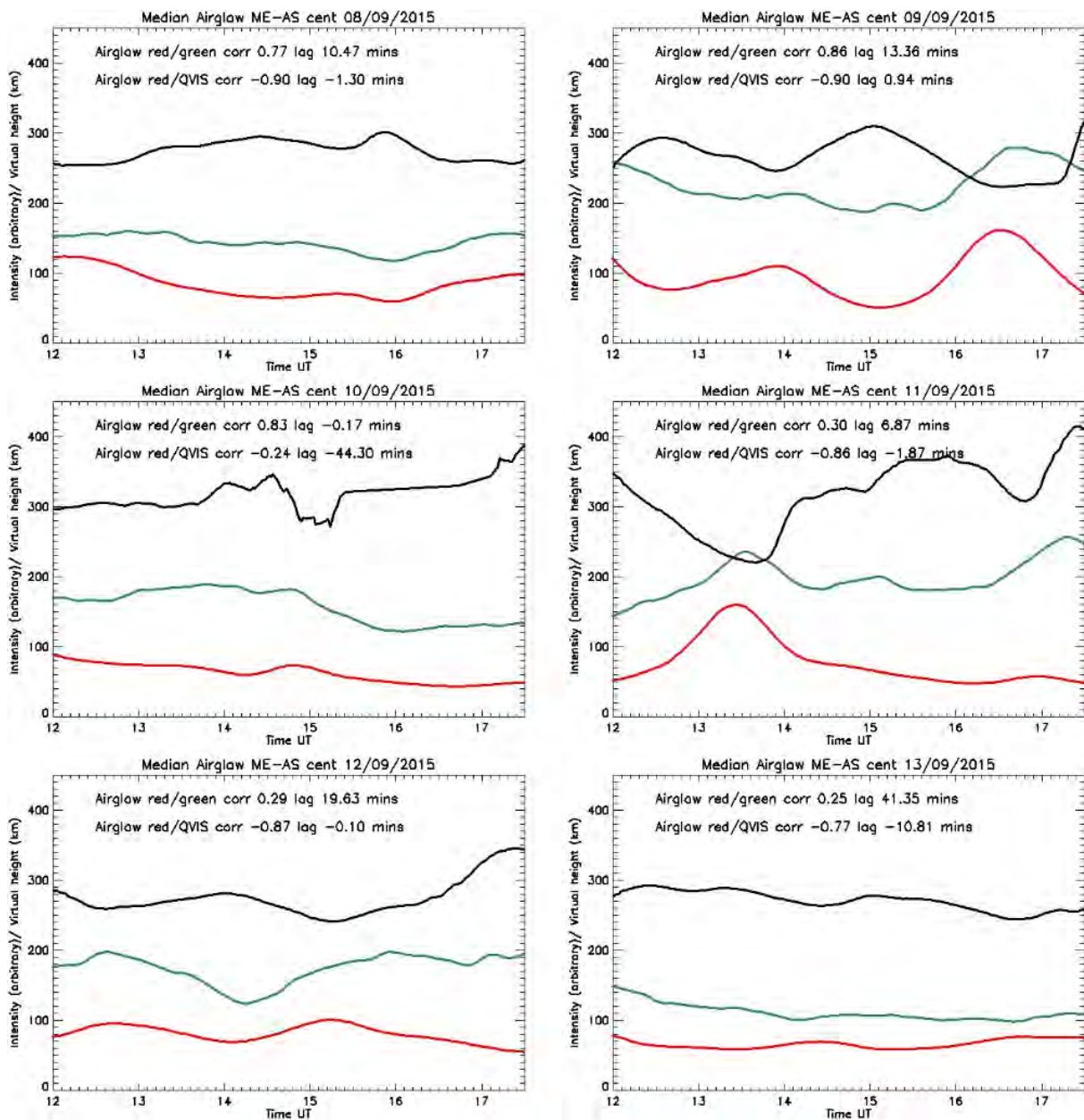


Figure 6 Median red and green airglow over time (UT) calculated for the ME-AS ionospheric probe point compared to QVIS virtual height at 2.4 MHz (black) from the 8th to the 13th of September 2015 over 12-17.5 UT. The virtual heights are in km, the airglow values are intensity in arbitrary units.

In general, the airglow measurements are correlated and the airglow/QVIS measurements are anti-correlated. This is especially true when strong enhancements or depletions are present such as the 2.5 hour period TID on the 9th of September and the airglow enhancement on the 11th of September. Very little sporadic E was observed during these days and times.

The anti-correlation between 630 nm airglow intensity and QVIS virtual height measurements [15] is due to neutral and charged atmospheric density perturbations which cause opposite effects in airglow intensity and QVIS virtual height measurements. Density depletions reduce the number of reactants available to produce airglow but results in an increased virtual height measurement as transmitted HF signals will penetrate further into the ionosphere.

Discussion

When a strong perturbation is present, it can often be detected in both 630.0 nm red and 557.7 nm green airglow emission and result in a high correlation between the two time series. If the time lag between two highly correlated time series is small then either F-layer 557.7 nm emission dominates the measured green emission during strong perturbations [3, 10] or the density perturbation extends at least 100 km in the vertical direction and has a vertical phase front so that it affects the E-layer and F-layer simultaneously [6, 27]. A large time lag between two highly correlated airglow time series indicates that either the density perturbation has a sloping phase front which affects the density of one layer before the other or that the perturbation is travelling in the vertical direction. This latter condition is only likely if the perturbation is generated in the lower levels of the atmosphere and travels upwards [14]. Sloping phase fronts may be mapped by the QVIS network by plotting a series of virtual height time series across a range of HF frequencies. As higher frequencies penetrate further into the ionosphere, they provide information about higher regions of the ionosphere.

The periodic TID seen in the airglow intensity time series of the 9th of September in Figure 6 is shown in detail in Figure 7a), the higher altitude 630.0 nm red airglow peaks and troughs precede the 557.7 nm green airglow peaks and troughs by more than 13 minutes implying that the green airglow originates primarily from the E-layer and that the density perturbation has a forward tilted phase front [28].

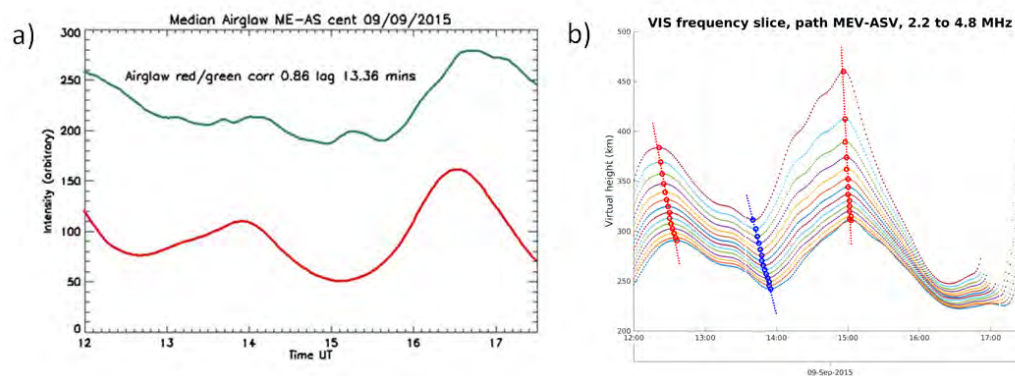


Figure 7 Airglow intensity time series on the ME-AS QVIS path for the 9th of September 2016 from 12.5-14.5 UT and b) the corresponding QVIS Frequency slices from 2.2 (bottom) to 4.8 MHz showing a forward sloping phase front.

This interpretation is supported by virtual height measurements on the ME-AS QVIS path across a range of frequencies from 2.2 (bottom) to 4.8 MHz (top) for the same time and day shown in Figure 7b). Lines through the crests (red) and troughs (blue) of the disturbance indicate the slope of the phase fronts where the features were distinct enough to calculate. It can be seen that as the disturbance passes through, the higher frequencies lead the lower

frequencies in phase. Note that this frequency-dependent phase relation implies that the phase lag between QVIS-measured virtual height and airglow is dependent on the QVIS frequency.

Conversely, the airglow intensity enhancement seen on the 11th of September from 12.5 – 14.5 UT, shown in detail in Figure 8a, has strongly correlated airglow but a small time lag relative to the sample spacing of 2.13 minutes. Figure 8b shows the corresponding time series of virtual height measured on the ME-AS QVIS path from 2.1 (bottom) to 3.8 MHz (top) at this time. A steeply tilted phase front is seen at 13.5 UT which tends to suggest that the green 557.7 nm airglow originates from the F-layer as E-layer 557.7 nm emission would exhibit a much longer time lag, depending on the actual height of the green airglow layer.

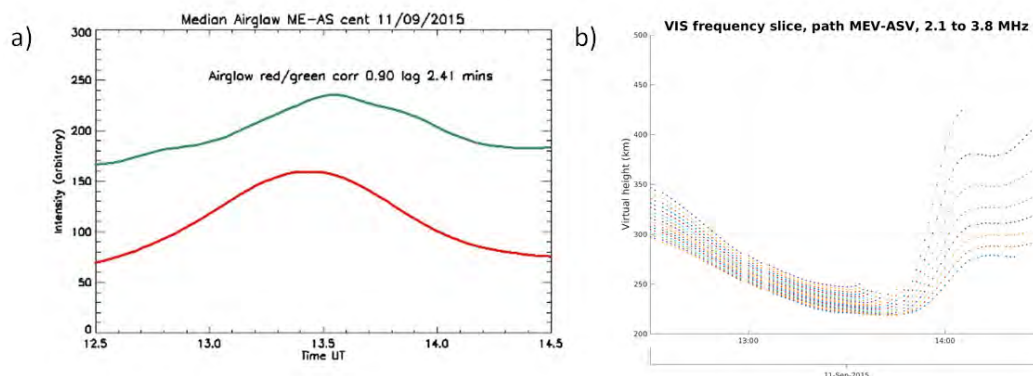


Figure 8 a) Airglow intensity time series on the ME-AS QVIS path for the 11th of September 2016 from 12.5-14.5 UT and b) the corresponding QVIS Frequency slices from 2.2 (bottom) to 4.8 MHz

It is possible that the broad intensity enhancement seen in the 557.7 nm green airglow intensity from 14.5 – 15 UT, shown in detail in Figure 9, is the E-layer 557.7 nm enhancement related to this steep phase front though it may be an unrelated enhancement in the 96 km altitude 557.7 nm green airglow.

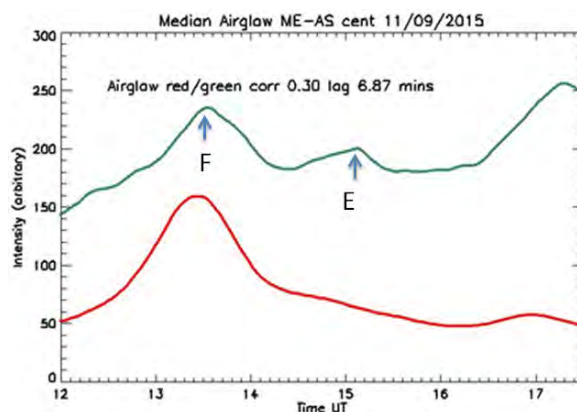


Figure 9 Airglow intensity time series on the ME-AS QIS path for the 11th of September, 2016 from 12-17.5 UT showing the possible E and F components of the green airglow.

The unusual HF virtual height increase and decrease seen in Figure 6 from 14 – 15.5 UT on the 10th of September corresponds to the onset of significant spread F as depicted in the QVIS time vs virtual height at 2.8 MHz plot of Figure 10 after 15 UT.

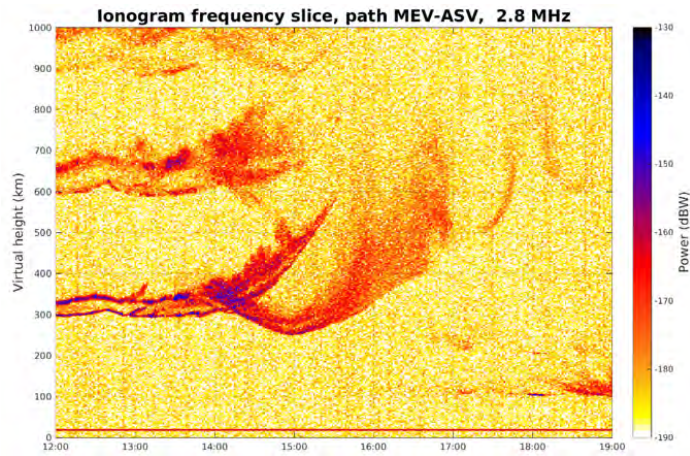


Figure 10 QVIS time vs 2.8 MHz virtual height on the QVIS ME-AS path for the 10th of September 2016.

This event will be the subject of a subsequent paper and corresponds to the appearance of an airglow depletion and brightness wave [16, 29] type feature which passed through the airglow field of view from 14 – 16 UT, just after local midnight (14.5 UT) on the 10th of September, 2015. The series of 2 minute exposure 630.0 nm red airglow images in Figure 11 shows the development of this travelling ionospheric disturbance feature over time. The brightness band was also faintly visible on the 557.7 nm green airglow image from around 15 UT. The nature of the spread F creates difficulties in creating QVIS frequency time series thus a phase slope cannot be calculated by this method for this feature. A similar relation between spread F and airglow depletion was reported by Lynn, *et al.* [17].

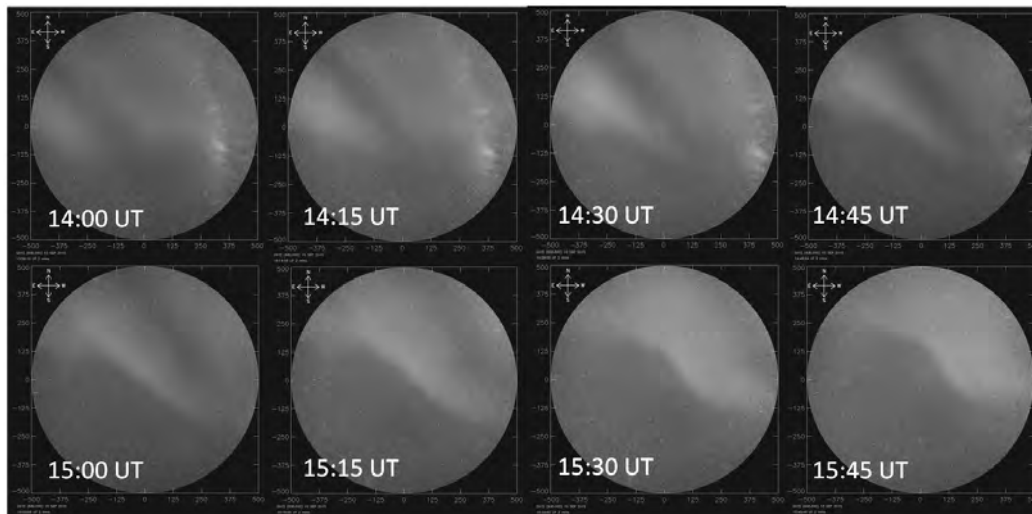


Figure 11 Fifteen minutes snapshots of a brightness-wave like event on the 10th of September 2015 from 14-16 UT.

Conclusion

This paper presents preliminary 630.0 nm red and 557.7 nm green airglow observations from the Defence Science and Technology Group (DST Group) ELOISE trial undertaken in August and September 2015 at Alice Springs, Australia and compares them to QVIS virtual height

measurements over the same region. Although ELOISE consisted of a large number of HF sounders over continental Australia, this report concentrates on results from one ionospheric probe point of a QVIS sub network co-located with the airglow imagers.

A general trend of correlated green and red airglow emission is seen as well as an anti-correlation of red airglow and QVIS virtual height measurements. This is especially true when significant enhancement or depletion of airglow intensity is present. As 557.7 nm green airglow originates from two different altitudes, time lags corresponding to the maximum correlation between 630 nm red and 557.7 nm green airglow time series during times of notable ionospheric perturbation were used to determine the altitude of the dominant 557.7 nm airglow emission. These results were supported using QVIS virtual height time series over a range of HF frequencies.

Data from three different days were examined in detail. Firstly, when peaks and troughs in red 630 nm airglow emission preceded green 557.7 nm airglow emission by 13 minutes in a quasi-periodic TID observed on the 9th of September, 2016, the green 557.7 nm airglow emission was found to be dominated by E-layer processes. The source of the perturbations was determined to have a forward tilted phase front. An airglow enhancement feature with a small time lag between airglow series seen on the 11th of September showed evidence of dominant F-layer 557.7 nm green airglow emission. Finally, a significant enhancement and depletion in QVIS virtual height measurements was found to be associated with spread F and a brightness wave type feature observed in airglow images. This event will be the subject of further work.

References

1. B. D. Ward, R. Gardiner-Garden, and A. Heitmann, "ELOISE - Towards an enhanced understanding of ionospheric variability and its impact on radio wave propagation," presented at the 15th Australian Space Research Conference, Canberra, September 29 - October 1, 2015.
2. A. Unewisse, *et al.*, "TRACE: A New Relocatable Airglow Imager," presented at the Proceedings of the 13th Australian Space Science Conference UNSW, Sydney, 2014.
3. R. A. Buriti, *et al.*, "OI557.7 nm nightglow intensity from F-region observed at 7.4°S," in *8th International Congress of the Brazilian Geophysical Society* ed: Sociedade Brasileira de Geofísica (SBGf), 2003.
4. I. S. Gullede, *et al.*, "Intensity profiles of the 6300-A and 5577-A O I lines in the night airglow," *Journal of Geophysical Research*, vol. 73, pp. 5535-5547, 1968, doi:10.1029/JA073i017p05535.
5. J. H. Klenzing, *et al.*, "Multi-instrument observations of an MSTID over Arecibo Observatory," in *General Assembly and Scientific Symposium, 2011 XXXth URSI*, 2011, pp. 1-4.
6. D. Fukushima, *et al.*, "Observation of equatorial nighttime medium-scale traveling ionospheric disturbances in 630-nm airglow images over 7 years," *J. Geophys. Res.*, vol. 117, p. A10324, 2012, doi:10.1029/2012ja017758.
7. M. J. Nicolls, "Radar and Airglow Studies of F-Region composition and Dynamics at low latitudes," PhD, Electrical Engineering, Cornell University, Ithaca, New York, 2006.

8. K. Shiokawa, Y. Otsuka, and T. Ogawa, "Propagation characteristics of nighttime mesospheric and thermospheric waves observed by optical mesosphere thermosphere imagers at middle and low latitudes," *Earth Planets Space*, vol. 61, pp. 479-491, 2009.
9. M. Kubota, *et al.*, "New Observational Deployments for SEALION - Airglow Measurements Using All-Sky Imagers,," *Journal of the National Institute of Information and Communications Technology*, vol. 56, pp. 299-307, 2009.
10. P. R. Fagundes, Y. Sahai, and H. Takahashi, "Investigation of OI 557.7 nm and OI 630.0 nm nightglow intensity ratios during the occurrence of equatorial F-region plasma bubbles," *Journal of Atmospheric and Terrestrial Physics*, vol. 57, pp. 929-932, 7// 1995, doi:[http://dx.doi.org/10.1016/0021-9169\(94\)00064-U](http://dx.doi.org/10.1016/0021-9169(94)00064-U).
11. D. C. M. Amorim, *et al.*, "Long-term study of medium-scale traveling ionospheric disturbances using O I 630 nm all-sky imaging and ionosonde over Brazilian low latitudes," *Journal of Geophysical Research: Space Physics*, vol. 116, p. A06312, 2011, doi:10.1029/2010JA016090.
12. I. Seker, D. J. Livneh, and J. D. Mathews, "A 3-D empirical model of F region Medium-Scale Traveling Ionospheric Disturbance bands using incoherent scatter radar and all-sky imaging at Arecibo," *Journal of Geophysical Research: Space Physics*, vol. 114, p. A06302, 2009, doi:10.1029/2008JA014019.
13. H. Takahashi, *et al.*, "Plasma bubble monitoring by TEC map and 630 nm airglow image," *Journal of Atmospheric and Solar-Terrestrial Physics*, vol. 130–131, pp. 151-158, 2015, doi:10.1016/j.jastp.2015.06.003.
14. F. Huang, *et al.*, "Statistical analysis of nighttime medium-scale traveling ionospheric disturbances using airglow images and GPS observations over central China," *Journal of Geophysical Research: Space Physics*, pp. n/a-n/a, 2016, doi:10.1002/2016JA022760.
15. A. Unewisse, *et al.*, "Observations of a Travelling Ionospheric Disturbance over Adelaide, Australia," presented at the Proceedings of the 15th Australian Space Science Conference, ADFA, Canberra, ACT, 2016.
16. Y. Otsuka, *et al.*, "Optical and radio measurements of a 630-nm airglow enhancement over Japan on 9 September 1999," *Journal of Geophysical Research: Space Physics*, vol. 108, p. 1252, 2003, doi:10.1029/2002JA009594.
17. K. J. W. Lynn, Y. Otsuka, and K. Shiokawa, "Simultaneous observations at Darwin of equatorial bubbles by ionosonde-based range/time displays and airglow imaging," *Geophys. Res. Lett.*, vol. 38, p. L23101, 2011, doi:10.1029/2011gl049856.
18. A. A. Pimenta, *et al.*, "Ionospheric plasma blobs observed by OI 630 nm all-sky imaging in the Brazilian tropical sector during the major geomagnetic storm of April 6–7, 2000," *Geophysical Research Letters*, vol. 34, p. L02820, 2007, doi:10.1029/2006GL028529.
19. T. J. Harris, M. A. Cervera, and D. H. Meehan, "SpICE: A program to study small-scale disturbances in the ionosphere," *Journal of Geophysical Research: Space Physics*, vol. 117, p. A06321, 2012, doi:10.1029/2011JA017438.
20. T. J. Harris, L. Pederick, and A. D. Quinn, "The DST Group Ionospheric Sounder Replacement for JORN," *Radio Sci.*, vol. 51, pp. 563-572, 2016, doi:10.1002/2015RS005881.
21. T. J. Harris and A. D. Quinn, "The DSTO Ionospheric Sounder Replacement for JORN (03B1)," in *Proceedings of the 14th International Ionospheric Effects Symposium*, Virginia, USA, 2015, p. 1087.

22. T. S. Trondsen, "Keo Sentinel Wide-Angle Monochromatic Imager," K. S. Ltd., Ed., ed. Calgary, Alberta, 2016.
23. "Outdoor racks 19 inch mounting IP55, IP65, IP66," OverIPGroupPty.Ltd., Ed., ed. OverIP Group Pty. Ltd., 2014.
24. A. Unewisse, A. Cool, and M. Cervera, "Observations of a Mesospheric bore over Edinburgh, Adelaide," presented at the Proceedings of the 14th Australian Space Science Conference, UNISA, Adelaide, 2015.
25. P. J. Van Rhijn, "On the brightness of the sky at night and the total amount of starlight," *Astrophys. J.*, vol. 50, 12/1919 1919, doi:10.1086/142513.
26. J. Yue, *et al.*, "Seasonal and local time variability of ripples from airglow imager observations in US and Japan," *Ann. Geophys.*, vol. 28, pp. 1401-1408, 2010, doi:10.5194/angeo-28-1401-2010.
27. I. Paulino, *et al.*, "Periodic waves in the lower thermosphere observed by OI630 nm airglow images," *Ann. Geophys.*, vol. 34, pp. 293-301, 2016, doi:10.5194/angeo-34-293-2016.
28. M. A. Cervera and T. J. Harris, "Modeling ionospheric disturbance features in quasi-vertically incident ionograms using 3-D magnetoionic ray tracing and atmospheric gravity waves," *J. Geophys. Res.*, vol. 119, pp. 431-440, 2014, doi:10.1002/2013JA019247.
29. K. A. Dick, G. G. Sivjee, and H. M. Crosswhite, "Aircraft airglow intensity measurements: Variations in OH and OI (5577)," *Planetary and Space Science*, vol. 18, pp. 887-894, 1970/06/01 1970, doi:[http://dx.doi.org/10.1016/0032-0633\(70\)90085-1](http://dx.doi.org/10.1016/0032-0633(70)90085-1).

Tradespace Exploration for CubeSats Bus Design using Principal Component Analysis and K-medoids Clustering

Li Qiao, Michael Ryan, Mahmoud Efatmaneshnik

Capability Systems Centre, School of Engineering and Information Technology, The University of New South Wales, Canberra, ACT, Australia

Summary: CubeSats are plug-and-play satellites that are convenient to build because of the availability of various miniaturised, Commercial-Off-The-Shelf (COTS) satellite components. A Cube satellite bus design can be viewed as a combination of sets of COTS components with variables such as mass, volume, cost etc. so that a design tradespace that consists of numerous design alternatives can be generated from all possible combinations. In order to handle the numerous design alternatives and to support engineering design, an effective method for the tradespace exploration is required. For example, designers need to reduce their cognitive workload in addressing so many options, by being able to select a subset of designs of interest and examine data from different dimensions, which will accelerate decision-making. As the design tradespace is naturally large-scale and multi-dimensional, the proposed approach integrates computational data clustering algorithms with principal component analysis (PCA) Visualisation. In the proposed approach, the k-medoids clustering provides a grouping model where similar designs are aggregated and uncovering hidden patterns within datasets are revealed; and PCA allow users to visualise the design samples on 2D scatter plots. A case study utilising a tradespace consisting of 900+ CubeSat design alternatives is used to demonstrate how this approach supports knowledge discovery of design options through tradespace exploration of multi-dimensional data.

Keywords: Design tradespace exploration, principal component analysis (PCA), k-medoids clustering, data mining, engineering design

Introduction

CubeSat is a member of the class of pico-satellites, but has specific design standards. The size and mass standards of CubeSat are 100 mm cube and 1kg, respectively [1]. Many university-class satellites are CubeSats as they are considered as ideal affordable space development projects for space education [2]. More than 80 documented CubeSat projects are in development and 36 university CubeSats have successfully launched since 2003 [3]. The European Union QB50 CubeSat project will launch 50 CubeSats from 27 Countries into space in the end of 2016 (www.qb50.eu). A growing number of CubeSats development programs are emerging across the world, partly encouraged by the increasing availability of Commercial-Off-The-Shelf (COTS) components within the commercial space market [4], such as CubeSat Shop (www.cubesatshop.com). When designers build CubeSats, they can directly take the components from the shop.

Following the conventional practises of designing satellites, the decision to choose components is influenced by expert judgement and historical data from a project with similar specifications. The satisfactory design decision is made as soon as the requirements are met, and then the following work is to build the physical system and test to make it a product. However, because of exogenous system disturbances such as budget reduction or changes in stakeholder requirements, the decisions made previously may need to be adjusted during system

development or operations. These changes will most likely introduce cost in terms of resources such as schedule and cost. In order to avoid unnecessary resource waste, it is essential to make informed decisions with a thorough understanding of the available design options when designing complex engineered systems [5]. It is therefore desirable to gain more knowledge on the possible designs for CubeSat before purchasing physical components in the design phase.

Although CubeSats have limited volume, most CubeSats still have similar multiple, interacting subsystems and components as larger satellites, albeit smaller and fully implemented at the board level. Because of the availability of various COTS components and standard specifications, CubeSats are plug-and-play satellites that are convenient to build. If we view a CubeSat bus as a combination of sets of COTS components; large datasets of candidate designs can be generated by considering alternatives of one or more system elements [4] (e.g. the COTS database). Each alternative is a coordinate in a hyperspace that represents the selected design parameters such as attributes (e.g. mass, volume, power consumption) or system parameters (e.g. total life cost, power distribution, deliver time and reliability) that represent different design objectives. The task is to identify the good designs; however, it is not an easy task as the amount of information is beyond human analytical capability and overwhelms designers [6].

In order to handle the enormous number of design alternatives and to support decision making in engineering design, an effective tradespace exploration technique is required. We propose an approach integrating a computational data-clustering algorithm with multidimensional scaling visualisation; and demonstrate how this approach supports knowledge discovery of CubeSat design tradespace exploration by supporting the use of intuition into complex design problems. We make the following contributions:

- The PCA, one of the multidimensional scaling techniques, is employed as a graphical tool to visualise the high-dimensional tradespace in 2D view, so that designers can gain intuition about the utility of various trades.
- The k-medoids cluster analysis is used to identify similar design alternatives. Segmented solutions are visualised in both decision and objective spaces, allowing designers to examine their behaviour in the objective space.
- The user interaction is to select of the preferred solution from the tradespace according to the interpretable ability in revealing the pattern. The user interaction is used to guide the iterations.
- An iterative process of identify interesting trends among design alternatives is demonstrated. The identification of the interesting design points is achieved and the workload burden is reduced, gradually. In addition, the dominance of the design variables is revealed through iterations.

Methodology Development

In this section, we present the proposed approach to the design tradespace exploration.

A tradespace contains the multitude of possible design alternatives generated from examination of all the available combinations of design elements. In other words a tradespace is a “potential solution space” [7]. Typically, a large system has millions of possibilities, so that enumerating every point in the design space can be prohibitive. Decision making in design of complex engineered systems involves the solution to a multi-objective optimisation problem. There are two approaches to solve this problem: design optimisation and design exploration. In design optimisation, a fully automated optimisation process is implemented on a formulated design problem. Most research in this domain focuses on novel formulations and algorithms for solving optimisation problems (see, for example, [8, 9]). However, this approach still has several

shortcomings [10]. For instance, the optimisation often leaves designers unsatisfied with their results because the problem is usually improperly formulated. As Baling noted [11], in many cases, people do not know what they really want until they see some designs.

The tradespace exploration refers to the activity of exploring design alternatives prior to implementation [12]. It allows designers to reduce their cognitive workload in addressing large numbers of options by selecting a subset of designs of interest and examining data from different dimensions. The idea is that, since the large number of points confuses the decision maker, a simplification of the problem is to focus only on the groups of similar solutions. Thus, it is important to understand what structure is behind the data. This requires an ability to compare the different groups. If the groups are well built, it reduces the comparisons problem. Only the groups of points need to be considered in the first step. In the second step, it is possible to focus only on the interesting groups. Obviously, the group of interest is smaller than in the previous step, reducing the data burden gradually via several iterations. At the end, we can make a decision among a relatively small subset of solutions of interest. An experienced human can make a final decision among the suggested solutions with additional knowledge or just by intuition, or perhaps even purely by a subjective preference.

Our main objective is to reduce the cognitive workload by identifying the design alternatives of interest. This proposed method (see Fig. 1) is an iterative process utilising both computers and users. The computer implements the process of the PCA visualisation and cluster analysis, which can quickly identify features that may be of interest in the data. The user select process is then employed to decide which group of data to explore in the next step and how to explore it, (e.g. to decide the number of clusters which is input of the clustering algorithm). This approach is made up of the following four steps:

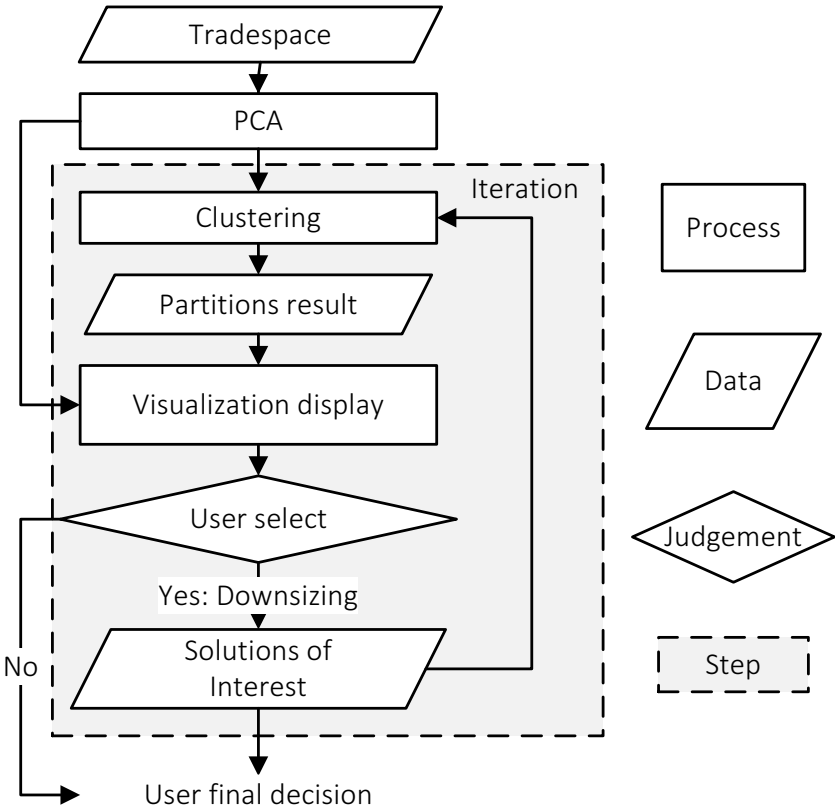


Fig. 1 Scheme of the proposed tradespace exploration approach

1) Dimension Reduction and Data Visualisation with PCA

Principal component analysis (PCA) is a statistical procedure that uses an orthogonal transformation to convert a set of observations of possibly correlated variables into a set of values of linearly uncorrelated variables called principal components [13]. Principal components (PCs) are uncorrelated and ordered such that the k^{th} PC has the k^{th} largest variance among all PCs. The k^{th} PC can be interpreted as the direction that maximises the variation of the projections of the data points such that it is orthogonal to the first $(k - 1)^{th}$ PCs. Using mathematical projection, the original dataset, which may have involved many variables, can often be interpreted in just a few variables (principal components). It is therefore often the case that an examination of the reduced dimension data set will allow the user to spot trends, patterns and outliers in the data, far more easily than would have been possible without performing the PCA. The rules to choose how many of the first PCs to retain are informal and ad-hoc [13]. Therefore, whether the number of first PCs captures most of the variation in the original data should be verified during implementation. For more details about PCA refer to [13].

2) Cluster Analysis using K-medoids

Cluster analysis is employed to access how intermediate variables affect design variables and objectives. Since PCs are uncorrelated and ordered, the first few PCs which contain most of the variations in the data, are used in cluster analysis[13]. i.e. the reduced dimension data points using PCs are clustered instead of the original full variables. The k-medoids clustering algorithm is applied to the reduced dimension data obtained by PCA, and the partition result is computed. The calculated partition result is expressed in both decision and objective space, so that the mapping information between the two spaces can be revealed.

Mathematically, k-medoids clustering takes as input a set of n objects S and an integer k (the number of clusters), and output a partition of S . Assume every design alternative is assigned to exactly one cluster, partitions are represented as a set of subsets $S = S_1, \dots, S_k$ such that $S = \bigcup_{i=1}^k S_i$ and $S_i \cap S_j = \emptyset$ for $i \neq j$. K-medoids starts with k initial seeds of clustering, where k is chosen *a priori*. All the n objects are then compared with each seed by a measure of distance such as Euclidean, and are assigned to the closest cluster seed. The procedure is then repeated, using the sum-of-squares of distances as the optimisation criterion. In particular, the k-medoids algorithm finds the centroid of each S_i , denoted S_i , is \hat{x}^i , if the algorithm is to optimize the function $c(S_i) = \sum_{v=1}^{|S_i|} d(\hat{x}_r^i, x_s^i)^2$. The goal of the algorithm is to minimise the objective function $c(S_1) + \dots + c(S_k)$. The algorithm stops when the changes in the cluster seeds from one stage to the next are smaller than a per-specified value. Clustering membership is determined by calculating the centroid for each group and assigning each object to the group with the closest centroid. For more details about k-medoids refer to [14].

3) Visualisation display

Three figures are shown as results to display the results of the previous two steps: 1) 2D scatter of the reduced dimension data in the decision space obtained from PCA; 2) 2D scatter of data in the objective space; and 3) Box plot of the combination of boards (the 6 design variables) in each cluster.

4) User select

The user selects the number of clusters and the group of interest, according to the clustering behaviour in the objective space. In this way, we ensure the knowledge generated is useful to decision makers. The distribution of the colour-coded points in the objective space changes with the setting of the clustering such as the input number of clusters. Then we examine how

the design space affects the objective space. Once the user selects which is the group of interest, a data downsizing is achieved by only looking into this group which the number of design points is reduced.

CubeSat Tradespace Data Set

In order to help the readers follow the proposed method, we construct an example CubeSat design tradespace that we will be referring to in the next sections. This section presents how we model the CubeSat design, as well as the construction of the CubeSat design tradespace.

In our example, we model a CubeSat bus using a structure that consists of six basic COTS components/subsystems, which are Communication, Power, Solar Panel, ADCS, Command Data Handling, and Antenna. The COTS components/subsystems are real boards from the online CubeSat Shop. Table 1 lists the specifications of COTS alternative for each component, where the Communication subsystem has four options and each of the rest five subsystems has three. We assume that all the COTS alternatives are available in the market and compatible with each other. Therefore, the key challenge for the system architect is to select the best combination of COTS boards that meets the system requirements.

Table 1 Components/Subsystems Alternatives

Subsystem	Options	Mass (g)	Vol (mm ³)	Cost (k€)	P.Con. (W)
(1)Communication	1 ISIS VHF/UHF	85	129.600	8.50	1.700
	2 ISIS UHF/VHF	75	129.600	8.50	4.000
	3 ISIS TXS	62	129.600	8.50	4.000
	4 NanoComU482C	75	154.800	8.80	5.500
(2)Power	1 NanoPower P31U	200	138.240	3.80	0.020
	2 NanoPower P31US	240	198.720	2.45	0.020
	3 Crystalspace P1U	270	12.320	2.90	0.015
(3)Solar panel	1 ISIS	50	16.170	2.50	0
	2 NanoPower 110	59	17.383	2.00	0
	3 NanoPower 110U	29	16.979	2.75	0
(4)ADCS	1 ESLCubeControl	115	259.200	4.80	0.220
	2 MAI400 1	694	559.000	30.80	3.170
	3 ISIS Magnetorquer	196	146.890	8.00	1.200
(5)Command Data Handling	1 NanoMind A712D	55	84.400	4.75	0.231
	2 ISIS On-board Computer	94	107.136	4.30	0.400
	3 Cube Computer	60	86.400	4.50	0.200
(6)Antenna	1 Patch HISPICO	110	8.000	4.86	0.010
	2 Turnstile antenna	100	37.228	5.50	0.060
	3 Dipole antenna	100	37.228	5.25	0.060

Note: Vol. is short for Volume. P.Con. is short for Power Consumption.

The tradespace is given in Table 2. The tradespace is an array of numbers, where n is the number of all design alternatives, and each alternative has multiple dimensions or variables. Each alternative is defined as a set of board decisions that consists of six design variables $\{k_1, k_2, k_3, k_4, k_5, k_6\}$, as follows.

k_1 , choose the k_1^{th} option for Communication subsystem, $k_1 = 1,2,3,4$

k_2 , choose the k_2^{th} option for Power subsystem, $k_2 = 1,2,3$

k_3 , choose the k_3^{th} option for Solar panel, $k_3 = 1,2,3$

k_4 , choose the k_4^{th} option for ADCS subsystem, $k_4 = 1,2,3$

k_5 , choose the k_5^{th} option for Command Data Handling subsystem, $k_5 = 1,2,3$

k_6 , choose the k_6^{th} option for Antenna subsystem, $k_6 = 1,2,3$

We vary the six components in Table 1 to generate all possible combinations of these boards. This results in $n = 4 \times 3 \times 3 \times 3 \times 3 \times 3 = 927$ design alternatives. For each CubeSat design alternative, we record four intermediate variables of interest, as follows.

- d_1 The total mass $M = \sum_{i=1}^6 m_{i,k}$
- d_2 The total volume $V = \sum_{i=1}^6 v_{i,k}$
- d_3 The total cost $C = \sum_{i=1}^6 c_{i,k}$
- d_4 The total power consumption $P. Con. = \sum_{i=1}^6 p. con_{i,k}$

where $m_{i,k}$, $v_{i,k}$, $c_{i,k}$, and $p. con_{i,k}$ signify the mass, volume, cost and power consumption of k_i^{th} option of subsystem/component i , respectively. d_1 to d_4 are dimensions in the 4D decision space. The requirement is to find design alternatives that satisfy the 2 objectives, as follows:

Minimise:

- Obj_1 Total cost d_3
- Obj_2 Power consumption per volume d_4/d_2

where Obj_1 and Obj_2 dimensions form the objectives space.

Table 2 Coordinates in the decision space and in the objective space

Variables	Design variables			Decision space			Objective space	
	k_1	...	k_6	d_1	...	d_4	Obj_1	Obj_2
Design alternative 1								
⋮								
Design alternative n								

Tradespace Visualisation with PCA

We use PCA to transform the original 927-by-4 data to a smaller 927-by-2 data for a 2D Visualisation (We will show 2 is a reasonable number later). As the variables are in different units (e.g. mass in kg , volume in mm^3), the original data is scaled before PCA implementation. We obtain information about the contributions of each principal component to the total variance of the coordinates, shown in Fig. 2. In our example, approximately 96% in total is accounted for by the first two principal components. As mentioned above, the goal of PCA is to identify the most meaningful basis to re-express a data set. This goal is achieved as we have accounted for the vast majority of the variation in the data using a two-dimensional plot, thus it is a reasonable way to reduce the dimensions to 2D.

Designers may want to know that how these variables are correlated. Table 3 gives the coefficients of correlation between each of the four variables. The correlation among some variables is as high as 0.93 and most correlation coefficients are relatively large (e.g. > 0.6), indicating the PCA could be effective. We use a dendrogram (see Fig. 3) to represent the relationships of similarity among the four variables, where the values on the horizontal axis are 1 minus the coefficients of correlation between variables shown in Table 3. We find that the variance of Power Consumption is different from others.

We plot all design alternatives from the design space in a lower 2D space in Fig. 4, where Dimension 1 and 2 is the first and second Principle Component (PC), respectively. Each point represents a unique design choice, pointing to a design alternatives in decision space. All design alternatives are plotted in the objective space in Fig. 5, where each point represents a unique design alternative as well. In our example, the points located in the lower left corner are preferred for minimising both objectives.

Table 3: Coefficients of correlation between four variables

Cost	0.91	0.96	0.62
	Mass	0.89	0.57
		Volume	0.66
			PowerCon

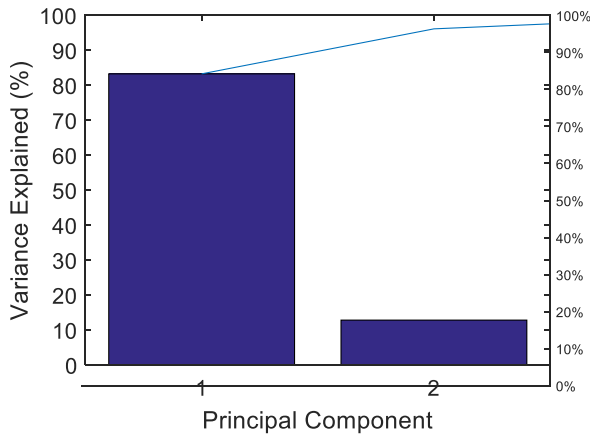


Fig. 2: Explained variance for the first two principal components

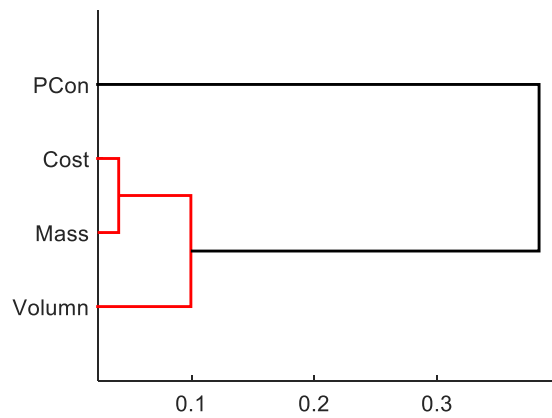


Fig. 3: Dendrogram of the coefficients of correlation between the four variables

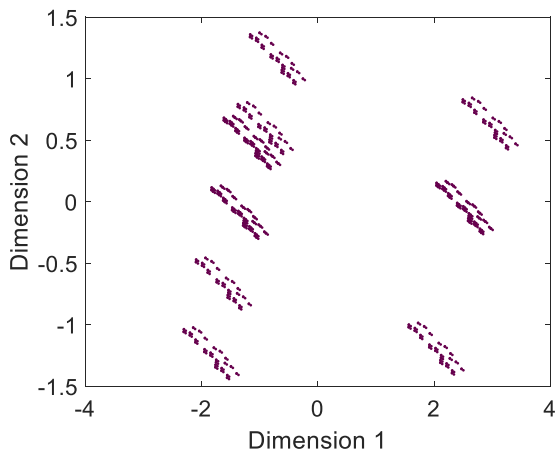


Fig. 4: 2D scatter of the design alternatives with respect to first and second principal components in the decision space

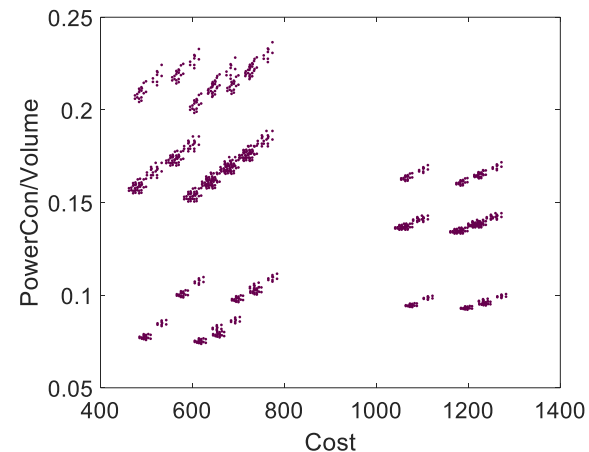


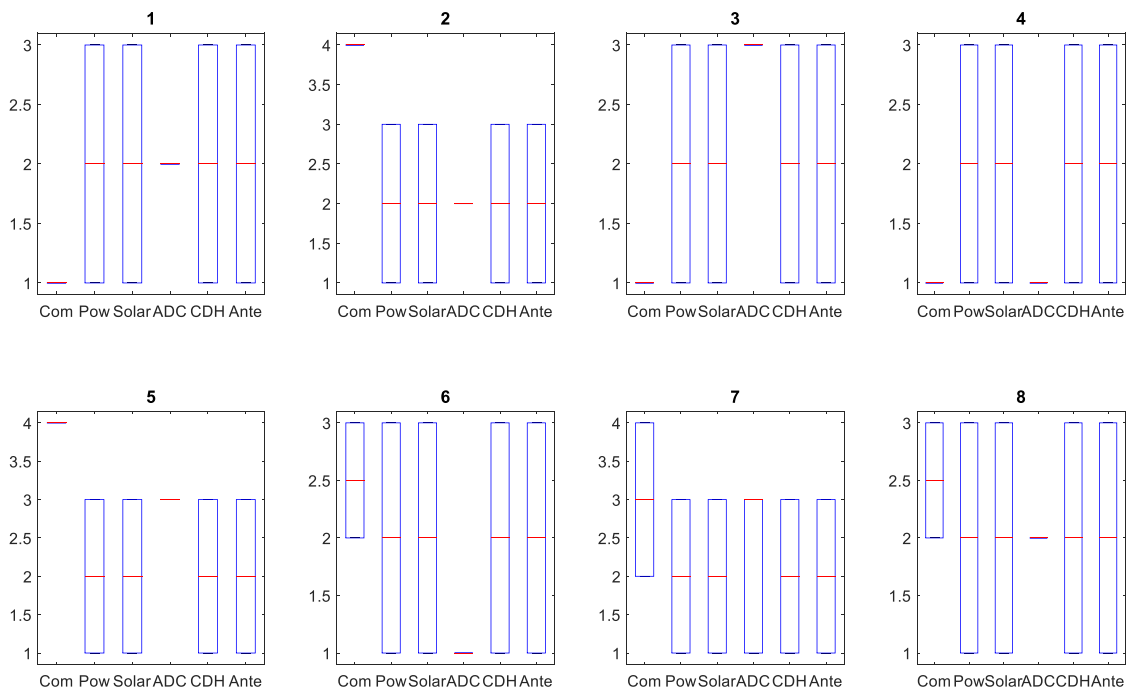
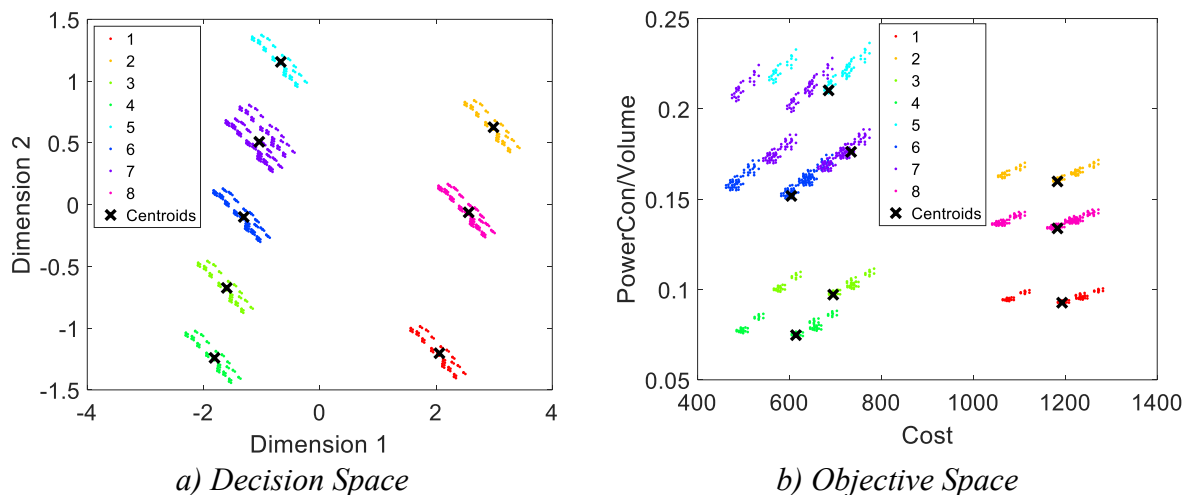
Fig. 5: 2D scatter of the design alternatives in the objective space

K-medoids Cluster Analysis

From Fig. 4 and Fig. 5 that obtained in last section, we do not know any mapping information from the decision space to the objective space. In this section, we illustrate how we use cluster analysis to reveal the hidden pattern between the decision and objective space.

Intuitively, we can see that there are eight potential clusters forming in Fig. 4, therefore we cluster the points to eight groups. (We will discuss how to select the number of cluster later.) The resulting partition is represented with different colours in the design space (see Fig. 6 a). Then we use the partition to distinguish the points in the objective space (see Fig. 6 b). The green points (Cluster 4) are located in the lower left corner in the object space where the values

of both objectives are minimised. In the procedure, we compare the centroid point (black cross) to decide the group of interest. The centroid point of Cluster 4 is located at in the lower left corner; therefore, Cluster 4 is marked as the group of interest in this iteration. We use box plots (see Fig. 6 c) to compare the distributions of the selection of the boards for each cluster. The number (e.g. 1) shown in the title of each subplot indicates the combination of Cluster 1. The red line in the box is the median value of the choices of options, and the blue box shows variation. For the Cluster 4 which we consider as the group of interest, the Communication and ADCS only have a red line without variation, which means the designs in this group all choose the 1st option in Communication boards and the 1st option in ADCS boards (see subplot of Fig. 6 c) for Cluster 4). We record the combination (design variables) of Cluster 4, {1, TBD, TBD, 1, TBD, TBD}, where TBD is short for to be determined. The group of interest has 81 design alternatives, i.e., after Iteration 1, we found 81 points of interest out of 927.



c) Distributions of the boards selection for each cluster

Fig. 6: Iteration 1 result display (927 design alternatives are divided to 8 clusters. Cluster 4 (81 green points) is marked as the group of interest.)

User Control and Iteration

Though 81 is much smaller than 927, it is still a big number for final decision. Therefore, we implement Iteration 2 to take a further examination of the subset. Before we reach a number of points that is reasonable for the final decision, more iterations might be required. This section will show how to reduce the cognitive workload via several iterations gradually. In the proposed method, the user interaction fully control the iterations selecting number of clusters k and the group of interest.

We cluster the 81 points into four groups in Fig. 7. We can see that the red points (Cluster 1) form the group of interest. We record the board combination of Cluster 1 as {1, 3, TBD, 1, TBD, TBD}, which indicates the design points of interest utilise the 3rd option in the Power boards. Comparing to the Iteration 1, we obtain more knowledge about the design variables of the desired designs. After Iteration 2, we found 26 red points of interest out of 81.

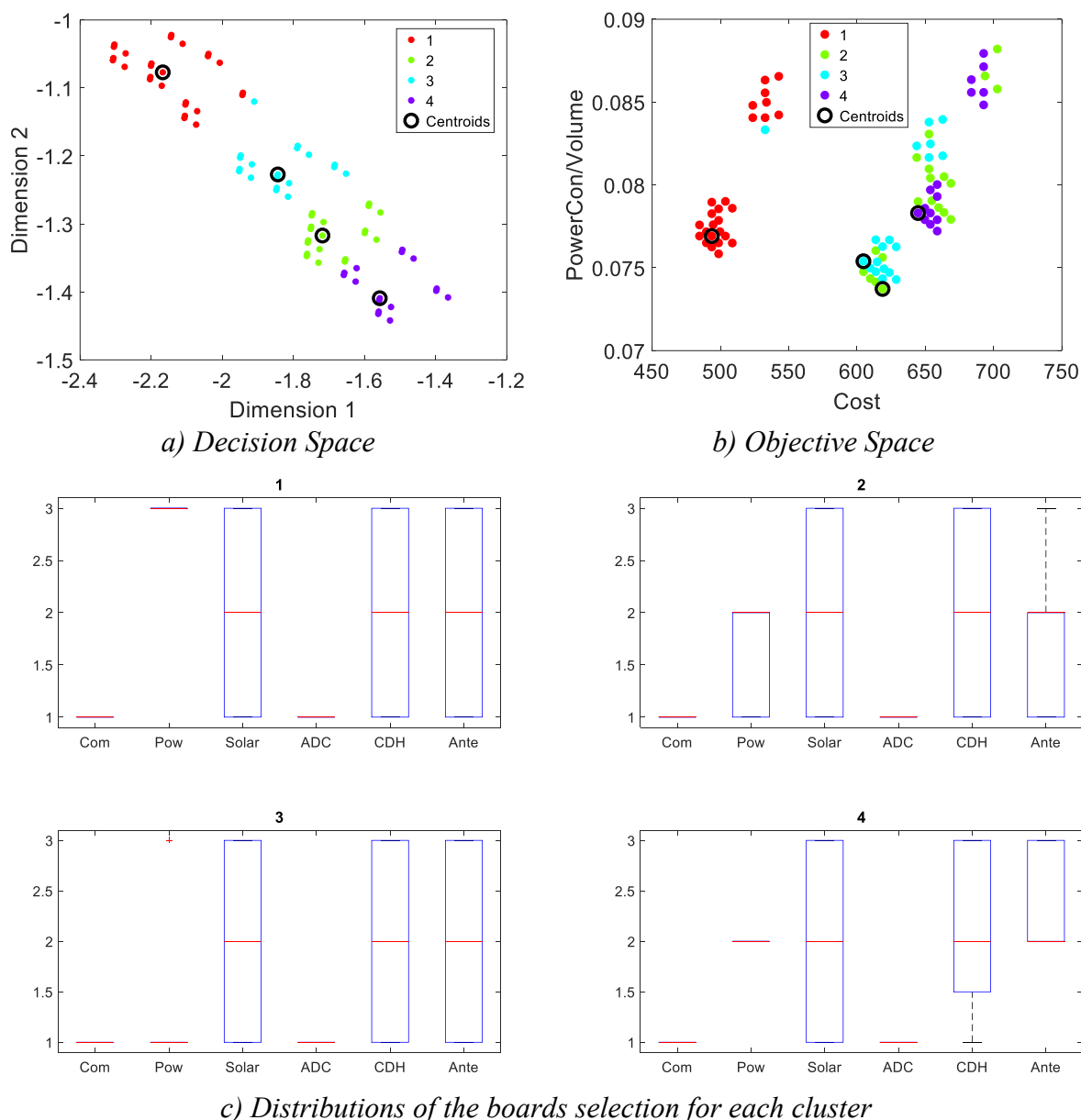


Fig. 7: Iteration 2 result display (81 design alternatives are divided to 4 clusters. Cluster 1(26 red points) is marked as the group of interest.)

The 26 is still too many to make the final decision, thus we implement Iteration 3. The results are shown in Fig. 8. We can see that Cluster 5 (6 blue points) is the group of interest. The combination of Cluster 5 is {1, 3, TBD, 1, TBD, 2}, which indicates the design points of

Finally, we discuss the selection of the number of cluster k . In each iteration, we try the number of cluster $k = 2, 3, \dots$ and then inspect the partition behaviour in the objective space until a number can best interpret and reveal the patterns. When the data in the decision space have natural clusters, e.g. the data in Iteration 1 (see Fig. 6 a), $k = 8$ is selected as a direct attempt because we intuitively see that there are eight potential clusters. The smaller number of clusters set, the more number of iterations are required to reach a small group of interest (e.g. the number of points are reasonable for the final decision).

Conclusions

This paper proposed a tradespace exploration method using PCA and k-medoids cluster analysis, as well as user interaction. We use a case study consisting of 927 CubeSat design alternatives to demonstrate the effectiveness of the proposed approach. The results indicate that designers can benefit from the proposed approach as it well supports knowledge discovery through the tradespace exploration.

The biggest challenge for the design tradespace exploration is that the amount of the data is going beyond humans analysing capability. We can see that both PCA and data clustering reduce the data burden, but they achieve this goal in different ways. PCA reduces the data amount by eliminating data dimensions; while clustering aggregates data points that share common features so that designers will see a small set of data groups rather than a large amount of data points.

This example is relatively simple for the demonstration purposes, thus we plan to enrich the variables in the design tradespace. For instance, the objective of power consumption per volume is a designer-determined metric; we plan to consider some stakeholder-defined metrics such as delivery time, reliability. What we address in this paper is a dual-objective problem; we plan to tackle some cases with three or more objectives in the future work. In addition, a formal procedure that evaluates and validates the results of the proposed tradespace exploration approach in a quantitative and objective fashion is required in the future work. For instance, we plan to define a criterion based on which we can choose the best value of the number of clusters, so that possible further acceleration of the tradespace exploration process occurs.

References

1. Puig-Suari, J., Turner, C., and Ahlgren, W. "Development of the standard CubeSat deployer and a CubeSat class PicoSatellite", *Proceedings of IEEE Aerospace Conference Proceedings*. 2001, 1/347-1/353 vol. 1.
2. Bouwmeester, J. and Guo, J., "Survey of worldwide pico- and nanosatellite missions, distributions and subsystem technology", *Acta Astronautica*, 2010. Vol. 67, No. 7–8, 2010, pp. 854-862.
3. Swariwout, M., "The first one hundred university-class spacecraft 1981-2008", *IEEE Aerospace and Electronic Systems Magazine*, 2009. Vol. 24, No. 3, 2009, pp. A1-A24.
4. Bonyan, H., *Looking into Future-Systems Engineering of Microsatellites*. Arif T.T.(ed.), Croatia, 2010.
5. Davison, P.L., *Tradespace exploration for space system architectures: a weighted graph framework*, in *Massachusetts Institute of Technology Department of Aeronautics and Astronautics*. 2014, Massachusetts Institute of Technology: Cambridge, Massachusetts.
6. Yan, X., Qiao, M., Li, J., et al. "A Work-Centered Visual Analytics Model to Support Engineering Design with Interactive Visualization and Data-Mining", *Proceedings of 45th Hawaii International Conference on System Science (HICSS)*. Hawaii (US), January 2012, 2012, 1845-1854.
7. Ross, A.M., Hastings, D.E., Warmkessel, J.M., et al., "Multi-attribute tradespace exploration as front end for effective space system design", *Journal of Spacecraft and Rockets*, 2004. Vol. 41, No. 1, 2004, pp. 20-28.
8. Deb, K., *Multi-objective optimisation using evolutionary algorithms*. Vol. 16. John Wiley & Sons, New York, 2001.

9. Konak, A., Coit, D.W., and Smith, A.E., "Multi-objective optimisation using genetic algorithms: A tutorial", *Reliability Engineering & System Safety*, 2006. Vol. 91, No. 9, 2006, pp. 992-1007.
10. Zhang, X.L., Simpson, T.W., Frecker, M., et al. "Supporting trade space exploration of multi-dimensional data with interactive multi-scale nested clustering and aggregation", *Proceedings of ASME 2009 International Design Engineering Technical Conferences and Computers and Information in Engineering Conference (IDETC/CIE)*. San Diego, CA, 2009, 1341-1353.
11. Balling, R. "Design by shopping: A new paradigm?", *Proceedings of Proceedings of the Third World Congress of structural and multidisciplinary optimisation (WCSSMO-3)*. 1999, 295-297.
12. Kang, E., Jackson, E., and Schulte, W. "An approach for effective design space exploration", *Proceedings of Monterey Workshop*. 2010, 33-54.
13. Jolliffe, I., *Principal component analysis*. Springer Verlag, New York, 1989.
14. Velmurugan, T. and Santhanam, T., "Computational complexity between K-means and K-medoids clustering algorithms for normal and uniform distributions of data points", *Journal of computer science*, 2010. Vol. 6, No. 3, 2010, pp. 363.

Optimising the Launch and Deployment of a Smallsat Constellation

Victor Lim¹, Hideaki Ogawa¹, George Coulloupas¹, Daniel Chadwick¹

School of Engineering, RMIT University, Melbourne, VIC 3001, Australia

Summary:

As satellite sizes and manufacturing costs fall, there is a renewed interest in affordably launching and deploying low-Earth orbit satellite constellations. One such upcoming service is Iceye, which is planned to be a radar-imaging satellite constellation operating in LEO. The design of such applications with multiple objectives represents a challenge to conventional design approaches. In this study a sophisticated design framework is developed by coupling high-fidelity orbit propagation tool, evolutionary algorithms assisted by surrogate modelling, and analytical approaches. A multi-objective design optimisation (MDO) study has been performed by employing the developed framework for the orbital deployment strategies of constellation satellites with respect to two competing objectives, namely the cost and deployment time of the whole distributed system. It has been demonstrated that orbital transfers can minimise either the time or cost of deploying the constellation. Through the use of MDO-based on surrogate-assisted evolutionary algorithms this paper ultimately aims to identify universal design factors and underlying mechanism.

Keywords: satellite constellation, low Earth orbit, orbital deployment strategies, co-orbital phasing, multi-objective design optimisation

Introduction

Satellite-based systems such as internet, telecommunications and global navigation represent an increasingly central part of our lives. They connect people around the world and are a pillar of modern society. Although all sections of a satellite's life cycle are important, the launch and deployment phase is the most crucial in terms of cost and overall system performance. Launching a satellite is a very expensive proposition, and cost-savings and efficiencies must be rigorously pursued. This is doubly true for deploying a distributed system of multiple individual satellites, or a constellation [1]. However, optimising the deployment of a satellite constellation is a multidisciplinary design task with many conflicting objectives, such as finding the optimum balance between payload mass and initial launch altitude.

Contemporary industry trends and developments

With technological developments such as the rise of the internet and the need for real-time communication and imaging, the launch industry is now dominated by private companies wishing to put their satellites into orbit. The miniaturisation of many electronic components and an increase in commercial off-the-shelf (COTS) parts has resulted in satellites which are significantly smaller and lighter than their forebears, leading to a new class of satellites called the smallsat [2]. In turn, this has greatly affected the launch vehicle industry, as demand for lighter rockets suited for smaller payloads has increased [3].

Smallsats can mass anywhere between 50kg to a few hundred kilograms, and typically orbit at LEO altitudes, which is any region in orbit below 2000km. In this regard, deploying smallsats

to LEO is advantageous, as propellant requirements are not so great, hence a greater payload of multiple smallsats is feasible [4]. Constellations of lighter and smaller satellites are more technically and economically feasible to launch and maintain, as multiple satellites can be placed within the payload bay of a single launch vehicle.

Unfortunately, the miniaturisation and optimisation of launch vehicles has not kept pace as well as the satellite manufacturing sector. Boltz (2001) [5] defines several classes of launch vehicles according to the mass of their payloads: very small payloads (5-50kg), small payloads (50-500kg), medium payloads (500-5000kg) and large payloads (5000-50,000kg). There has been a growing interest in procuring smaller launch vehicles for small to medium payloads, as previous launch vehicles were too large. Demand for such vehicles has been met to an extent by a range of small rockets such Pegasus, Minotaur I, Epsilon, Long March II, Start-1 and Vega. For this study, only launch vehicles with sufficient data available will be used, as information for some models (Long March II, Start-1) remains proprietary. See Appendix E for more details on surveyed launchers.

Case study: The Iceye satellite

The basis of this research project is optimising and simulating the launch and distribution of the future Iceye satellite constellation. Research will be performed by RMIT with collaboration from Iceye Oy.

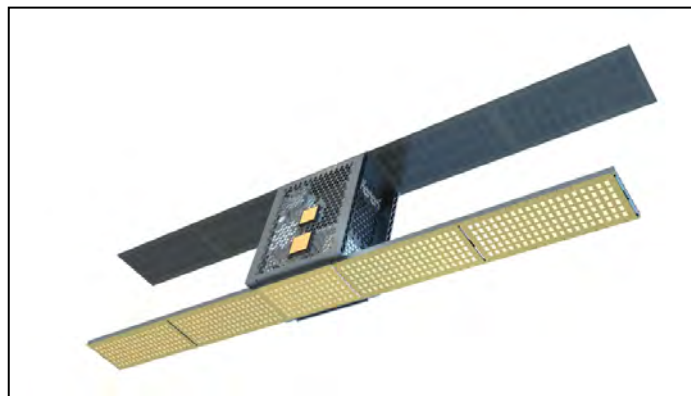


Fig.1 – Concept art of a deployed Iceye satellite [6]

As a relatively new Finnish satellite company, Iceye Oy plans to launch its first satellite in late 2017 [7]. Iceye is a fast-response radar imaging smallsat, with a mass of only around 75kg. Its mission objectives include real-time ice tracking, geographical and agricultural surveying, as well as the ability to be repurposed to other functions such as disaster monitoring. Although the unit cost has not been announced yet, Iceye's use of commercial-off-the-shelf components should lower the cost significantly [6]. This mirrors the industry trend of reducing cost via using reliable but generic parts. This service could be a lucrative industry niche, as there is a lack of non-optical imaging satellites in the northern latitudes, despite the obvious benefits to shipping in those regions. To succeed, it is of vital importance for the company to consider early on the most effective launch and deployment methods for their service. See the mission specifications in the Appendix A.

Directly relevant literature concerning the multidisciplinary optimisation of the launch and deployment of a satellite constellation is found in only a few texts. Gavish & Kalvenes (1997) [8] use a probabilistic and reliability viewpoint to find the optimum LEO satellite launch policy for given numbers of satellites in a constellation. The research also incorporated launch site costs, replacement costs and the financial effect of delays. The interrelationships between

cost, payload and launcher reliability are discussed by Jafarsalehi & Mirshams (2012) [9], and an emphasis on discretising mission segments to simplify analysis was apparent. For any given launch and deployment mission, the three broad stages are: launch strategy, injection and orbit transfer and constellation set-up strategy [10].

Research methodology

Optimising the Iceye mission, or any other similar scenario, is a confronting task with many interrelated stages. To break this problem space down into manageable areas, discretisation is important. Key segments that are strongly related are grouped by themes, solved for and then their results are fed back into the main analysis.

Cornara *et al.* (2001) states that a constellation launch and deployment strategy should be split into three distinct segments [11]:

1. **Launch strategy** (selection of launch site and launch vehicle, based on mission requirements)
2. **Evaluation of injection and orbital transfer strategies** (derived from direct and indirect injection methods using impulsive manoeuvres – results will be compared to preliminary analysis of manoeuvring via low thrust engines)
3. Constellation set-up strategy (intermediate constellation configurations to final generic constellation configuration)

The first two points are shown in bold as they relate to the main concern of this study. A constellation design study in STK found the coverage design requirements can be met with a 30-satellite Walker configuration of 6 planes with 5 satellites per plane. This configuration has 75% global coverage at any given time with a cumulative coverage of 100% and a maximum revisit time of 13 minutes, and is visually represented in Appendix C.

- **1st phase:** 10 satellites, 2 planes, 5 satellites each
- **2nd phase:** 30 satellites, 6 planes, 5 satellites each

A combination of qualitative, analytical and numerical studies will be used to determine the optimal parameters for this case study. MDO will be applied where appropriate, particularly for problems with many complex interrelationships, such as performing orbital transfer and phase changes. Data has been collected on candidate launch vehicles and launch sites, in order to keep findings grounded in reality, and maximising the practical utility of this study for future researchers (see Appendices B and E).

Results and discussion

Launch site selection

For this project, it is assumed that Iceye Oy will make use of an existing launch site, or at least one that may come into service in the near future. The choice of launch sites is therefore finite, and evaluation and selection of potential candidates has been done on a largely parametric and qualitative basis, rather than via MDO. Although highly comprehensive, MDO cannot fully address all the factors surrounding launch site selection; such as political, legal and economic reasons, hence human input is required and Iceye will need to look further into

this aspect of the mission in order to minimise these outside risks. A list of potential launch sites is included in Table 1 with their related azimuth values. The equations linking the two possible launch azimuths ‘A’ (when applicable) for a given location are:

$$A(\text{north}) = \sin^{-1}\left(\frac{\cos(i)}{\cos(\varphi)}\right) \quad \text{and} \quad A(\text{south}) = 180 - \sin^{-1}\left(\frac{\cos(i)}{\cos(\varphi)}\right) \quad (1)$$

where i is the desired orbit inclination (degrees) and φ is the latitude of launch site (degrees).

Mathematically, it can be seen that $i > \varphi$, lest there be no solution for the arcsin function. In the physical world, this translates to there being no way to directly inject a launch vehicle into an orbital plane, which is the most efficient way to launch. Failing to do so results in very costly plane changes to reach the required orbital plane. However, the high inclination of the final SSO orbit means that only launch sites at extremely high latitudes around the poles are disqualified from selection (past latitudes of 82°). This is demonstrated by the following graph.

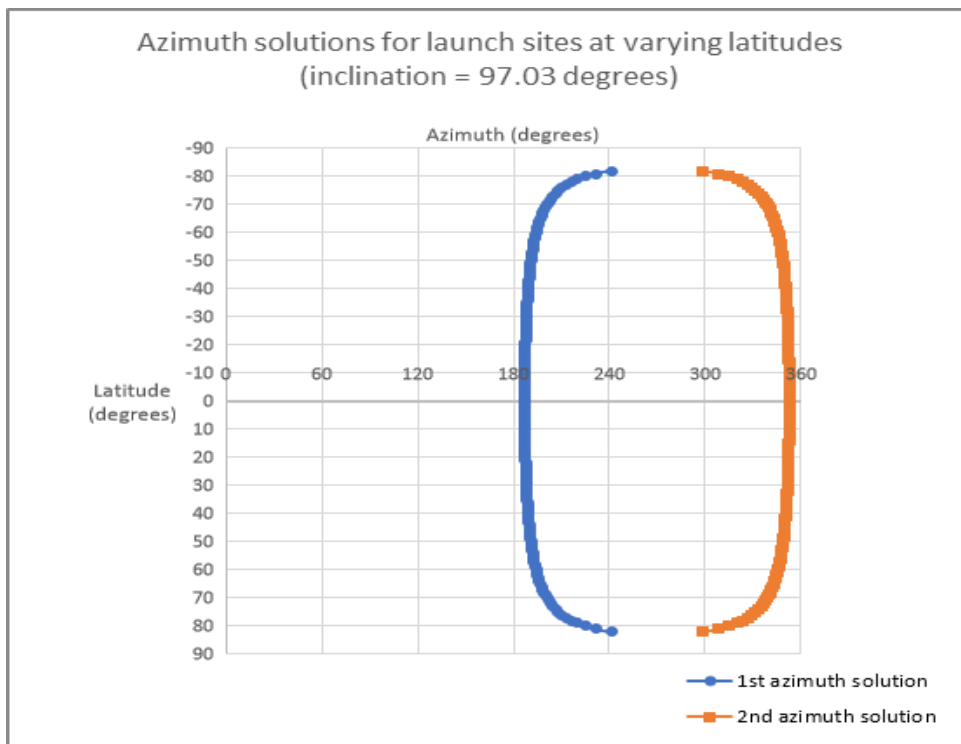


Fig. 2: Possible azimuths for $i = 97.03^\circ$ are largely confined to two near-constant values irrespective of launch latitude; note that all solutions are westward launches

For prograde launches, selecting a launch location near the equator is advantageous as this takes advantage of the Earth’s rotational velocity [12]. At the equator, this is approximately 0.46km/s eastwards and diminishes as one approaches the poles (with increasing latitude ϕ) according to the rule:

$$v_{\text{rotational}} = v_{\text{equatorial}} \cos(\phi) \quad (2)$$

Evidently, proximity to the equator for a westwards launch is not beneficial, as this is an inherent velocity disadvantage for any rocket launched to reach the project’s required inclination. The greater the starting velocity advantage, the greater the payload mass can be, or higher altitudes may be reached.

Azimuth restrictions are different for each launch site, as launching rockets over and around populated landmasses is both unsafe and undesirable in the event of an accident. Azimuth restrictions may also be the result of geopolitical factors in a particular region. Calculations were performed using Eqn. 1 to determine a launch site's physical suitability for a direct launch. Further vetting of these results took into account known – or in a few cases inferred – azimuth restrictions. The launch sites were narrowed down to the following candidates.

Table 1: Existing launch facilities with suitable azimuths for the project mission (see Fig. 3 for graphical representation)

Site name	Latitude	Specialisation in launches and notes	Allowable azimuth launch path	Direct launch to 400km SSO possible?
Vandenberg Air Force Base, USA	34.7582°	North-south polar orbits	158° SE to 201° SW	YES (188.56° SW)
Reagan Test Site, Kwajalein Atoll, Marshall Islands	8.7167°	Moderately inclined orbits (38° for HETE-2)	All azimuths allowed	YES (352.89° NW and 187.11° SW)
Kodiak Island, USA	57.4913°	Polar orbits, unobstructed downrange flight paths	116° SE to 244° SW	YES (193.16° SW)
Omelek, Marshall Islands	9.0482°	Equatorial satellite launch facility (SpaceX Falcon 1)	All azimuths allowed	YES (352.88° NW and 187.12° SW)
Plesetsk Cosmodrome, Russia	62.9356°	Highly inclined orbits, Molniya orbits	341.5° NW to 76.2° NE	YES (344.40° NW)
Guiana Space Centre, French Guiana	5.2374°	Equatorial launch facility, government and commercial launches (ESA, Arianespace)	349.5° NW to 93.5° SE	YES (352.94° NW)
Taiyuan Satellite Launch Center, China	39.1432°	Polar orbits <ul style="list-style-type: none"> • Generally closed to foreigners 	180° S to 190° SW (estimated)	YES (189.08° SW)
Baikonur Cosmodrome, Kazakhstan	45.9552°	Highly inclined orbits, large number of commercial and government launches	347° NW to 65° NE	YES (349.86° NW and 190.14° SW)

High latitude sites such as Kodiak Island and Plesetsk Cosmodrome stand as likely candidates. However, due to Baikonur Cosmodrome's extensive network of launch-supporting infrastructure, it may be cheaper and quicker to launch from that location.

Launch site candidates that will be able to accommodate a direct launch to 400km SSO are marked as blue points, with the allowed azimuth launch paths in green. Possible launch sites that are proposed future launch sites, currently not used or under construction are marked as red points.

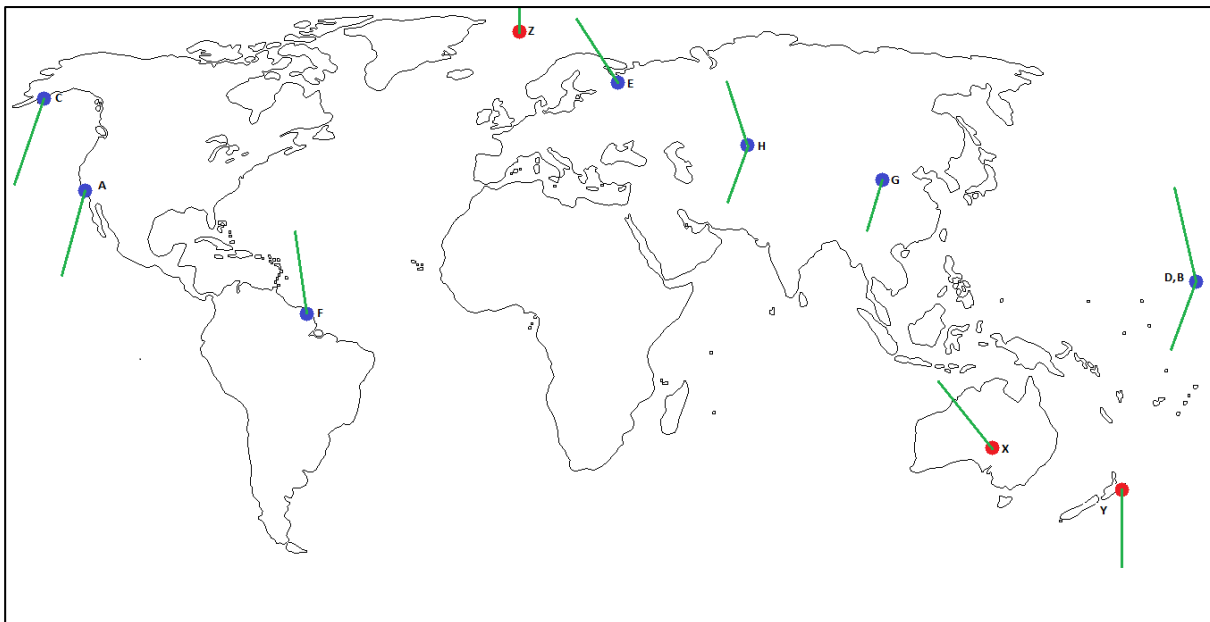


Fig. 3: Possible launch site locations, as follows: A (Vandenberg AFB, USA), B (Reagan Test Site, Marshall Islands), C (Kodiak Island, USA), D (Omelek, Marshall Islands), E (Plesetsk Cosmodrome, Russia), F (Guiana Space Centre, French Guiana), G (Taiyuan Satellite Launch Centre, China), H (Baikonur Cosmodrome, Kazakhstan), X (Woomera Test Range, Australia), Y (Mahia Peninsula Launch Site, New Zealand), Z (SvalRak, Norway). Please note that the diagram is not to scale.

Launcher selection

The optimum choice of launch vehicle relates to the number of orbital planes of a constellation, particularly for direct injections. In this case, at least six separate launches are required to deploy the constellation's six planes, each with five satellites. Cornara *et al.* (2001) notes that only a few very heavy launch vehicles (Ariane 5 and Rockot) are capable of multiple plane insertions, and only in the order of a difference of a few degrees [12]. Multi-plane insertions are therefore assumed to be impossible for the surveyed small launch vehicles. For such a large number of satellites, it would be ideal and cost-effective to deploy multiple satellites from the same launcher in a clustered initial state. Multiple satellites included in the same launcher will require additional mass and volume for their adapters. Jafarsalehi & Mirshams (2012) estimate each adaptor weighs close to 15% of the satellite's dry mass [10]. This approach would be necessary if large launchers indirectly injecting many satellites into orbit are selected. Such an approach mirrors the FORMOSAT-3/COSMIC mission, which is the only mission to simultaneously deploy a constellation of six weather satellites from a single launch vehicle, namely the Minotaur I [13].

A summary of launcher specifications that can be used can be found in the Appendix E, where several combinations of launchers are suggested to fill single planes of the final constellation. With reference to these tables, the specific cost of each satellite rises as launcher payload mass decreases. There are significant economies of scale associated with using larger launchers [14]. Parts become simpler and the technological requirements are not so advanced for larger rockets, hence reducing the cost. Having a large amount of unused payload space is not necessarily detrimental, as long as a willing 'piggybacking' partner can be found to help share launch costs. However, this may be difficult with such large amounts of empty space, as Iceye's payload is actually the minority if using the Vega rocket. It is more likely that the company will use the smaller launchers, most notably Electron, if it is released onto the market with the current advertised price. Due to its low projected cost, Electron has the lowest

specific cost of USD5 million. It is also used to cheaply ‘fill out’ launch schedules to single planes, for the launchers (Pegasus, Minotaur I and Epsilon) that cannot simultaneously launch all five satellites of a plane using this estimated payload bay mass of each Iceye satellite.

When choosing launchers, it is important to design the mission in such a way that extra mass attached to the satellite, most notably in the form of propellant, is minimised without compromising mission success. Hence, launcher selection is strongly tied not only to cost, but also to delta-v requirements stemming from orbital transfers. Other practical factors affecting the choice of launcher include availability, insurance, shipping and transport, as well as choice of fuel. The last point could be a legal and safety concern depending on the country from where the rocket is launched.

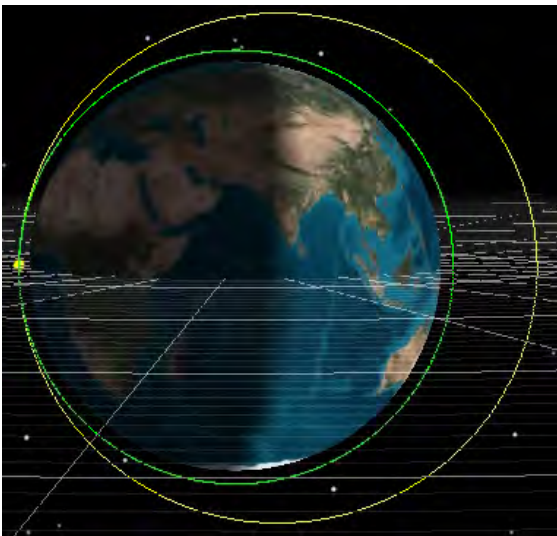
Orbital transfer and multidisciplinary design optimisation (MDO)

Hohmann transfer from initial 600km orbit

A Hohmann transfer is a coplanar manoeuvre that is the most efficient means to move a spacecraft, or in this case a satellite, from one orbit to another. For this project, a stated initial altitude of 600km has been given by Iceye Oy. It is assumed that the inclination of any initial orbit will match the final orbit at an inclination of 97.03° to keep the manoeuvre coplanar, thus avoiding any expensive plane change manoeuvres. The question of optimising the transfer is dependent on the mission designer’s planned purpose for the higher initial orbit. It may be used as a parking orbit to test or deploy mission-critical systems before descending to a lower altitude, or to phase a cluster launch in preparation for transfer to the lower final orbit

As Iceye Oy currently considers it necessary to initially launch to 600km altitude (based on provided information), the optimal initial orbit would be an elliptical orbit with an apogee altitude of 600km, and a perigee altitude of 400km. Because this parking orbit is already tangential to the final circular 400km orbit, transferring the satellites only requires one burn as opposed to two, which is the typical Hohmann transfer. This results in the lowest delta-v or propellant requirement from all possible initial states, save launching directly to the final 400km circular orbit. The results are summarised in the table below.

Table 2: Orbital parameters for the optimum initial launch state. The initial 400 × 600km parking orbit is marked in yellow, the final circular 400km orbit is marked in green

Apogee altitude	600km	 <p>(not to scale)</p>
Perigee altitude	400km	
Delta-v required (analytical)	0.05555km/s	
Delta-v required (STK 11)	0.05107km/s	
Transfer time	46.28 minutes	

In comparison to analytical results, the STK 11 simulation yielded a lower delta-v requirement for transferring from the parking to final orbit. In short, this is due to the software package modelling orbital perturbations: chiefly atmospheric drag and nodal precessions. Because the satellite is descending to a lower energy orbit, atmospheric drag aids in reducing the delta-v requirement needed to retrofire. The use of STK 11 is highly advantageous as it can analyse these real-life effects that cannot be adequately addressed by analytical means.

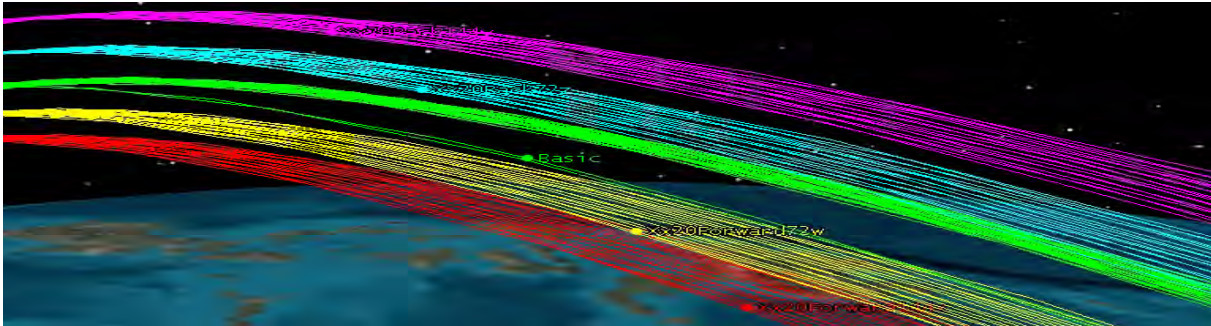


Fig. 4: Phasing orbits precess and are affected by atmospheric drag, resulting in wide bands of phasing orbits with some variation in altitude, resulting in non-tangential burns in reality

Phasing manoeuvres using impulsive and low-thrust manoeuvres

For the Iceye scenario, an even spread of five satellites per plane requires a phase angle of 72° between each satellite. Only four out of the five need to affect phase changes, with one non-maneuvring satellite acting as the reference point. This is the most efficient way to set up a single plane, as propellant for phasing manoeuvres does not need to be allocated to one of the satellites. Two satellites will phase forwards (72° and 144° forward) and two satellites phasing behind (72° and 144° back). See Fig. 5 below for clarification.

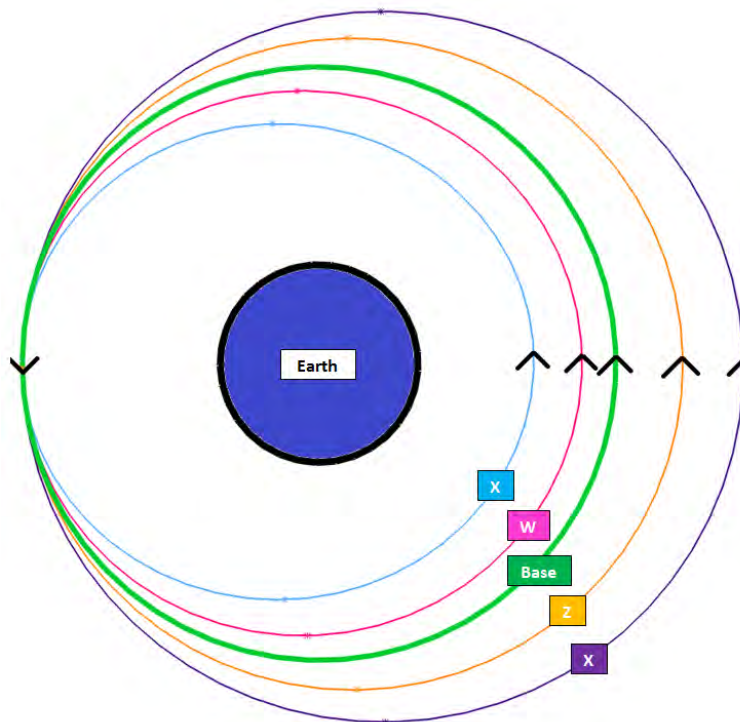


Fig. 5: Phasing orbit definitions for the four manoeuvring satellites. Satellites W and X go forward 72° and 144° , respectively, Z and X go backwards 72° and 144° , respectively (note that the reference satellite orbit (green) does not perform a phase change).

The possible three scenarios for manoeuvring the five satellites of each plane to their final positions, and their respective advantages and disadvantages are presented in the table below:

Table 3: An analysis of the advantages and disadvantages of the three deployment schemes (impulsive manoeuvre cases marked in green, low thrust manoeuvre case marked in red)

	Phase change at 400km • Impulsive manoeuvres	Phase change at 600km (or any other initial altitude) • Impulsive manoeuvres	Simultaneous phasing and altitude change • Low thrust engine
Stages	1. Cluster launch to 600km 2. Perform Hohmann transfers to the final 400km orbit 3. Conduct phase changes	1. Cluster launch to 600km 2. Conduct phase changes at 600km (satellites phased to final relative spacing) 3. Perform Hohmann transfers to the final 400km orbit	1. Cluster launch to 600km 2. Conduct simultaneous phasing and altitude change to 400km into final operational positions
Advantages	<ul style="list-style-type: none"> • Simplest case to analyse and simulate • Low delta-v and propellant requirement • Phasing at 400km is not reliant on the shape of the initial orbit • Phasing at 400km occurs at lower energy final orbit 	<ul style="list-style-type: none"> • Simple to analyse in the case of a circular initial orbit • Delta-v savings for the Hohmann transfer increase as eccentricity increases • Phasing angle is lower (68.9° spread) 	<ul style="list-style-type: none"> • Fastest deployment time to final orbital configuration • Excellent for low thrust manoeuvring, as the propellant mass required is very low
Disadvantages	<ul style="list-style-type: none"> • Phasing angle is higher (72° spread), resulting in higher delta-v requirement • Phasing occurs at lower altitudes – the effect of atmospheric drag and other orbital perturbations increases 	<ul style="list-style-type: none"> • Phasing occurs at a higher energy initial altitude (delta-v requirement increases) • More difficult to analyse in the case of elliptical initial orbits • Launcher requires more propellant to reach higher, more eccentric initial orbits, reducing payload mass 	<ul style="list-style-type: none"> • Most difficult case to analyse (non-tangential burns) • Much greater delta-v and propellant requirement • Poor choice for impulsive manoeuvring, as propellant mass required is very high

Initial low-thrust manoeuvring results

A preliminary study was performed using a low-thrust ion engine, with the satellite undergoing simultaneous phasing and altitude change. Because of the long transfer times associated with such manoeuvres, the initial unpowered drifting time was also taken into account. The numerical results are presented below for a single plane of four manoeuvring satellites with one non-manoevring satellite acting as the reference.

Table 4: Initial numerical results for the low-thrust orbital transfer case

Specific impulse	1500s	Deployment time per plane	146.8 hours
Thrust	20mN	Last satellite in position	Drift time: 30 hours Descending burn time: 116.8 hours
Initial altitude	600km	Highest individual fuel usage	0.574kg
Final altitude	400km	Total propellant for cluster	2.854kg

Unsurprisingly, the delta-v and propellant requirements are low for this phasing case, particularly when compared to impulsive manoeuvres. Further exploration of transfers using low-thrust manoeuvres should also include the possibility of plane changes, allowing only a few large launchers to theoretically deploy all satellites simultaneously.

Impulsive manoeuvring MDO results

The coupled use of surrogate-assisted evolutionary algorithms (SAEA) MDO and STK 11 was applied to analyse phase changes from the final 400km circular orbit to generate a range of Pareto optimal solutions, as seen in Fig. 6 (see Fig. 10 in Appendix G for an enlarged version). The automated nature of this process generated a wide range of results that were unexpected, particularly in the fact that the phasing satellites in a plane could use different numbers of phasing orbits to achieve their phase changes. A summary of the MDO process, key parameters and a detailed breakdown of the 400km MDO run is presented in Appendices D and F. It is the virtue of MDO that both delta-v and time may be co-optimised.

A powerful feature of SAEA MDO is its ability to learn after a number of successful individuals are generated, in this case after ten such individuals are encountered every five generations. Populations of results subsequently undergo cross-over, selection, reproduction and mutation; evolving in ways inspired by evolutionary processes found in nature. In order to expedite the optimisation process, surrogate modelling is capable of predictive output for objective functions over the course of subsequent generations or iterations for given decision variables. Because of this, 50 generations each with a population of 48 were modelled and optimised, resulting in 2400 unique individuals – albeit not all were viable. The two competing objective functions to be optimised were minimising the total delta-v against minimising mean transfer time for a single plane of five Icyeye satellites. The two objective functions were interpreted in the following ways:

- **Total delta-v:**

$$\sum \Delta v = \Delta v_{Lead72} + \Delta v_{Lead144} + \Delta v_{Trail72} + \Delta v_{Trail144} \quad (3)$$

- The summation of the four satellites' delta-v requirements for phasing is indicative of how much propellant mass must be allocated for phasing, which will be added to the mass budget in the launcher's payload bay.

- **Mean phasing time:**

$$Mean t_{phase} = \frac{P_{Lead72} + P_{Lead144} + P_{Trail72} + P_{Trail144}}{4} \quad (4)$$

- Each phasing orbit period (*e.g.* P_{Lead72}) is strictly defined as the phasing orbit(s) only, without the initial and final drift time.
- The average phasing time is indicative of how long it will take for each particular plane to reach near-half of its full functionality, as preliminary surveying can already begin as soon as two or three satellites reach their final orbital slots.
- While time is not as critical, decreasing phasing time requires more propellant burn, increasing total payload mass and decreasing the spare mass available for additional propellant (which may extend operational life) or extra revenue from piggybacking cubesats. See Table 7 for propellant mass differences.

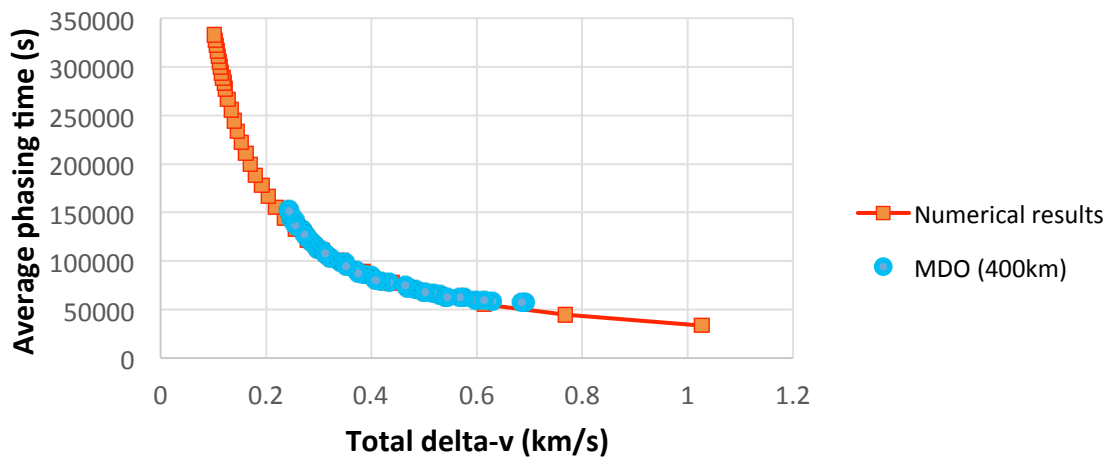


Fig. 6: MDO-derived Pareto optimal results (blue points) nestled in the ‘elbow’ of the numerical curve are slightly more efficient than their numerically-calculated counterparts (orange), requiring less delta-v and phasing time to achieve phase changes

A recurring pattern was clear throughout all MDO-generated runs. The MDO appeared to be using the Trailing 144° satellite’s phasing orbit to lower the plane’s mean phasing time, by using only one or two phasing orbits on average for that particular satellite. This resulted in a much larger phasing orbit for the Trailing 144° satellite than its counterparts, whose number of phasing orbits ranged anywhere from five to thirty revolutions, thus staying very close to the base orbit. See Fig. 7 below for details.



Fig. 7a & 7b: A typical MDO-generated optimal solution (note the Trailing 144° satellite’s phasing orbit relatively large size compared to its counterparts (purple line) and the base orbit is marked in green)

In practical terms, this means that two of the five satellites of each plane: the non-maneuvring reference and Trailing 144° satellites, will arrive in their final operational positions relatively quickly. Furthermore, a similar trend was for the Trailing 72° satellite (marked in light blue in Fig. 7b) to use about 4 to 10 phasing orbits to complete its phase change, meaning that it too arrived not long after the Trailing 144° satellite. As a result, three of the five satellites of a plane would usually be in their final operational configurations in at most ten hours since commencing their phase change manoeuvres.

Three Pareto optimal mission approaches are named by their central theme: ‘low delta-v’, ‘balanced’ and ‘fast’. From the 400km MDO-generated Pareto optimal front (refer to Fig. 5), these scenarios represent the left-most, middle and right-most points respectively. Assuming an engine specific impulse of 200s using hydrazine propellant [15], a satellite dry mass of 75kg and using impulsive manoeuvres, the following optimal total transfer times, delta-v and propellant masses can be determined for each case.

Table 5: Summary of the three approaches in terms of total delta-v, total deployment time and propellant mass – a mission designer can pick the most suitable approach based on needs

Approach	Delta-v (km/s)		Time to deployment (hr)		Propellant mass for one plane (kg)
Low delta-v	Hohmann transfer	0.0511	Hohmann transfer time	0.7713	41.77
	Total phase change	0.243	Average phasing time	42.3886	
	Total delta-v	0.2941	Total time to deployment	43.1599	
Balanced	Hohmann transfer	0.0511	Hohmann transfer time	0.7713	62.69
	Total phase change	0.4087	Average phasing time	22.361	
	Total delta-v	0.4598	Total time to deployment	23.1323	
Fast	Hohmann transfer	0.0511	Hohmann transfer time	0.7713	94.68
	Total phase change	0.6927	Average phasing time	15.8039	
	Total delta-v	0.74377	Total time to deployment	16.5753	

Conclusion

Using the discretisation method outlined previously [12], the problem space of launching and deploying the Iceye satellite constellation was broken down into two manageable areas relevant to this study: the launch phase and the injection and orbital transfer stage. Candidate launch sites and combinations of launch vehicles to deploy the two phases of the Iceye satellite constellation have been outlined through parametric and qualitative means. The deployment phase has been extensively demonstrated in the second, more complicated stage. Through realistic simulation and multi-disciplinary design optimisation, the problem space of deployment from an initial clustered state of a plane of five smallsats has been thoroughly explored. Significant trade-offs and sources of uncertainty such as RAAN and effects of orbital perturbations have been identified and their effects quantified via sensitivity analysis and numerical verification. The automated, adaptive optimisation loop provided by the coupled use of SAEA MDO and STK 11 proved to be a powerful and versatile tool that greatly expedited the optimisation process. A major assumption of this project involved using the limited initial mission information provided by Iceye Oy without in-depth verification, for the sake of beginning the academic exercise regarding MDO. Future work could include aspects such as verifying power budgets, PESTLE analysis regarding launcher and launch site selection and arranging transportation and logistics. Of course, this depends on the business trajectory of Iceye Oy itself, which will be very interesting to watch over the next few years.

Acknowledgements

The authors are grateful to Tapabrata Ray at The University of New South Wales at Canberra for the original MDO framework and Jeremy Lui at Iceye Oy for the general information on Iceye. We are also thankful to George Coulloupas at RMIT University for valuable advice and discussions.

References

1. Morgan, L, Morton, A & Daniels, R 2006, "Simultaneously determining the mix of space launch vehicles and the assignment of satellites to rockets", *European Journal of Operational Research*, vol. 172, issue 3, pp. 747-760
2. Duret, F 1997, "Small and medium launch vehicles to extend the Ariane 5 transportation service", *Acta Astronautica*, vol. 40, issue 2, pp. 171-182
3. Ridolfi, L, Pontani, M & Teofilatto, P 2010, "Effect of different flight conditions at the release of a small spacecraft from a high performance aircraft", *Acta Astronautica*, vol. 66, issue 5, pp. 665-673
4. Orbital ATK 2015, *FORMOSAT-3/COSMIC*, Orbital ATK, viewed 18 March 2016, https://www.orbitalatk.com/space-systems/science-national-security-satellites/science-environment-satellites/docs/FS003_04_OA_3862%20FORMOSAT-3.pdf
5. Boltz, F 2001, "Miniature Launch Vehicles for Very Small Payloads", *Journal of Spacecraft and Rockets*, vol. 38, issue 1, pp. 126-128
6. Iceye 2015, *Space Technology Startup Iceye Raises \$2.8 Million Series A*, PR Newswire, viewed 21 March 2016, <http://www.prnewswire.com/news-releases/space-technology-startup-iceye-raises-28-million-series-a-546560572.html>
7. Howard, C 2015, *Iceye raises millions to launch first radar-based microsattellites*, Intelligent Aerospace, viewed 21 March 2016, <http://www.intelligent-aerospace.com/articles/2015/11/iceye-raises-millions-to-launch-first-radar-based-microsatellites.html>
8. Gavish, B & Kalvenes, J 1997, "LEOS – optimal satellite launch policies: the static case (low earth orbit satellite)", *Management Science*, vol. 43, issue 8, pp. 1164-1176
9. Jafarsalehi, Z & Mirshams, M 2012, "Collaborative Optimization of Remote Sensing Small Satellite Mission Using Genetic Algorithms", *Iranian Journal of Science and Technology*, October, vol. 36, issue 2, pp. 117-128
10. Jilla, C & Miller, D 2004, "Multi-Objective, Multidisciplinary Design Optimization Methodology for Distributed Satellite Systems", *Journal of Spacecraft and Rockets*, vol. 41, issue 1, pp. 39-50
11. Cornara, S, Beech, T, Bello-Mora, M & Janin, G 2001, "Satellite constellation mission analysis and design", *Acta Astronautica*, vol. 48, issue 5, pp. 681-691
12. Curtis, H 2014, *Orbital Mechanics for Engineering Students*, 3rd edn., Elsevier Aerospace Engineering Series, USA
13. eoPortal 2016, *FORMOSAT-3*, eoPortal Directory, viewed 25 May 2016, <https://directory.eoportal.org/web/eoportal/satellite-missions/f/formosat-3>
14. Koelle, D 2000, "The cost-optimal size of future reusable launch vehicles", *Acta Astronautica*, vol. 47, issue 2, pp. 205-213
15. AstroRecon 2015, *Small Satellite Propulsion*, NASA, viewed 13 October 2016, <http://ntrs.nasa.gov/archive/nasa/casi.ntrs.nasa.gov/20150002945.pdf>

Appendix A

Table 6: Iceye specifications

Iceye	
Type of satellite	Radar imaging (SAR)
Estimated mass	75kg ± 5kg
Estimated stowed dimensions (L x W x H)	0.75 x 0.55 x 0.35m
Desired type of orbit	Sun-synchronous orbit (SSO), retrograde
Desired eccentricity of orbit	0 (circular orbit)
Desired operational altitude (orbit altitude)	400km
Calculated inclination	97.03°
Possible altitude of insertion	600km
Manoeuvring capability	Possible Hall-effect thruster or ion engine for orbital transfer, station keeping and collision avoidance purposes
Constellation phases	<u>First phase</u> <ul style="list-style-type: none"> • 5 to 10 satellites • Revisit time = 2-3 hours
	<u>Second phase</u> <ul style="list-style-type: none"> • 30 to 50 satellites • Revisit time = 0.5-1 hour

Appendix B

Table 7: Combinations of launchers and varying specific costs for deploying a single plane

Launcher(s)	Payload mass to LEO (kg)	Number of satellites per launcher	Estimated leftover payload mass (kg)	Specific cost per satellite (USD million)	Total launcher cost (USD million)
Vega	1500 (estimated)	5	1000	8.4	42
Epsilon	450	4	60kg in total	8.6	43
1 x Electron	110	1			
Minotaur I	331	3	51kg in total	7.76	38.8
2 x Electron	110	1			
Pegasus	443	4	53kg in total	12.26	61.3
1 x Electron	110	1			
5 x Electron	110	1	50kg in total	5	25

Appendix C

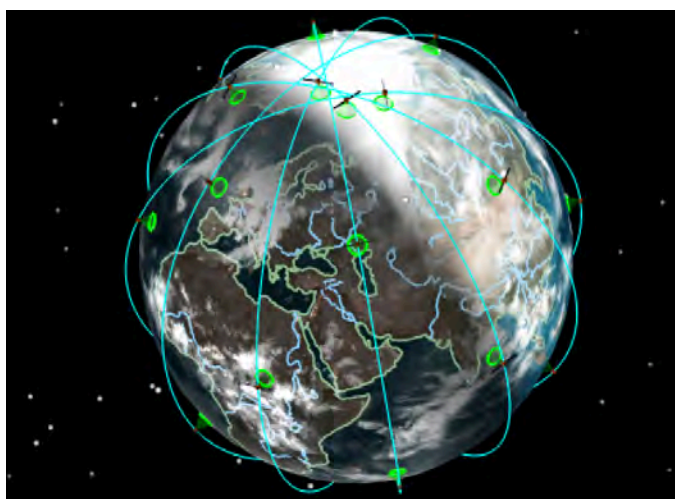


Fig. 8: Final Icyeye satellite constellation configuration (6 planes, 5 satellites each)

Appendix D

A summary of what each parameter represents in the MDO is presented here, and relevant examples from the performed MDO runs are presented in brackets. Please refer to Appendix F for further details.

- **Constants** – Parameters defined by the final Iceye mission requirements and are regarded as fixed (initial and final eccentricity e , altitude of final orbit h_f)
- **Fixed inputs** – Variables that represent very significant choices, that if changed alter the scenario entirely, and hence must be analysed in separate MDO runs (number of satellites per plane, no plane changes, scenario starting date: 1 January 2018)
- **Constraint functions** – These provide limits on possible values of decision variables to prevent the MDO from iterating solutions outside of the specified boundary conditions or generating invalid or impossible solutions (maximum phasing time, maximum/minimum orbit period times)
- **Outputs** – A range of solutions generated by the MDO which are usually open to interpretation (total delta-v, average phasing time)
- **Decision variables** – Key variables for study that can be easily changed to gauge their effect on the desired objective functions and are likely to have a major impact on mission outcomes (initial RAAN, phasing orbit periods)
- **Objective functions** – Areas that are either minimised or maximised to provide optimal solutions and are often competing parameters that require an optimal trade-off (minimising delta-v, minimising phasing time t_{phase})

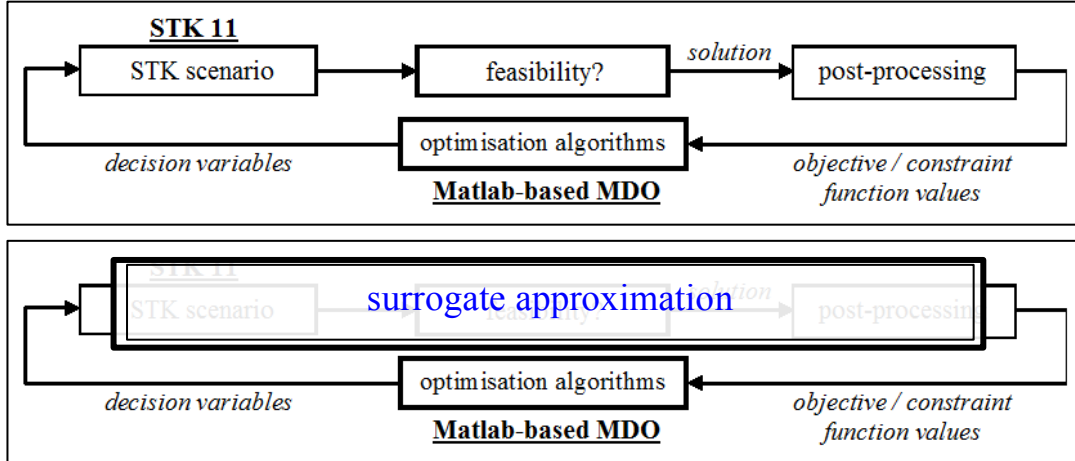


Fig. 9: MDO methodology overview (note how surrogate modelling can predictively generate output in the lower diagram)

Table 8: Launch vehicle specifications

Launch vehicle and operator	Number of stages	Payload to LEO (kg)	Specific LEO altitude (km)	Payload container dimensions	Number of launches	Vehicle gross mass (kg)	Cost (USD)	Height (m)	Diameter (m)	Specific impulse stage (s)
Epsilon (JAXA)	3	1200	250-500	D = 2.5m H = 3m	1	91000	38 million	24.4	2.5	1. 283.6
	3	700	500							2. 283.6
	4	450	500 (to SSO)							3. 301
										4. 215 (PBS)
Minotaur I (Orbital Sciences/Orbital ATK)	4	580	185	D = 3.8m H = 2.23m	10	36200	28.8 million	19.21	1.67	1. 237 (atmosphere)
										2. 288 (vacuum)
										3. 289
										4. 287
	5	331	500 (to SSO)							1. 237 (atmosphere)
				2. 288 (vacuum)						
				3. 289						
				4. 287						
				5. 229 to 232 (HAPS)						

Pegasus (Orbital ATK)	3	443	500 to 700	D = 1.18m H = 2.13m	42	18500	56.3 million	16.9	1.27	1. 295 2. 289 3. 287 4. 229 to 232 (HAPS)
Electron (Rocket Lab)	2	110	500 (to SSO)	D = <1m H = 1m (approximately)	0 (in testing)	10500	5 million (projected)	18	1	1. 327 2. 327
Vega (Arianespace)	4	300 to 2500	300 to 1500 (depending on orbital inclination)	D = 2.6m H = 7.88m	6	137000	42 million	29.9	3.03	1. 280 2. 289 3. 295 4. 315.5 (AVUM)

Appendix F

Table 9: MDO parameters for performing a phase change at 400km

Decision variables	Objective functions	Constraint Functions	Fixed inputs	Outputs	Constants and assumptions
<p>Initial orbit parameters:</p> <ul style="list-style-type: none"> $x(1)$ = Initial RAAN (degrees) $x(2)$ = Orbit period of 'Leading 72° satellite' (seconds) $x(3)$ = Orbit period of 'Leading 144° satellite' (seconds) $x(4)$ = Orbit period of 'Trailing 72° satellite' (seconds) $x(5)$ = Orbit period of 'Trailing 144° satellite' (seconds) 	<p>Minimise (f_1)</p> $\sum \Delta V_{sat} = f_1(x(1), x(2), x(3), x(4), x(5))$ <ul style="list-style-type: none"> ΔV_{sat} relates directly to the total satellite propellant needs (M_{extra}) that will be added to the payload mass Explore the effect of different initial RAAN <hr/> <p>Minimise (f_2)</p> $Mean t_{phase} = f_2(x(1), x(2), x(3), x(4), x(5))$ <ul style="list-style-type: none"> Competes with first objective Higher delta-v expenditure, lower phasing time Lower delta-v expenditure, higher phasing time 	<p>Time constraint</p> $t_{phase} < 2 months$ <ul style="list-style-type: none"> Transfer time should not be excessively long <p>RAAN constraint</p> $0^\circ \leq x(1) \leq 360^\circ$ <p>Explores all possible RAAN values</p> <p>Phasing orbit period constraints</p> <ul style="list-style-type: none"> $5350 < x(2) < 5553$ $5330 < x(3) < 5553$ $5554 < x(4) < 7774$ $5554 < x(5) < 9000$ <p>Prevents phasing orbit periods that require less than 0.5 phasing orbits, or collide with Earth</p>	<p>Plane</p> <ul style="list-style-type: none"> 5 satellites per plane 4 phasing satellites 1 satellite does not phase (reference) <p>Initial orbit</p> <ul style="list-style-type: none"> 400km circular orbit Inclined at 97.03° <p>Phasing orbits</p> <ul style="list-style-type: none"> No plane change (no change in inclination) All satellites begin phasing orbits at the same time 	<p>Optimal results</p> <p>MDO will generate a range of optimal combinations for:</p> <ul style="list-style-type: none"> Minimised total delta-v needs (f_1) Minimised phasing time (f_2) <p>Insights</p> <p>The MDO will also explore the effect of initial RAAN on these decision variables</p>	<p>Final orbit parameters are largely determined by the final SSO altitude and inclination</p> <ul style="list-style-type: none"> Final altitude $h_f = 400\text{km}$ Inclination (i) = 97.03° Eccentricity $e = 0$ Final orbit period = 5553.459 seconds Scenario start date: 1st January 2018 00:00:00 <p>The number of phasing orbits is based on the rounded number of phasing orbits according to MDO-generated orbit periods from the relation:</p> <ul style="list-style-type: none"> $P_2 = P_1 \pm \frac{t_{AB}}{\pi}$ Phasing orbits must be integers There must be at least one phasing orbit Orbit cannot intersect with Earth

Appendix G

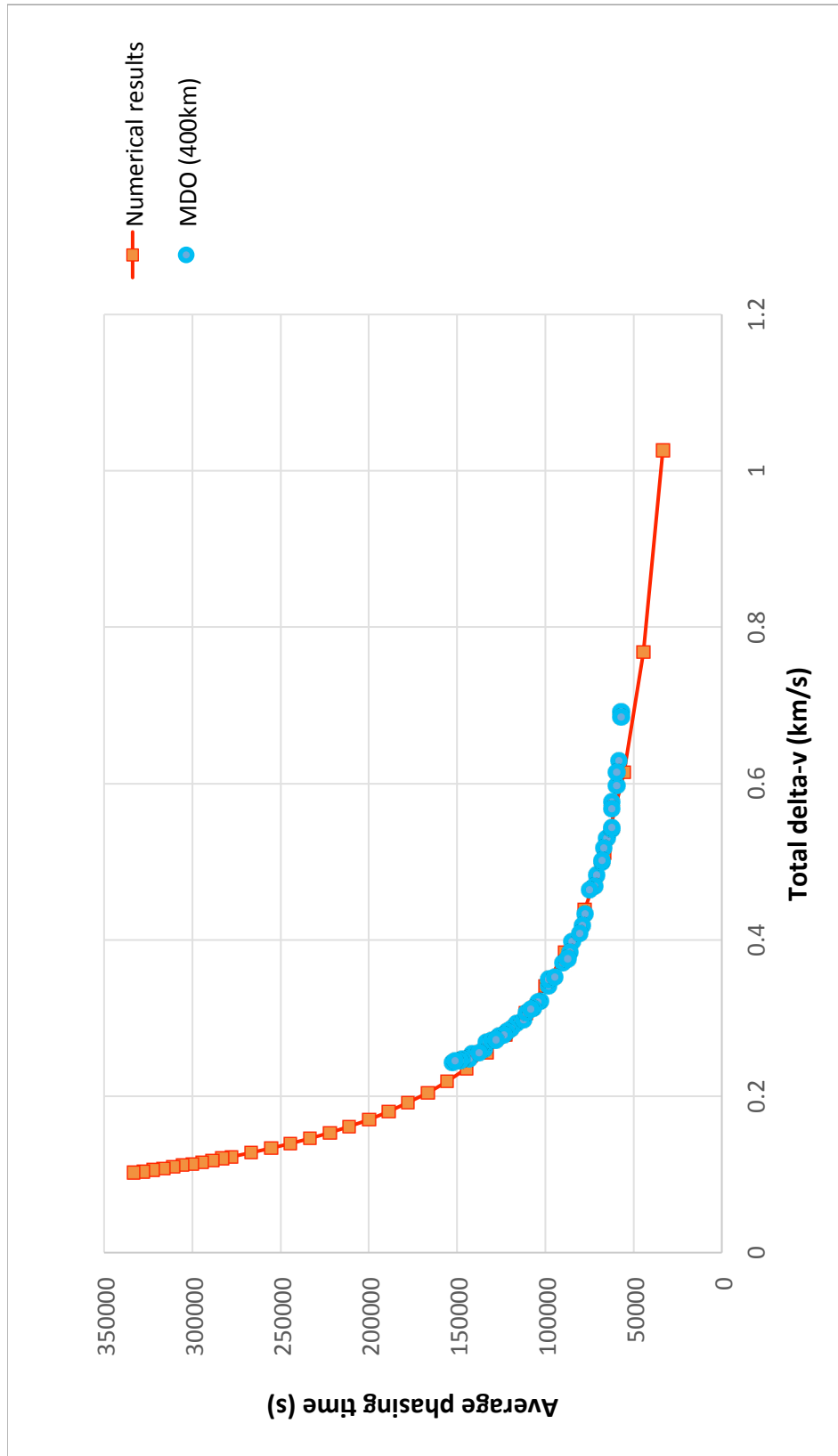


Fig. 10: Comparison of analytical and MDO-derived results

Multi-objective Design Optimisation of a small scale Cusped Field Thruster for micro-satellite platforms

Angus T. R. Muffatti¹, Hideaki Ogawa¹

¹ *School of Engineering, RMIT University, Buildings 56 and 57, Level 3, Corner of Queensberry and Lygon Streets Carlton, Melbourne, Victoria, 3053, Australia*

Summary:

The High Efficiency Plasma Thruster (HEMP-T) or Cusped Field Thruster (CFT) is a new concept in the field of electric propulsion that employs a permanent periodic magnet arrangement to confine and accelerate plasma. Efforts have been made to characterize the performance of the thruster, while efforts to down scale the design have lead to significant losses in performance. An advanced design methodology is applied combining a power distribution calculation and evolutionary algorithms to a multi-objective optimization for the performance optimisation and characterisation of the CFT. Optimization is performed for maximisation of performance defined by 8 design parameters while simultaneously aiming to maximize 3 objectives (thrust, efficiency and specific impulse). A global sensitivity analysis is employed to assess the optimization results to identify key design factors. Significant effects of the anode power and magnet radii have been observed design with the anode current exhibiting the most significant degree of influence.

Keywords: Electric propulsion, HEMP-T, high efficiency multi-stage plasma thruster, CFT, cusped field thruster, multi-objective design optimisation, evolutionary algorithm, micro-satellite.

Introduction

Electric propulsion (EP) is quickly becoming the standard for in-situ space operations. The incredible performance benefits of EP over traditional chemical propulsion is having effects felt in many areas of the space industry (commercial and scientific) such as increasing operational lifetimes of satellites, reducing fuel usage and launch costs as well as providing new opportunities for scientific exploration [1]. The most efficient types of EP used are the gridded ion thruster (GIT) and the Hall effect thruster (HET). Both of these propulsion concepts are well understood and provide values of specific impulse (Isp) ranges from 1500-6000s [2] and even higher into the tens of thousands [3]. Both of these designs provide great performance but also come with drawbacks such as system complexity and thruster erosion from impinging ions on grids or channel walls [4], which limits their operational lifetimes. The High Efficiency Multi-Stage Plasma thruster (HEMP-T) avoids these characteristics and simplifies thruster design while providing similar performance ranges of 2000-3000s and above [5, 6]) and expected worst-case lifetimes of over 16000 hours of continuous operation [7]. Since the first HEMP-T patent by Thales Electron Devices (TED) in 1999 similar thruster designs have been developed and tested by different institutions around the world; MIT's DCFT [8], Stanford's DCF [9] and the Harbrin Institute of Technology's CFT [10]. The HEMP-T or the Cusped Field Thruster avoids the negative characteristics of GITs and HETs through a novel method of plasma confinement usually employed in travelling wave tube technology [4]. The confinement method consists of a series of permanent ring magnets aligned co-axially with reversing polarity known as a permanent periodic magnet (PPM) system. This significantly reduces plasma contact with the discharge chamber walls as the majority of the magnetic field is parallel to the inner walls and hence decreases charge losses by restricting the radial movement of the plasma. This leads to higher

beam power efficiencies in the range of 80-90% [4]. This was also the reasoning behind the TED group's name "High Efficiency" for the design. The PPM system also impedes the axial translation of electrons up-stream of the magnetic cusp regions by means of the magnetic mirror condition [4, 5, 11]. The cusp regions effectively divide the engine into separate magnetic cell stages, which have been shown in particle-in-cell (PIC) simulations [12-14]. The magnetic field (B) strength is chosen such that the Larmor radius of the electrons is much smaller than the inner geometry of the discharge chamber. This effectively confines the electrons to the centre of the engine that in turn helps to electrostatically confine the ions, of which the magnetic field has little effect upon because the mean free path of the ion is significantly smaller than its gyro radius and is not considered magnetized [7]. Ions that escape this confinement contribute to an overall positive charge of the chamber wall and therefore an enhancement of ion beam formation [5]. The thruster also features a steep potential drop occurring just after the exit cusp whilst the plasma potential is maintained at a relatively constant level throughout the engine [4, 5, 12]. This is due to the electron cloud (from the neutralizer cathode) confined at the exit cusp that acts as a virtual acceleration grid resulting in high acceleration efficiencies with the majority of ions close to anode potential [5]. From this, a clear separation of ionization and acceleration regions is occurring likening the thruster acceleration to a grid-less GIT [4,5]. A diagram of the thruster layout is shown in Fig 1.

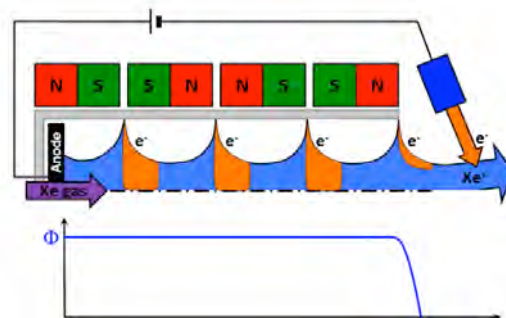


Fig. 1: Cusp impediment of electrons and potential profile of the thruster [5]

Efforts in recent years have seen some attempt to scale down the HEMP-T technology but the performance of the micro-newton thruster remains low. Keller et al [15] have produced a study of the performance parameterization of the HEMP-T design. In their efforts to scale down the size of the thruster into the micro-newton thrust range they have shown the relation of several inter-related sizing parameters. Testing various thruster configurations and the sensitivity of parameters (chamber diameter, magnetic ring outer diameter, the distance between magnetic stages and the number of stages) to four output performance measures (mass flow, anode current, plume divergence, acceleration efficiency) an approximate range of values for the micro-newton thrust level was obtained. These specifications provide some insight into the sizing sensitivity of the design and deliver key indicators in the way of thruster sizing ratios such as increasing magnetic field intensity for decreasing discharge chamber diameters to reduce losses. However, the performance remains quite low in comparison with the larger scale counterparts with a maximum I_{sp} achieved of 860 s whereas the higher end of performance range upwards of 3000 s [6, 16].

A state-of-the-art methodology to achieve such design requirements has been developed by coupling an analytical global-variable based steady-state power and plasma model solver and a multi-objective design optimization (MDO) capability based on evolutionary algorithms. This approach enables robust and effective population-based optimization, assisted by surrogate modelling, which can effectively reduce the computational cost by approximating the model calculation in lieu of expensive true computational evaluation. The coupled simulation/MDO approach has been applied successfully to numerous design optimization

problems (CFD/MDO) [36-38] however this appears to be the first application of this methodology to this design problem. In the present study, a multi-objective design optimization of a small-scale HEMP-T, being the first example of the advanced MDO capability based on surrogate-assisted evolutionary algorithms applied to the design of electrostatic plasma propulsion, in particular the HEMP-T or CFT design. This paper presents the outcomes of the optimization analysis that has been conducted for 3 major objectives commonly targeted in the area of spacecraft propulsion, that is, 1) Thrust (T), 2) Efficiency (η_t), and 3) Specific Impulse (I_{sp}). The magnetic topology is examined for representative high-performance configurations to investigate the underlying thruster physics. The surrogate models are trained with the archive of solutions evaluated during the optimization. They are used to perform variance-based global sensitivity analysis to identify the key design factors as well as an additional large-scale optimization solely employing the surrogates to better capture the effects of the design parameters on the HEMP-T's design space.

Methodology

Performance characterisation

Performance metrics used to characterize the Hall thruster can also be used to quantify the function of the HEMP-T/CFT because of their similarities in operation. Starting with the basic relations of spacecraft propulsion thrust (T) equating with force on a charged particle in an electric field, specific impulse (I_{sp}) and power (P_a) – both electric and kinetic [7,19,20].

$$T = v \cdot m_f = e \cdot E \quad (1)$$

$$I_{sp} = T / (m_f g) \quad (2)$$

$$P = \frac{1}{2} \cdot m_f \cdot v^2 = U_a \cdot I_a \quad (3)$$

Where E is the potential difference in an electric field, U_a and I_a are the anode voltage (subscript a refers to the anode) and current respectively and m_f is the mass flow rate of propellant (anode and cathode). Where $I_a = dq / dt$ this gives the power to thrust ($PTTR$) ratio in Eqn 4 [4].

$$PTTR = \sqrt{(e \cdot U_a / 2M)} \quad (4)$$

$$\eta_t = T \cdot v / P_a = T^2 / (2m_f P_a) \quad (5)$$

Where M is the mass of propellant atoms (2.18×10^{-25} kg for Xe), e is the elementary charge (1.602×10^{-19}). The total efficiency of the thruster can be calculated through the ratio of the jet power to the anode power (P_a). The component efficiencies that comprise parts of the total efficiency relate to the processes involved in converting the electrical energy input to the kinetic energy of the exhaust plume; the beam efficiency (η_b) is the ratio of anode current to the plasma beam current, utilization efficiency (η_u) the maximum current obtainable from the supplied beam current assuming only singly charged ions, acceleration efficiency (η_{ac}) the percentage of ions accelerated at anode potential and the coefficient of plume divergence ($\cos^2(\theta_b)$), which accounts for ions that are not accelerated parallel to the thruster axis. Defined as follows [19, 21].

$$\eta_b = I_a / I_b \quad (6)$$

$$\eta_u = I_b / (m_f e / M) \quad (7)$$

The subscript b refers to the ion beam. The acceleration efficiency would be measured experimentally by and calculated from the data received from a retarding potential analyser.

The current density around the thruster exit i.e. plume divergence (measured by the angle from the thruster centreline to the point where ~90% of the discharge in the plume is encompassed, (θ_b)) and the total beam current would be measured with faraday probes, which would allow for the calculation of beam and utilization efficiencies. These efficiencies combine to make the total efficiency, commonly referred to as the anode efficiency.

$$\eta_b = \eta_b \cdot \eta_b \cdot \eta_{ac} \cdot \cos^2(\theta_b) \quad (8)$$

Thruster model

Kornfeld *et al* [4] describe a simplified power balance description of the HEMP-T based in plasma fluid theory. A one-dimensional set of equations (28 in total) to be solved simultaneously that can be used to provide a rough estimate of the thruster performance. As the only known values in the equation set are the probabilities to reach the channel wall at the cusp locations, and these probabilities are based on magnetic field strength, thruster performance can be estimated through only a few parameters. These are anode potential, anode current and the ratio of magnetic field strength from the axially aligned region to where the fields radially cross the discharge channel walls i.e., the magnetic mirror strength. It is also important to note that the ratios (described in [4]) of power transferred to excitation, ionization and thermalisation are only estimations. It is also stated that inclusion of angular and ionization efficiencies could allow for predictions of total thruster efficiency. The following description was derived from the equation system presented by Kornfeld *et al* [4], where a full description of the power model can be found.

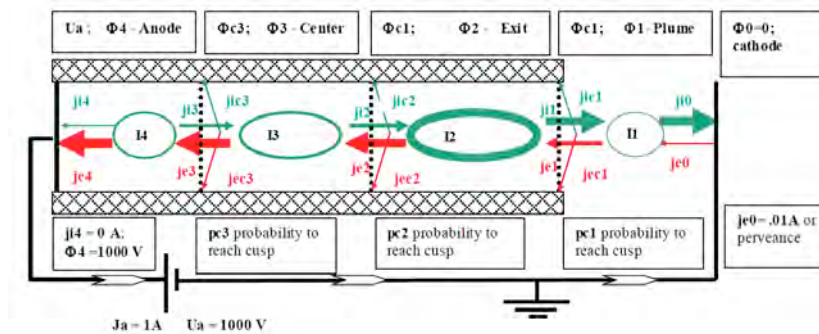


Fig. 2: Simplified circuit of the HEMP-T [4]

The PPM system that defines the main operational characteristic of this thruster type relies on the magnetic mirror principal to reduce losses at the plasma chamber walls where the magnetic field radially crosses (cusp region) [4]. It states that as a particle moves into the mirror region (B is increasing), with a constant kinetic energy (K) (the B field does no work on the particle) and ignoring B drifts that it experiences a longitudinal axial force (F_z) proportional to the increase of the magnetic field in the opposite direction of its motion, given by the Lorentz force defined in a cylindrical field [11,20].

$$F_z = - (m \cdot v_r^2 / 2B) \nabla_1 \cdot B \quad (9)$$

$$F = \mu \cdot \nabla_1 \cdot B \quad (10)$$

Where v_r is the cyclotron motion of the particle – in terms of magnetic moment (μ) this gives. As can be seen in the above equations, the force is increasing negatively with increasing field strength. In [11,20] it states that a particle moving through a field of increasing strength (i.e. field strength is time dependent) that the magnetic moment is constant, which when equating the magnetic moment of two points (low and high field areas) delivers.

$$v_{\perp 0}^2 / B_0 = v_{\perp m}^2 / B_m \quad (11)$$

Subscript 0 refers to low field and m for the high field mirror region. As the flux linked in the particle orbit remains constant, the particle is reflected at the point where its velocity parallel to the increasing field (flux lines are contracting) reaches zero due to the perpendicular component of its velocity (a rotational velocity) that elicits reflective force normal to the B field and hence a component in the opposite direction (still parallel but negative); it is wholly dependent on the strength of the magnetic field. Because the particle kinetic energy is conserved and is itself comprised of both the parallel and perpendicular components of velocity i.e.

$$K = m \cdot (v_{\parallel 0}^2 + v_{\perp 0}^2) / 2 \quad (12)$$

$$v_{\parallel} = [2(K - \mu \cdot B)]^{1/2} \quad (13)$$

This magnetic mirror trap however is not completely efficient. The velocity direction of the charged particle (an electron in this case) must be within the acceptance angle to escape the mirror condition [11, 20] or, as in the case of electron confinement in the thruster, arrive at the chamber wall and contribute to the ion beam energy losses [4]. The acceptance angle comes from the conservation of kinetic energy in Eqn 12 and is the angle between the vectors of the particle's forward and rotational velocity. Eqn 14 is known as the mirror ratio.

$$B_m / B_0 = (v_{\parallel 0}^2 + v_{\perp 0}^2) / v_{\perp 0}^2 \quad (14)$$

$$= 1 / \sin^2(\theta_m) \quad (15)$$

$$\theta_m \leq \sin^{-1} [\sqrt{(B_0 / B_m)}] \quad (16)$$

$$p_c \equiv \frac{2\pi \left(\int_0^{\theta_m} \sin(\theta) d\theta \right)}{4\pi} \quad (17)$$

The acceptance angle, θ_m , is the angle at which all incident ions that are under are not reflected by the magnetic mirror. The arrival probability of electrons at the dielectric wall in the HEMP thruster can be calculated by integrating over all angles from 0 to θ_m , where the subscript c denotes the cusp number [4]. The magnetic field topology is measured in FEMM – a validation of the software accuracy can be found in [35].

Design Optimisation

Shown in Fig. 3 is the process chain followed for the production of decision variables and delivery of the objective functions. The decision variables are pre-processed to assure the geometry is physically possible before they are passed onto the software FEMM for model construction and the computation of the magnetic field. The data is then extracted from the magnetic topology to compute the cusp arrival probability for each location throughout the thruster. These conditions are subsequently passed to the power distribution calculation. The resultant solutions from this are post processed to deliver the objectives and check they're within the set of physical constraints, which are then submitted to the MDO Algorithms for evaluation. This cycle then repeats and as more designs are produced and evaluated according to the set criteria. The optimisation progressively learns the sensitivity of the decision variables and delivers more favourable results and refined guesses with each generation.

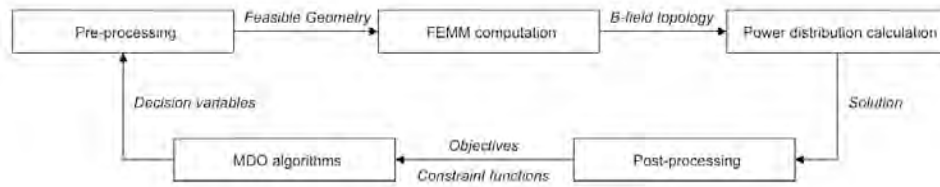


Fig. 3: MDO Process chain

An evolutionary algorithm originally developed at University of New South Wales (UNSW) Canberra [24, 25] performs the design optimization. In particular, use is made of the elitist non-dominated sorting genetic algorithm [26] assisted by surrogate modelling. It is a population-based approach where the candidate solutions in the population pool evolve over generations. A population size of $N = 96$ is used in this study to be evolved over 67 generations. These values have been chosen to sufficiently explore the design space for a 3 objective design problem with 8 decision variables within reasonable computational effort. Applying recombination operators are applied to the previous generation's decision variable values to create offspring. A simulated binary crossover and polynomial mutation are used as recombination operators at a given probability (1.0 and 0.1, respectively, in this study) with a specified distribution index (10 and 20, respectively) [25]. Surrogate modeling [27] is commissioned to estimate the possible values of the objectives and constraints in an inexpensive manner, imitating the simulation of the solutions from the magnetic and power analyses with meta-models characterized by appropriate mathematical functions. The surrogates are constructed by using a fraction (90% in this study) of the actual solutions calculated from the magnetic and power distribution models to prevent over fitting, whereas the remainder (10%) of the evaluated solutions are used to assess the quality of the surrogate models [25]. Surrogates for each of the objective and constraint functions are trained by using a subset of the archive, which is created by selecting the solutions closest to the centroids of the k clusters obtained through k -means clustering [28]. Multiple surrogate models are employed and evaluated: quadratic response surface model [29], artificial neural network (ANN) models including the radial basis function network [30] and multilayer perceptron model [31], which are single-layer and feed forward types of ANN models, respectively, and Kriging model based on Gaussian process regression [32]. The mean squared error (MSE) in the actual and predicted values of the objectives and constraints is calculated for the remaining (10%) solutions and used as the measure to validate the surrogate models. Prediction from the best surrogate model with a minimum error is adopted to replace Simulation analysis, only if the MSE is within a threshold value of 5% for all objective and constraint functions and the distance to the closest point in the archive is smaller than 5% [25]. The 3 objective functions used to evaluate design performance are thrust (T), efficiency (η_t) and specific impulse (I_{sp}). The efficiency term with the subscript t is somewhat of a misnomer, usually descriptive of total efficiency, it must be stated that the model presented in this paper does not take in to consideration plume divergence losses or an accurate representation of acceleration efficiencies. The η_t term is comprised of the measures of efficiencies within the thruster model, that is, the beam efficiency (η_b), the mass utilisation efficiency (η_m) and the grid efficiency (η_g). η_b is relatively straightforward; Kornfeld's power balance model returns a value for the thruster beam power, which is then compared to the anode power i.e.,

$$\eta_b = P_b / (I_a \cdot U_a) \quad (19)$$

$$\eta_g = 1 - (\Phi_1 / \Phi_2) \quad (20)$$

$$T = \sqrt{(2I_a \cdot U_a \cdot m_f \eta_t)} \quad (21)$$

The grid efficiency is a measure of the ratio between the last downstream internal magnetic cell and the plume cell potentials (see Fig. 2). Maintaining a large value of η_b seeks to maintain the desired large potential drop at the exit cusp while promoting consistent plasma potential throughout the engine. This measure also serves as a weak approximation for acceleration efficiency. The mass utilisation efficiency is shown in Eqn 7, T is calculated by rearranging Eqn 5 and I_{sp} through Eqn 2. The decision variables and their input ranges chosen to represent the main design factors investigated in this study (shown below) are U_a [V], I_a [A], m_f [sccm], IMR [mm], OMR [mm], ISR [mm], OSR [mm], and OER [mm]. The objectives; $-T$, $-\eta_b$, $-I_{sp}$ (the negative sign denotes a maximization problem) are subject to (Decision variable [upper range:lower range]) in the units listed above; U_a [0:1000], I_a [0:10], m_f [0.2:50], IMR [2:50], OMR [2:50], ISR [2:50], OSR [2:50], OER [2:50].

Sensitivity Analysis

Variance-based global sensitivity analysis is executed to investigate the influence of each decision variable $x(i)$ as input (i.e., design parameter) on the objective functions y as output (i.e., thruster performance parameter). A numerical procedure (Sobol's variance decomposition [33]) is employed to derive the sensitivity indices, facilitated by surrogate modelling [27]. Input matrices X of a base sample quantity of 10,000 and multiple columns for the decision variables are built by using quasi-random numbers [33] within the range for each variable. Output vectors Y are obtained by forwarding the input matrices to the surrogate model that are of the greatest prediction accuracy. The first-order indices S_i and total-effect indices ST_i are calculated by the method outlined in [34], defined as

$$S_i = [E(Y|X_i)]/V(Y), \quad ST_i = 1 - V[E(Y|X_{-i})] / V(Y) \quad (22)$$

Model Description

The HEMP-T model created in FEMM for use in the MDO design is designed to remain as simple as possible. This is for ease of calculation but also to simplify the input design parameters that will affect the outcome of the simulation and therefore allow for a clearer derivation of the cause-and-effect relation between the decision variables and the objectives. The thruster itself features a consistently straight chamber, 3 magnet stages with spacers (doubling as field guides), a magnetic shield that creates a secondary magnetic circuit and the thruster housing. Used in the simulation are SmCo 27 MGOe magnets stacked with reversing polarity and the thruster housing material used is Al 6061-T6. Both the 'shield' and spacers are made from pure Iron due to the high conductivity of the material as well as to improve commonality with other HEMP-T/CFT designs [5, 9, 15, 19]. Several geometric constraints were implemented to restrict the scope and output of the design space that is IMR , OMR , ISR , OSR and OER . The basic physical constraints implemented into the model are quite simple in nature, that is, rejection of geometries that overlap in regions. The somewhat arbitrary limitations selected are those for the inner thruster channel geometry (2 mm radius) as a lower limit and the upper limit (50 mm radius) to remain approximately within the limits of the standard cubesat form. Further restrictions are placed on the utilisation of propellant regarding anode current. Described in eq. 7, the upper limit is set in the pre-processing stage where I_b is replaced with I_a and cannot produce a value exceeding 1, as the only ion species under consideration are the singly charged variety.

Results

Optimisation

A multi-objective optimization by surrogate-assisted evolutionary algorithms is performed up to 67 generations with a population size of 96. Fig. 8 displays the non-dominated individuals obtained as a result, where a vector of the objective functions $f(x')$ is said to be non-

dominated if there exists no other vector $f(x)$ that satisfies $f(x) \leq f(x')$ with $f_i(x) < f_i(x')$ for at least one index $i \in \{1, 2, 3\}$. It also shows all 6472 solutions that have been evaluated during the optimization from a three dimensional viewpoint and projections on three planes. Also included in these plots are 4 selected individuals (S1– 4) that have been selected to investigate the key design factors and associated context of their creation. S2, and S3 are non-dominated solutions that perform the best with respect to each design criterion, that is, η_t (S2), T and I_{sp} (S3) with S1 occupying a place on the pareto-optimal front between S2 and S3. S4 is a sub-optimal solution, characterized by low performance in all 3 objective categories. The surrogate models trained during the optimization have been found to be, at this stage incapable of predicting the objective functions (output parameters) from decision variables (input parameters) within reasonable accuracy, with the errors being 6.51 % in T via the rsm model, 13.9 % in η_t via the orsm model, and 6.17 % in I_{sp} via the orsm model. Table 1 displays the variable interaction observed after 67 generations. A positive sign (+) denotes that there is a correlation between the increase of the absolute variable magnitude with an increase of the objective, however, there remain outlying data points (>20). Two positive signs (++) indicate that an increase in the absolute value of a decision variable strongly correlates with an absolute increase in the objective. The same statement is true for that of the negative signs ($-$, $--$) but the increase of the absolute value of the objective is coupled with a decrease in the absolute value of the variable. Following this same methodology, the ($\approx+$) and ($\approx-$) sign indicates a slight trend but no conclusive trends can be deduced, those present are most likely due to the non-linear nature of the problem i.e., secondary influence from variable interactions, the ($=$) sign indicates no apparent trend.

Table 1: Effects of design parameters on performance parameters

Parameter	U_a	I_a	m_f	IMR	OMR	ISR	OSR	OTR	P	IMR/OMR
T mN +	+	+	++		$\approx+$	$\approx+$	==	==	++	$\approx-$
η_t +	$\approx-$	+	-	==	$\approx+$	$\approx+$	==	==	-	$\approx+$
I_{sp} +	++	+	==	$\approx-$	$\approx-$	$\approx+$	==	==	++	$\approx-$

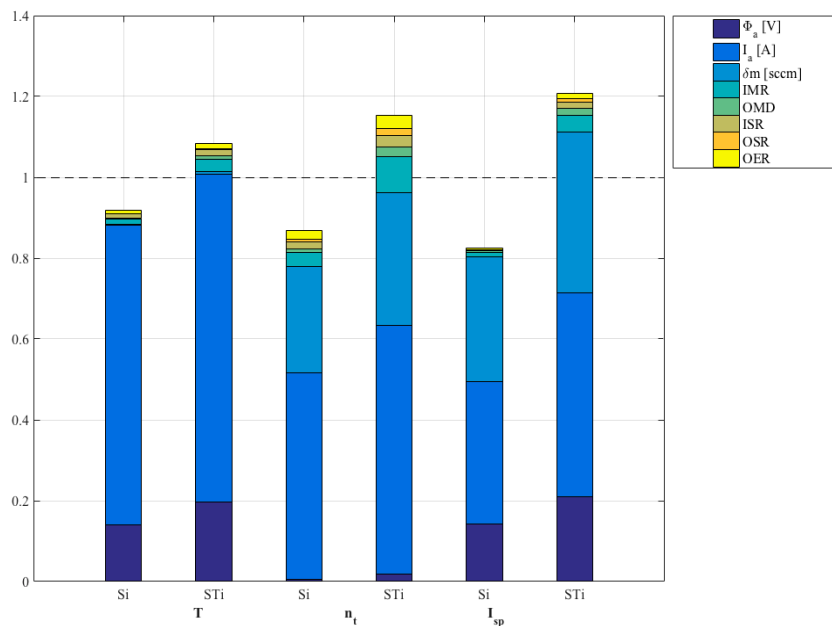


Figure 4 - Sensitivity indices for influence of decision variables on objective functions

Sensitivity Analysis

A variance-based global sensitivity analysis is completed to examine the effect of the decision variables on the objective and functions by applying the technique outlined in Sec. II-D. Presented in Fig. 8 are the first-order sensitivity indices S_i and total-effect indices S_{Ti} , which

represent the main and overall effects of the input parameters (decision variables) respectively, i.e., U_a , I_a , m_f , IMR and OMR , inner and outer shield radii, and the outer engine radius on the output parameters (objective functions), i.e., thrust, efficiency, and specific impulse. The differentiation between the total-effect index ST_i and the first-order index Si is indicative of the degree of the influence of the decision variable in combination with other decision variables on the objective functions [34]. If the decision variables are characterized by the sum of both first-order and total-effect indices being near unity (i.e., $\sum S_i \approx 1$ and $\sum ST_i \approx 1$), this indicates that the effects of individual decision variables interact linearly. Considering the design objectives presented in Fig. 8 we can see that the majority of influence on the design overall comes from 3 critical design parameters, that is, U_a , I_a and m_f , with the anode current delivering the highest degree of influence across all 3 objectives. Considering the physical design factors of the design output, the inner magnet radius is clearly the most influential on thruster performance across all objectives. It is worth noting that the surrogate model prediction error (used for calculating the sensitivity indices) was approximately 6% for T and η_t and 10% for I_{sp} .

The first order effects for thrust are dominated by I_a (0.741) followed by U_a (0.141) with the next most influential parameter being IMR (0.012), all other decision variables registering and at or below 0.01. The summation of first order effects is 0.981. Second order effects are apparent as well, illustrating the non-linear nature of the problem. Again the indices follow the same order of influence but with each increasing slightly in magnitude giving 0.811, 0.197 and 0.031 for I_a , U_a and IMR respectively again, with the other variables remaining just above or under 0.01. In terms of the growth of influence from first to second order effect i.e., the greatest variability observed in the growth of design variable influence, the OMR experienced the largest increase (439 %) followed by IMR (262 %) and m_f (259 %). While maintaining I_a as the most influential first order variable at 0.510, the following variables in order of influence are m_f (0.262), IMR (0.035), OER (0.022) and ISR (0.018) with the rest remaining below 0.01. Second order effects follow this same trend giving indices values of 0.614, 0.329, 0.089 and 0.032 for I_a , m_f , IMR and OER respectively. Relative increases of variable influence show that U_a increases by 319 %, IMR by 253 % and OMR by 253 %. The large influence that m_f and I_a have on η_t is not entirely unexpected due to the highly inter-related nature of the mass utilisation calculation. These results perhaps indicate the importance of matching these two parameters to achieve nominal conditions. However it is important to note that other measures of efficiency such as acceleration efficiency and beam divergence losses are not taken into consideration in this model. The parameter influence on I_{sp} follow the trends observed with η_t but with a much larger influence from U_a . The respective first order influence of I_a , m_f and U_a 0.351, 0.308, 0.142, show again that the optimisation of the parameters plays an important role on thruster performance and that a precise level of power delivery to the thruster is required for nominal operation at a selected values of m_f . This is further reinforced by the nonlinear nature of variable interaction illustrated in figure 8. The indices for I_a , m_f and U_a are 0.504, 0.398 and 0.211. The largest relative increases were witnessed with IMR (318 %) and OMR (438 %).

Objectives & Configurations

After the evaluation of 67 generations consisting of 96 individual design evaluations the following plots are produced in Fig. 8. These plots show the feasible evaluated solutions along with the 3 selected points from the non-dominated solutions (a total of 6 were generated) and a single sub-optimal solution for comparison. The data trends described in table 4 are subsequently reflected in the design configurations presented in tables 5 showcasing the variation in performance and geometry. A discussion of this variation relative to the design objectives shall follow.

Table 2 – Selected points (s1-4)

Configuration	T	η_t	I_{sp}	U_a	I_a	m_f	IMR	OMR	ISR	OSR	OTR
S1	69.90	99.61	3387	638.14	1.826	21.408	19.931	27.092	30.365	42.177	47.330
S2	64.16	99.99	3141	542.43	1.822	21.189	19.602	26.385	31.030	44.031	46.762
S3	85.42	96.74	4192	997.33	1.820	21.135	9.275	26.281	32.200	44.714	48.869
S4	31.74	42.13	1491	464.43	1.187	22.080	13.869	25.835	26.587	26.662	38.656

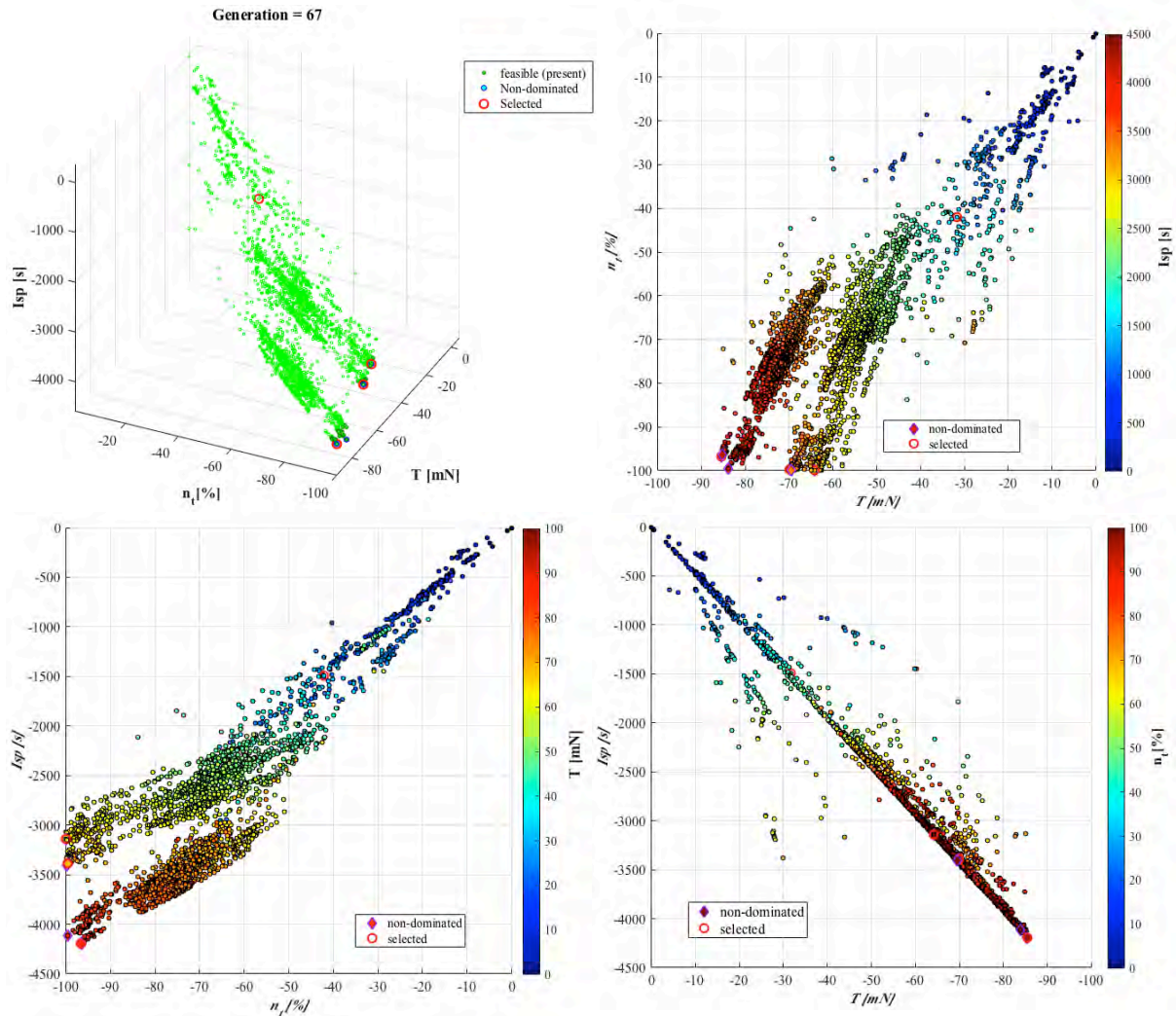


Fig. 5: Optimisation solutions of analytical evaluations (at 67th generation with $n = 96$)

The third selected point (S3) provides the greatest measure of thrust generated in the cohort of simulation evaluations and of the non-dominated solutions it exhibits the lowest measure of efficiency. The high thrust value is reflected in the anode potential the thruster exhibits, given the approximate non-variation of the anode current among its non-dominated peers this indicates a reliance on high power operation to achieve significant momentum exchange (intuitively grasped from eq. 20). Comparing S2 with S3, a drop of approximately 20 mN is observed at 54.4 % of the input power. The sub-optimal S4 design point operates at 30.4 % of the power level of its S3 counterpart however delivering a reduction in thrust of 53.68 mN. Following the relation in eq. 20, should the power level be the only variable at play a thrust level of 38.38 mN should be apparent (a variation of 20.9 % from the output). The only large geometric variation between the S3 and S4 designs is that of the IMR indicating its role in achieving high thrust densities (also seen in Fig. 7). The highest thrust achieved by S3 is coupled with the highest peak field strength within the discharge chamber (Fig. 9) however

this is not entirely indicative of thruster performance as the field strength does not pertain to the force output but to the power losses which are relative to the high and low field regions at each magnetic cusp.

Little variation in efficiency is seen between the non-dominated solutions, all featuring values above 96 %, with S3 being the lowest. S4 shows significantly reduced levels of efficiency (42.13 %) mostly in part to the level of propellant utilisation, which sits at 62.0 %. Variation in efficiency levels between the non-dominated points is almost non-existent however there is a general trend where the higher T or I_{sp} will be coupled with a reduced value of η_t . The variation in magnetic field strength and topology between the non-dominated results is quite small with peak B field strengths occurring in the discharge chamber of approx. 0.3 T. As the cusp arrival probability is a major component of inefficiencies in the thruster is no surprise to see the sub-optimal point (S4) with such a low peak field strength, almost half that of its non-dominated counterparts. Clearly standing out among the cohort S3 delivers an impressive value of I_{sp} (4192 s) reaching in excess of 805 s greater than the closest in the selected points (S1). This is, however, not unexpected given that the S3 point has the largest power input at the anode. In terms of effective specific impulse gained for power input one finds that S2 is the most cost effective in this regard delivering 0.31 W/s compared with S3's 0.43 W/s.

Perhaps more interesting is the power to thrust ratio (PTTR), where we can see which designs provide us with the most cost effective thrust production; a critical component when considering the thruster in the context of small spacecraft whom are often power limited. A clear distinction can be seen in Fig. 15 where those with the lowest values (dark blue) do not occupy the regions of the solution space that are maximised with regard to all 3 objectives. Considering the selected points (S1-4) from section III-H-9, S1, S2, S3 and S4 exhibit PTTR values of 16.7, 15.4, 21.2 and 17.4 respectively. Therefore measured against this metric the so-called sub-optimal point achieves greater performance than that of S3 providing a more cost effective method to achieve thrust i.e., more mN per W. for small spacecraft platforms this is most likely the metric of most benefit. Given minimum requirements for thrust and I_{sp} design should be sought for the most cost effective method of producing the impulse required.

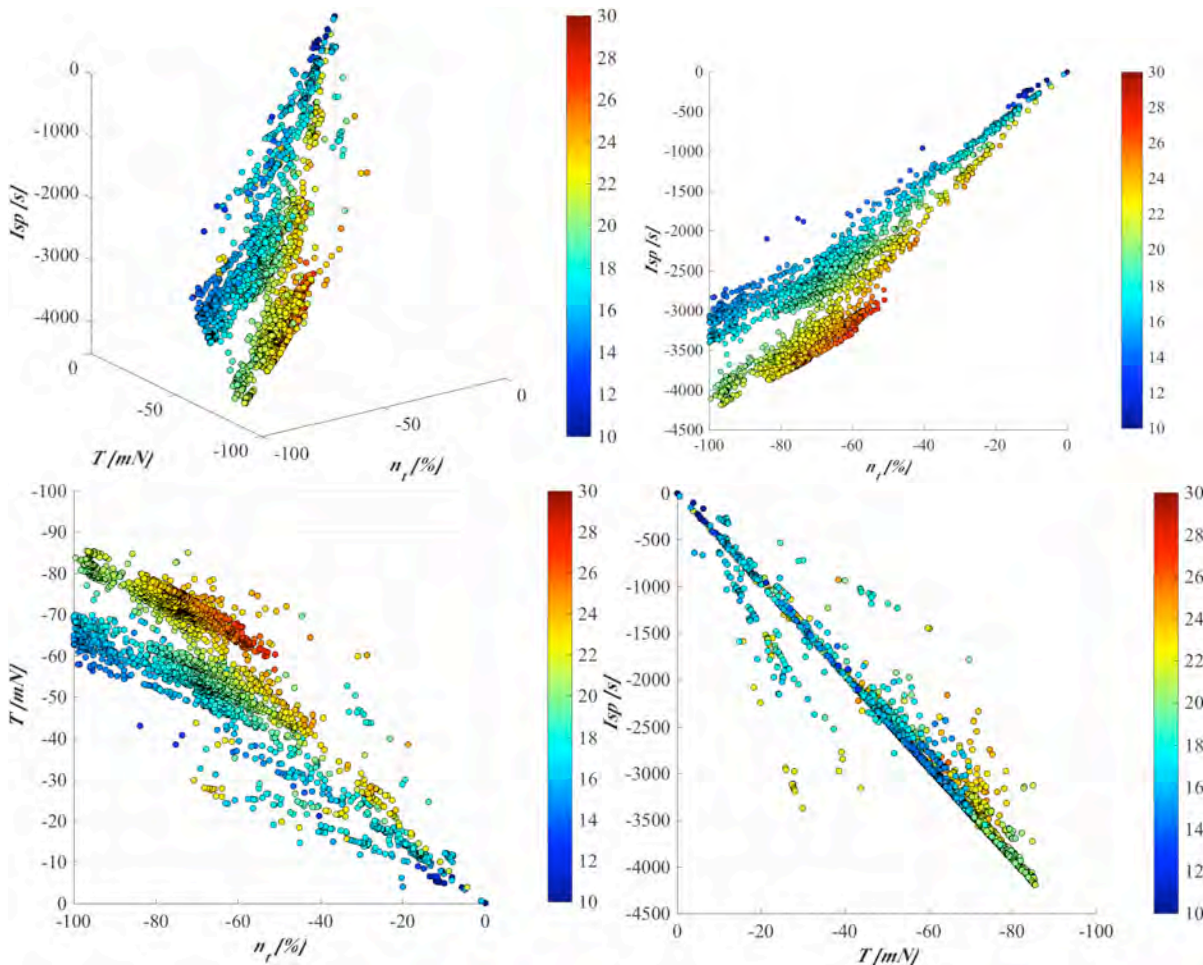


Fig. 6: Power to thrust ratio (W/mN)

Conclusion

A computational study has been conducted to investigate the characteristics and behaviour of the HEMP-T design, aiming at the application of a scaled down thruster for micro-satellite platforms. A multi-objective design optimization using surrogate-assisted evolutionary algorithms has been performed to maximize 3 performance measures, namely, thrust, efficiency and specific impulse, by incorporating magnetic field design with a global equilibrium power distribution calculation. A global sensitivity analysis based on surrogate models has identified the anode power, mass flow rate and magnet sizing as key design parameters for most performance parameters under the presented conditions [describe your simulation context]. The design performance was found to be highly sensitive to the anode current across all 3 objectives, which was found to be the most influential variable. The 3 objectives (maximisation of T , η_t , I_{sp}) have been examined for four representative configurations to scrutinize the underlying mechanism that has led to the performance trends observed here. The performance point S2 appears to deliver the most beneficial thruster configuration delivering the highest efficiencies of all design points as well as the lowest values of PTTR. Several important trends in the data have been recognised such as maintaining a high anode potential and matching the anode current with mass flow rate to achieve high utilisation efficiencies. The high efficiency achieved is also a reflection of magnetic field configuration with a maximum in chamber strength of approx. 0.3 T delivering low probability of electron arrival in the cusp regions.

Acknowledgements

The author is grateful to T. Ray and A. Isaacs for the original MDO framework. The first author would also like to acknowledge Mr George Coulloupas for the many discussions and help throughout the project.

References

- 1 Saccoccia, G. and del Amo, G., 2000. Electric propulsion- A key technology for space missions in the new millennium. *ESA bulletin*, (101), pp.62-71.
- 2 Boyd, Ian D. *Simulation Of Electric Propulsion Thrusters*. Ann Arbor, Michigan: Department of Aerospace, University of Michigan, 2011. Print.
- 3 ".: Space Propulsion Laboratory | About Electric Propulsion :.". *Web.mit.edu*. N.p., 2016. Web. 8 Mar. 2016.
- 4 Kornfeld, G., Koch, N. and Harmann, H.P., 2007, September. Physics and evolution of HEMP-thrusters. In *Proceedings of the 30th International Electric Propulsion Conference* (pp. 17-20).
- 5 Koch, N., Schirra, M., Weis, S., Lazurenko, A., van Reijen, B., Haderspeck, J., Genovese, A., Holtmann, P., Schneider, R., Matyash, K. and Kalentyev, O., 2011, September. The HEMPT Concept-A Survey on Theoretical Considerations and Experimental Evidences. In *32nd International Electric Propulsion Conference, Wiesbaden, Germany September* (Vol. 11, p. 15).
- 6 Koch N, Weis S, Schirra M, Lazurenko A, van Reijen B, Haderspeck J, Genovese A, Holtmann P. Development, qualification and delivery status of the HEMPT based ion propulsion system for SmallGEO. In *Proceedings of the 32d International Electric Propulsion Conference* 2011.
- 7 Eichmeier JA, Thumm M, editors. *Vacuum electronics: components and devices*. Springer Science & Business Media; 2008 Mar 4.
- 8 Courtney DG, Lozano P, Martinez-Sanchez M. Continued investigation of diverging cusped field thruster. *AIAA Paper*. 2008 Jul;4631:2008.
- 9 Young CV, Smith AW, Cappelli MA. Preliminary characterization of a diverging cusped field (DCF) thruster. In *Proc. 31st Int. Electric Propulsion Conf.(Ann Arbor, MI) 2009* Sep 20.
- 10 Ma, C., Liu, H., Hu, Y., Yu, D., Chen, P., Sun, G. and Zhao, Y., 2015. Experimental study on a variable magnet length cusped field thruster. *Vacuum*, 115, pp.101-107.
- 11 *Chapter 4 SINGLE PARTICLE MOTIONS* [Internet]. 1st ed. Australian National University; 2016 [cited 28 March 2016]. Available from: <http://people.physics.anu.edu.au/~jnh112/AIIM/c17/chap04.pdf>

- 12 Schneider, R., Matyash, K., Kalentev, O., Taccogna, F., Koch, N. and Schirra, M., 2009. Particle-in-Cell Simulations for Ion Thrusters. *Contributions to Plasma Physics*, 49(9), pp.655-661.
- 13 Hui L, Peng-Bo C, Yin-Jian Z, Da-Ren Y. Particle-in-cell simulation for different magnetic mirror effects on the plasma distribution in a cusped field thruster Project. *Chinese Physics B*. 2015 Jun 20;24(8):085202.
- 14 Matyash K, Schneider R, Mutzke A, Kalentev O, Taccogna F, Koch N, Schirra M. Kinetic simulations of SPT and HEMP thrusters including the near-field plume region. *Plasma Science, IEEE Transactions on*. 2010 Sep;38(9):2274-80.
- 15 Keller A, Kohler P, Hey FG, Berger M, Braxmaier C, Feili D, Weise D, Johann U. Parametric Study of HEMP-Thruster Downscaling to N Thrust Levels. *Plasma Science, IEEE Transactions on*. 2015 Jan;43(1):45-53.
- 16 Zhurin VV, Kaufman HR, Robinson RS. Physics of closed drift thrusters. *Plasma Sources Science and Technology*. 1999 Feb;8(1):R1.
- 17 Iceye - Global monitoring, when it matters [Internet]. Iceye.fi. 2016 [cited 4 April 2016]. Available from: <http://iceye.fi/>
- 18 Kornfeld, Günter, Norbert Koch, and Grégory Coustou. "First Test Results of the HEMP thruster concept." *Proceedings of the 28th International Electric Propulsion Conference*. 2003.
- 19 Courtney DG. "Development and characterization of a diverging cusped field thruster and a lanthanum hexaboride hollow cathode" (Masters dissertation, Massachusetts Institute of Technology).
- 20 Goebel DM, Katz I. *Fundamentals of electric propulsion: ion and Hall thrusters*. John Wiley & Sons; 2008 Dec 22.
- 21 Kim V. Main physical features and processes determining the performance of stationary plasma thrusters. *Journal of Propulsion and Power*. 1998 Sep;14(5):736-43.
- 22 "The elements of the periodic table sorted by ionization energy", *Lenntech.com* Available: <http://www.lenntech.com/periodic-chart-elements/ionization-energy.htm>.
- 23 D. C. Meeker, Finite Element Method Magnetics, Version 4.2 (12 Jan 2016 Build), <http://www.femm.info>
- 24 Ray, T., and Smith, W., "A Surrogate Assisted Parallel Multiobjective Evolutionary Algorithm for Robust Engineering Design," *Engineering Optimization*, Vol. 38, No. 8, 2006, pp. 997–1011. doi:10.1080/03052150600882538
- 25 Ray, T., Isaacs, A., and Smith, W., "Multi-Objective Optimization Using Surrogate Assisted Evolutionary Algorithm," *Multi-Objective Optimization: Techniques and Applications in Chemical Engineering*, World Scientific, Singapore, 2008, pp. 131–151.

- 26 Deb, K., Pratap, A., Agarwal, S., and Meyarivan, T., "A Fast and Elitist Multiobjective Genetic Algorithm: NSGA-II," *IEEE Transactions on Evolutionary Computation*, Vol. 6, No. 2, 2002, pp. 182–197. doi:10.1109/4235.996017
- 27 Queipo, N. V., Haftka, R. T., Shyy, W., Goel, T., Vaidyanathan, R., and Tucker, P. K., "Surrogate-Based Analysis and Optimization," *Progress in Aerospace Sciences*, Vol. 41, No. 1, 2005, pp. 1–28. doi:10.1016/j.paerosci.2005.02.001
- 28 Lloyd, S. P., "Least Squares Quantization in PCM," *IEEE Transactions on Information Theory*, Vol. 28, No. 2, 1982, pp. 129–137. doi:10.1109/TIT.1982.1056489
- 29 Box, G. E. P., and Wilson, K. B., "On the Experimental Attainment of Optimum Conditions," *Journal of the Royal Statistical Society*, Vol. 13, No. 1, 1951, pp. 1–45.
- 30 Buhmann, M. D., *Radial Basis Functions: Theory and Implementations, General Methods for Approximation and Interpolation*, Cambridge Univ. Press, Cambridge, England, U.K., 2003, pp. 36–47, Chap. 3.
- 31 Rosenblatt, F., *Principles of Neurodynamics: Perceptrons and the Theory of Brain Mechanisms, The Existence and Attainability of Solutions in Elementary Perceptrons*, Spartan Books, Washington, D.C., 1962, pp. 97–127, Chap. 5.
- 32 Krige, D. G., "A Statistical Approach to Some Mine Valuations and Allied Problems at the Witwatersrand," M.S. Thesis, Univ. of Witwatersrand, Johannesburg, 1951.
- 33 Sobol, I. M., "Uniformly Distributed Sequences with Additional Uniformity Properties," *U.S.S.R. Computational Mathematics and Mathematical Physics*, Vol. 16, No. 5, 1976, pp. 236–242. doi:10.1016/0041-5553(76)90154-3
- 34 Saltelli, A., Ratto, M., Andres, T., Compolongo, F., Cariboni, J., Gatelli, D., Saisana, M., and Tarantola, S., *Global Sensitivity Analysis. The Primer*, Wiley, London, 2008, pp. 164–167.
- 35 Keller, A., "Feasibility of a down-scaled HEMP Thruster", Phd, Justus-Liebig-University Gießen, 2014.
- 36 Ogawa, H., "Physical Insight into Fuel-Air Mixing for Upstream-Fuel-Injected Scramjets via Multi-Objective Design Optimization", *Journal of Propulsion and Power*, Vol. 31, No. 6, 2015, pp. 1505-1523.
- 37 Ogawa, H., Brown, L., Boyce, R. R., and Ray, T., "Multi-Objective Design Optimisation of Axisymmetric Scramjet Nozzle and External Components Considering Static Stability by Using Surrogate-Assisted Evolutionary Algorithms," *Proceedings of the 20th International Symposium on Air-Breathing Engines, International Soc. for Air Breathing Engines Paper 2011-1513*, Göteborg, Sweden, Sept. 2011, <http://www.proceedings.com/12869.html>.
- 38 Ogawa, H., and Boyce, R. R., "Nozzle Design Optimization for Axisymmetric Scramjets by Using Surrogate-Assisted Evolutionary Algorithms," *Journal of Propulsion and Power*, Vol. 28, No. 6, 2012, pp. 1324–1338.

Geometrical assessment of Multi-GNSS prospects for Space Service Volume

Arunkumar Rathinam*, Andrew G. Dempster*

* *Australian Centre for Space Engineering Research (ACSER),
University of New South Wales, Australia, 2052*

Summary: This paper presents a geometrical assessment of multi-GNSS based positioning for the space service volume, especially for altitudes between the MEO GNSS constellations and geostationary altitudes. The navigational systems considered for positioning includes GPS, GLONASS, Galileo, Beidou, QZSS and SBAS. The line-of-sight availability analysis (from a GNSS-satellite to a space user and vice-versa) is performed in MATLAB for two multi-GNSS combinations. This analysis includes a wide array of orbital altitudes and inclination combinations to characterize the signal availability at higher altitudes. Two specific multi-GNSS combinations are simulated and the results shows that both of them offer near 100% performance at higher altitudes/lower inclinations and near 97% at higher altitudes/larger inclination orbits. Future missions should consider exploiting the large potential offered by multi-GNSS systems.

Keywords: Space Service Volume; Multi-GNSS; global navigation satellite systems; GPS; Galileo; GLONASS; BeiDou; Quazi-Zenith Satellite System; QZSS; SBAS

Introduction

Global Navigation Satellite Systems (GNSS) provide users with accurate Position, Navigation, and Timing (PNT) services. GNSS based positioning becomes an integral component in spacecraft navigation in low earth orbits (LEO). A LEO satellite equipped with a GNSS receiver on-board enables precise orbit determination and makes the spacecraft more autonomous. As spacecraft's intended orbit shifted towards medium or high earth orbits, it loses the direct access to GNSS satellites (above) and becomes dependant on the GNSS signals over the limb of the Earth (from the other side). Previous studies [1], [2] on positioning at high earth orbits using the GPS constellation suggests that the users are vulnerable to significant outage over a longer time period, with limited or no satellites available for positioning. In another study [3], a multi-GNSS based positioning for missions targeting highly elliptical orbits (e.g. Proba-3) were analyzed and the result shows less outage time period and also improved number of GNSS satellites available for positioning. In [4], a geometrical assessment of multi-GNSS based positioning for satellites in geostationary orbit were studied and it considered all constellations in a certain frequency band for single analysis. This approach maximises the number of satellites available and the results suggests continuous coverage is possible through a multi-GNSS based positioning at the Geostationary orbit, but didn't highlight the availability at intermediate altitudes.

In this paper, we present a geometrical assessment of multi-GNSS based positioning between medium earth orbit (MEO) (i.e. above MEO GNSS constellations) and geostationary

altitude. The line-of-sight visibility is calculated between each GNSS-satellite in the multi-GNSS combination and a space user and vice-versa, using their propagated orbits in MATLAB. To characterize the signal availability over the interested region, the analysis is extended over an array of orbital altitudes and inclinations combinations. For each combination the percentage of user's orbital time (between MEO and geostationary altitude) where four or more GNSS satellites available for positioning is presented as the percentage of availability. The results also included the percentage of availability at geostationary altitude at 1° spatial resolution of latitudes and longitudes.

GNSS constellations and service regions

The two prominent global navigation systems, namely United States' Global Positioning System (GPS) and Russian Global Navigation Satellite System (GLONASS) are in a fully operational state, while the other systems i.e., Chinese Beidou and European Galileo, are currently under development. Regional support systems, including the Japanese Quasi-Zenith Satellite System (QZSS) and Indian Regional Navigation System (IRNSS/NAVIC) are yet to be fully operational. Also, there are Satellite Based Augmentation Systems (SBAS) operational at GEO. This includes the European EGNOS (European Geostationary Navigation Overlay Service) (3 sat), United States' WAAS (Wide Area Augmentation System) (3 sat), Japanese MSAS (Multi-functional Satellite Augmentation System) (2 sat), Indian GAGAN (GPS and GEO Augmented Navigation) (2 sat) and Russian SDCM (System for Differential Corrections and Monitoring) (3 sat).

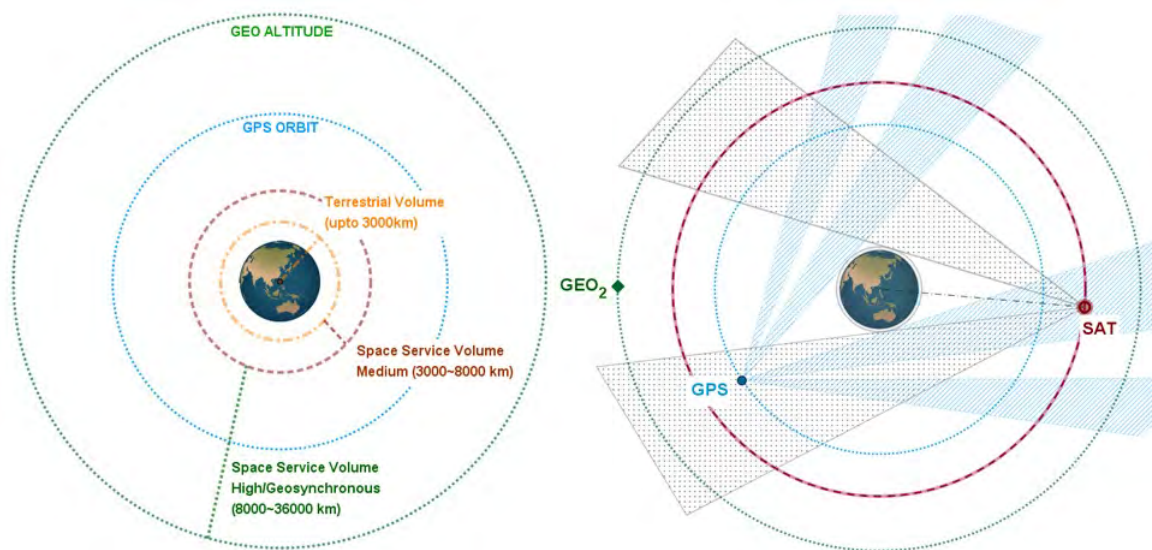


Fig. 1: SSV Visibility - GPS constellation with only main lobe available

GNSS service regions are classified into Terrestrial Service Volume (TSV) and Space Service Volume (SSV), as shown in Figure 1. TSV encloses the Earth's surface and orbital altitudes up to 3000km, whereas the SSV encloses the the region between 3000km and 36000km. In the TSV, users have a relatively uniform distribution of GNSS satellites above with relatively uniform received signal power levels. The SSV can be divided into two, based on GNSS availability; they are MEO SSV and HEO SSV. MEO SSV encloses altitudes from 3000km to 8000km and here the users have continuous access to four GNSS satellites from

any single constellation either from the satellites above or over the limb of the earth. In the HEO SSV, the users depend on the signals available over the edge of the Earth except for signals from SBAS where they have possibility to access from both directions with dual antenna design. This poses a serious challenge, as it results in significant outage when using a single constellation for GNSS positioning.

Analysis Methodology

The performance of GNSS positioning in the SSV can be assessed based on three major parameters: minimum received power level, GNSS availability (antenna beam width) and pseudo range accuracy. However, this study is limited to a geometrical assessment of GNSS availability using the antenna beam width of both transmitting and receiving antennas. To analyze the GNSS availability, we performed a line-of-sight visibility simulation over the range of altitude and inclination angles of a SSV user, where altitude varies from 25,000 km to 36,000 km and the inclination from 0° to 60°. The orbital positions of the GNSS constellation and a receiving satellite are propagated in MATLAB from the Keplerian parameters in the Earth Centered Earth Fixed (ECEF) frame. Then the synodic period is calculated between the SSV user orbital time period and the nearest GNSS constellation's orbit period. The synodic period is then divided into intermediate time steps. Then, for each time step, the elevation angle between the position vectors of each GNSS satellite and a SSV user and vice-versa are calculated. The calculated angles are compared against their corresponding (receiving or transmitting) beam width angle of the antenna pattern. The GNSS satellite is assumed to be available for positioning, when the angle formed by both the GNSS satellite and receiving satellite are within each other's beam width angle. The transmission beam width of L1 frequency band for different constellations and their received signal strength (available over the limb of the earth) at GEO is provided in Table 1. For each combination, the percentage of user's orbital time (between MEO and geostationary altitude) where four or more GNSS satellites available for positioning is calculated. The results are plotted with the percentage of availability, user's altitude and inclination combinations.

Table 1: GNSS Transmitter beamwidth and min. received power

GNSS constellation	Signal	Beam width (°)	Approx. minimum received power at GEO (dBW)
GPS	L1	23.5	-184.0 [1]
GLONASS	L1	20	-185.0 [6]
GALILEO	E1	20.5	-182.5 [7]
BEIDOU - MEO	B1	24	-184.1 [8]
BEIDOU - GEO/IGSO	B1	18	-185.8 [8]
QZSS	L1	22	-185.3 [9]

Results

Single Constellation approach - GPS

The availability of the GPS constellation for positioning in SSV is analyzed through two specific cases: case 1 - using only main lobe signals and case 2 - using both main lobe and first side lobe signals. For the GPS constellation, terrestrial service covers approximately a 13.5° half-beam width in the main lobe. In addition, 50km is added to the Earth radius to avoid the dense atmospheric region. Also, the half-beam width angle equivalent of 0dB directivity is only considered for the main lobe. This allows only $14^\circ - 22^\circ$ of the main lobe signal for positioning in the SSV. The values considered are based on the antenna pattern data presented in [5]. This angle is very limited and it affects the GPS performance at higher altitudes as seen in Figure 2. After considering the first side lobe signal available ($24^\circ - 32^\circ$) for positioning at the L1 frequency in case 2, the GPS availability increases depending up on orbital altitude and varies from 60% to 80% as shown in Figure 3. This shows the importance of the side lobe signal for positioning at higher altitudes.

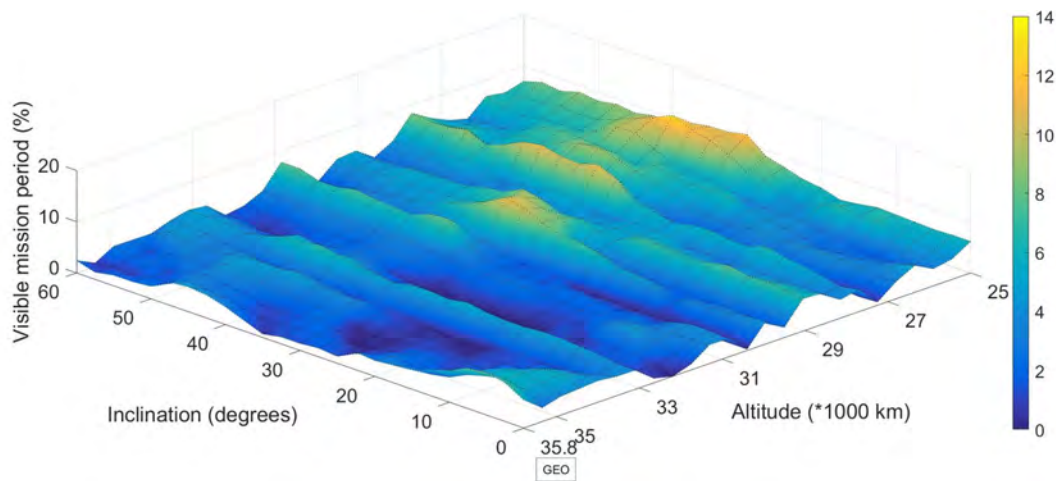


Fig. 2: SSV Visibility - GPS constellation with only main lobe available

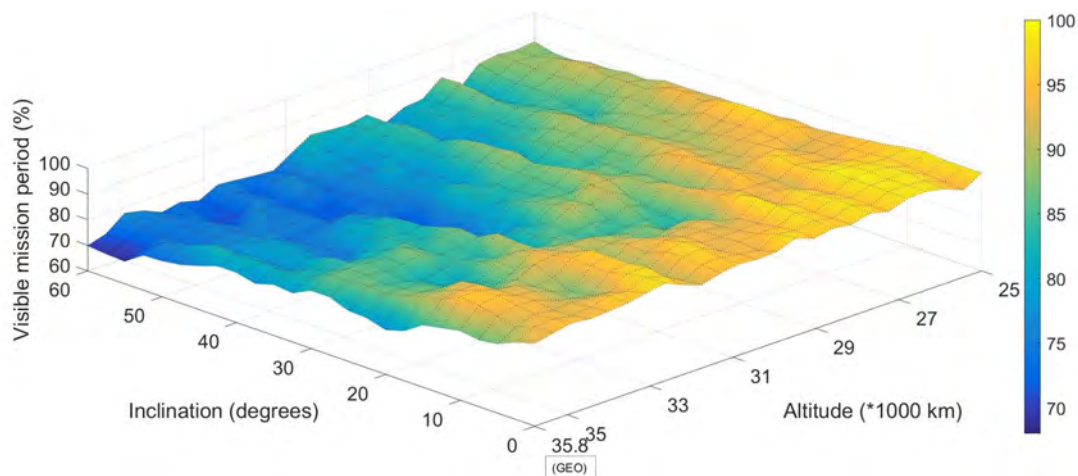


Fig. 3: SSV Visibility - GPS constellation with main and side lobe available

Multi-GNSS approach

In the multi-GNSS approach, two specific configurations are considered to include all the GNSS constellations. They are

- 1) GPS, GLONASS, GALILEO, SBAS and QZSS
- 2) GPS, GLONASS, BEIDOU, SBAS and QZSS

GPS + GLONASS + GALILEO + SBAS + QZSS

The three MEO constellations (GPS, GLONASS and Galileo) along with the SBAS and QZSS satellites is considered for simulation in this case. When compared to a single constellation this combination offers near 100% availability of four GNSS satellites for positioning at lower altitudes as seen in Figure 4.

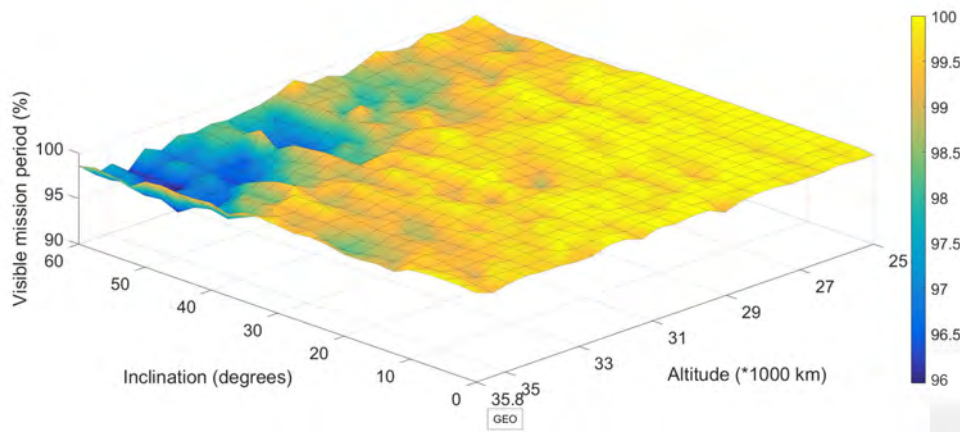


Fig. 4: Multi-GNSS simulation (altitude vs inclination)

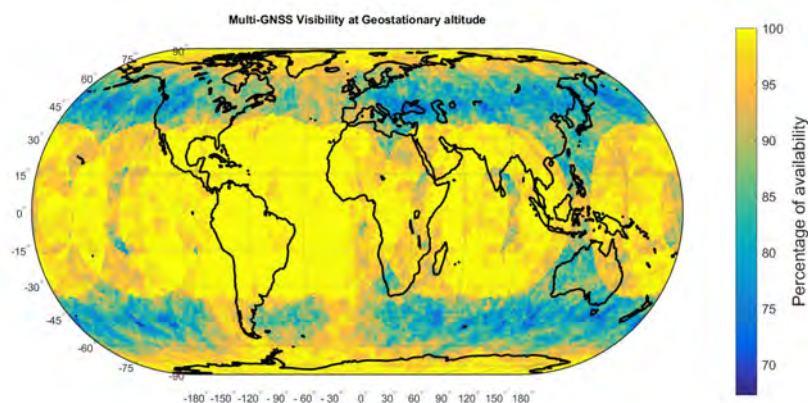


Fig. 5: Multi-GNSS simulation for GEO altitude

But as we move towards higher altitudes (i.e. near GEO) the availability of GNSS satellites drops by approximately 4%, with the lowest percentage at 34000km. The results shown for GEO in Figure 4 correspond to one particular longitude. To analyze the complete visibility, we

performed a second GEO only altitude simulation for every latitude and longitude combination and the result is presented in Figure 5. This shows the near 100% visibility at GEO altitude with few significant low availability locations at higher latitudes.

GPS + GLONASS + BEIDOU (MEO & GEO/IGSO) + SBAS + QZSS

For case 2, MEO constellations along with the Beidou (GEO/IGSO), SBAS and QZSS satellites are simulated. With additional GEO/IGSO satellites, the visibility improved compared to the previous case. At lower altitudes/inclinations, the availability is close to 100%, whereas, at the higher altitudes/inclinations there are some outages of approximately 2~3% as shown in Figure 6. Also, the availability at geostationary altitude varies such that 100% at lower latitudes and drops to 70% lowest at higher latitudes, as shown in Figure 7. The results suggest both configurations offer similar overall performance, with the Beidou combination offering a slender advantage with the availability of additional GEO/IGSO satellites.

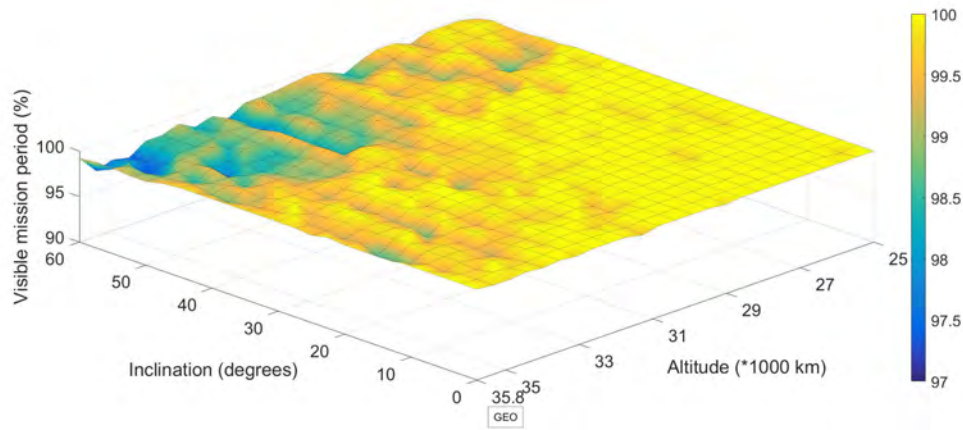


Fig. 6: Multi-GNSS simulation (altitude vs inclination)

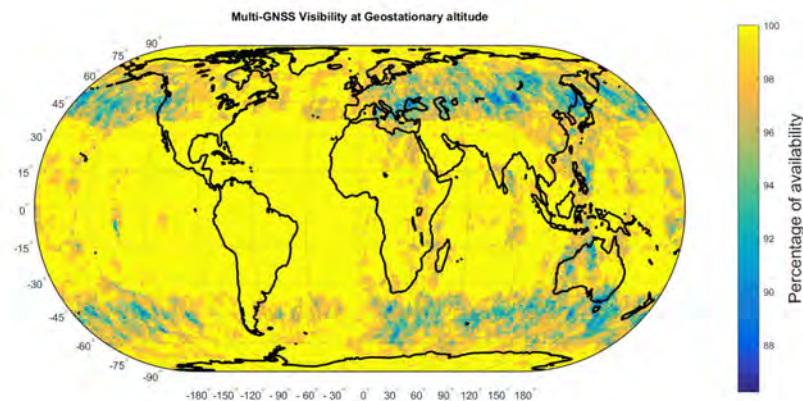


Fig. 7: Multi-GNSS simulation for GEO altitude

Conclusion

This paper presented a geometrical assessment of multi-GNSS based positioning in the SSV. It confirms that the multi-constellation approach offers good GNSS availability at the higher altitudes with nearly 100% at near equatorial latitudes and as the inclination of the orbit increases the percentage drops by nearly ~3%. There are other design parameters (such as weak signal acquisition and tracking, and a better algorithm for satellite selection, etc.) one needs to consider for efficient operation of a multi-GNSS receiver. Also, inclusion of better orbital models and navigational filters will help to position even with fewer than four satellites available. This suggests that multi-GNSS based positioning systems offer huge potential at higher altitudes and future missions should consider taking advantage of this.

References

- [1] Bauer, F.H., Moreau, M.C., Dahle-Melsaether, M.E., Petrofski, W.P., Stanton, B.J., Thomason, S., Harris, G.A, Sena, R.P., Temple, L. Parker, III, The GPS Space Service Volume, *Proceedings of the 19th International Technical Meeting of the Satellite Division of The Institute of Navigation (ION GNSS 2006)*, Fort Worth, TX, September 2006, pp. 2503-2514.
- [2] Ruiz, J.L. and Frey, C.H., Geosynchronous satellite use of GPS. *Proceedings of the 18th International Technical Meeting of the Satellite Division of The Institute of Navigation (ION GNSS 2005)*, Long Beach, CA, September 2005, pp. 1227-1232.
- [3] Kahr, E., Prospects of multiple global navigation satellite system tracking for formation flying in highly elliptical earth orbits, *Int. J. of Space Science and Engineering*, 2013, Vol.1, No.4, pp.432 - 447.
- [4] Welch, Bryan W., Geometrical-Based Navigation System Performance Assessment in the Space Service Volume Using a Multiglobal Navigation Satellite System Methodology, *Technical Report - NASA/TM-2016-219143*, Sep 01, 2016, URL: hdl.handle.net/2060/20160011241
- [5] Marquis, W.A., Reigh, D.L., The GPS block IIR and IIR-M broadcast L-band antenna panel: Its Pattern and Performance, *Journal of the Institute of Navigation*, 2015, 62: 329347, doi:10.1002/navi.123.
- [6] Kosenko, V., Grechkoseev, A., Sanzharov, M., GLONASS Space Service Volume, *9th ICG - UNOOSA*, 2014.
- [7] Wallner, S., Galileos Contribution to Interoperable GNSS SSV, *10th ICG - UNOOSA*, 2015.
- [8] Chang, X. n., Mei, X., Yang, D. H., Space Service Volume Performance of BDS, *10th ICG - UNOOSA*, 2015.
- [9] Kogure, S., Kishimoto, M., MICHIBIKI (QZS-1) and Space Service Volume, *International Committee on GNSS (ICG)*, 2012.

Position and Velocity estimation of Re-entry Vehicles using Fast Unscented Kalman Filters

Sanat Biswas*, Li Qiao†, Andrew Dempster*

* *Australian Centre for Space Engineering Research, UNSW Australia, NSW, Australia, 2052*

† *School of Engineering and Information Technology, UNSW Australia, Canberra, ACT, Australia, 2600*

Summary: The application of two new Unscented Kalman Filter (UKF) based estimation techniques with reduced processing time in a re-entry vehicle position and velocity estimation problem using ground-based range and elevation measurements is presented. The first method is called the Single Propagation Unscented Kalman Filter (SPUKF) where the *a posteriori* state is propagated only once and then the sampled sigma points at the next time state are approximated by the first-order Taylor Series terms. In the second method, called the Extrapolated Single Propagation Unscented Kalman Filter (ESPUKF), the sigma points are approximated to the second-order Taylor Series terms using the Richardson Extrapolation. The Extended Kalman Filter (EKF), SPUKF, ESPUKF and the UKF are utilized in a re-entry vehicle navigation scenario using range and elevation measurements. The estimation accuracies and the processing times for different algorithms are compared for the scenario. The result demonstrates that the UKF provides better accuracy than the EKF but requires more processing time. The SPUKF accuracy is better than the EKF and the processing time is significantly less than the UKF. However, the accuracy of the SPUKF is less than the UKF. The ESPUKF provides estimation accuracy comparable to the UKF and the processing time is also significantly reduced.

Keywords: Re-entry vehicle, Unscented Kalman Filter, Navigation, Estimation

Introduction

Estimation of the position and velocity of a re-entry vehicle is a challenging task due to the highly non-linear nature of the vehicle dynamics. Accurate position and velocity estimation is essential for proper re-entry procedures and vehicle recovery [1, 2]. Generally for a re-entry mission, the position and velocity information of the vehicle is estimated from radar based observations using Kalman Filter.

Out of several types of sequential estimators, the Kalman Filter is designed for the state estimation of stochastic dynamic systems [3]. It is the most popular estimation technique due to the computational efficiency and frequently used in space vehicle navigation and attitude estimation.

The Kalman Filter is a statistical approach to optimal state estimation for linear systems and measurements with random noise [4]. The Extended Kalman Filter (EKF) was developed to apply the Kalman Filter framework in non-linear systems [5, 6]. Application of the EKF spans

almost all the engineering disciplines. However, this algorithm provides sub-optimal estimation for mildly non-linear problems [7, 8] due to the first-order Taylor series approximation of the mean and conditional error covariance [9]. It is long established that the degree of non-linearity of a dynamic system is one of the decisive factors for the accuracy of the EKF. To address the non-linearity, several techniques involving analytical and numerical computation of the Jacobian and Hessian were developed [8, 10]. Julier et al. suggested a deterministic sampling approach to compute the *a priori* mean state vector and the error covariance to capture the non-linearity of the dynamic system [11, 12, 13, 14, 15]. This approach is known as the Unscented Kalman Filter. The estimation accuracy is significantly better than the EKF for systems with Non-linearity Index higher than 0.7 [16].

The UKF relies on propagation of multiple sample state vectors to predict the *a priori* mean state vector and the error covariance at an epoch. For a system with n state variables, $2n + 1$ sigma points must be propagated. This requires a substantial amount of processing time compared to the EKF. Other notable Bayesian non-linear estimation techniques are the Gauss-Hermite Filter (GHF) and Cubature Kalman Filter (CKF). The GHF exploits the Gauss-Hermite Quadrature (GHQ) rule to compute the *a priori* state vector and the error covariance [17]. The UKF can be viewed as a special case of the GHF. For a multi-dimensional estimation problem, the GHQ rule is applied to evaluate the integral over each dimension and then a tensor product is applied successively to obtain the multi-dimensional *a priori* state vector. This implies that, if a m point GHQ rule is applied, then a total of m^n grid points must be constructed for a n -dimensional estimation problem, which is shown to be more computationally expensive than the UT [18, 19]. Jia et al. introduced the Sparse-grid Gauss-Hermite Filter (SGHF), where a sparse-grid technique is used to determine grid points for the GHQ [19]. Arasaratnam et al. proposed a different variant of the GHF called the CKF which uses the spherical-radial cubature rule to evaluate the multi-dimensional integral to get more prediction accuracy [18]. This method requires parameterization of the system function in spherical-radial form. However, all these methods cannot alleviate the curse of dimensionality and cannot be used for high dimensional estimation problems when computation resources are limited.

From this discussion of state of the art non-linear filters, it is discernible that the UKF is the most tractable solution for highly non-linear estimation problems in real-time. Spherically Simplex Unscented Kalman Filter (SSUKF) [14] and Marginal Unscented Transform (MUT) [20] were also proposed to reduce the computation time of the UKF. However, the reduction of computation time by the SSUKF is intuitively less than 50% and the MUT can be applied only to the non-linear systems with linear substructures.

To reduce the computation time of the UKF significantly, two new UKF based estimation techniques called the Single Propagation Unscented Kalman Filter (SPUKF) and the Extrapolated Single Propagation Unscented Kalman Filter (ESPUKF) were proposed in [21]. In these new methods, only one sample state vector is propagated and the other samples are computed using the Taylor Series approximation. These new filters were applied to a vertical re-entry problem and an LEO satellite navigation problem and the performance were compared with the EKF and the UKF. In [22] the EKF, UKF, SPUKF and ESPUKF was applied to a launch vehicle trajectory estimation problem using GNSS observations. The ESPUKF provided the most optimal estimation performance in terms of the processing time and the estimation accuracy.

Estimation performance of the CKF, UKF, GHF and SGHF for a vertical re-entry of a

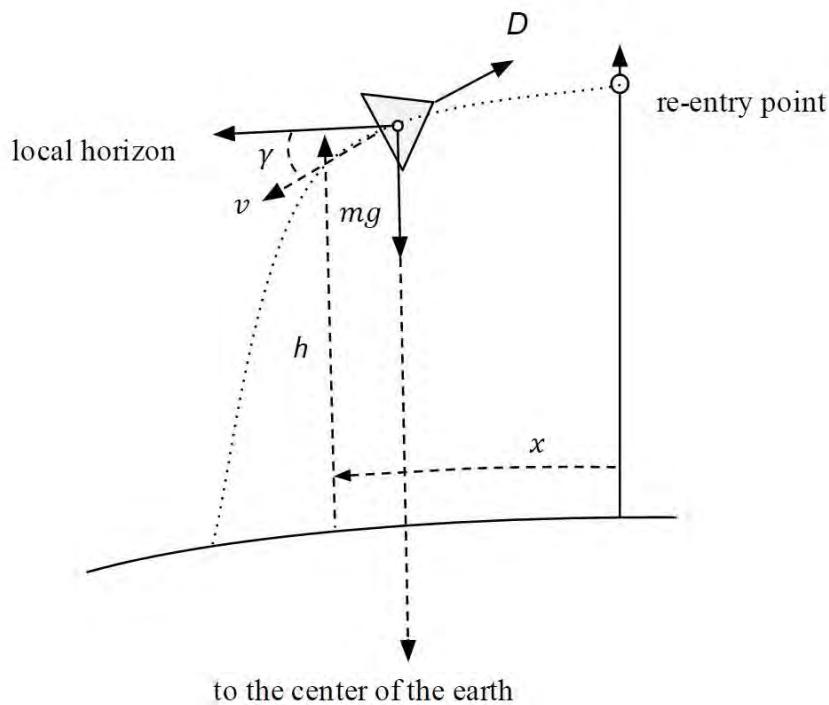


Fig. 1: Re-entry vehicle trajectory

ballistic missile were compared in [23]. Lu et. al. proposed an estimation scheme with local estimators based on Interacting Multiple Model (IMM) Filter and a central Gaussian Mixture Fusion for ballistic target tracking in the re-entry phase [24]. This method is complex from the implementation point of view as it requires local estimators and a fusion center. Also, the performance improvement is not significant compared with the conventional estimation methods. A minor modification of the IMM Filter was proposed in [25] to improve the IMM filter performance in the re-entry vehicle tracking problem.

In this paper, the estimation performance of the SPUKF and the ESPUKF in a ballistic realistic re-entry mission is compared with the performance of the UKF and the EKF. The performance of the CKF, GHF, SGHF and IMM based algorithms are not compared because the estimation accuracy of all these filters was the same order of the UKF and the processing times of the Gauss-Hermite type filters were higher than the UKF [23]. A detailed re-entry vehicle motion considering both the horizontal and vertical motion is simulated. The radar range and elevation observations corresponding to the trajectory is generated. These observations are used in the EKF, UKF, SPUKF and the ESPUKF for the position and the velocity estimation. The performance of the SPUKF and the ESPUKF are compared with the EKF and the UKF.

Re-entry Vehicle Dynamics

The re-entry vehicle follows a curved path during atmospheric re-entry. In a detailed re-entry dynamics the downrange x , altitude h , velocity v , flightpath angle γ and the aerodynamic co-efficient C are considered as state variables. A planar re-entry vehicle trajectory is provided in Fig. 1.

The re-entry dynamics can be expressed as [26]:

$$\begin{bmatrix} \dot{x} \\ \dot{h} \\ \dot{v} \\ \dot{\gamma} \\ \dot{C} \end{bmatrix} = \begin{bmatrix} \frac{R_E}{R_E+h} v \cos \gamma \\ v \sin \gamma \\ -\frac{D}{m} - g \sin \gamma \\ -\frac{1}{v} \left(g - \frac{v^2}{R_E+h} \right) \cos \gamma \\ 0 \end{bmatrix} + \boldsymbol{\nu}(t) \quad (1)$$

where m is the mass of the re-entry vehicle, R_E is the mean radius of the Earth, g is the gravitational acceleration, D is the aerodynamic drag and $\boldsymbol{\nu}(t)$ is the process noise vector. Similar to the launch vehicle model, D is modelled using the following equation [27]:

$$D = \frac{1}{2} AC \rho_0 e^{-\frac{h}{H}} v^2 \quad (2)$$

where A is the effective area of the re-entry vehicle, ρ_0 is the density of the atmosphere at sea level and H is the scale height.

Reference Trajectory Generation

The reference re-entry trajectory is generated by numerically integrating equation (1). The initial true state vector is

$$\begin{bmatrix} h \\ d \\ v \\ \gamma \\ C \end{bmatrix} = \begin{bmatrix} 100 \text{ km} \\ 0 \text{ km} \\ 6 \text{ km/s} \\ -10^\circ \\ 0.7 \end{bmatrix} \quad (3)$$

The reference trajectory, velocity, flightpath angle and aerodynamic co-efficient profile are shown in figures 2a, 2b, 3a and 3b.

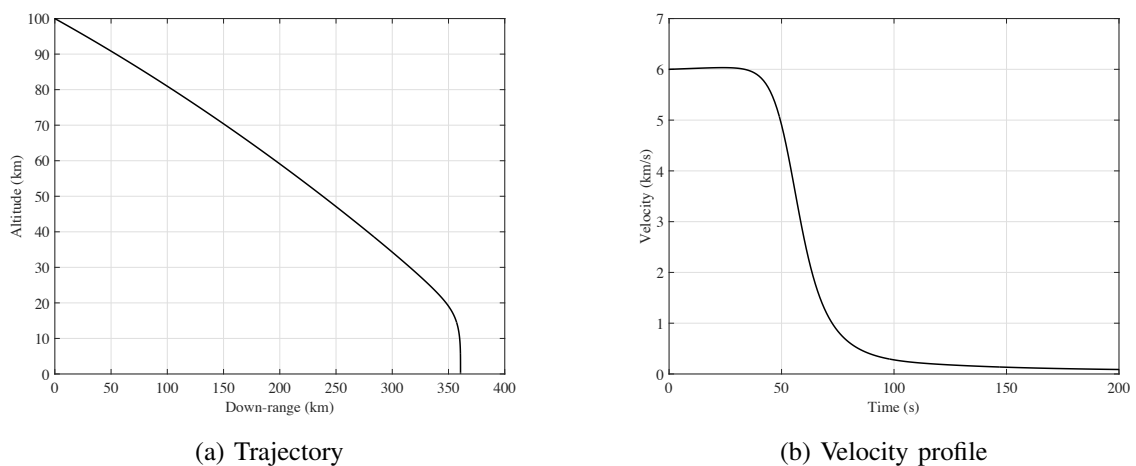
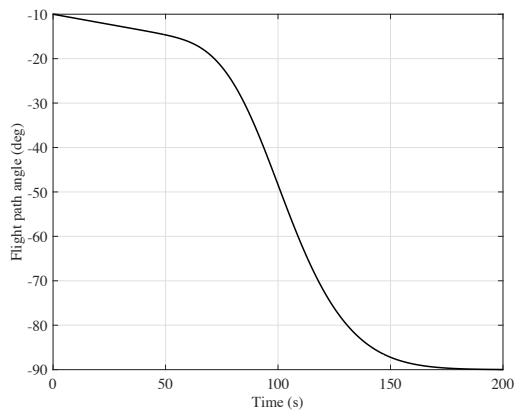
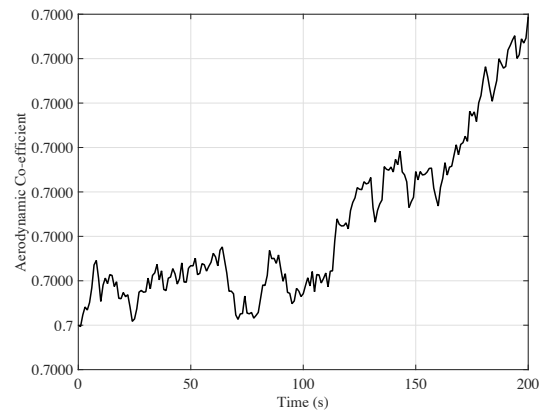


Fig. 2: Re-entry vehicle trajectory and velocity profile



(a) Flightpath angle



(b) Aerodynamic co-efficient

Fig. 3: Flightpath angle and aerodynamic co-efficient profile

Simulation of Radar Observations

Radar observations are used in the launch vehicle and re-entry vehicle state estimation scenarios. It is assumed that the radar is situated in the trajectory plane of the vehicle and hence the azimuth angle is fixed.

For the curved re-entry trajectory the range and elevation are considered as the observations. The effect of the Earth's curvature is considered in the measurement simulation. The geometry of radar tracking for a re-entry vehicle in a curved path is shown in Fig. 4.

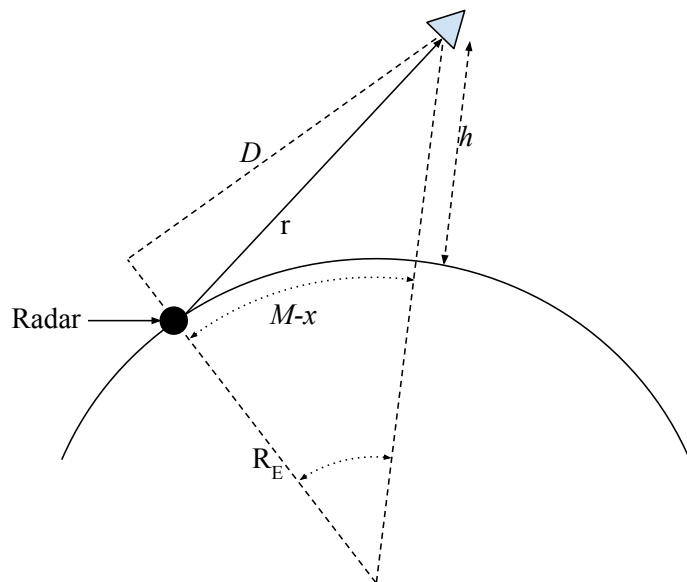


Fig. 4: Radar tracking geometry for a re-entry vehicle in a curved trajectory

In the figure, r is the geometric distance of the re-entry vehicle, M is the initial down-range distance of the radar from the re-entry point, h is the altitude and x is the downrange distance of the re-entry vehicle from the re-entry point. ϕ is the angular distance between the radar

and the re-entry vehicle and can be written as

$$\phi = \frac{M - x}{R_E} \quad (4)$$

δH and δD can be expressed as

$$\delta H(t) = (R_E + h(t)) \sin \phi - R_E \quad (5)$$

$$\delta D(t) = (R_E + h(t)) \sin \phi \quad (6)$$

The range r and elevation E is modeled as

$$r(t) = \sqrt{\delta H(t)^2 + \delta D(t)^2} + \omega_r(t) \quad (7)$$

$$E(t) = \tan^{-1} \frac{\delta D(t)}{\delta H(t)} + \omega_E(t) \quad (8)$$

here, $\omega_r(t)$ and $\omega_E(t)$ are zero mean white noise with standard deviation of 20m and 17.5 milirad respectively. The range and elevation measurements are generated using equations (7) and (8).

Implementation of Unscented Filters

In unscented filtering, the evolution of the process noise statistics over time is addressed by augmenting the state vector with the process noise terms [12]. The augmented state vector is

$$\mathbf{X}_a(t) = \begin{bmatrix} \mathbf{X}(t) \\ \boldsymbol{\nu}(t) \end{bmatrix} \quad (9)$$

In the UKF, the sigma points are calculated from [11]

$$\mathbf{X}_a^+(t) = \begin{bmatrix} \mathbf{X}^+(t) \\ \mathbf{0}_{5 \times 1} \end{bmatrix} \quad (10)$$

$$\mathbf{P}_a(t) = \begin{bmatrix} \mathbf{P}(t) & \mathbf{P}_{X\nu}(t) \\ \mathbf{P}_{X\nu}(t) & \mathbf{Q}(t) \end{bmatrix} \quad (11)$$

Here, $\mathbf{X}^+(t)$ and $\mathbf{X}_a^+(t)$ are the *a posteriori* state vector and the augmented state vector respectively at epoch t . The augmentation terms are zero because the process noise distribution is considered as zero mean Gaussian. $\mathbf{P}(t)$ and $\mathbf{P}_a(t)$ are the error covariance and the augmented error covariance matrices respectively. $\mathbf{P}_{X\nu}(t)$ is the cross covariance of \mathbf{X} and $\boldsymbol{\nu}$. $\mathbf{Q}(t) = \mathbf{E}[\boldsymbol{\nu}\boldsymbol{\nu}^T]$ is the process noise covariance matrix. The dimension of the augmented state vector is 10. Therefore, a total of 21 sigma points must be propagated to the next epoch to predict the weighted *a priori* mean state vector and the error covariance. The sigma points and the corresponding weights are

$$\mathbf{X}_0(t) = \mathbf{X}_a^+(t) \quad (12)$$

$$\mathbf{X}_i(t) = \mathbf{X}_a^+(t) + \Delta \mathbf{X}_i, (i = 1, 2, 3...32) \quad (13)$$

$$W_0 = \frac{\kappa}{n + \kappa} \quad (14)$$

$$W_i = \frac{1}{2(n + \kappa)}, (i = 1, 2, 3...32) \quad (15)$$

and

$$\begin{aligned}\Delta \mathbf{X}_i &= (\sqrt{(n+\kappa)\mathbf{P}_a})_i \quad \text{for } i = 1, 2, 3, \dots, 16 \\ \Delta \mathbf{X}_i &= -(\sqrt{(n+\kappa)\mathbf{P}_a})_i \quad \text{for } i = 17, 18, 19, \dots, 32\end{aligned}$$

where $(\sqrt{(n+\kappa)\mathbf{P}_a})_i$ is the i th column of the matrix $\sqrt{(n+\kappa)\mathbf{P}_a}$. κ is a parameter and generally it is selected in such a way that $(n+\kappa) = 3$ [11]. Corresponding to all the 21 propagated sigma points the measurement vectors are computed using the measurement equations (7) and (8). The weighted mean of these is considered to be the predicted measurement vector. The measurement error covariance and the cross covariance between the measurement vector and the state vector is computed using the predicted mean state and measurement vector, the predicted sigma points and the corresponding measurement vectors [11]. Then the conditional mean state vector and the error covariance is computed using the Kalman Filter equations [11].

Single propagation Unscented Kalman Filter

In the SPUKF, only $\mathbf{X}_0(t)$ is propagated to the next epoch. The other sigma points are not propagated. To calculate the sigma points at the next epoch $t + \delta t$, the following equation is utilized [21]

$$\mathbf{X}_i^-(t + \delta t) = \mathbf{X}_0^-(t + \delta t) + e^{\mathcal{J}\delta t} \Delta \mathbf{X}_i \quad (16)$$

Here $\mathbf{X}_0^-(t + \delta t)$ propagated augmented state vector at $t + \delta t$ and

$$\begin{aligned}\mathcal{J} &= \left. \frac{\partial \dot{\mathbf{X}}_a}{\partial \mathbf{X}_a} \right|_{\mathbf{X}_a^+(t)} \\ &= \begin{bmatrix} \left. \frac{\partial \dot{\mathbf{X}}}{\partial \mathbf{X}} \right|_{\mathbf{X}^+(t)} & \mathbf{0}_{5 \times 5} \\ \mathbf{0}_{5 \times 5} & \mathbf{0}_{5 \times 5} \end{bmatrix} \quad (17)\end{aligned}$$

After calculation of all the sigma points the standard weighted mean and covariance calculation method of the UT [11] is used to compute the *a priori* mean state vector and the error covariance matrix. The correction stage of the SPUKF is the same as the UKF.

Extrapolated Single propagation Unscented Kalman Filter

In the ESPUKF, the sigma points are computed using the following equations [21]:

$$N_1(\Delta \mathbf{X}_i) = \mathbf{X}_0^-(t + \delta t) + e^{\mathcal{J}\delta t} \Delta \mathbf{X}_i \quad (18)$$

$$N_2(\Delta \mathbf{X}_i) = \mathbf{X}_0^-(t + \delta t) + e^{\mathcal{J}\delta t} \frac{\Delta \mathbf{X}_i}{2} + e^{\mathcal{J}'\delta t} \frac{\Delta \mathbf{X}_i}{2} \quad (19)$$

$$\mathbf{X}_i^-(t + \delta t) = 2N_2(\Delta \mathbf{X}_i) - N_1(\Delta \mathbf{X}_i) \quad (20)$$

Here,

$$\mathcal{J}' = \left. \frac{\partial \dot{\mathbf{X}}_a}{\partial \mathbf{X}_a} \right|_{\mathbf{X}_a^+(t) + \frac{\Delta \mathbf{X}_i}{2}}$$

Computation of sigma points using equation 20 results in inclusion of the second-order Taylor series terms in the approximation [21]. The rest of the calculation procedure in the ESPUKF is the same as for the SPUKF.

Simulation

The block diagram for the launch vehicle and re-entry vehicle trajectory estimation experiments using radar observations is shown in Fig. 5.

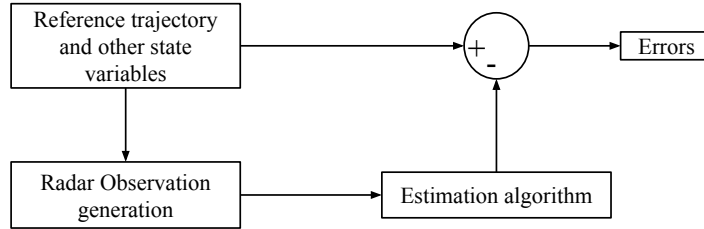


Fig. 5: Estimation using radar observations

The radar observations corresponding to the reference trajectory are generated using the measurement equations (7) and (8). Measurement noise is also included in the observation simulation. True range and angle measurement noise standard deviation are selected as 50 m and 0.1° . These observations are used in various estimation algorithms to estimate the trajectory of the re-entry vehicle and compared with the reference trajectory for performance analysis. For all the estimation algorithms, the initial state vector and error covariance are:

$$\widehat{\mathbf{X}}(0) = \begin{bmatrix} 101 \text{ km} \\ 5 \text{ km} \\ 6.050 \text{ km/s} \\ -10^\circ \\ 0.7 \end{bmatrix} \quad (21)$$

$$\mathbf{P}(0) = \text{diag} \begin{bmatrix} 6 \\ 6 \\ .1 \\ .1 \\ .1 \end{bmatrix} \quad (22)$$

The process noise covariance matrix is selected as

$$\mathbf{Q} = 10^{-15} \mathbf{I}_{5 \times 5} \quad (23)$$

Simulation Results

The estimation performance of the EKF, UKF, SPUKF and ESPUKF are examined in the re-entry vehicle trajectory estimation scenario. Using the simulation process described in the previous section, the re-entry trajectory is estimated using all the four Kalman Filters separately. The altitude, down-range and velocity errors are shown in Fig. 6a. It can be observed that the estimation error of the EKF is much higher than the UKF and the new variants of the UKF. Estimation errors for the UKF, SPUKF and ESPUKF are shown separately in figure 6b. The UKF provides the most accurate state estimate of all the Kalman Filters under consideration. The performance of the SPUKF is significantly better than the EKF.

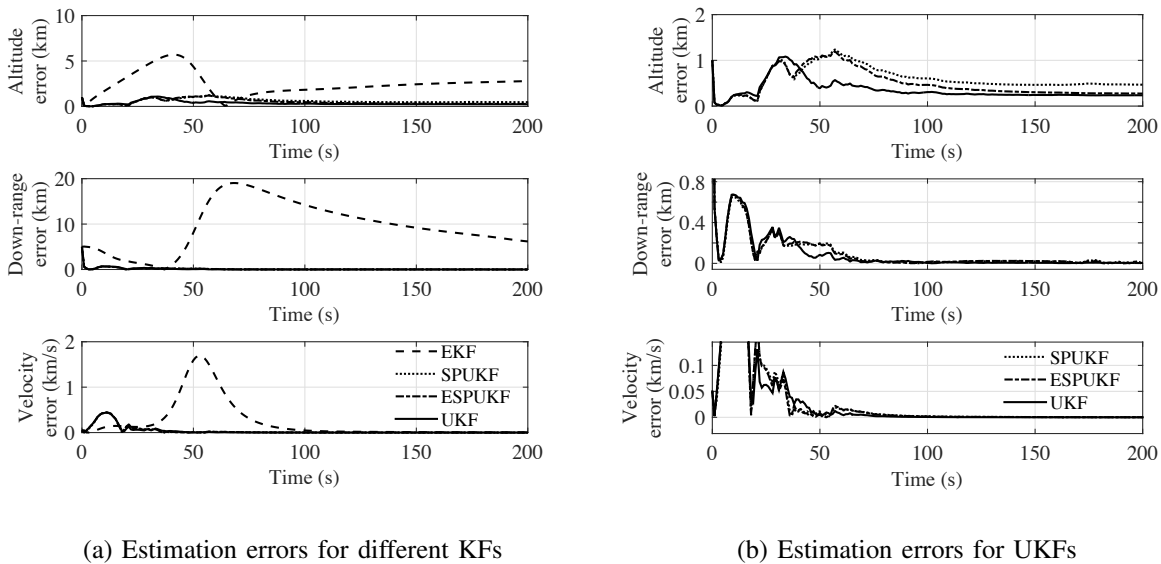


Fig. 6: Estimation errors for different algorithms

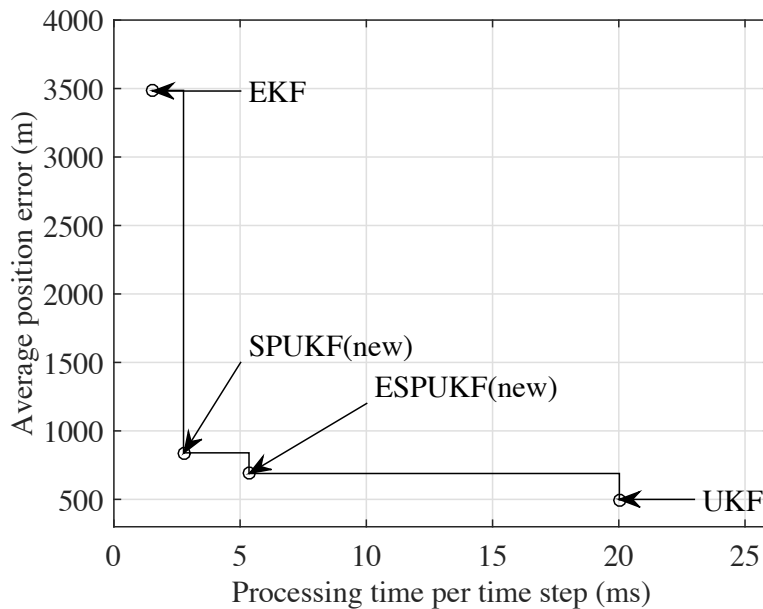


Fig. 7: Processing time vs. estimation error

The performance of the ESPUKF almost matches the UKF. The processing time required in every time step is also recorded for all the estimation algorithms. The time average absolute position estimation error vs. the processing time is shown in Fig. 7. The processing time of the EKF is the lowest. However the average estimation error of the EKF is significantly more than the SPUKF, ESPUKF and the UKF. The UKF provides the lowest average estimation error and the processing time is significantly higher than the other Kalman Filters.

Conclusion

In this paper the application of two new variants of Unscented Filters is proposed for the re-entry vehicle trajectory estimation. The results demonstrate that the UKF provides better accuracy than the EKF but requires more processing time. The SPUKF accuracy is better than the EKF and the processing time is significantly less than for the UKF. The processing time reduces by 86.2% for the SPUKF compared to the UKF. However, the accuracy of the SPUKF is less than the UKF. The ESPUKF provides estimation accuracy comparable to the UKF and the processing time reduces by 73.3% compared to the UKF.

References

- [1] Lu, P., "Entry guidance and trajectory control for reusable launch vehicle," *Journal of Guidance, Control, and Dynamics*, vol. 20, no. 1, pp. 143–149, 1997.
- [2] Johnson, E. N., Calise, A. J., and Corban, J. E., "Reusable launch vehicle adaptive guidance and control using neural networks," in *AIAA Guidance, Navigation and Control Conference*, vol. 4381, Montreal, Canada: AIAA, 2001.
- [3] Bar-shalom, Y., Li, X.-r., and Kirubarajan, T., *Estimation with applications to tracking and navigation: theory algorithms and software*. John Wiley & Sons, 2004.
- [4] Kalman, R. E., "A New Approach to Linear Filtering and Prediction Problems," *Transactions of the ASME-Journal of Basic Engineering*, vol. 82, no. Series D, pp. 35–45, 1960.
- [5] Smith, G. L., McGee, L. A., and Schmidt, S. F., "Application of Statistical Filter Theory to the Optimal Estimation of Position and Velocity on Board a Circumlunar Vehicle," tech. rep., 1962.
- [6] Smith, G. L., "Multivariable Linear Filter Theory Applied to Space Vehicle Guidance.," *Journal of the Society for Industrial & Applied Mathematics, Series A: Control*, vol. 2, no. 1, pp. 19–32, 1964.
- [7] Cox, H., "On the estimation of state variables and parameters for noisy dynamic systems," *IEEE Transactions on Automatic Control*, vol. 9, no. 1, pp. 5–12, 1964.
- [8] Athans, M., Wishner, R., and Bertolini, a., "Suboptimal state estimation for continuous-time nonlinear systems from discrete noisy measurements," *IEEE Transactions on Automatic Control*, vol. 13, pp. 504–514, oct 1968.
- [9] Bernstein, I. and Friedland, B., "Estimation of the state of a nonlinear process in the presence of nongaussian noise and disturbances," *Journal of the Franklin Institute*, vol. 281, no. 6, pp. 455–480, 1966.
- [10] Nørsgaard, M., Poulsen, N., and Ravn, O., "New developments in state estimation for nonlinear systems," *Automatica*, vol. 36, no. 11, pp. 1627–1638, 2000.
- [11] Julier, S., Uhlmann, J., and Durrant-Whyte, H., "A new method for the nonlinear transformation of means and covariances in filters and estimators," *IEEE Transactions on Automatic Control*, vol. 45, pp. 477–482, mar 2000.
- [12] Julier, S. and Uhlmann, J., "A New Extension of the Kalman Filter to Nonlinear Systems," in *SPIE*, vol. 3068, pp. 182–193, Orlando, FL, 1997.
- [13] Julier, S. J., "A Skewed Approach to Filtering," in *Proceedings of SPIE—the international society for optical engineering*, vol. 3373, pp. 271–282, 1998.
- [14] Julier, S., "The spherical simplex unscented transformation," *Proceedings of the 2003 American Control Conference, 2003.*, vol. 3, pp. 2430–2434, 2003.
- [15] Julier, S. and Uhlmann, J., "Unscented Filtering and Nonlinear Estimation," *Proceedings of the IEEE*, vol. 92, pp. 401–422, mar 2004.
- [16] Biswas, S. K., Qiao, L., and Dempster, A. G., "A quantitative Relationship between Non-linearity and Unscented Kalman Filter Accuracy," *submitted at IEEE Transactions on Aerospace and Electronic Systems*, 2016.
- [17] Ito, K. and Xiong, K., "Gaussian filters for nonlinear filtering problems," *IEEE Transactions on Automatic Control*, vol. 45, no. 5, pp. 910–927, 2000.
- [18] Arasaratnam, I. and Haykin, S., "Cubature Kalman Filters," *IEEE Transactions on Automatic Control*, vol. 54, pp. 1254–1269, jun 2009.
- [19] Jia, B. J. B., Xin, M. X. M., and Cheng, Y. C. Y., "Sparse Gauss-Hermite Quadrature filter for spacecraft attitude estimation," *American Control Conference (ACC), 2010*, vol. 34, no. 2, pp. 2873–2878, 2010.
- [20] Chang, G., "Loosely Coupled INS/GPS Integration with Constant Lever Arm using Marginal Unscented Kalman Filter," *Journal of Navigation*, vol. 67, pp. 419–436, 2013.
- [21] Biswas, S. K., Qiao, L., and Dempster, A. G., "A Novel a priori State Computation Strategy for the Unscented Kalman Filter to Improve Computational Efficiency," (*in early access*) *IEEE Transactions on Automatic Control*, 2016.
- [22] Biswas, S. K., Qiao, L., and Dempster, A. G., "Computationally Efficient Unscented Kalman Filtering Techniques for Launch Vehicle Navigation using a Space-borne GPS Receiver," in *ION GNSS+*, 2016.
- [23] Nikhil Kumar Singh., Bhaumik, S., and Bhattacharya, S., "A comparison of several nonlinear filters for ballistic missile tracking on re-entry," in *IEEE First International Conference on Control, Measurement and Instrumentation (CMI)*, 2016.

- [24] Lu, K. and Zhou, R., "Sensor fusion of Gaussian mixtures for ballistic target tracking in the re-entry phase," *Sensors (Switzerland)*, vol. 16, no. 8, 2016.
- [25] Shin, S.-J., "Re-entry vehicle tracking with a new multiple model estimation applicable to highly non-linear dynamics," *IET Radar, Sonar & Navigation*, vol. 9, no. August 2014, pp. 581–588, 2015.
- [26] Regan, F. J., *Dynamics of atmospheric re-entry*. AIAA, 1993.
- [27] Curtis, H. D., *Orbital Mechanics for Engineering Students*. Butterworth-Heinemann, 2010.

Contemporary Space-based GNSS Remote Sensing

Changjiang Hu¹, Craig Benson¹, Li Qiao¹

¹ *School of Engineering and Information Technology
University of New South Wales, Canberra, 2612, Australia*

Summary: This paper focuses on near-term space-based GNSS remote sensing, including imminent space missions and applications. Firstly addressing GNSS-R, this paper compares ground-based, airborne and space-borne scenarios in the respects of data collection, measuring scale, and the quality of results, reaching the conclusion that the greatest potential of GNSS-R is to use space-based receivers. Secondly, after reviewing the evolution of GNSS remote sensing space missions, from CHAMP and UK-DMC-1 to COSMIC and TechDemonSat-1, we describe six forthcoming missions, such as COSMIC-2, CICERO, GRACE-FO and CYGNSS. These missions have different tasks, data collecting capabilities, data processing strategies and parameters of the antennas, which are the aspects to be analysed in this paper. Finally, some future applications are discussed including mesoscale ocean altimetry, catastrophe weather alarming, and the detection of ocean surface targets.

Keywords: GNSS remote sensing, GNSS Reflectometry, GNSS Radio Occultation.

Introduction

Remote sensing is a powerful technology to understand the environments of the Earth, including weather, climate and energy circulation. In order to know the Earth from different respects, scientists try to explore as many as possible ways to remotely sense the Earth. Two decades ago when the concepts of GNSS Radio Occultation (GNSS-RO) and GNSS Reflectometry (GNSS-R) were proposed [1, 2], the utilisations of GNSS signals have extended from traditional navigation and positioning to sounding the Earth's surface and the atmosphere around it, providing a new optional remote sensing manner. Fig. 1 is an illustration of GNSS-RO and GNSS-R. The GNSS signals carry the information about the properties of the media they pass through, it is thus possible for GNSS-RO and GNSS-R to retrieve the parameters of the atmosphere and the Earth's surface.

GNSS-RO uses the bending angle measurement, which indicates the refractive index of the atmosphere that the signals travel through to infer the atmospheric properties, such as temperature, pressure, and humidity [3]. The first dedicated mission was GPS Meteorological experiment (GPS/MET) carried out by NSF, FAA, NOAA and NASA in 1995. The success of the pioneering mission attracts considerable attention from many other countries and regions, which leads to around 20 missions in the following two decades. Table 1 lists them by launch time. Among these missions, the COSMIC constellation which consists of 6 satellites is the most productive one, providing 1500 to 2000 soundings per day.

With the support of the large amount of data from a wide range of missions, GNSS-RO has rapidly become a valuable technique, providing unprecedented high accuracy, time-space resolution, and worldwide coverage for atmospheric and ionospheric products. The chief application of the products is in Numerical Weather Prediction (NWP) models to improve the performance of weather forecasting. After the launch of the COSMIC constellation, weather forecasting centres, including the European Centre for Medium-Range Weather Forecasts (ECMWF) and the US National Centre for Environmental Prediction (NCEP),

assimilated the real-time soundings into their NWP models and showed positive impact of the GNSS-RO data on weather forecasting [4, 5]. GNSS-RO measurements can be also applied into climate studies, thanks to its global coverage, high accuracy, vertical resolution and long-term stability [6]. In addition, GNSS-RO observations are also useful for calibrating radiance measurements of microwave sensors [7], and assessing the quality of radiosonde data [8].

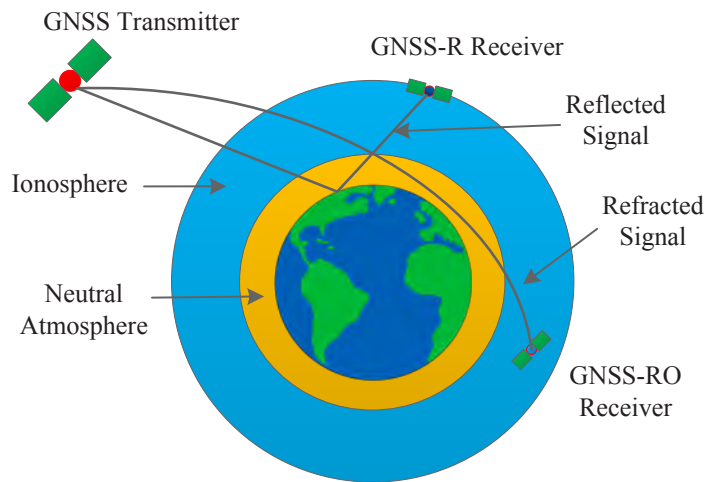


Fig. 1: Illustration of GNSS-RO and GNSS-R

Table 1: GNSS Radio Occultation Missions

Launch Time	Mission	Sponsors	Launch Time	Mission	Sponsors
1995	GPS/MET	America	2006	MetOp-A	ESA
1999	Ørsted	Denmark	2007	TerraSAR-X	German
1999	Sunsat	South Africa	2008	CNOFS	America
2000	CHAMP	German	2009	Oceansat-2	India
2000	SAC-C	Argentina	2010	TanDEM-X	German
2001	PicoSAT	America	2011	SAC-D/Aquarius	America
2002	GRACE	German and US	2012	MetOp-B	ESA
2002	Fdesat	Australia	2013	KOMPSAT5	South Korea
2006	COSMIC	US and Taiwan	2013	FY-3C	China

GNSS-R is another important branch of GNSS remote sensing, using the GNSS signals reflected from ocean, land, and ice. However, unlike GNSS-RO, which has been facilitated by approximately 20 missions, there are only four missions exploring the feasibility of GNSS-R. The pioneer was the UK-Disaster Monitoring Constellation-1 (UK-DMC-1) that ceased in 2011. The reflected signals collected by this mission demonstrate the feasibility of GNSS-R [9]. Another mission is Technology Demonstration Satellite-1 (TDS-1), which was launched by UK in 2014. The data from TDS-1 has been used to study ocean wind [10], sea surface height [11] and Delay-Doppler Maps (DDMs) [12]. In 2016, ³Cat-2 developed by UPC and CYGNSS supported by NASA were launched, but there are no publications using the data from the two missions yet. Contrary to space missions, many ground and air-based campaigns have been conducted, from aircraft experiments over the Chesapeake Bay and the Eastern Shore of Virginia [13] to most recent ground-based campaigns [14].

Depending on the reflecting surfaces, GNSS-R can be applied to different purposes, such as soil moisture, snow depth, wind speed, and ocean altimetry. GNSS-R altimetry basically uses

the path delay between the reflected and direct signals to estimate the height of receiver over the reflecting surface or the height of reflecting surface with respect to a given reference surface, like WGS-84 ellipsoid surface. GNSS-R altimetry has achieved cm-level results in precision and accuracy in low-platform scenarios [14-16]. However, most research relating to space-borne altimetry is theoretical [17, 18]. The first space-based altimetry using real data was reported recently, with a general conclusion that the altimetric result is in agreement with the global DTU10 mean sea surface height [11]. Wind speed is another application of GNSS-R. In 2000, Zavorotny and Voronovich theoretically studied the relationship between wind speed and the power of the reflected signals [19]. In 2015, results with a precision of about 2.2 m/s were obtained using the TDS-1 data [10]. Other applications, such as soil moisture and snow depth, were also pursued by researchers [20-22].

Since GNSS-R is much less developed than GNSS-RO, especially in space missions, more attention is paid to GNSS-R in this paper. The remainder of this paper is organised as follows. Following the introduction is the comparison between different platforms of the GNSS-R. Then, six forthcoming space missions relating to the GNSS remote sensing will be introduced. Afterwards, several future applications are discussed. The final section is a conclusion.

Comparisons between Three Scenarios of GNSS-R

In GNSS-R, there are three scenarios (ground-based, airborne and space-borne) according to the height of receivers' platform, as shown in Fig. 2. In the ground-based situation, the receivers are usually fixed on a cliff, bridge or tower, and the heights of the receivers are low. When the receivers are mounted on an aircraft, the height can be several thousand meters. In the space-based scenario, the altitude of the receivers ranges from 200 km to over 1000 km.

In Fig. 2, the specular reflection point is the point through which the reflected path has the shortest length. If there is no special comment, the elevation angle in this paper means the angle between the tangent plane of the reflecting surface at the specular reflection point and the vector from the specular reflection point to the transmitter or receiver. This section compares the three scenarios regarding the ability of data collection, measuring scale, and quality of results.

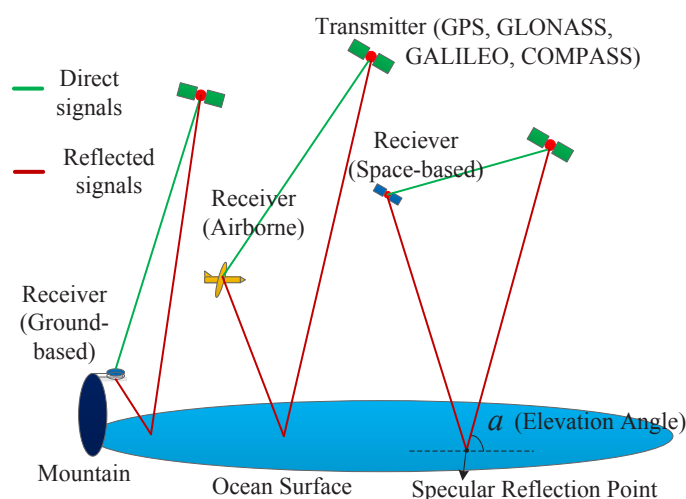


Fig. 2: Illustration of Ground, Air and Space-based GNSS-R.

Utility

The utility of GNSS-R is driven by many factors, such as data sampling rate, the maximum data rate of downlink, the number of available receivers, the number of visible transmitters, and observation period. Here, we focus on the number of visible transmitters.

GNSS-R receivers contain two antennas, one up-looking right-handed circularly polarized (RHCP) antenna to receive direct signals and one down-looking left-handed circularly polarized (LHCP) antenna to receive reflected signals. We first study the number of visible transmitters for the up-looking antenna. Fig. 3 shows the view of the up-looking antenna when it is placed on a platform h metres above the Earth surface. In Fig. 3, B represents the receiver's position. O is the Earth's centre. A is the intersection point of OB and the Earth's surface. θ is the viewing angle of the receiver. T_1 and T_2 are the edging points within the antenna's view, which are symmetrical with respect to OB . Θ is the angle between B and T_2 as seen from the Earth's centre. p is the radius of the transmitter, and d is the distance between T_2 and B . Θ can be deduced by the following equations.

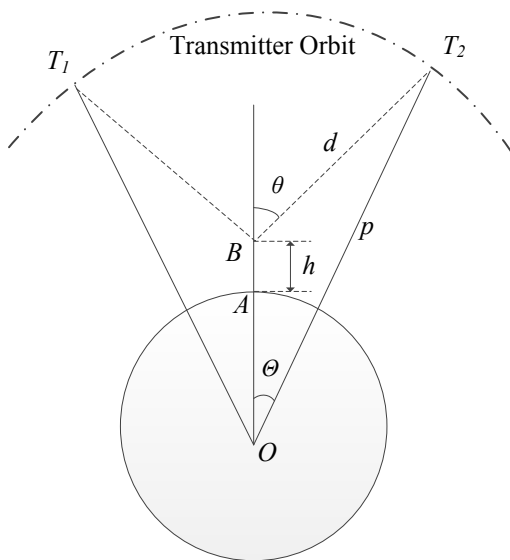


Fig. 3: The view of up-looking antenna.

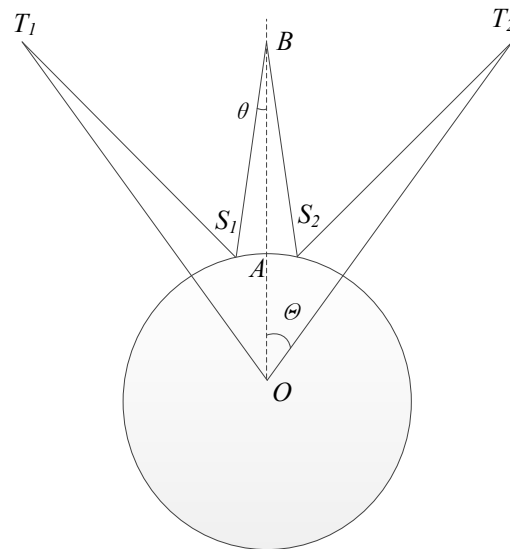


Fig. 4: The view of down-looking antenna.

$$(R+h)^2 + d^2 - 2d(R+h)\cos(\theta) = p^2 \quad (1)$$

$$(R+h)^2 + p^2 - 2p(R+h)\cos(\Theta) = d^2 \quad (2)$$

where R represents the radius of the Earth. In order to quantitatively study the number of visible transmitters, we use the solid angle Ω that the antenna covers with a full azimuthal view, and consider that GNSS satellites (transmitters) are uniformly distributed in space. Then the number of transmitters that can be seen by the antenna is given by (4), which only considers GPS system.

$$\Omega = 2\pi \left(1 - \cos \theta\right) \quad (3)$$

$$N = 32 \frac{\Omega}{4\pi} \quad (4)$$

Since the ground and air-based platforms are significantly lower than that of the space-based scenario, in the following analysis, they are taken as one group (low platform). Given that the Earth's radius is of 6731 km, and the altitude of GPS satellites is about 20000 km, the number

of visible transmitters can be obtained for different platforms with a given antenna viewing angle. Table 2 presents the results for the platform heights of 1, 5, 300, and 800 km when the viewing angle is 80° . The number of visible transmitters is about 9 for the four platform heights. Although the number of visible transmitters decreases with the height of platform, the influence of the platform height is negligible. So, the height of receiving platform cannot significantly affect the number of visible transmitters for the up-looking antenna.

Table 2: Number of visible transmitters for the up-looking antenna with 80° viewing angle

Platforms	Low Platform		Space Platform	
Altitudes (km)	1	5	300	800
Visible Transmitters' Number	9.6	9.5	9.4	9.1

Table 3: Number of visible transmitters for down-looking antenna

Viewing Angle of Down-looking Antenna	45°	60°
Heights of Low Platform	1 km	2.2
	5 km	2.2
Heights of Space Platform	300 km	2.8
	800 km	4.2

For the down-looking antenna, Fig. 4 shows the antenna's view in this case. The deduction of θ can be found in [23]. Similarly, the number of visible transmitters is given for the platform heights of 1, 5, 300 and 800 km when the viewing angle is 45° and 60° respectively, as shown in Table 3. When the viewing angle is 45° , only 2.2 transmitters can be seen by the receiver for the low platform scenario, compared to 2.8 and 4.2 for the 300 and 800 km space-based platforms respectively. Around 10 transmitters' reflected signals can be received by the receiver at 800 km altitude with the viewing angle of 60° , but only 4 for the low platform. Thus, receivers at the space-based platform can receive reflected signals from more transmitters than that at the low platform, this is particularly so as the height of space platform increases.

From the above analysis, it is clear that the receivers' heights have negligible impact on the ability to receive the direct signals, while the receivers mounted on higher platform have significant advantages over these on low platform in receiving the reflected signals. Therefore, in respect to the number of visible transmitters, the space-based scenario has stronger data collecting ability than the low platform scenario. When considering that space mission usually consists of several satellites (receivers), such as 8 satellites in CYGNSS constellation, while low-platform campaigns often operate in single-receiver model, the advantage of data collection will be further enhanced in space-borne GNSS-R.

Measuring Scale

The measuring scale is associated with data distribution, which relates to the receivers' track. For the ground-based scenario, the data is limited to a small area around the receiver. Flight campaigns can obtain data from a wider area, but the data is still limited to a narrow area along the footprint of the flight track. However, the space-based mission will collect data worldwide. This has been confirmed by several simulated studies, such as [23]. Fig. 5 takes TDS-1 as an example, showing the distribution of the specular reflection points that have an elevation angle of over 15° during one day. The red curves are the loci of the specular reflection points. Although only GPS satellites are considered in Fig. 5 and TDS-1 is a single-satellite mission, it has clearly shown the global coverage ability. Thus, the space-based

GNSS-R measurements are able to cover the whole Earth surface, while the low platform GNSS-R cannot.

Quality of Results

In this section, the quality of GNSS-R results is compared between the low and space platforms. GNSS-R involves a range of applications, such as wind speed, soil moisture and altimetry. This section focuses on the quality of altimetric results.

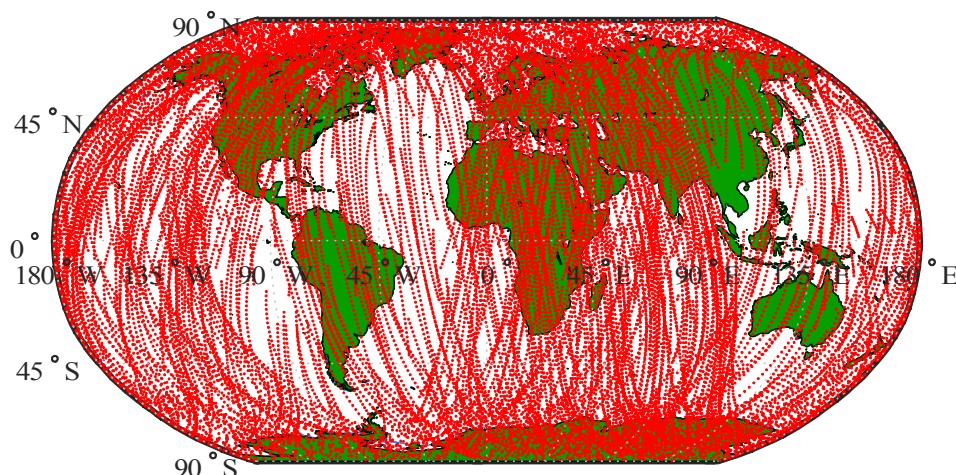


Fig. 5: Data distribution of the TDS-1 in one day

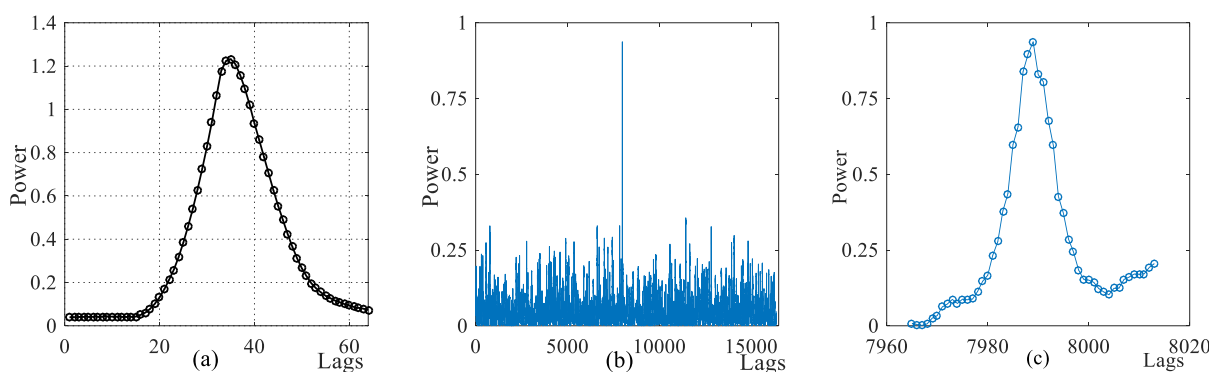


Fig. 6: Waveforms of reflected signals: (a) waveform from a flight-based experiment, (b) waveform from TDS-1 mission, (c) the partial enlarged figure of (b) around the peak.

The cross-correlation waveform function between received signals and their local replicas is a key concept for GNSS-R altimetry, from which the observations of path delay are measured. The waveform is approximately a triangle function in theory, and this property is retained in the waveforms of the direct signals, but the waveforms of the reflected signals are distorted by a host of factors, such as multi-path scattering, and the roughness of reflecting surface. Theoretically studying all these factors is beyond the scope of this paper. Here, we analyse the quality of the waveforms of low and space platforms by an example, as shown in Fig. 6. Fig. 6 (a) is a waveform of the reflected signals collected by a flight-based campaign using the receiver described in [24]. Each channel of this receiver contains 64 single-lag correlators, putting out 64-lags waveforms [24]. Fig. 6 (b) is a waveform of the reflected signals collected from the TDS-1. This waveform is generated by 1-ms coherent integration. Fig. 6 (c) is the partial enlarged figure of (b) around the peak. The waveform in (b) is an ‘ideal’ one because in many cases, reflected waveforms generated by 1-ms coherent integration have no clear correlation peak. But in comparison with the curve in (a) which is very smooth, the curve in

(c) is considerably distorted. Therefore, long-term coherent and non-coherent integrations are usually adopted to obtain high quality waveforms in processing the reflected signals from space-based mission, such as [25]. Thus the reflected signals from space mission are generally noisier than these from low platform receivers.

Another factor which influences the quality of altimetric results are the errors relating to atmosphere. For the low platform GNSS-R altimetry, the atmospheric environments that the direct and reflected signals pass through are nearly the same, so it can be assumed that the direct and reflected signals are equally affected by ionosphere and troposphere. Consequently the path delay is nearly free of atmospheric errors. However, this assumption does not work in space-based GNSS-R altimetry, where the direct and reflected signals are usually separated far away from each other. In this case, the direct signals are free of tropospheric error and just affected by the upper layer of the ionosphere, while the reflected signals travel through the troposphere twice, and the ionosphere nearly twice. Even if the two errors can be compensated by using classical models or atmospheric products, the path delay measurements still suffer from residual errors. Thus, the space-based measurements are more vulnerable to atmospheric errors than these of the low-platform.

As mentioned in the introduction part, cm-level precision and accuracy altimetry results have been achieved in the low-platform scenario, while the precision of first experimental result from space is not given [11]. The quality of the reflected signals and atmospheric errors play a non-negligible role here. Based on the analysis in this section and the results reported in the literature, such as [11, 14], we can see that the low-altitude platform tends to obtain higher quality altimetric results than the space-platform.

After comparing the ground, air and space-based GNSS-R in the three respects, the space-based GNSS-R shows stronger ability in data collection, and wider measuring scale than that of the low-platform GNSS-R. Therefore, the greatest potential of GNSS-R is in the space-based receiver scenario.

Missions

Evolution of Space Missions

GNSS-RO space mission has a history of over 20 years, starting from the launch of GPS/MET in 1995. From then on, a number of space missions have been carried out. However, most missions launched before 2006 can only provide several hundred measurements per day, such as CHAMP and SAC-C. When the COSMIC constellation, delivering 1500 to 2000 soundings per day, was launched in 2006, GNSS-RO stepped into a new stage such that GNSS-RO measurements are now an operational data source for weather prediction and ionospheric studies. Other missions which make significant contributions to GNSS-RO are METOP-A, OCEANSAT-2, and METOP-B.

By contrast, GNSS-R is poor in space missions. The first mission was the UK-DMC-1, which served from 2003 to 2011. It was successful in demonstrating the concept of GNSS-R, but with very limited ability in data collection because during its lifetime only around 60 collections and 5000 DDMs were gathered. The other mission was TDS-1, which is currently in operation. This mission holds a far stronger capability in data collection than the first one, providing approximately 630000 DDMs within 2 days. In addition, TDS-1 has some improvements in the LHCP antenna gain, with 13 dBi compared to 12 dBi of the UK-DMC-1. Nevertheless, they are single-spacecraft missions and because of competing payloads, do not

operate continuously. For example TDS-1 opens GNSS-R on only 2 out of every 8 days. In order to fully develop the potential of the GNSS-R, it is necessary to develop dedicated missions, especially those with multiple spacecraft.

Near Future Missions

In the near future, a series of space missions relating to GNSS remote sensing will be carried out, such as COSMIC-2 and CYGNSS. Six of them are focused in this section. Table 4 lists the main information of the six missions, from which the difference between them can be easily seen.

Table 4: Main information of the six space missions

Missions	Altitude(km)	Inclination(°)	Task	Frequency	Spacecraft
GRACE-FO	~490	~89	GNSS-RO	L1+L2+L5	2
COSMIC-2	~520&720	~24 & 72	GNSS-RO	L1+L2+L5	12
CICERO	~750	~72	GNSS-RO	L1+L2+L5	> 24
GEROS-ISS	~400	~52	Altimetry	At least L1+L2	1
³ Cat-2	~500	~97	Altimetry	L1+L2	1
CYGNSS	~500	~35	Wind Speed	L1	8

Since the GRACE spacecraft have been in a slowly decaying orbit, the GRACE-FO mission, which is the successor of the GRACE, has been planned in order to minimise the data gap. The GRACE-FO mission is expected to be launched in August 2017 with an expected life of over 5 years. Similar to its predecessor, GRACE-FO's main task is to map spatial and temporal changes in the gravity field from space, continuing the radio occultation measurements for numerical weather services as a secondary objective. GRACE-FO will use the Tri-GNSS (GPS+GALILEO+GLONASS) radio occultation receiver developed by JPL instead of the previous BlackJack receiver, which means the number of daily soundings will be significantly increased.

COSMIC-2 is the follow-on mission of the COSMIC-1, organised by Taiwan, NOAA, USAF and NASA. COSMIC-2 is a dedicated mission for radio occultation, which will employ a constellation of 12 microsattellites to collect atmospheric data. These 12 satellites will be sent to space by two launches. The first launch will send 6 satellites to a low-inclination (24°) orbit with an altitude of approximately 520km, and the other launch aims to a high-inclination (72°) orbit with an altitude of around 720km. The two launches are expected to be finished in the first quarter of 2017 and early 2019, separately. Moreover, this mission is equipped with Tri-GNSS radio occultation receivers, which enables the mission with the capability of capturing signals from GPS, GALILEO and GLONASS simultaneously. So it is predicted that COSMIC-2 will be able to provide over 8,000 sounding profiles daily, which is 4 to 5 times that of the COSMIC-1.

CICERO is another radio occultation project sponsored by GeoOptics Inc, a private environmental Earth observation company. This mission will deploy a constellation of at least 24 micro-satellites to produce atmospheric temperature, pressure and moisture profiles and ionospheric electron density profiles. These satellites are designed to work in high inclination (72°) orbits with an altitude of around 750km. The receiver on this mission is a tailored version of the 'Pyxis' receiver developed by Broad Reach Engineering. The specialised receiver works in three frequencies, L1, L2 and L5, receiving the GPS and GALILEO signals. In order to demonstrate the capabilities of micro-satellites, two micro-satellites will be

launched first as the pathfinder of the CICERO. The initial operational constellation (CICERO-1) is expected to be in operation at the end of 2016. The constellation will be expanded to 12 satellites in 2017 and 24 in 2018.

GEROS-ISS (GNSS Reflectometry, Radio Occultation and Scatterometry on board the International Space Station) is a GNSS remote sensing project proposed by ESA and supported by many scientific institutes, such as GFZ, IEEC and JPL. Apart from GPS and GALILEO systems, other systems, including GLONASS, BEIDOU and QZSS, also tend to be used in the GEROS-ISS. The primary goals of this mission are to explore the potential of the GNSS-R. One of them is to measure the sea surface height of the ocean using reflected signals. Another main goal is to retrieve ocean surface mean square slope, which is associated with sea roughness and wind speed. The secondary objectives relate to the GNSS radio occultation and scatterometry, such as collecting occultation soundings and exploring the potential of land application. The GEROS-ISS can map ocean altimetry at the scales of about 10 to 100 km in less than four days, compared to current satellite altimeter providing altimetry measurements at a scale of around 80 km every ten days. The orbit altitude and inclination of the GEROS-ISS are around 400 km and 52° respectively, and the launch is scheduled in 2019.

³Cat-2, launched in 15 August 2016, is a nano-satellite mission developed by UPC. The chief goal of this mission is to demonstrate dual frequency (L1+L2) GNSS-R altimeter. The main payload is P(Y) and C/A reflectometer (PYCARO) which has been tested in actual experiments. ³Cat-2 is a multi-systems mission, using the signals of GPS, GLONASS and GALILEO. In addition, the LHCP antenna capturing reflected signals is two antenna arrays of 3 by 2 elements (each element with a gain of 5.6 dB). With the high gain LHCP antenna, precise code and dual-frequency measurements, this mission is expected to obtain high precision and accuracy altimetric results.

CYGNSS is another space mission specially designed for the GNSS-R, which will be launched in November 2016. The primary goal is to measure ocean surface wind in all conditions, including severe ones like the eyewall of a cyclone. The CYGNSS mission is comprised of 8 micro-satellites on the same orbit that the altitude is approximately 500 km and the inclination 35°. The Space GPS Receiver Remote Sensing Instrument (SGR-ReSI), which works on the TDS-1, will be employed on the CYGNSS mission, and the LHCP antenna gain increased to 14 dB. The SGR-ReSI runs automatically to generate DDMs, and then downlinks to ground station. When an interested area is identified, the SGR-ReSI operates in raw data mode.

Future Applications

Mesoscale ocean altimetry is vitally important to understand energy transfer between ocean surface and atmosphere, to study current characteristics, and to investigate eddies. The requirements of mesoscale ocean altimetry are 5-cm height accuracy, 100 km along-track spatial resolution, two-day revisit time, and global coverage [17]. This is a very challenging issue because currently no technologies can meet this demand, such as satellite altimetry. Although GNSS-R also cannot reach the requirements now, it shows great potential to solve this issue because of its unprecedentedly high spatial and temporal coverage. In 2011, Martin-Neira proposed an in-orbit demonstration that would reach the altimetric accuracy suitable for mesoscale ocean altimetry [17]. In 2014, Cardellach theoretically expected the altimetric precision of space-based scenario based on air-borne experimental measurements, reaching the conclusion that interferometric GNSS-R has the capability to conduct mesoscale ocean altimetry [18].

Catastrophic weather, such as tsunamis and cyclones, are a great threat to property and life. The prediction of catastrophic weather remains a challenging issue. Tsunamis, which are usually triggered by an earthquake under deep-ocean, causes small vertical variation (a few decimetres) but with very large horizontal pattern (several hundred kilometres in wavelength) in open ocean. Although a satellite altimeter can be as accurate as a few centimetres, it is unlikely to detect a tsunami due to the limited coverage. An alternative approach of studying tsunami is by means of GNSS-R technique, using its advantage in coverage. GFZ has done some work in using the space-based GNSS-R altimetric measurements to German Indonesian Tsunami Early Warning System (GITEWS) [26]. In addition, K. Yu focuses on tsunami-wave parameter estimation and weak tsunami detection using GNSS-R sea surface height measurements recently [27, 28]. GNSS-R can also be applied to cyclone forecasts, which have high ocean surface winds. Remarkable results have been obtained using GNSS-R to retrieve the wind speed with the support of the TDS-1 mission. In the near future, cyclone forecasting using the GNSS-R technique may become a reality with the aid of the forthcoming CYGNSS mission, which is dedicated to studying wind speed.

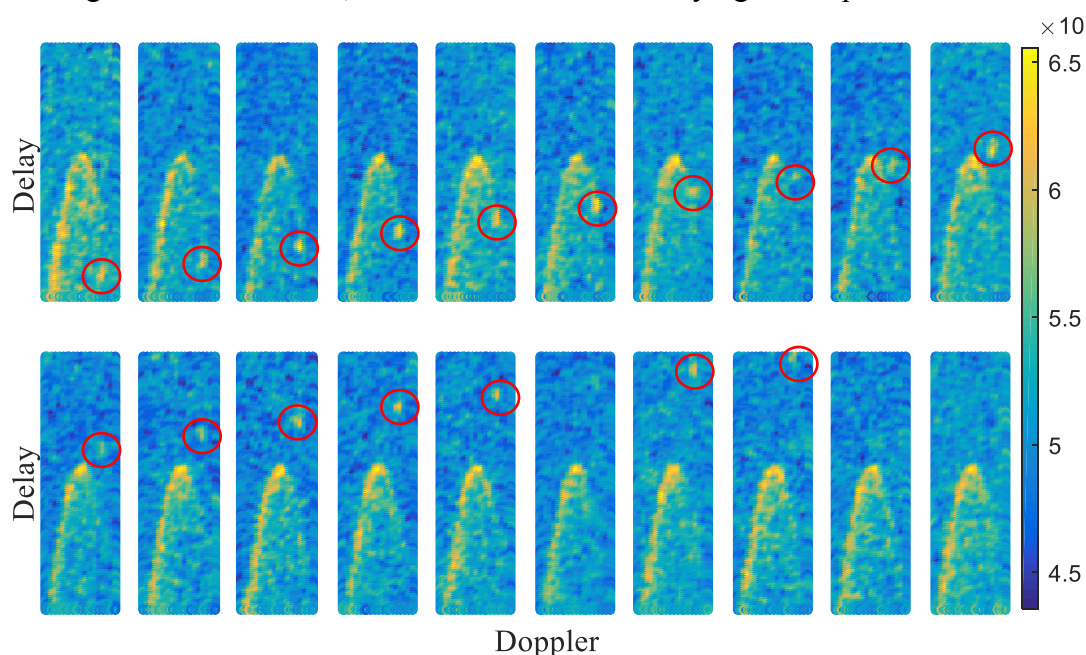


Fig. 7: Evidence of Target Detection from TDS-1 [made by authors]

Target detection is an interesting issue, attracting a range of technologies to do so, such as InSAR system [29], and remote sensing images [30]. Soon after the proposal of the concept of GNSS-R, researchers found that the GNSS-R could be an alternative approach to detect targets, especially on the ocean surface. Using the GNSS-R for ocean surface target detection is first proposed in [31]. In 2014, a study based on simulated DDM to detect and position ocean surface target was reported [32]. For GNSS-R, the target had considerably higher or lower reflecting coefficient than that of the objects around it could be detected because this significant difference in reflecting coefficient will lead to a bright or dark spot in the DDMs. Fig. 7 shows the evidence of target detection from the TDS-1. In this figure, 20 DDMs from the RD06 of the TDS-1 are shown. The red circles in the DDMs mark the track of the target, from the occurrence at the lower right of the first DDM to the disappearance at the upper right of the 18th DDM.

Conclusion

In this paper, we made comparisons between the three GNSS-R scenarios (ground, air and space-based) based on their ability to collect data, their measuring scale, and the quality of their results. We concluded that the greatest potential for GNSS-R is in the space-borne receiver scenario. Then, after reviewing the evolution of space-based GNSS remote sensing, six forthcoming space missions relating to the GNSS remote sensing were discussed, especially their primary objectives, data collection abilities and working frequencies. Finally, three potential applications of GNSS-R were investigated, including mesoscale ocean altimetry, catastrophic weather alarms and ocean surface target detection. Evidence of target detection using GNSS-R was discovered in a TDS-1 dataset.

References

1. Yunck T.P., Lindal G.F., and Liu C.-H., "The role of GPS in precise Earth observation", in Position Location and Navigation Symposium, 1988. Record. Navigation into the 21st Century. IEEE PLANS'88., IEEE, 1988, pp. 251-258.
2. Martin-Neira M., "A passive reflectometry and interferometry system (PARIS): Application to ocean altimetry", *ESA journal*, Vol. 17, 1993, pp. 331-355.
3. Kursinski E., Hajj G., Schofield J., Linfield R., and Hardy K.R., "Observing Earth's atmosphere with radio occultation measurements using the Global Positioning System", *Journal of Geophysical Research: Atmospheres*, Vol. 102, No. D19, 1997, pp. 23429-23465.
4. Cucurull L. and Derber J., "Operational implementation of COSMIC observations into NCEP's global data assimilation system", *Weather and forecasting*, Vol. 23, No. 4, 2008, pp. 702-711.
5. Healy S., "Forecast impact experiment with a constellation of GPS radio occultation receivers", *Atmospheric Science Letters*, Vol. 9, No. 3, 2008, pp. 111-118.
6. Qiao L., Glennon E., Dempster A. G., and Chaoui S., "Using cubesats as platforms for remote sensing with satellite navigation signals", in *Geoscience and Remote Sensing Symposium (IGARSS), 2013 IEEE International*, 2013, pp. 852-855.
7. Ho S.-P., Goldberg M., Kuo Y.-H., Zou C.-Z., and Liam Schreiner W., "Calibration of Temperature in the Lower Stratosphere from Microwave Measurements Using COSMIC Radio Occultation Data: Preliminary Results", *Terrestrial, Atmospheric and Oceanic Sciences*, Vol. 20, 2009, pp. 87-100.
8. He W., Ho S.p., Chen H., Zhou X., Hunt D., and Kuo Y.H., "Assessment of radiosonde temperature measurements in the upper troposphere and lower stratosphere using COSMIC radio occultation data", *Geophysical Research Letters*, Vol. 36, No. 17, 2009, pp. 1-7.
9. Gleason S., Hodgart S., Yiping S., Gommenginger C., Mackin S., Adjrad M., and Unwin M., "Detection and Processing of bistatically reflected GPS signals from low Earth orbit for the purpose of ocean remote sensing", *IEEE Transactions on Geoscience and Remote Sensing*, Vol. 43, No. 6, 2005, pp. 1229-1241.
10. Foti G., Gommenginger C., Jales P., Unwin M., Shaw A., Robertson C., and Roselló J., "Spaceborne GNSS reflectometry for ocean winds: First results from the UK TechDemoSat-1 mission", *Geophysical Research Letters*, Vol. 42, No. 13, 2015, pp. 5435-5441.

11. Clarizia M.P., Ruf C., Cipollini P., and Zuffada C., "First spaceborne observation of sea surface height using GPS-Reflectometry", *Geophysical Research Letters*, Vol. 43, No. 2, 2016, pp. 767-774.
12. Giangregorio G., di Bisceglie M., Addabbo P., Beltramonte T., D'Addio S., and Galdi C., "Stochastic Modeling and Simulation of Delay-Doppler Maps in GNSS-R Over the Ocean", *IEEE Transactions on Geoscience and Remote Sensing*, Vol. 54, No. 4, 2016, pp. 2056-2069.
13. Garrison J.L. and Katzberg S.J., "Detection of ocean reflected GPS signals: theory and experiment", in *Southeastcon'97. Engineering new New Century., Proceedings. IEEE*, 1997, pp. 290-294.
14. Kucwaj J.C., Stienne G., Reboul S., Choquel J.-B., and Benjelloun M., "Accurate Pseudorange Estimation by Means of Code and Phase Delay Integration: Application to GNSS-R Altimetry", *IEEE Journal of Selected Topics in Applied Earth Observations and Remote Sensing*, DOI. 10.1109/jstars.2016.2538728. 2016, pp. 1-11.
15. Treuhaft R.N., Lowe S.T., Zuffada C., and Chao Y., "2-cm GPS altimetry over Crater Lake", *Geophysical Research Letters*, Vol. 28, No. 23, 2001, pp. 4343-4346.
16. Lowe S.T., Zuffada C., Chao Y., Kroger P., Young L.E., and LaBrecque J.L., "5-cm-Precision aircraft ocean altimetry using GPS reflections", *Geophysical Research Letters*, Vol. 29, No. 10, 2002, pp. 13-1-13-4.
17. Martin-Neira M., D'Addio S., Buck C., Flourey N., and Prieto-Cerdeira R., "The PARIS Ocean Altimeter In-Orbit Demonstrator", *IEEE Transactions on Geoscience and Remote Sensing*, Vol. 49, No. 6, 2011, pp. 2209-2237.
18. Cardellach E., Rius A., Martin-Neira M., Fabra F., Nogues-Correig O., Ribo S., Kainulainen J., Camps A., and D'Addio S., "Consolidating the Precision of Interferometric GNSS-R Ocean Altimetry Using Airborne Experimental Data", *IEEE Transactions on Geoscience and Remote Sensing*, Vol. 52, No. 8, 2014, pp. 4992-5004.
19. Zavorotny V.U. and Voronovich A.G., "Scattering of GPS signals from the ocean with wind remote sensing application", *IEEE Transactions on Geoscience and Remote Sensing*, Vol. 38, No. 2, 2000, pp. 951-964.
20. Rodriguez-Alvarez N., Bosch-Lluis X., Camps A., Vall-Llossera M., Valencia E., Marchan-Hernandez J.F., and Ramos-Perez I., "Soil moisture retrieval using GNSS-R techniques: experimental results over a bare soil field", *IEEE Transactions on Geoscience and Remote Sensing*, Vol. 47, No. 11, 2009, pp. 3616-3624.
21. Chen Q., Won D., and Akos D.M., "Snow depth estimation accuracy using a dual-interface GPS-IR model with experimental results", *GPS Solutions*, DOI. 10.1007/s10291-016-0517-1, 2016, pp. 1-13.
22. Yu K., Ban W., Zhang X., and Yu X., "Snow Depth Estimation Based on Multipath Phase Combination of GPS Triple-Frequency Signals", *IEEE Transactions on Geoscience and Remote Sensing*, Vol. 53, No. 9, 2015, pp. 5100-5109.
23. Hajj G.A. and Zuffada C., "Theoretical description of a bistatic system for ocean altimetry using the GPS signal", *Radio Science*, Vol. 38, No. 5, 2003, pp. 1089.
24. Nogues-Correig O., Cardellach Gali E., Sanz Campderros J., and Rius A., "A GPS-Reflections Receiver That Computes Doppler/Delay Maps in Real Time", *IEEE Transactions on Geoscience and Remote Sensing*, Vol. 45, No. 1, 2007, pp. 156-174.

25. Gleason S., Adjrad M., and Unwin M., "Sensing ocean, ice and land reflected signals from space: results from the UK-DMC GPS reflectometry experiment", in *Proceedings of the 2005 ION GNSS Technical Meeting*, 2005, pp. 13-16.
26. Stosius R., Beyerle G., Semmling M., Helm A., Hoehner A., Wickert J., and Lauterjung J., "Tsunami detection from space using GNSS Reflections: Results and activities from GFZ", in *Geoscience and Remote Sensing Symposium (IGARSS), 2010 IEEE International*, 2010, pp. 3047-3050.
27. Yu K., "Tsunami-Wave Parameter Estimation Using GNSS-Based Sea Surface Height Measurement", *IEEE Transactions on Geoscience and Remote Sensing*, Vol. 53, No. 5, 2015, pp. 2603-2611.
28. Yu K., "Weak Tsunami Detection Using GNSS-R-Based Sea Surface Height Measurement", *IEEE Transactions on Geoscience and Remote Sensing*, Vol. 54, No. 3, 2016, pp. 1363-1375.
29. Howard D., Roberts S., and Brankin R., "Target detection in SAR imagery by genetic programming", *Advances in Engineering Software*, Vol. 30, No. 5, 1999, pp. 303-311.
30. Sun H., Sun X., Wang H., Li Y., and Li X., "Automatic target detection in high-resolution remote sensing images using spatial sparse coding bag-of-words model", *IEEE Geoscience and Remote Sensing Letters*, Vol. 9, No. 1, 2012, pp. 109-113.
31. Pascazio V., Schirinzi G., and Farina A., "Moving target detection by along-track interferometry", in *International Geoscience and Remote Sensing Symposium*, 2001, pp. VII: 3024-3026.
32. Ji W., Xiu C., Li W., and Wang L., "Ocean surface target detection and positioning using the spaceborne GNSS-R Delay-Doppler maps", in *2014 IEEE Geoscience and Remote Sensing Symposium*, 2014, pp. 3806-3809.

A Systems Engineering Approach to Miniaturised Satellite Constellation Design Optimisation

George Coulloupas^{1,2}, Hideaki Ogawa¹, John Mo¹

¹ School of Engineering, RMIT University, Melbourne, GPO Box 2476, VIC 3001, Australia

² Aerospace Systems Pty. Ltd., Prahran, VIC 3181, Australia

Summary: The recent advent of miniaturised satellites has seen success as an economically viable and attractive spacecraft platform for scientific and technology demonstration missions by national space agencies and private enterprise, some with scarce space engineering experience. In response, this study presents the use of advanced design methodologies to iteratively assist systems engineering of spacecraft. In an automated manner, the resultant framework combines numerical integration of orbit propagation and surrogate modelling to multi-objective optimisation for a conceptual 12 asset co-planar constellation operating in low-Earth orbit. Optimisation was performed for 11 orbital-rendezvous manoeuvres simultaneously minimising three objectives; summation of the magnitude of ΔV for all manoeuvres of each satellite, duration of constellation formation and the radiation dose depth experienced by one reference satellite. Identification of decisive and performance influencing constellation design factors then followed by means of a global sensitivity analysis employing statistical surrogates.

Keywords: systems engineering, multi-objective design optimisation, low-Earth orbit (LEO), co-planar orbital phasing, satellite constellation.

Introduction

The motivation for this study is the application of the systems engineering (SE) approach within the domain of commercial-off-the-shelf (COTS) components and state-of-the-art software for miniaturised spacecraft design, specifically constellation design optimisation conducted in an automated manner. In particular, miniaturised spacecraft have had recent success as an economically viable and accessible satellite platform for scientific research and space technology demonstration missions conducted by research/education institutions, national space agencies and private enterprise, some with scarce

space engineering experience. Miniaturised spacecraft are defined in this paper as modular, capability-limited satellites with quintal mass (100kg) or less for low-Earth orbit applications. Table 1 adopted from [1] provides common satellite categories by mass. Notably, the 'CubeSat' program as a miniaturised satellite form factor, jointly developed in 1999 by Stanford University and California Polytechnic State University [2] have increased in popularity since their precedent launch in 2003 [3-4]. The most common rationale for adopting a miniaturised platform appears to be majorly influenced by the reduction in launching costs, typically

Table 1: Satellite categories adopted from Evans (1999)

Category	Mass (kg)
Large	>1,000
Medium	500-1,000
Mini	100-500
Micro	10-100
Nano	1-10
Pico	0.1-1
Femto	<0.1

evaluated and advertised by specific cost (\$/kg). As a result, efforts to maximise performance of miniaturised satellites have led to the emergence of a high capital international marketplace for COTS designing tools, and pre-manufactured satellite subsystems, primarily targeting the CubeSat platform [5]. Thus, new satellite constellation and space mission concepts in the interest of investors, research outcomes and organisations have emerged at reduced cost while increasing sub-system capability and market resilience. The reductions in payload mass made through the adoption of a smaller satellite platform offer launch opportunities for the satellite to be deployed as an auxiliary item of a much heavier payload. The CubeSat [6] includes details on one of the interfaces which exist between a CubeSat and the primary payload, and launch vehicle, such as the Poly Picosatellite Orbital Deployer (P-POD), a spring-glided rail system that is controlled by the primary payload. This launching paradigm is argued to partially address the issue of access-to-orbit in the absence of smaller or cost-effective launch vehicles supplying only the miniaturised satellite market, however it is still highly restrictive on mission outcomes as miniaturised satellites must be able to satisfy missions requirements within the orbital plane of the primary payload. The spacecraft may not be optimally designed to function within its deployed orbital plane. It is suggested that unless arranged under launching educational or other framework, such as NASA’s CubeSat Launch Initiative [7] often at subsidy, secondary payload launch costs are generally higher than the specific cost of the launch vehicle itself [8-9]. Moreover, miniaturised satellites launched as an auxiliary payload must adhere to strict regulation of volume and pressure of on-board propellant and stored electrical energy, aimed at protecting the primary payload [6]. A review of a number of in-development launch vehicles [10] addressing the capability gap [8,11] between conventional and miniaturised satellite deployment which will support the dedicated launch and increase the orbital deployment precision of miniaturised satellites, while enabling cluster launches of spacecraft. In response, state-of-the-art design methodology utilised in this study favours a cluster launch, or a dedicated launch service.

Therefore, a constellation of miniaturised satellites launched in a cluster/in high numbers offers further advantage owing to the lower cost of unit development. Successful deployment of miniaturised satellite constellations has demonstrated two generations of capability: single-plane and multi-plane constellations. Multi-plane constellations exhibit superior capability to single-plane in regards to revisit times and coverage, which influence on-board data storage requirements [12-13]. Satellites belonging to the CubeSat form-factor which have successfully demonstrated multi-plane constellations (of which 2 instances are observed between 2003 and 2014) were designed and operated by Planet Labs Incorporated Flock-1A of 28 satellites, Flock-1C of 11 satellites [14] and Skybox Imaging’s planned constellation of 24 satellites for launch in 2018. Skybox’s efforts in the field of micro-propulsion utilising ‘green’ monopropellant

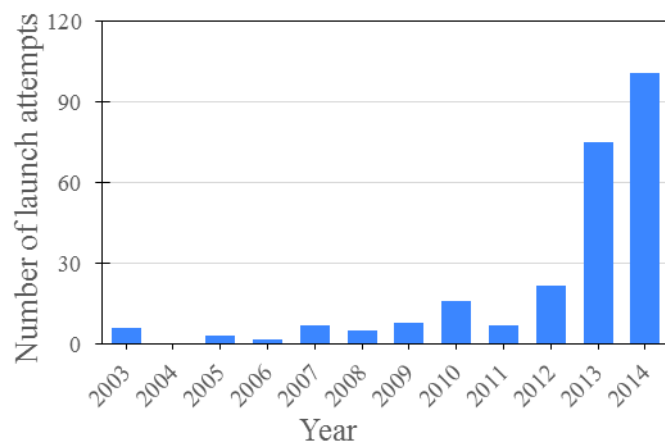


Fig 1: CubeSat launches over time

systems holds great promise for propulsion systems with low life-cycle cost [15]. The objectives of these constellations surround Earth observation with global or near-global coverage. The Flock constellations achieved orbit by manifestation on a re-supply mission to the International Space Station as well as deployment via a launch vehicle as an auxiliary payload, resulting in multiple orbital planes [14]. At present, the only example of a multi-plane miniaturised satellite constellation deployed from a single launch vehicle is the FORMOSAT-3/COSMIC mission (6 micro satellites), which demonstrated a novel strategy involving multi-plane separation through the use of nodal precession due to J2 perturbations [16].

Historically, an SE approach has been highly favourable and exploitable to explore complex, inter-disciplinary design problems exhibiting unknown performance trade-offs by initially adopting a holistic paradigm [17]. Traditionally, when applied to space vehicle design, it is suggested SE follows a top-down design approach with iterative refinement, applying specialist knowledge and experience to satisfy system requirements and constraints [18]. More recently, the maturation of similar approaches to describe and evaluate feasible solutions, such as model-based SE (MBSE) [19] and System-of-System (SoS) thinking have been largely discussed in the context of rapid spacecraft design in order to address the inherent inter-disciplinary requirements [20,21]. Figure 2 communicates the systems engineering approach and processes therein adopted by the proposed framework.

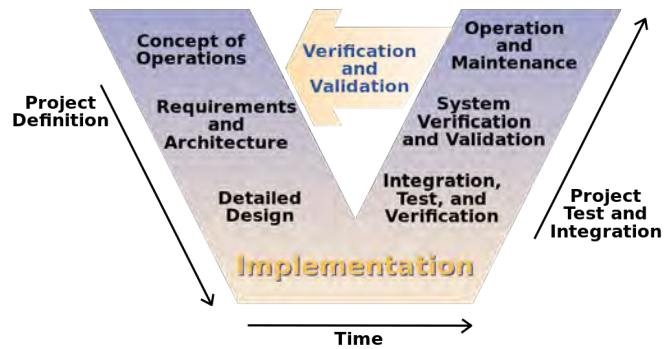


Fig. 2: Simplified Systems Engineering “V” model

While SE approaches are said to be commonplace and favourable for spacecraft design, the practices of SE processes therein are typically applied on a case-by-case basis and cannot be generalised across multiple scenarios. This may be due to the aforementioned nondeterministic relationship between the design and solution spaces of a whole system and the inter-disciplinary nature of the problem and relative uniqueness of individual systems.

Single-objective optimisation algorithms in SE processes have been widely applied in aerospace design problems and high-level space mission planning problems for an effective and efficient evaluation of system performance trade-offs. As it has been demonstrated that spacecraft design is an inter-disciplinary effort, such techniques lack detail, often centric to one outcome constrained by opinion or experience. The limited nature of miniaturised satellites is described as being advantageous to extensively understanding performance trade-offs when employing multi-objective optimisation. Stated in [9] this quality as a promising prospect for the CubeSat platform, when considering a large number of design solutions. It is in the interest of decision-makers that computation time for system evaluation should be reduced, however this is inherently limited as the design variable inputs are constrained in the context of a resource-limited system.

In terms of specific cost, dedicated miniaturised satellite launches as secondary payloads are in the order of magnitude of tens of thousands of dollars, while dedicated launches are in the range of hundreds of thousands of dollars [23]. Space agency and government-based funding initiatives have provided some opportunities for access to space for miniaturised satellite efforts at a reduced or waived cost. However, the risks and uncertainties of orbital deployment for miniaturised satellites as auxiliary payloads provides a great barrier for achieving optimal capability for an already resource-limited system. For these reasons, the ‘ride-share’ launching paradigm is said to be “falling out favour” [22].

Some satellite missions of the past have exhibited long durations (months to years) between the system verification process to orbital deployment. In the interest of private enterprise, economic risks associated with unforeseen or sudden changes in markets or services during this time may be mitigated with constellation assets that are able to deploy increasing capability in multiple mission phases. The ‘staged’ deployment strategy of a constellation is shown to maintain performance in the event of the loss of a constellation asset as reconfiguration can fill the performance gap [24]. In the instance of favourable market conditions, deploying new assets to operating or additional orbital planes can increase performance whilst tempering financial risk. Conceptually, the addition of a new unit would incur a higher capital cost associated with a high number of launches, however the use of a miniaturised satellite platform reduces launching cost. Further efforts to reduce costs associated with the launching segment, miniaturised satellite constellations may be deployed such that, the number of dedicated and/or auxiliary launches shall be optimally minimised leveraging phased asset design and increased capability. To this end, phased multi-asset orbital deployment is an attractive cost and risk minimisation strategy.

A commonly executed and conceptually simple method of satellite deployment resulting in constellation formation is by means of co-planar orbital phasing with respect to a reference satellite, in essence an orbital rendezvous problem [25]. The first known instance of a co-planar manoeuvre to be performed belongs to the Sputnik I mission of 1957 [26]. The conception of the so-called orbital rendezvous problem came about during the height of the 20th century space race with a number of historically significant missions said to symbolise its beginning such as Vostok, Gemini, Soyuz and Apollo [27]. Missions of this era also implemented the first instances of small spacecraft designs for some aspects of missions.

Orbital rendezvous in this context occurs after separation from the launch vehicle and orbital deployment. Spacecraft phase within a common orbital plane in either a trailing or leading manner to a reference satellite or position. Prior to any manoeuvre, the state of the reference satellite is considered as a common initial state among all assets. The term rendezvous is used conceptually and does not necessarily imply that a spacecraft physically docks or otherwise interfaces with another spacecraft at its target state in orbit.

Conversely, this study exploits publicly available two-line element data of a large number of past CubeSat missions by automating the statistical inference of missions by launch site, determining feasible ranges for the initial state of a clustered constellation following launch. Thus, decision variable simplification is further complemented through the collective analysis of successful miniaturised satellite missions of the past. The term state refers to a spacecraft’s

position, velocity magnitude and direction, for any point in time that can be characterised by six orbital elements [25]. The results of the case study provide practical insight into mission outcomes. The outcomes are also visualised in commercial space mission modelling software, Systems Tool-Kit developed by Analytical Graphics Incorporated.

Methodology

This paper presents the results of an optimisation study minimising three objectives characterising the performance of a whole spacecraft constellation system. That is, minimisation of 1) the summation of the magnitude of all impulses (ΔV) of all satellites in a coplanar constellation, 2) duration between initial and final state and 3) radiation dose depth as experienced by the reference satellite. The study incorporated state-of-the-art multi-objective design optimisation (MDO) algorithms assisted by surrogate modelling, coupled with precise orbital numerical integration utilising STK functions. Specifically, extensive use was made of a population-based evolutionary algorithm, the so-called elitist non-dominated sorting genetic algorithm (NSGA-II) implemented in MATLAB®, originally developed at the University of New South Wales, Canberra [28]. Combined with the STK-MATLAB application programming interface, this framework enables automated and robust computation for spatially complex space mission architectures. In order to design an optimally performing constellation and gain insight into decision variable sensitivity without incurring high computational cost, statistical surrogate modelling is used in absence of true numerical evaluation to reasonably predict better performing mission design configurations with respect to the objective functions.

MDO algorithms have been used advantageously to extensively explore inter-disciplinary design spaces by evaluating a high number of configurations; sets of decision variables subject to constraints. Pareto-optimal solutions [29] are observed without traditional cost functions representing weights of objective functions. For the purposes of this study aligning with an SE approach to the benefit of satellite designers and stakeholders, optimal solutions belonging to the Pareto set are to be interpreted as autonomously and objectively derived high-level system requirements. A number of exemplary works using MDO algorithms to solve for conceptual constellation design problems for a wide-range of applications provide many opportunities for the validation of the approach [30-34],

Following the review of relevant literature, the CubeSat case study facilitated conceptual exploration of feasible operations. CubeSats launched from 2003 and 2014 were considered relevant to the concept of operations to the problem at hand and formed the population investigated in the case study, conducted in STK providing access to a large data federate containing position data, as two-line element data. Figure 3 is the result of automated visualisation compositing orbital planes of the CubeSat missions included in the case study based on first observations.

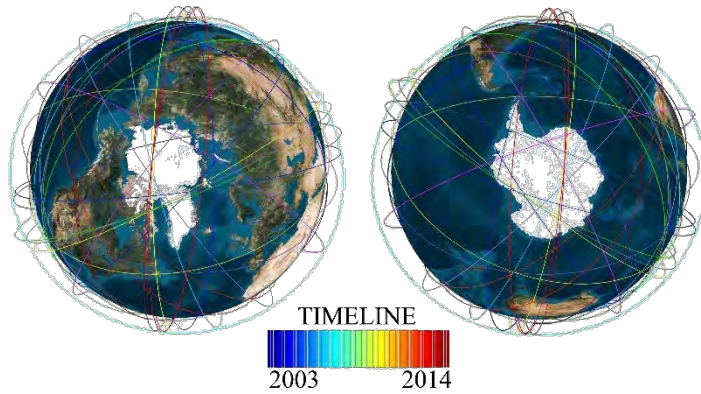


Fig. 3: Visualisation of CubeSat orbits (2003-2014)

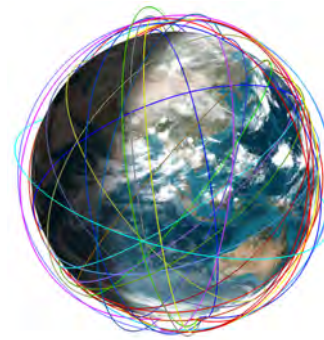


Fig. 4: Visualisation of mean

CubeSat elements coloured by launch

The objectives of the case study were to determine feasible ranges of some orbital elements, statistically inferred by the Brouer-Lyddane long mean method between spacecraft with common launch sites shown in Fig. 4. This range was later implemented to constrain inputs to the MDO algorithm hence constrain the search space to reflect realistic operations. Furthermore, exploiting the STK-MATLAB application programming interface to automate TLE data and subsequent analysis of a large number of space missions was computationally inexpensive.

Satellite co-planar manoeuvres are modelled as an impulsive type occurring in three-dimensional space. Described in [35] a phasing manoeuvre in either terms of sub- or super-synchronous transfer with respect to a reference satellite or position. Sub-synchronous orbit phasing occurs when spacecraft is leading the reference position in the velocity vector direction, relative to an orbiting, non-maneuvring reference satellite/position subject to perturbations. Conversely, super-synchronous orbit phasing occurs when spacecraft is trailing the reference. The introduction of the term phase angle, hereafter denoted as α describes the relative Argument of Latitude between the reference position and one sub- or super-synchronous spacecraft. Modelling the formation of a co-planar constellation involves 4 impulsive manoeuvres from a clustered initial state; 1) a change in altitude such that sub-synchronous phasing warrants lowering altitude while super-synchronous raises altitude; 2) circularisation of the spacecraft's orbit in a parking orbit to achieve required α ; 3) retro-impulse to return to original altitude corresponding to the initial state and 4) final circularisation of the spacecraft's orbit. Fig. 5 visualises sub- and super-synchronous phasing following the first impulsive manoeuvres.

It is conceivable to observe performance trade-offs for decisions necessitated by spacecraft performing co-planar manoeuvres in this manner. Ideal initial states of the cluster, and ideal changes in altitude for each spacecraft, denoted hereafter as ΔH , exist by virtue of achieving an optimal or minimum summation of ΔV for all manoeuvres for a given phase angle for an optimal or minimised manoeuvring duration, denoted hereafter as Δt .



Fig. 5: Visualisation of the first impulsive manoeuvre and satellites phase from the initial state

A description of impulse budgets for sub- and super-synchronous phasing is explained in [24]. These lack eccentricity corrective budgets and perturbations as shown

$$\Delta V_{\text{sub}} = 2\sqrt{GM_e} \times \left(\sqrt{\frac{1}{a}} - \sqrt{\frac{2}{a} - \left(\frac{\pi - \alpha}{\pi} + k\right)^{\frac{2}{3}} \frac{(k+1)^{\frac{2}{3}}}{a}} \right) \quad (1)$$

$$\Delta V_{\text{super}} = 2\sqrt{GM_e} \times \left(\sqrt{\frac{2}{a} - \left(\frac{\pi - \Delta\theta}{\pi} + k\right)^{\frac{2}{3}} \frac{k^{\frac{2}{3}}}{a}} - \sqrt{\frac{1}{a}} \right) \quad (2)$$

where G represents the Universal gravitational constant, M_e represents the mass of the Earth, a represents the semi-major axis of the Earth and k represents an integer number of orbital revolutions.

Noted in [35] one may set ΔV to an arbitrarily small value resulting in very long phasing durations. However, as this framework adopts a practical perspective, too long of a phasing duration may be an undesirable consequence to deliver efficient on-orbit capability. Thus, simultaneous minimisation of ΔV and Δt yield optimal constellation designs.

Additionally, a radiation environment model was also implemented following a worst-case scenario. Utilising data collected by the Combined Release and Radiation Effects Satellite (CRRES) after the famous 24 March 1991 solar storm event, the model assumes the maximum observed solar activity via the NASA computational mode and recommended energy levels with a silicon detector. The reference satellite was modelled to have a finite-slab radiation shield with the detector embedded on one side of a planar slab with 2 millimetres (78.7402 Mils) of Aluminium shielding, irradiated through the slab.

Experimental Design

A co-planar constellation of 12 satellites was modelled, 5 of which phase sub-synchronously to positions $\alpha_{\text{sub-synchronous}} \{+30^\circ, +60^\circ, +90^\circ, +120^\circ, +150^\circ\}$ while 6 satellites phase super-synchronously to positions $\alpha_{\text{super-synchronous}} \{-30^\circ, -60^\circ, -90^\circ, -120^\circ, -150^\circ, 180^\circ\}$ with respect to one non-phasing reference satellite. In order to perform constellation design optimisation, an automated process chain, as shown in Fig. 6, was formulated by taking advantage of the STK-MATLAB application programming interface.

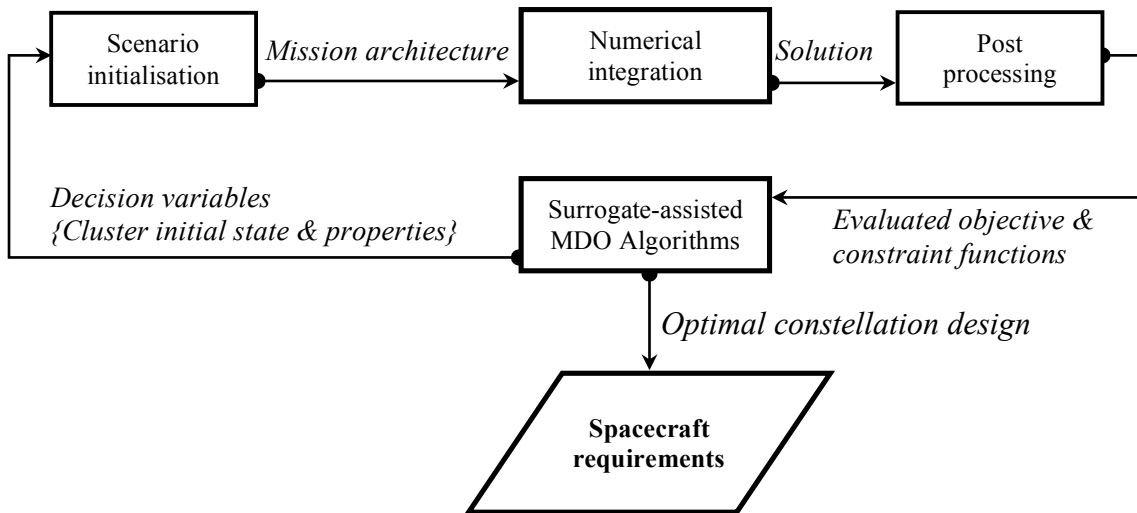


Fig. 6: Automated process chain

The objective and automated derivation of spacecraft requirements begins with the use of evolutionary algorithms to randomly seed input values as decision variables into the high-fidelity modelling environment. The astrodynamics model is initialised accordingly and numerical integration of the individual mission architecture involving all satellites is executed, which may be computed in parallel with other architectures. Lastly, the solution is evaluated against any constraints and discarded if detected to be unfeasible. A proportion of the successful evaluations are selected to breed a new generation of potentially successful and optimal candidates. The breeding process is inspired by biological evolution with cross-over and mutation acting as the main genetic operators. Plausible solutions are then used to routinely train statistical surrogates to predict values of the objective and constraint functions as the evolutionary algorithms take a population-based approach for searching the wide solution space.

The predictive capability of the surrogate models is assessed by evaluating the mean square error (MSE) against a portion of the population; the surrogate must achieve less than 5% MSE to be considered adequate. Multiple surrogates were employed in this study; quadratic response surface models, kriging models based on Gaussian regression as well as artificial neural networks namely radial basis functions. Additionally, variance-based global sensitivity analysis is performed to gain physical insight into the constellation design search space by determining the key design parameters with respect to the objective functions. Once a sufficient population of Pareto-optimal solutions are found and surrogate models perform under the MSE threshold, the best performing surrogate (lowest MSE) is employed to build a base sample using a quasi-random sequence of a much larger population in-lieu of true numerical integration. Based on Sobol's variance decomposition (Sobol 1976), first-order and total effect sensitivity indices are determined.

The robustness of the framework for requirement derivation was explored through two MDO problem definitions which differ by complexity and fidelity, summarised in Table 2. Results from both problems are presented in the results section. Orbits are described by the Keplerian elements n mean angular motion, e eccentricity, i inclination, Ω right ascension of the ascending

node, u argument of latitude while E represents accumulative radiation dose experienced by the reference satellite.

Table 2: Summary of MDO Problem Definitions

	Problem Definition 1	Problem Definition 2
Decision variables	$0.0471705 < n < 0.063414$ deg/s	
Cluster initial state	$0 < e < 0.005$ $0 < i < 180$ deg	
Search Space	$0 < \Omega < 360$ deg $0 < u < 360$ deg	
Manoeuvre	$\{\Delta H_{sub} = \Delta H_{super}\}$ for $ \alpha_{sub} = \alpha_{super} $	Unique $\{\Delta H\}$ for α
Search space	$0 < \Delta H_{30^\circ, 60^\circ, 90^\circ} < 40$ km $0 < \Delta H_{120^\circ, 150^\circ, 180^\circ} < 60$ km	$0 < \Delta H < 50$ km
Objective functions	$f_1 = (\sum \Delta V_{x,y,z})$ km/s (3) Minimise $f_2 = \Delta t_{phase}$ sec (4) Minimise $f_3 = E_{total}$ rads (5) Minimise	
Constraint functions	Valid solution $\rightarrow g = 1$ Infeasible solution $\rightarrow g = -1$	
Propagator Fidelity	<ul style="list-style-type: none"> • Earth: J2 effect only 	<ul style="list-style-type: none"> • Earth: GRACE gravity model 03 (degree, order = 50) with ocean tides (degree = 4) • Atmosphere: NRLMSISE 2000 • Moon: GRAIL gravity model 0660B (degree, order = 8) • Sun: ZonalsToJ4 (degree = 4) • Third-body effects of Mercury, Venus, Phobos, Deimos, Mars, Ceres, Jupiter system, Saturn system, Neptune system, Uranus system & Pluto system • General relativity acceleration correction
Numerical integration	Runge-Kutta-Fehlberg integration method of 7 th order with 8 th order error control	

MDO for the listed objective functions in both problem definitions seek to identify global Pareto-optimal and feasible solutions by simultaneously minimising Eqs. (3) – (5). The quality of a feasible solution is evaluated as a vector, f , with a corresponding decision vector x . Pareto-optimal solutions are said to be non-dominant such that no vector exists for $f(x) \leq f(x')$ with $f_o(x) < f_o(x')$ supposing $o = \{1,2,3\}$. This quality is often expressed as if a solution is not worse than another solution in all objectives, and the solution is strictly better than the other in at least one objective, the solution dominates the other.

Results

Multi-objective design optimisation assisted by surrogate modelling has been completed for Problems 1 & 2. Problem 1 was performed over 50 generations, with a population size of 96 individuals. Of the 4800 functional evaluations, 3503 were found to be feasible solutions. Figure 7 displays the non-dominated (Pareto-optimal) solutions with the entire truly evaluated population in the style of tri-objective projection upon three planes for Problem 1. Figure 8 displays only the non-dominated solutions for MDO Problem Definition 2 derived from the high-fidelity modeling environment, performed over 30 generations.

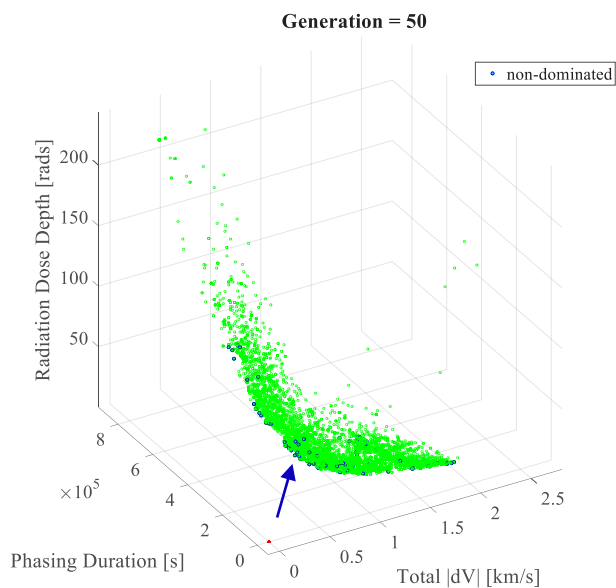


Fig. 7: - Problem 1 solution in 3D

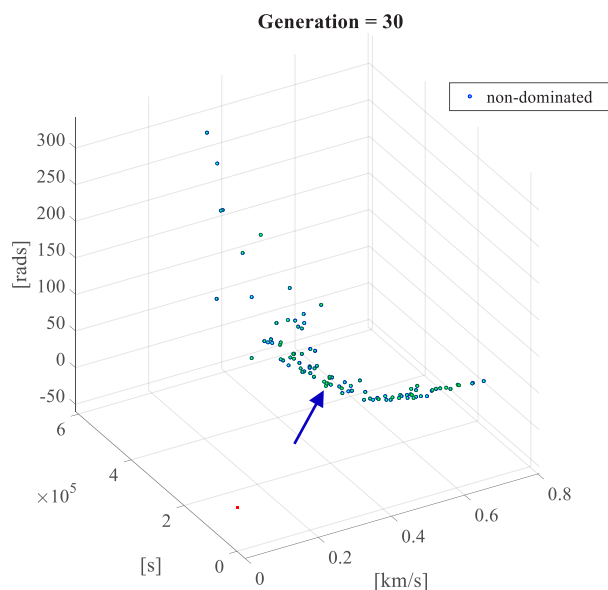
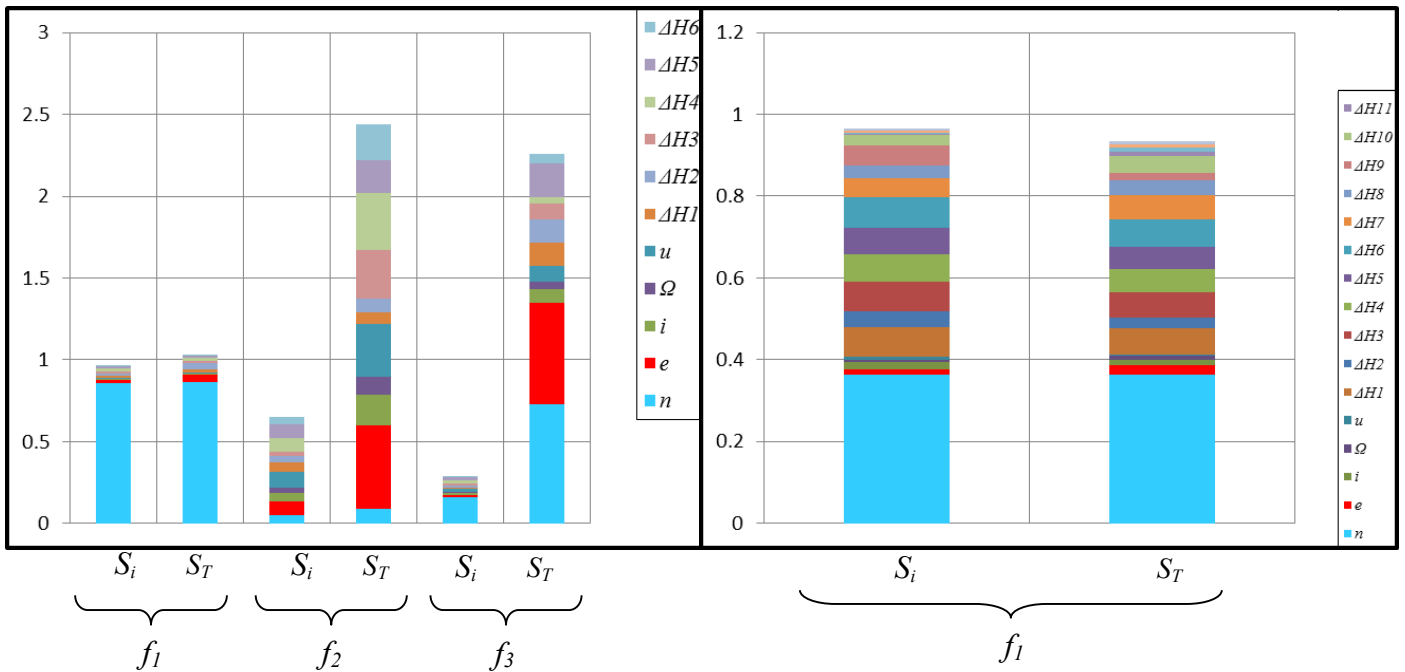


Fig. 8: - Problem 2 solution in 3D

It is observed in Figs. 7 and 8 non-dominated solutions reveal deterministic behaviour between f_1 with obvious performance trade-offs with other objectives. Indicated by the arrow, optimal constellation design configurations exist about $f_1 \approx 0.47$ km/s and $f_2 \approx 70$ hours for both problem definitions with a number of solutions exhibiting local f_3 minima. Low radiation doses experienced by the reference satellite can be explained by the low operating altitude of the spacecraft as well as cluster initial states found to be favourable for this objective. Specifically, the initial state (determined by decision variables) which put the cluster on a trajectory out of the domain of the Earth's inner Van Allen radiation belt significantly reduce radiation dose depth to low levels in the order of hundreds of millirads to orders of magnitudes larger. However, radiation dose is significantly increased if ΔV and time optimal trajectories exhibit several revisits over the South Atlantic Anomaly during the mission, increasing radiation dose depth experienced to the order of a hundred *rads*.

Variance-based global sensitivity analysis was performed for the 3 objective functions for Problem Definition 1, presented in Fig. 9 while Fig. 10 presents the first order, S_i , and total-effects, S_T , of f_1 as measured in the high-fidelity modelling environment.



Figs. 9 & 10: - Problem 1 Sensitivity Analysis (Left) and Problem 2 Sensitivity Analysis (Right)

Surrogate models trained over the course of optimisation were employed to extrapolate the sample to $N = 50,000$ and conducted the sensitivity analysis to acceptable accuracy. For Problem Definition 1, it was found that the responsive surface model performed best for predicted ΔV values however Problem Definition 2 elected the use of kriging approximation. It is notable that operational altitude by virtue of mean motion has a major influence on f_1 for both Problem Definitions, as well as f_3 however it is not a significant influence on f_2 . The difference between the total-effects and first order indices for f_2 and f_3 indicates interaction with most of the decision variables to a higher degree than f_1 . Additional performance parameters may be warranted in future studies to gain further insight. Furthermore, granting satellites and the MDO algorithms to make decisions on individual satellites yields a noteworthy finding shown in Fig. 10; the influence of each manoeuvre decision shows similar effect by magnitude on f_1 between the decisions, as well as a comparable influence to the altitude of the initial state.

Conclusion

A computational optimisation study utilising precise numerical integration and validated optimisation methodologies was conducted to derive high-level spacecraft requirements for a conceptual constellation consisting of 12 co-planar satellites. Specifically, surrogate assisted multi-objective design optimisation coupled with STK was used to perform two optimisation studies in response to commercial trends involving miniaturised spacecraft. A global sensitivity analysis for a large sample ($N = 50,000$) based on suitably performing surrogate models identified that all of the decisions considered, initial state mean motion of the cluster was the most significant design parameter with respect to ΔV , followed closely by manoeuvring requirements, namely target phasing altitudes ΔH . Additionally, specific orbital configurations provided insight to very high performing constellations for single objectives, of particular interest, radiation dose depth. Use of the framework has demonstrated its potential for research organisations and private enterprise concerned with miniaturised satellite concepts that may have scarce space engineering experience. The study has also demonstrated the appropriation

of the employed methodology in alignment with an SE approach applied to complex, inter-disciplinary design problems by which the results of the study provide insight to performance trade-offs and justified high-level system requirement derivation with objectivity, in an automated manner.

References

1. Evans, B. G., "Satellite Communication Systems." London, UK, *Peregrinus On Behalf of The Institution of Electrical Engineers*, 1999.
2. Heidt, H., Puig-Suari, J., Moore, A., Nakasuka, S. and Twiggs, R., "CubeSat: A New Generation of Picosatellite for Education and Industry Low-Cost Space Experimentation." *14th Annual AIAA/USU Conference on Small Satellites*, 2000.
3. Woellert, K., Ehrenfreund, P., Ricco, A. J. and Hertzfeld, H., "Cubesats: Cost-Effective Science and Technology Platforms For Emerging and Developing Nations." *Advances In Space Research*, Vol. 47, No. 4, 2008, pp. 663-684.
4. Muteanu, A., "Nanosat/Cubesat Constellation Concepts." Master's Thesis, Cranfield University, 2009.
5. Toorian, A., Diaz, K. and Lee, S., "The CubeSat Approach To Space Access", *EEE Aerospace Conference*, 2008.
6. Lee, S., Hutputanasin, A., Toorian, A., Lan, W. & Munakata, R., "Cubesat Design Specification". Available: <www.cubesat.org>
7. N.A.S.A., "Educational Launch of Cubesats", Available: <http://www.nasa.gov/Mission_Pages/Smallsats/Elana/>
8. Crisp, N., Smith, K. and Hollingsworth, P., "Small Satellite Launch to LEO: A Review of Current and Future Launch Systems", *29th International Symposium on Space Technology and Science*, 2014.
9. Lowe, C. and Macdonald, M., "Rapid Model-Based Inter-Disciplinary Design Of A Cubesat Mission", *Acta Astronautica*, Vol. 105, No. 1, 2014, pp. 321-332.
10. Crisp, N., Smith, K. and Hollingsworth, P., "Launch and Deployment of Distributed Small Satellite Systems." *Acta Astronautica*, Vol. 114, 2015, pp. 65-78.
11. Charania, A., Isakowitz, S., Pomerantz, W., Morse, B. and Sagis, K., "Launcherone: Revolutionary Orbital Transport For Small Satellites", *27th Annual AIAA/USU Conference On Small Satellites*, 2013.
12. Waydo, S., Henry, D. and Campbell, M. "CubeSat Design For LEO-Based Earth Science Missions", *IEEE Aerospace Conference*, 2002.

13. Barnhart, D. J., Vladimirova, T. & Sweeting, M. N., "Very-Small-Satellite Design For Distributed Space Missions", *Journal of Spacecraft and Rockets*, Vol. 44, No. 6, 2007, pp. 1294-1306.
14. Boshuizen, C., Mason, J., Klupar, P. and Spanhake, S., "Results From The Planet Labs Flock Constellation", *28th Annual AIAA/USU Conference On Small Satellites*, 2014.
15. Dyer, J., Dinardi, A. and Anflo, K., "First Implementation of High Performance Green Propulsion in A Constellation of Small Satellites." *27th Annual AIAA/USU Conference On Small Satellites*, 2013.
16. Anthes, R. A., Ector, D., Hunt, D., Kuo, Y., Rocken, C., Schreiner, W., Sokolovskiy, S., Syndergaard, S., Wee, T. and Zeng, Z. "The Cosmic/Formosat-3 Mission: Early Results", *Bulletin of The American Meteorological Society*, Vol. 89, 2008, No. 3, pp. 313-333.
17. INCOSE, "INCOSE Systems Engineering Handbook: A Guide For System Life Cycle Processes and Activities", John Wiley & Sons Ltd., 2000.
18. Aguilar, J. A., Dawdy, A. B. and Law, G. W. "The Aerospace Corporation's Concept Design Center", *8th Annual International Symposium Of The International Council On Systems Engineering*, 1998.
19. Spangelo, S. C., Cutler, J., Anderson, L., Fosse, E., Cheng, L., Yntema, R., Bajaj, M., Delp, C., Cole, B. and Soremekum, G., "Model Based Systems Engineering (MBSE) Applied To Radio Aurora Explorer (RAX) Cubesat Mission Operational Scenarios", *IEEE Aerospace Conference*, 2013.
20. Chaieb, S., Wegerson, M., Kading, B., Straub, J., Marsh, R. and Whalen, D., "The OpenOrbiter CubeSat as a System-Of-Systems (SoS) and How SoS Engineering (SoSE) Aids CubeSat Design", *10th System Of Systems Engineering Conference (SoSE)*, 2015, pp. 47-52.
21. Chen, P. and Clothier, J., "Advancing Systems Engineering for Systems-Of-Systems Challenges", *Systems Engineering*, Vol 6. No. 3, 2003, pp.170-183.
22. Lowe, C. and Macdonald, M., "Rapid Model-Based Inter-Disciplinary Design Of A Cubesat Mission", *Acta Astronautica*, Vol. 105, No. 1, 2014, pp. 321-332.
23. Puig-Suari, J., Turner, C. and Twiggs, R., "Cubesat: The Development and Launch Support Infrastructure for Eighteen Different Satellite Customers On One Launch", *15th Annual AIAA/USU Conference On Small Satellites*, 2001.
24. Chaize, M., "Enhancing the Economics of Satellite Constellations via Staged Deployment and Orbital Reconfiguration", Master's thesis, Massachusetts Institute of Technology, 2003.
25. Larson, W. J. and Wertz, J. R., "Space Mission Analysis and Design." Microcosm, Inc., California, 1992.

26. Anderson, J. D., "Introduction To Flight", Mcgraw-Hill Ltd, Boston, 2005.
27. Woffinden, D. C. and Geller, D. K., "Navigating The Road To Autonomous Orbital Rendezvous." *Journal of Spacecraft and Rockets*, Vol. 44, No. 4, 2007, pp. 898-909.
28. Ray, T., Isaacs, A. and Smith, W., "Surrogate Assisted Evolutionary Algorithm For Multi-Objective Optimization", *47th AIAA/ASME/ASCE/AHS/ASC Structures, Structural Dynamics and Materials Conference*, 2006.
29. Deb, K., Pratap, A., Agarwal, S. and Meyarivan, T., "A Fast and Elitist Multiobjective Genetic Algorithm: Nsga-Ii. Evolutionary Computation", *IEEE Transactions on Evolutionary Computation*, Vol. 6, 2002, pp. 182-197.
30. Savitri, T. and Bang, H., "Multi Objective Optimization Of Satellite Constellation Orbit Design Using NSGA-II." *Korean Society for Aeronautical & Space Sciences Spring Conference*, 2014, pp. 733-736.
31. Hinds, C. A., "A Pareto-Frontier Analysis of Performance Trends for Small Regional Coverage Leo Constellation Systems", Master's Thesis, California Polytechnic State University, 2014.
32. Jilla, C. D. and Miller, D. W., "Multi-Objective, Multidisciplinary Design Optimization Methodology For Distributed Satellite Systems." *Journal of Spacecraft and Rockets*, Vol. 41, No. 1, 2004, pp. 39-50.
33. Ferringer, M. P., Spencer, D. B. and Reed, P., "Many-Objective Reconfiguration of Operational Satellite Constellations with The Large-Cluster Epsilon Non-Dominated Sorting Genetic Algorithm-Ii", *IEEE Congress on Evolutionary Computation*, 2009. pp.340-349.
34. Wang, L., Wang, Y., Chen, K. and Zhang, H., "Optimization Of Regional Coverage Reconnaissance Satellite Constellation By NSGA-II Algorithm", *International Conference On Information and Automation*, 2008.
35. De Weck, O. L., Scialom, U. and Siddiqi, A., "Optimal Reconfiguration of Satellite Constellations with The Auction Algorithm." *Acta Astronautica*, Vol. 62, 2008, pp. 112-130.

Evaluation of Current and Projected CubeSat Propulsion Technologies for Navigating Cislunar Space

Noor Taofiqul Huq and Andrew G Dempster

Australian Centre for Space Engineering Research, Faculty of Engineering, UNSW Australia, University of New South Wales, Sydney, New South Wales 2052, Australia

Summary: The CubeSat architecture has reduced the cost of access to space significantly, allowing small organisations the ability to access Low Earth Orbit. Many groups have begun developing miniature propulsion systems to aid CubeSats in extending mission length. A propulsion system carrying sufficient energy will open the door for CubeSat missions beyond Low Earth Orbit, such as to the Moon. This research evaluates current and upcoming CubeSat propulsion systems capable of propelling a 6U CubeSat to beyond the Moon's orbit. Research has been undertaken into the work being done in CubeSat propulsion. The BET-1mN, BET-100 μ N, BIT-3 and CubeSat Ambipolar Thruster are identified as the most promising thrusters under development. Two body and three body models are used to show that each of these thrusters could pass the Moon in less than 500 days. The feasibility of using current and future propulsion systems aboard CubeSats for beyond LEO missions is demonstrated.

Keywords: CubeSat, propulsion, survey, orbital mechanics, spiral transfer, beyond LEO, cislunar

Introduction

CubeSats are the leading standard for nanosatellites, a class of satellite within the mass range of 1-10kg. The basic CubeSat consists of a 10x10x10cm box (1U), while larger versions will consist of multiples of these units attached together. For example, a 10x10x30cm CubeSat will be a 3U CubeSat, and a 10x20x30cm CubeSat will be a 6U CubeSat. Each U of a CubeSat weighs 1.33kg or less. [1] [2] CubeSat technology has been enabled by rapid advances in miniaturised consumer electronics, as seen in tablets and smartphones. Much of the hardware used on CubeSats is standardised and can be bought off the shelf, dropping the costs of manufacturing a CubeSat to as low as \$50,000 per unit. [3] The small size of CubeSats allows them to hitchhike into orbit on launches of larger spacecraft. These rideshare agreements enable a launch cost of less than \$100,000 per unit. [4] Emerging small rocket launchers such as Rocket Lab promise to drop the price even further, to as low as \$50,000 per unit. [5] These low construction and launch costs have enabled the development of the NewSpace sector of the spacecraft industry. A key example of this is Earth imaging company Planet. [6] Academia has also taken advantage of the CubeSat platform, as seen with the upcoming QB50 mission, which will explore the lower thermosphere. [7]

To date, CubeSats have not used propulsion systems to the degree that traditional spacecraft do. This means that drag from Earth's upper atmosphere inevitably robs CubeSats of the energy required to maintain orbit, resulting in a fiery end of life for most CubeSats after only a year or two in orbit. [8] [9] [10] CubeSats have generally not utilised propulsion systems as an increased mission length does not justify the extra costs involved. [9] However, for CubeSats to become as feasible and attractive to industry and academia for beyond Low Earth Orbit (LEO) missions as they have become for LEO missions, this research proposes that CubeSat propulsion systems will be necessary.

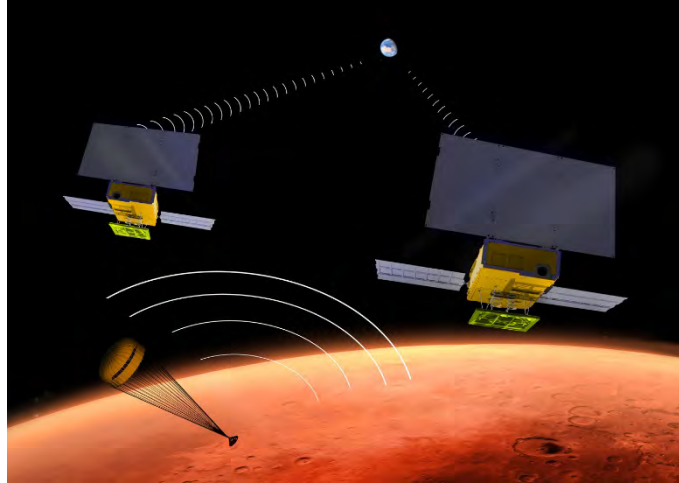


Figure 1 – An artist's impression of JPL's MarCO mission performing its relay mission at Mars. [11]

Proposed beyond LEO missions for CubeSats, such as JPL's MarCO (shown in Figure 1) and Cornell University's Cislunar Explorers will be ridesharing missions. MarCO will be boosted to a Mars transfer trajectory with Mars InSight aboard an Atlas V 401 and Centaur in May 2018. Cislunar Explorers will launch on Exploration Mission 1 (EM-1) aboard the Space Launch System (SLS) in September 2018. EM-1 is to fly a free return trajectory around the Moon. [11] [12] [13] [14] [15] While these missions are expected to provide significant research outcomes, the fact that they require rideshare agreements on pre-existing missions removes much of the cost and flexibility advantages of ridesharing. For example, the cost of each SLS launch is expected to fall between \$500 and \$700 million, and the second launch of SLS will not occur until 2023. [16] Without government subsidy, part of this immense launch cost must be assumed by prospective beyond LEO CubeSat developers. The scarcity of launches ensures that competition for space aboard the SLS launches will be fierce. As for Mars, regular ridesharing opportunities may become available on missions launched by space agencies due to the regularity of Mars launch windows. However, a lack of a sufficiently powerful propulsion system on a CubeSat mission to Mars will preclude the possibility of achieving Mars orbit on most missions, limiting the data that can be harvested. In addition, missions to asteroids have been irregularly spaced to date. [17] As such, there are no regular opportunities for missions to asteroids, leading to the same issues as for launching on the SLS.

To solve these issues, this research proposes that CubeSats conducting missions beyond LEO, such as for exploring the Moon, asteroids or Mars, carry a propulsion system of sufficient power and energy to reach the mission target with no outside assistance. In this research, a hypothetical mission architecture consisting of a CubeSat travelling beyond Lunar orbit is considered. The key design specifications and constraints of such a mission are:

- The mission rideshares to or near Geostationary Orbit (GEO);
- The spacecraft is a 6U system with a dry mass of 8kg;
- Carries a propulsion system and enough fuel for 2500m/s Δv ; and
- Capable of passing Lunar orbit in 500 days or less.

While the challenges involved in designing and executing such a mission are various, the main focus of this research is on the propulsion subsystem. The aim of this research is to evaluate the current state of CubeSat propulsion in the context of the aforementioned hypothetical cislunar

CubeSat mission. An online survey of organisations developing CubeSat propulsion systems has been conducted. The specifications of 30 propulsion systems are recorded from 14 organisations, ranging from commercial entities to universities. Of these, 7 electric propulsion systems are identified as suitable for a cislunar CubeSat mission by examining their specifications. The field is further narrowed to 4 systems using examinations of their scalability and an estimation of the time they would need to propel the CubeSat past lunar orbit using a 2 body approximation. These 4 engines are finally tested in a Restricted Circular 3 Body Problem (RC3BP) model created using numerical computation software Octave. The 4 propulsion systems are finally compared in terms of the length and variance of time required to pass lunar orbit. Conclusions are drawn on the state of the CubeSat propulsion industry and the feasibility of a cislunar CubeSat mission.

Prospective CubeSat Missions Beyond LEO

The rise of CubeSats in the spacecraft industry represents a significant opportunity for scientific missions beyond LEO. This has been encouraged by the National Aeronautics and Space Administration (NASA) with EM-1 set to take 13 CubeSats to beyond LEO in the inaugural launch of the SLS in September 2018. Ten of these 13 CubeSats have already been determined. These are:

- Skyfire – will perform a flyby of the Moon and improve knowledge of the Lunar surface;
- Lunar IceCube – will search for water ice and other resources from Lunar orbit;
- Near-Earth Asteroid Scout (NEA Scout) – will perform reconnaissance of a Near Earth asteroid;
- Bio Sentinel – will measure the effect of deep space radiation on living creatures through use of yeast;
- Lunar Flashlight – will look for ice deposits and places from which resources can be extracted from the Moon;
- CubeSat to study Solar Particles (CuSP) – will measure particles and magnetic fields in space and act as a space weather station; and
- Lunar Polar Hydrogen Mapper (LunaH-Map) – will map hydrogen at the Moon’s south pole.
- Equilibrium Lunar-Earth point 6U Spacecraft (EQUULEUS) – will improve understanding of the radiation environment around the Earth;
- Outstanding Moon exploration Technologies demonstrated by Nano Semi-Hard Impactor (OMOTENASHI) – will attempt to land on the Moon; and
- Argomoon – will perform operations in close proximity to the Interim Cryogenic Propulsion Stage. [18]

Three missions are being determined from NASA’s ongoing Cube Quest Challenge. Another three missions are to be sourced from the international community. [19] Of the participants in the Cube Quest Challenge, the following missions have made the top 5 in both competition stages so far:

- Cislunar Explorers – will perform technology demonstrations, including water propulsion and optical navigation; [13]
- MIT Kitcube – will attempt to enter lunar orbit and test a laser communication system; [20] and
- Team Miles – will attempt to enter lunar orbit and then navigate to an asteroid. [21] [22]

The Jet Propulsion Laboratory (JPL) is also working on the Mars Cube One (MarCO) mission that will rideshare aboard the Mars InSight mission to Mars. Twin 6U CubeSats are to be deployed from Mars InSight, and will relay information from Mars InSight as it attempts to land on the surface of Mars. [11] MarCO and Mars InSight are expected to launch in May 2018. [12]

Table 1 – List of beyond LEO missions either chosen or expected to be chosen for launch [23] [13] [20] [21] [24]

Mission	Organisation/s	Goal	Propulsion
Skyfire	Lockheed Martin	Lunar flyby	
Lunar IceCube	Morehead State University	Low Lunar Orbit	Ion engine
NEA Scout	Marshall SFC	Asteroid slow flyby	Solar Sail
Bio Sentinel	Ames Research Center	Heliocentric orbit	
Lunar Flashlight	JPL, UCLA, Marshall	Lunar Polar Orbit	Green monopropellant
CuSP	Southwest Research Institute	Heliocentric Orbit	
LunaH Map	Arizona State University	Lunar Polar Orbit	Solar Sail
EQUULEUS	JAXA, University of Tokyo	Lunar flybys	
OMOTENASHI	JAXA, University of Tokyo	Lunar landing	Unknown
Argomoon	Argotec	Heliocentric orbit	
Cislunar Explorers	Cornell University	Lunar orbit	Water electrolysis
KitCube	MIT	Lunar orbit	Green monopropellant
Miles	Team Miles	Lunar orbit, asteroid flyby	Unknown
MarCO	Jet Propulsion Laboratory	Mars flyby	Green monopropellant

Of the 14 beyond LEO CubeSat missions discussed here, 9 are expected to employ propulsion systems, as seen in Table 1. Of these, 2 missions will employ solar sails, which, while promising, are not considered in this research. The propulsion methods of 2 missions are unknown. Of the 5 remaining, 3 use green monopropellant thrusters, 1 uses water electrolysis and combustion, and the other makes use of an ion engine. It is apparent here that these CubeSat missions plan to take advantage of the considerable amounts of energy the SLS will provide them. The missions carrying propulsion systems need to carry only small amounts of Δv to take advantage of ballistic captures and gravitational assists. Low specific impulse chemical propulsion systems are thus acceptable. Such systems would need to be scaled enormously if CubeSats are to use them to travel from Earth orbit to the Moon, asteroids or Mars. Propulsion methods and their advantages and disadvantages are discussed further in the Propulsion System Survey.

Concept for a Self-Propelled Cislunar CubeSat

Propulsion systems evaluated in this research will be evaluated in the context of a hypothetical Lunar flyby CubeSat mission. Such a mission would be capable of conducting flybys of the Moon and asteroids, or impactor missions. Entering lunar orbit may also be possible, but is not considered in this research. The specifications and constraints of this mission are chosen to

minimise cost and maximise flexibility in launch opportunities. These specifications and constraints are identified and justified in this section.

Ridesharing to GEO

The Cislunar CubeSat mission is to rideshare to GEO aboard Space System Loral's (SSL) Payload Orbital Delivery System (PODS) [25] or a similar system. The CubeSat should ideally be launched into a Supersynchronous Orbit (SSO) just above GEO to mitigate the risk of colliding with valuable GEO satellites. After deployment, the CubeSat will then begin propelling itself outwards. Deployment from GEO is chosen ahead of LEO due to issues with fuel requirements. As calculated using the equations for a low thrust spiral transfer described by Stansbury [26], travelling from a GEO orbit to a circular orbit of Lunar altitude requires only 2.07km/s of Δv . Travelling from LEO to a circular orbit of Lunar altitude requires in excess of 6.5km/s of Δv . Carrying the amount of fuel required to travel from a starting orbit in LEO is not feasible for a CubeSat. In terms of flexibility of opportunities, LEO deployment of CubeSats is well established compared to GEO deployment of CubeSats. As such, in the short term until SSL's PODS system becomes a mature service, there is a loss of flexibility in launch opportunities. In the medium to long term, however, the large number of GEO satellite launches per year will ensure flexibility of accessing GEO launch opportunities for CubeSats will approach that of LEO launch opportunities.

6U Bus

A 6U CubeSat bus is chosen for this mission. The 6U size is an intermediate CubeSat size from which the spacecraft could be scaled up or down as necessary. The CubeSats described in the Prospective CubeSat Missions Beyond LEO section are all 6U CubeSats. In addition, Nanoracks is now providing the ability to deploy 6U and 12U CubeSats from the International Space Station (ISS), signalling that the 6U bus is becoming an accepted standard for CubeSat design. [27] An image of a 6U CubeSat bus is shown in Figure 2.

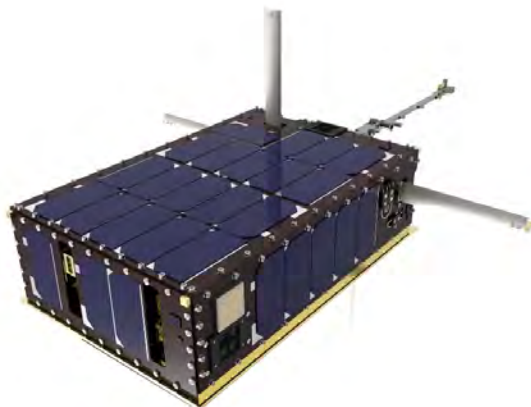


Figure 2 – An artist's impression of a 6U CubeSat. [28]

Propulsion system carrying 2500m/s Δv

The Cislunar CubeSat mission should carry approximately 2500m/s of Δv for this mission. As will be described in the Selection using 2 Body Model section, approximately 2.07km/s of Δv is estimated to be required to progress a spiral transfer from GEO to beyond Lunar orbit. An additional 430m/s of Δv is allocated to round off the amount that is carried to 2500m/s. The

reason for this is that the actual 3 body simulation may require a greater amount of fuel for the mission than is estimated. In addition, in an actual mission, additional Δv not used up in the spiral transfer may be used for station keeping, off-axis manoeuvres for changing direction, and for entering orbit.

Capable of passing Lunar orbit within 500 days

The mission is to be allowed no more than 500 days to pass the orbit of the Moon. The 500-day figure itself is somewhat arbitrary and chosen to allow examination of the 4 propulsion systems chosen in the Selection using 2 Body Model section. However, the need to set a time limit on mission length is important for spacecraft missions and CubeSats in general due to the expense of operating a spacecraft, and the increasing need for heavy radiation countermeasures the longer a mission is stretched. Currently CubeSats deployed from the ISS have operational lifespans of around 2 years. [9] Considering this, allowing 500 days of travel time is quite reasonable.

Propulsion System Survey

An extensive online survey of propulsion systems was conducted. 30 CubeSat propulsion systems were found from 13 organisations with varying levels of information available on their specifications. Propulsion systems were found through the websites of research and development organisations and through research papers published via conferences and journal papers. Organisations whose propulsion systems were examined are shown in Table 2. Time constraints ensured that the survey done was not completely exhaustive. Nonetheless, this survey is a sufficient overview of the state of the CubeSat propulsion industry.

Table 2 – An overview of the organisations whose propulsion systems were surveyed in this research.

Organisation	Systems	Organisation	Systems
Busek	7	Micro Aerospace	2
CubeSatShop	1	Firestar	1
Aerojet Rocketdyne	6	George Washington University	1
VACCO	6	MIT	1
University of Michigan	1	USYD	1
Tethers Unlimited	1	ANU	1
Surrey Satellite Technologies	1		

Initial Classification

Of the 30 propulsion systems examined as part of the propulsion system survey, specifications on thrust, specific impulse (I_{SP}) and system mass were available for 18 of these systems. This allows classification of these 18 propulsion systems according to their I_{SP} and Thrust-to-Weight Ratio (TWR). This classification is shown in Figure 3. This chart can be used to classify these 18 propulsion systems into three groups:

- Pressure fed and microresistojet systems (middling TWR and low I_{SP}) in the green ellipse;
- Chemical propulsion systems (high TWR and low I_{SP}) in the red ellipse; and
- Electric propulsion systems (low TWR and high I_{SP}) in the purple ellipse.

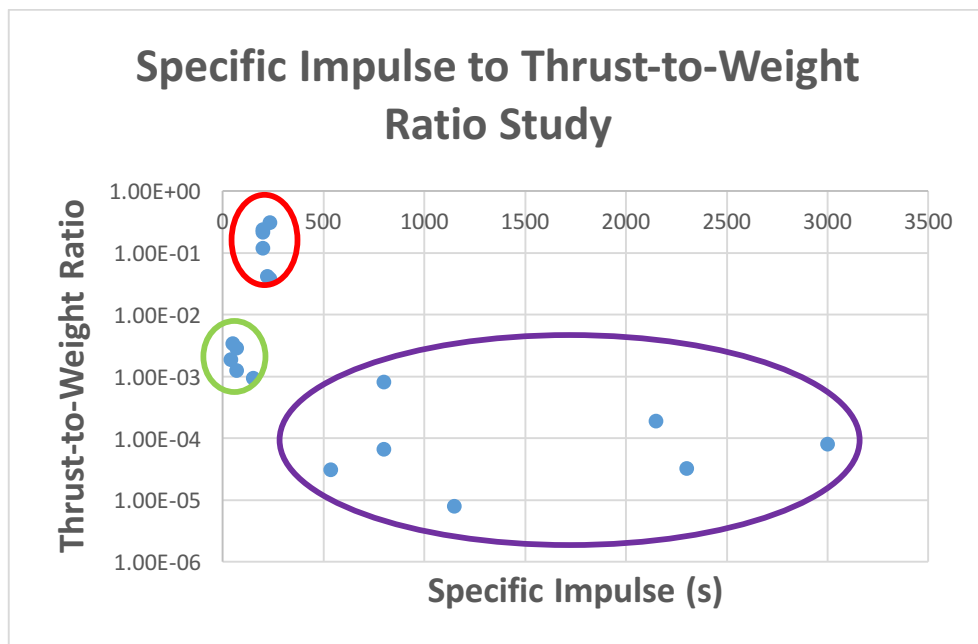


Figure 3 – Specific Impulse to Thrust-to-Weight Ratio study of 18 CubeSat propulsion systems. The green ellipse encircles pressure fed and microresistojet systems, the red ellipse encircles chemical systems, and the purple ellipse encircles electric propulsion systems.

The volume constraint of CubeSats suggests that the high I_{SP} electric propulsion systems are best for a Cislunar CubeSat mission. Immense propellant tanks far beyond the volume available in a 6U CubeSat would be needed to use the low I_{SP} pressure fed and microresistojet, and chemical propulsion systems. The 7 electric propulsion systems thus proceed to the next selection stage. However, of these 7 systems, the George Washington University’s Micro Cathode Arc Thruster (μ CAT) is unsuitable due to its inability to scale well. This inability to scale well is due to the fact that the solid fuel it uses must be built into the engine itself, requiring redesign of the entire engine for the Cislunar CubeSat mission. [29] This engine is thus eliminated.

Selection using 2 Body Model

Due to the choice of low thrust electric propulsion, the instantaneous impulse change assumption used for Hohmann transfers is not valid. As such, if the 6 CubeSat electric propulsion systems are to be tested under the 2 body problem, it must be assumed that they will use spiral transfers. The difference between a spiral transfer trajectory and a Hohmann transfer trajectory is shown in Figure 4. While a spiral transfer will take a longer amount of time and fuel than a Hohmann transfer, Hohmann transfers are simply not possible if thrust is too low, as is typically the case with electric propulsion. [26]

To compare the 6 remaining electric propulsion systems in a 2 body system, the system of equations described by Stansbury must be used. [26] These equations describe the amount of Δv required to progress from one circular orbit to another circular orbit using a spiral transfer. The generalised procedure for these questions is:

1. Determine the initial and final velocities at the initial and starting orbits;
2. Determine the acceleration of the spacecraft from the spacecraft’s mass and thrust;
3. Calculate the required spiral transfer Δv using the provided equations; and
4. Divide the required Δv by the acceleration to find time required to complete the transfer.

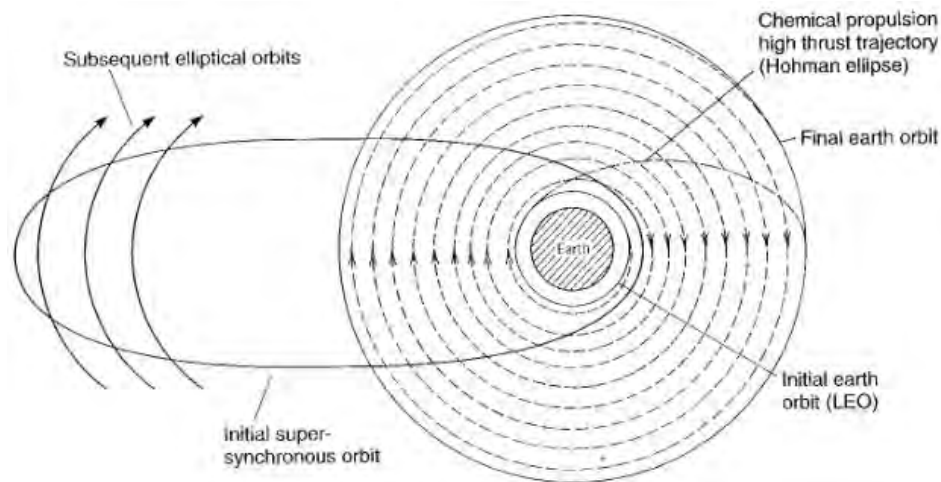


Figure 4 – Different methods of transfer from LEO to GEO. Of note are the high thrust trajectory taken during a Hohmann transfer, and the low thrust spiralling outwards of the spiral transfer trajectory. [26]

By calculating the time required to transfer from GEO to a circular orbit of equal energy to the orbit of the Moon, the performance level of each engine was determined. Of the 6 electric propulsion engines that were chosen in the previous section, 2 are eliminated due to having too low thrust to make the 500 day cut-off. The 4 selected propulsion systems are the BET-1mN, the BET-100 μ N, the BIT-3, and the CubeSat Ambipolar Thruster (CAT).

This method suffers from a few key issues. Being a restricted 2 body model, only the gravity of the Earth is taken into account. This method cannot model the gravity and motion of the Moon. The acceleration number used can only take one value for mass, and is thus time invariant in a system in which acceleration will increase as the spacecraft's mass decreases due to using up fuel. The mass number used for calculations here is the spacecraft's dry mass plus half of the fuel mass. Finally, this method assumes that the spacecraft will move from a circular orbit to another circular orbit. This assumption may not hold true, as the propulsion system may be sufficient to propel the spacecraft to Earth escape before reaching the orbit of the Moon.

While these issues are significant, the Stansbury method for spiral transfer calculations remains a good way to provide validation to a numerical 3 body model. The numerical 3 body model used will be described in the Modelling Engines using R3CBP in Octave section. This model will be able to overcome the issues encountered in the Stansbury method.

Selected Propulsion Systems

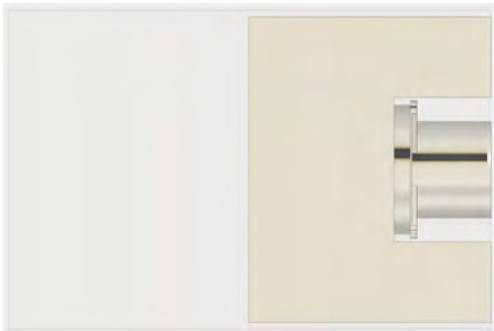
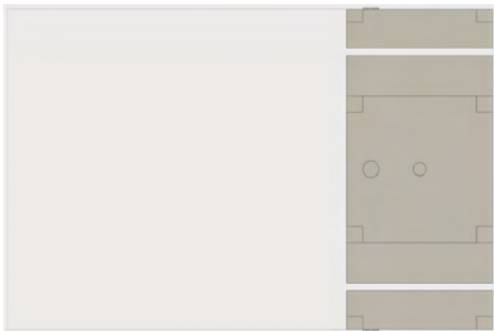
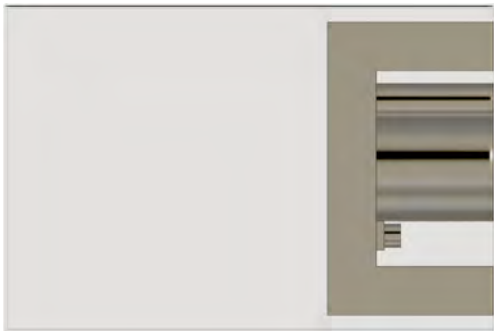
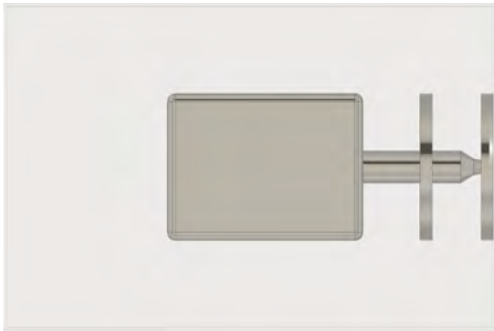
Specifications and mock-ups of each of the chosen propulsion systems are provided in Table 3.

Even these highly efficient electric propulsion systems require significant fractions of the 6U volume. Even the most efficient of these engines, the BET-100 μ N and BIT-3 leave only 4U for the other subsystems and payload. This demonstrates that the less efficient propulsion systems listed previously would require too much of a 6U CubeSat's volume to be viable.

Of these engines, it is worth noting that there is significant doubt as to the veracity of the claimed thrust level of the CAT system. The fact that it has a very low technology readiness level (TRL) is

further indication of this. However, as it requires a significant amount of power to run, the system will still be modelled in this research.

Table 3 – Specifications and mock-ups of each of the chosen propulsion systems. Each propulsion system is shown with the required fuel volume inside a 6U CubeSat. The thrust vector for each propulsion system is to the right.

BET-1mN [30]																			
	<table border="1"> <thead> <tr> <th>Specification</th> <th>Value</th> </tr> </thead> <tbody> <tr> <td>Thrust (mN)</td> <td>0.7</td> </tr> <tr> <td>Specific Impulse (s)</td> <td>800</td> </tr> <tr> <td>Power Required (W)</td> <td>15</td> </tr> <tr> <td>Dry Mass (kg)</td> <td>1.06</td> </tr> <tr> <td>Technology Readiness Level</td> <td>7</td> </tr> <tr> <td>Propellant</td> <td>Ionic liquid</td> </tr> <tr> <td>Prop. Volume Required (mL)</td> <td>1936</td> </tr> <tr> <td>Time to pass Lunar Orbit (days)</td> <td>319.5</td> </tr> </tbody> </table>	Specification	Value	Thrust (mN)	0.7	Specific Impulse (s)	800	Power Required (W)	15	Dry Mass (kg)	1.06	Technology Readiness Level	7	Propellant	Ionic liquid	Prop. Volume Required (mL)	1936	Time to pass Lunar Orbit (days)	319.5
	Specification	Value																	
	Thrust (mN)	0.7																	
	Specific Impulse (s)	800																	
	Power Required (W)	15																	
	Dry Mass (kg)	1.06																	
	Technology Readiness Level	7																	
	Propellant	Ionic liquid																	
Prop. Volume Required (mL)	1936																		
Time to pass Lunar Orbit (days)	319.5																		
BET-100µN x 4 [31]																			
	<table border="1"> <thead> <tr> <th>Specification</th> <th>Value</th> </tr> </thead> <tbody> <tr> <td>Thrust (mN)</td> <td>0.4</td> </tr> <tr> <td>Specific Impulse (s)</td> <td>2300</td> </tr> <tr> <td>Power Required (W)</td> <td>22</td> </tr> <tr> <td>Dry Mass (kg)</td> <td>1.26</td> </tr> <tr> <td>Technology Readiness Level</td> <td>7</td> </tr> <tr> <td>Propellant</td> <td>Ionic Liquid</td> </tr> <tr> <td>Prop. Volume Required (mL)</td> <td>605</td> </tr> <tr> <td>Time to pass Lunar Orbit (days)</td> <td>498.5</td> </tr> </tbody> </table>	Specification	Value	Thrust (mN)	0.4	Specific Impulse (s)	2300	Power Required (W)	22	Dry Mass (kg)	1.26	Technology Readiness Level	7	Propellant	Ionic Liquid	Prop. Volume Required (mL)	605	Time to pass Lunar Orbit (days)	498.5
	Specification	Value																	
	Thrust (mN)	0.4																	
	Specific Impulse (s)	2300																	
	Power Required (W)	22																	
	Dry Mass (kg)	1.26																	
	Technology Readiness Level	7																	
	Propellant	Ionic Liquid																	
Prop. Volume Required (mL)	605																		
Time to pass Lunar Orbit (days)	498.5																		
BIT-3 [32]																			
	<table border="1"> <thead> <tr> <th>Specification</th> <th>Value</th> </tr> </thead> <tbody> <tr> <td>Thrust (mN)</td> <td>1.15</td> </tr> <tr> <td>Specific Impulse (s)</td> <td>3500</td> </tr> <tr> <td>Power Required (W)</td> <td>75</td> </tr> <tr> <td>Dry Mass (kg)</td> <td>1.5</td> </tr> <tr> <td>Technology Readiness Level</td> <td>4</td> </tr> <tr> <td>Propellant</td> <td>Xenon</td> </tr> <tr> <td>Prop. Volume Required (mL)</td> <td>195</td> </tr> <tr> <td>Time to pass Lunar Orbit (days)</td> <td>170.0</td> </tr> </tbody> </table>	Specification	Value	Thrust (mN)	1.15	Specific Impulse (s)	3500	Power Required (W)	75	Dry Mass (kg)	1.5	Technology Readiness Level	4	Propellant	Xenon	Prop. Volume Required (mL)	195	Time to pass Lunar Orbit (days)	170.0
	Specification	Value																	
	Thrust (mN)	1.15																	
	Specific Impulse (s)	3500																	
	Power Required (W)	75																	
	Dry Mass (kg)	1.5																	
	Technology Readiness Level	4																	
	Propellant	Xenon																	
Prop. Volume Required (mL)	195																		
Time to pass Lunar Orbit (days)	170.0																		
CubeSat Ambipolar Thruster [33] [34]																			
	<table border="1"> <thead> <tr> <th>Specification</th> <th>Value</th> </tr> </thead> <tbody> <tr> <td>Thrust (mN)</td> <td>20</td> </tr> <tr> <td>Specific Impulse (s)</td> <td>800</td> </tr> <tr> <td>Power Required (W)</td> <td>100</td> </tr> <tr> <td>Dry Mass (kg)</td> <td>2.5</td> </tr> <tr> <td>Technology Readiness Level</td> <td>2</td> </tr> <tr> <td>Propellant</td> <td>Xenon</td> </tr> <tr> <td>Prop. Volume Required (mL)</td> <td>968</td> </tr> <tr> <td>Time to pass Lunar Orbit (days)</td> <td>11.2</td> </tr> </tbody> </table>	Specification	Value	Thrust (mN)	20	Specific Impulse (s)	800	Power Required (W)	100	Dry Mass (kg)	2.5	Technology Readiness Level	2	Propellant	Xenon	Prop. Volume Required (mL)	968	Time to pass Lunar Orbit (days)	11.2
	Specification	Value																	
	Thrust (mN)	20																	
	Specific Impulse (s)	800																	
	Power Required (W)	100																	
	Dry Mass (kg)	2.5																	
	Technology Readiness Level	2																	
	Propellant	Xenon																	
Prop. Volume Required (mL)	968																		
Time to pass Lunar Orbit (days)	11.2																		

The high levels of power required by these engines cannot be realistically provided by solar panels currently available on the market, such as the GOMSpace P110, which only provides 37W/kg. [35] However, the advent of solar panels like the HAWK Solar Array developed by MMA Design will be sufficient. Each HAWK panel provides 36W of power, at a far superior 130W/kg. [36]

An important specification not considered in Table 3 is the working life of these thrusters. Working life for the BET-1mN and the BET-100 μ N is not explicitly given by Busek. It has been noted by another source that these engines face a lifetime challenge, and may not be able to burn for the hundreds of days required here. [37] This is a concern for these engines, but for the purposes of this research, it is assumed that this lifetime challenge will be solved. On the other hand, the BIT-3 and CAT are both expected to achieve working lives in excess of 20,000 hours (833 days) which is more than sufficient. [32] [33]

Modelling Engines using R3CBP in Octave

A 3-body model was constructed using numerical computation software Octave. The Earth and Moon were placed on circular approximations of their real world motion for the sake of simplicity. In other words, the Earth and Moon were put “on rails”. The relatively miniscule mass of the spacecraft meant that the gravitational forces exerted by the spacecraft on the Earth and Moon were not accounted for. These simplifications are standard for R3CBP models. Newton’s equation for universal gravity was applied to calculate the gravitational acceleration experienced by the Cislunar CubeSat caused by the gravity of both the Earth and Moon.

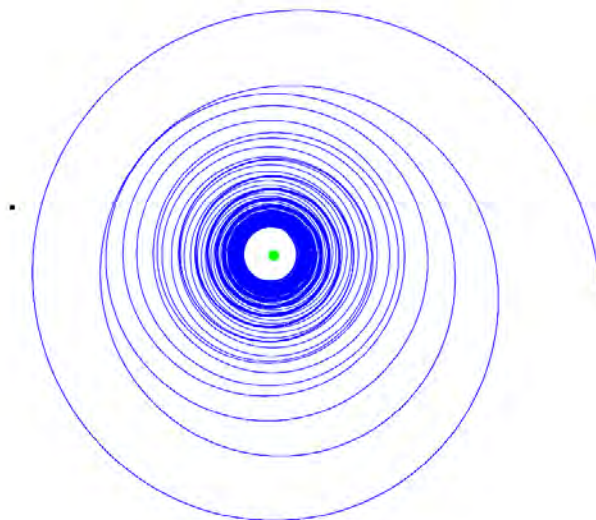


Figure 5 – Example spiral transfer past the Moon to an escape trajectory modelled in Octave. The green point is the Earth, the black point the Moon, and the red point is the spacecraft. In this case, the engine used is the BET-1mN.

The starting position and velocity was determined from the starting orbit and true anomaly. Starting orbit was set to GEO, and true anomaly kept as an input variable. With the starting position and velocity known, the model could progress forward step by step, with each step integrating the acceleration to velocity and position. The chosen step size was 100 seconds. This step size was chosen as a compromise between precision and required processor time. Fuel mass

was also decremented from the mass of the spacecraft as the simulation progressed. An example of the output of this model is shown in Figure 5.

While this model represents a significant step forward from the 2 body model used earlier, there remain issues with the model that should be improved in the future. These include:

- Motion of the Earth and Moon is assumed circular;
- Gravity of other solar system bodies are not taken into account;
- Solar radiation pressure is not taken into account; and
- The Octave package is a very high level package and is less computationally efficient than a dedicated model made from scratch.

Inputs for this modelling are the 4 chosen engines and the starting true anomaly, which was varied between 0 and 360° at 22.5° intervals. The main output for this modelling is the time required to pass lunar orbit. The trajectory path taken by each engine at each starting true anomaly is an additional qualitative output.

Results and Discussion

The time required to pass lunar orbit for each engine are given in Table 4. The time calculated from the Stansbury method and the time modelled from the Octave R3CBP simulation are both given. As the time required to pass Lunar orbit varied significantly due to influence from the Moon’s gravity for 3 of the 4 engines, average, minimum and maximum time are given to demonstrate variation of outputs from the simulation. Examination of trajectories has shown that the minimum time cases occurred when the simulated spacecraft passed close to the Moon and received a gravitational assist. Maximum time cases occurred when the Moon’s gravity did not influence the spacecraft’s trajectory as it passed the orbit of the Moon. Two videos containing two simulation runs are provided [here](#) and [here](#). The first linked video shows the CAT entering into an escape trajectory long before it approaches lunar orbit, which is a typical situation for the high thrust CAT. The second linked video shows the BIT-3 colliding with the Moon. Because there is no collision detection, the BIT-3 equipped spacecraft slingshots through the centre of the Moon.

Table 4 – Time required to pass lunar orbit for each engine. The calculated row shows the output calculated from the Stansbury method and the Modelled rows show the output determined from Octave R3CBP simulations.

	Engine	BET-1mN	BET-100uN	BIT-3	CAT
Calculated	Expected Time (days)	319.5	498.5	170.0	11.2
Modelled	Minimum Time (days)	311.4	472.7	164.8	12.8
	Average Time (days)	324.6	494.7	172.0	12.9
	Maximum Time (days)	336.1	514.5	177.3	13.0

It is clear that the two methods have produced broadly similar results. The calculated time value for all but the CAT falls within the minimum to maximum range of modelled time results. In the case of the CAT, the difference between the calculated output and the modelled outputs can be

explained by the assumptions inherent in the Stansbury method. The Octave R3CBP can thus be considered a valid method for determining the time required to pass lunar orbit.

The reason that the CAT did not see much variance in the time required to pass lunar orbit was due to its high thrust causing it to enter an escape trajectory long before passing lunar orbit. This was observed in the CAT linked video. Lunar gravity will not have a great effect on the speed of such a trajectory. As was seen in the other linked video showing the BIT-3's collision with the Moon, the BIT-3 and other engines do not have enough thrust to achieve an escape trajectory before reaching the orbit of the Moon, and will still be on a near circular orbit. Such an orbit is much more easily influenced by the Moon's gravity, and is what causes the BIT-3, BET-1mN, and BET-100 μ N to have such variation in their time result.

Of these 4 engines, the CAT has by far the best performance, but there remain issues with its low Technology Readiness Level. Its specifications are expected to change markedly as it is developed further. If a Cislunar CubeSat mission were to be designed today, the BIT-3 would likely be chosen, especially given the lifetime challenges faced by Busek's BET series thrusters. If these lifetime challenges are solved, then any one of the Busek engines may be chosen, with the choice ultimately depending on the amount of power available for the propulsion system and the desired flight time.

Conclusion

Self-propelled CubeSats are needed if accessing beyond LEO space is to become practical for groups that cannot partake in rare ridesharing opportunities aboard traditional beyond LEO missions. Such missions must make use of CubeSat propulsion technologies, particularly low thrust, high efficiency electric propulsion systems. There are a large number of groups working on CubeSat propulsion, with Busek leading the field in providing space ready hardware suitable for the purpose. The 4 most promising systems under development were found to be the BET-1mN, the BET-100 μ N, the BIT-3 and the CubeSat Ambipolar Thruster. These systems were able to reach the Moon in under 500 days, with the CAT fastest, followed by the BIT-3, BET-1mN, and the BET-100 μ N in order of time needed. Analysis was done using two body and three body modelling. The low TRL of the CAT remains an issue, and it is likely to see changing specifications as it is developed further. The lifetime challenges of the BET series are also an issue that will need to be overcome for these engines to be suitable for a beyond LEO CubeSat mission. Nonetheless, the technology to propel a CubeSat from geostationary orbit to the Moon, asteroids or Mars is clearly available.

Acknowledgements

Noor would first like to acknowledge the support of his parents. Without their support, this research project would not have been possible. Noor would also like to acknowledge Professor Andrew Dempster, whose expert supervision and guidance has helped immensely.

References

[1] SpaceWorks, "2016 Nano/Microsatellite Market Forecast," 2016. [Online]. Available:

- <http://spaceworksforecast.com/2016-market-forecast/>. [Accessed 2 October 2016].
- [2] NASA, “CubeSats Overview,” 31 July 2015. [Online]. Available: http://www.nasa.gov/mission_pages/cubesats/overview. [Accessed 2 October 2016].
- [3] DIY Space Exploration, “CubeSats explained and why you should build one,” 2016. [Online]. Available: <https://www.diyspaceexploration.com/blogs/news/cubesats-explained-and-why-you-should-build-one>. [Accessed 2 October 2016].
- [4] Spaceflight, “Schedule & Pricing,” 2016. [Online]. Available: <http://www.spaceflightindustries.com/schedule-pricing/>. [Accessed 2 October 2016].
- [5] Rocket Lab, “Space is open for business, online,” 2016. [Online]. Available: <https://rocketlabusa.com/space-is-open-for-business-online/>. [Accessed 2 October 2016].
- [6] Planet Labs Inc., “Planet,” 2016. [Online]. Available: <https://www.planet.com/>. [Accessed 2 October 2016].
- [7] The von Karman Institute for Fluid Dynamics, “QB50,” 2016. [Online]. Available: <https://www.qb50.eu/>. [Accessed 2 October 2016].
- [8] M. Wall, “New Space Engine Could Turn Tiny CubeSats into Interplanetary Explorers,” 8 July 2013. [Online]. Available: <http://www.space.com/21867-cubesat-deep-space-propulsion-kickstarter.html>. [Accessed 3 October 2016].
- [9] P. de Selding, “1 in 5 Cubesats Violates International Orbit Disposal Guidelines,” 23 July 2015. [Online]. Available: <http://spacenews.com/1-in-5-cubesats-violate-international-orbit-disposal-guidelines/>. [Accessed 2 October 2016].
- [10] W. de Vries, “Cubesat Drag Calculations,” 8 September 2010. [Online]. Available: <https://e-reports-ext.llnl.gov/pdf/433600.pdf>. [Accessed 2 October 2016].
- [11] Jet Propulsion Laboratory, “Mars Cube One (MarCO),” 2016. [Online]. Available: <http://www.jpl.nasa.gov/cubesat/missions/marco.php>. [Accessed 2 October 2016].
- [12] National Aeronautics and Space Administration, “NASA Targets May 2018 Launch of Mars InSight Mission,” 10 March 2016. [Online]. Available: <http://www.nasa.gov/press-release/nasa-targets-may-2018-launch-of-mars-insight-mission>. [Accessed 9 October 2016].
- [13] Cislunar Explorers, “Cislunar Explorers: Streamlined, Sustainable Spacecraft,” 2016. [Online]. Available: <https://cislunarexplorers.wordpress.com/>. [Accessed 3 October 2016].
- [14] B. Hill, “NASA Advisory Council: Exploration Systems Development Status,” March 2012. [Online]. Available: http://www.nasa.gov/pdf/630149main_5-Hill_SLS%20MPCV%20GSDO_508.pdf. [Accessed 3 October 2012].
- [15] P. Sloss, “SLS Program working overtime to make 2018 debut,” 24 August 2016. [Online]. Available: <https://www.nasaspaceflight.com/2016/08/sls-program-working-overtime-2018-debut/>. [Accessed 9 October 2016].
- [16] L. Grush, “NASA officials admit Space Launch System is a rocket without a plan,” 12 January 2016. [Online]. Available: <http://www.theverge.com/2016/1/12/10758110/nasa-ksc-meeting-sls-rocket-uncertain-launch-dates>. [Accessed 3 October 2016].
- [17] National Aeronautics and Space Administration, “Asteroids,” 31 March 2016. [Online]. Available: <http://nssdc.gsfc.nasa.gov/planetary/planets/asteroidpage.html>. [Accessed 3 October 2016].
- [18] J. Harbaugh, “International Partners Provide Science Satellites for America’s Space Launch System Maiden Flight,” 27 May 2016. [Online]. Available: <http://www.nasa.gov/exploration/systems/sls/international-partners-provide-cubesats-for-sls-maiden-flight>. [Accessed 9 October 2016].
- [19] K. Northon, “NASA Space Launch System’s First Flight to Send Small Sci-Tech Satellites

- Into Space,” 3 February 2016. [Online]. Available: <https://www.nasa.gov/press-release/nasa-space-launch-system-s-first-flight-to-send-small-sci-tech-satellites-into-space>. [Accessed 6 October 2016].
- [20] crowdfundMIT, “MIT KitCube Lunar Orbiter,” 25 January 2016. [Online]. Available: <https://crowdfund.mit.edu/project/1501>. [Accessed 6 October 2016].
- [21] Miles, “Miles,” 2016. [Online]. Available: <http://miles-space.com/>. [Accessed 6 October 2016].
- [22] J. Harbaugh, “NASA Awards Second-Round Prizes in Cube Quest Challenge,” 22 March 2016. [Online]. Available: http://www.nasa.gov/directorates/spacetech/centennial_challenges/cubequest/awards-second-round-prizes-in-cube-quest-challenge. [Accessed 6 October 2016].
- [23] Gunter's Space Page, “Gunter's Space Page,” 2016. [Online]. Available: <http://space.skyrocket.de/index.html>. [Accessed 9 October 2016].
- [24] J. Cardin, J. Essmiller and A. Klesh, “Mars Cube One Interplanetary Propulsion System,” 2016. [Online]. Available: <https://icubesat.org/papers/2016-2/2016-b-3-1/>. [Accessed 9 October 2016].
- [25] A. Tadros and D. King, “SSL Payload Orbital Delivery System (PODS): “FedEx to GTO/GEO”,” 27 May 2015. [Online]. Available: https://icubesat.files.wordpress.com/2015/06/icubesat-2015_org_b-1-1_pods_king.pdf. [Accessed 10 October 2016].
- [26] S. Stansbury, “Low Thrust Transfer to GEO: Comparison of Electric and Chemical Propulsion,” 10 December 2009. [Online]. Available: http://ccar.colorado.edu/asen5050/projects/projects_2009/stansbury/. [Accessed 10 October 2016].
- [27] Nanoracks, “NanoRacks Announces 6U and 12U CubeSats for ISS Deployment,” 27 September 2016. [Online]. Available: <http://spaceref.com/news/viewpr.html?pid=49567>. [Accessed 12 October 2016].
- [28] [Online]. Available: http://www.nasa.gov/sites/default/files/thumbnails/image/dellingr_artist_concept.jpg. [Accessed 12 October 2016].
- [29] M. Keidar, “Micro-Cathode Arc Thruster for Small Satellite Propulsion,” 2016. [Online]. Available: <http://dcspacegrant.org/affiliatemeeting2016/GWU2016.pdf>. [Accessed 12 October 2016].
- [30] Busek, “BET-1mN Busek Electro Spray Thruster,” 2016. [Online]. Available: http://www.busek.com/index_htm_files/70008500%20BET-1mN%20Data%20Sheet%20RevH.pdf. [Accessed 13 October 2016].
- [31] Busek, “BET-100uN Busek Electro Spray Thruster,” 2016. [Online]. Available: http://www.busek.com/index_htm_files/70008516%20BET-100uN%20Data%20Sheet%20RevE.pdf. [Accessed 13 October 2016].
- [32] Busek, “BIT-3 Busek RF Ion Thruster,” 2016. [Online]. Available: http://www.busek.com/index_htm_files/70010819%20BIT-3%20Data%20Sheet%20RevB.pdf. [Accessed 13 October 2016].
- [33] PEPL, “PEPL Thrusters: CubeSat Ambipolar Thruster,” 23 January 2016. [Online]. Available: <http://pepl.engin.umich.edu/thrusters/CAT.html>. [Accessed 13 October 2016].
- [34] J. Sheehan, T. Collard, F. Ebersohn and B. Longmier, “Initial Operation of the CubeSat Ambipolar Thruster,” in *Presented at Joint Conference of 30th International Symposium on Space Technology and Science, 34th International Electric Propulsion Conference and 6th*

Nano-satellite Symposium, Hyogo-Kobe, 2015.

- [35] GOMSpace, “NanoPower Solar Panels,” 2016. [Online]. Available: <http://www.gomspace.com/index.php?p=products-p110>. [Accessed 27 January 2017].
- [36] MMA Design, “HAWK Solar Array,” 2017. [Online]. Available: <http://mmadesignllc.com/products/hawk-solar-arrays/>. [Accessed 27 January 2017].
- [37] “Small Satellite Propulsion,” 8 January 2015. [Online]. Available: <https://ntrs.nasa.gov/archive/nasa/casi.ntrs.nasa.gov/20150002945.pdf>. [Accessed 27 January 2017].

Rationale and Strategies for Lunar and Martian Pit Crater Reconnaissance

Graham. E. Dorrington

School of Engineering, RMIT University, PO Box 71, Bundoora VIC 3083, Australia

Summary: Reasons for exploring pit craters on the surface of the Moon and Mars are outlined: first, to answer scientific questions concerning their formation; second, in the context of future human utilisation, the need to establish whether, or not, they have subsurface caverns or lava tubes associated. In order to establish the spatial extent of the subsurface void of any pit crater, it is proposed that preliminary reconnaissance missions using “micro-hoppers” are needed to acquire lateral images from near the pit floor. In the case of the Moon, the propulsive requirements to hop several kilometres into a pit crater from a nearby landing site are found to be relatively modest and could be met using well-established monopropellant propulsion systems. However, in the case of Mars, it is suggested that the higher surface gravitational acceleration and the issue of contamination prevention leads to the possible selection of lithium-ion powered micro-rotorcraft or probes involving parachute deployment.

Keywords: skylight, lava tube, sink-hole, habitation, exobiology, exploration, planetary.

Introduction

The geological explanation for “pit craters” (or “skylights”) on the surfaces of both the Moon [1, 2] and Mars [3, 4] has not yet been resolved. Two prominent examples of these enigmatic features are shown in Fig. 1 and 2. Aside from the scientific interest in their formation, it has been speculated that naturally occurring subsurface voids could be useful for future habitation [e.g., 5-7] and - in the case of Mars - they may also be sites of high exobiological promise [8]. At this juncture, the sizes of the subsurface voids of the known pit craters have not been established. They may all be closed with little lateral void extent, or it is possible that some or all of them offer open entrances to much larger subsurface caverns or lava tubes.

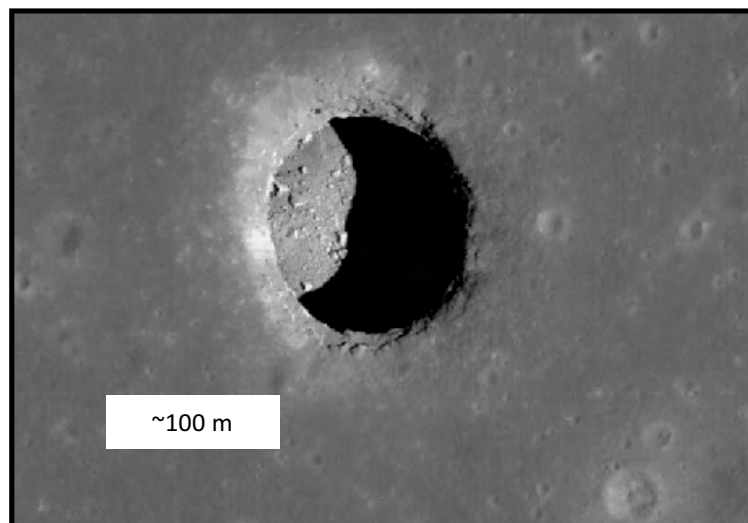


Fig. 1: Mare Tranquillitatis Pit Crater, credit: NASA/GSFC/Arizona State University)

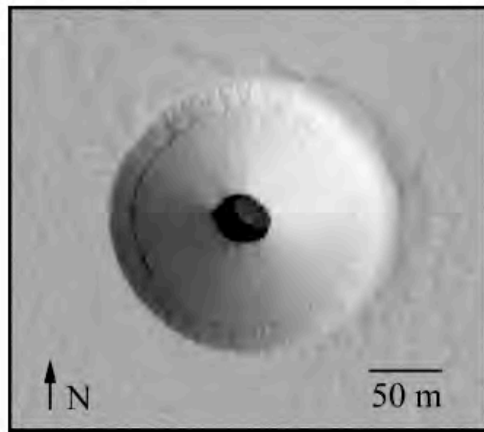


Fig. 2: Martian pit crater, credit: HiRISE image ESP-0235231-1840

On Earth, lava tubes such as “Undara” in Queensland are often revealed by (multiple) collapse skylights [9]. The existence of lunar and Martian lava tubes has long been suspected [10, 11], but not yet been confirmed. On first appearance, the Moon’s Mare Tranquillitatis Pit Crater (MTPC), shown in Fig. 1, appears to be similar to the near-circular sinkholes that are associated with the gradual water erosion of karst or pyroclastic pumice sediments on Earth. Immediately, it should be stressed that the Moon probably never had any surface water flows (unlike Mars) and the sinkhole analogy is misleading. On the other hand, lunar lavas are known to be far less viscous than those on Earth [12] and it is tempting to suggest that, at some ancient time in the Moon’s volcanically active past, lava erosion may have been instrumental in the formation of these pit craters [13] as well as its well-known rilles [14]. Consequently, the volcanically formed Wood Valley Pit Crater in Hawaii [15], depicted in Fig. 3, is most likely to provide one of the best Earth-based analogues.

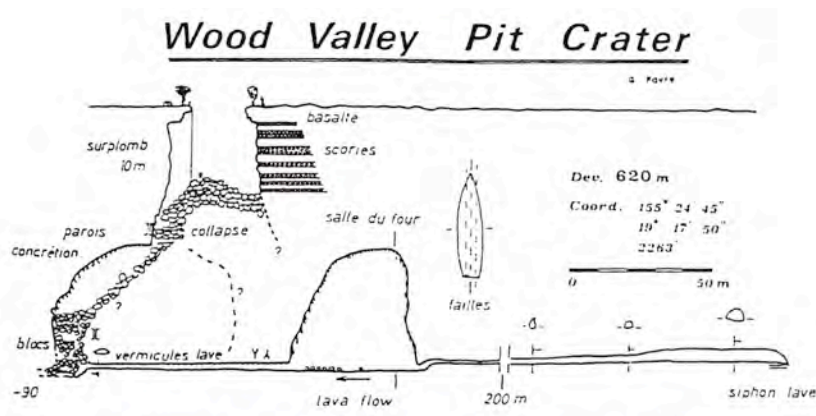


Fig. 3 Wood Valley Pit Crater, Hawaii, copied from ref. [15]

If some/all of the known lunar pit craters do lead to extensive, easily-accessible subsurface caverns or tubes, then these naturally occurring voids could provide several advantages over artificial surface constructions for future human lunar habitation. First, they would have much reduced radiation levels [16]. Second, they would not suffer from the extreme temperature variations occurring at the surface [5]. And third, they would offer natural protection from micro-meteoroid impacts. On Mars, some of these voids may also contain large quantities of useful volatiles (in particular, water ice) that could be utilised [8].

Unfortunately, using currently available orbital images it is not possible to determine the full lateral extent of any of the voids of the known pit craters. The MTPC (Fig. 1) and the example of a Martian pit crater (Fig. 2) certainly both have overhang regions, but there is no

evidence of any substantial subsurface-lateral void (tube or cavern) in any pit crater. Whilst it might be possible in the near-future to use time-of-flight photon photography from orbit in order to obtain a first order measure of the void size [17], this technology is still at a low level of maturity, hence it seems likely that *in situ* reconnaissance will be required and arguably should be regarded as having relatively high priority.

There are many possible concept strategies [e.g., 17-24] that could be adopted for preliminary reconnaissance missions, including use of tethered rovers, astronauts with abseils, etc., but one of the most promising near-term ideas is to use a remotely-operated “micro-hopper” that is capable of performing a ballistic-hop or hover-translation manoeuvre into the pit crater of primary interest [24] in order to acquire lateral images (or LIDAR scans) nearby to its floor. In the case of the MTPC, these images might then be transmitted directly back to Earth since a small portion of the pit floor comes within direct line-of-sight of the Earth at certain libration conditions. Alternatively, the micro-hopper could transmit the images via a relay orbiter, and/or hop back out of the pit - in order to acquire line-of-sight prior to transmission. In the case of the near-vacuum conditions of the Moon, such hops are probably best achieved using throttled rocket propulsion. In the case of Mars, with its tenuous atmosphere, rotary-wing craft may also be considered [25-27]. The remainder of this paper considers these options in a little more depth and maintains that such propulsive micro-hoppers are likely to be a promising solution with an acceptably low mission risk.

Lunar Micro-Hopper Concept

Performance Considerations

In the following development it is assumed that a lunar micro-hopper of ~10 kg gross mass is deployed from a main landing craft, which itself lands on the lunar surface some kilometres from the selected pit crater (e.g., the MTPC). Once the exact landing coordinates of the main landing craft are established the micro-hopper would be instructed to perform the following sequence: a propulsive ballistic hop translation to within ~50 m of the pit entrance; hover translation to within ~10 m distance from the vertical axis centreline (possibly determined by LIDAR sensors); vertical descent into the pit crater at ~5 m/s; acquisition of the lateral images (including the pit side walls during descent) whilst hovering at ~5 m from the pit floor; possible re-ascent and transmission of the images.

Using a simple trajectory model (a flat Moon approximation in which flight velocities remain much lower than orbital velocity and the lunar surface gravitational acceleration is fixed at $g_{lunar} = 1.62 \text{ ms}^{-2}$), a short impulsive burn at an initial flight angle of 45 degrees to the zenith, results in a ballistic hop with a constant lateral horizontal velocity, $V_x = V_0 / \sqrt{2}$, and a vertical velocity given by $V_y = V_0 / \sqrt{2} - g_{lunar} t$, where V_0 is the velocity immediately after the impulse burn. It follows, therefore, that the total delta-V required to accelerate and decelerate back to rest is,

$$V = 2\sqrt{g_{lunar} R_{hop}} \quad (1)$$

For example, to achieve a hop of ~2500 m, the delta-V requirement is ~130 ms^{-1} . The amount of propellant required to achieve this hop, is $m_{prop,hop} = m_0(1 - \exp(-V/I_{sp}))$ where m_0 is the initial gross mass of the micro-hopper and I_{sp} is the specific impulse of the propulsion system measured in ms^{-1} . In this case the use of a standard hydrazine monopropellant thruster would require a 10 kg micro-hopper to consume just ~0.6 kg of propellant.

To bring about a subsequent sequence of slow descent and hover, the thrust must approximately balance the micro-hopper weight and it is easy to show that the hover time is,

$$t_{\text{hover}} = \frac{I_{sp}}{g_{\text{lunar}}} \ln \frac{m_2}{m_2 - m_{\text{prop,hover}}} \quad (2)$$

The free-fall time into the pit is $t_{\text{descent}} = \sqrt{(2h_{\text{pit}} / g_{\text{lunar}})}$ where the depth, h_{pit} , of the largest known pit (MTPC) is ~ 100 m. The propellant consumed to hover for a similar time span is $m_{\text{prop,hover}} = m_2(1 - \exp(-g_{\text{lunar}}t_{\text{hover}} / I_{sp})) \sim m_2(1 - \exp(-\sqrt{(2g_{\text{lunar}}h_{\text{pit}} / I_{sp}))})$. It is worth noting that the same result is obtained by assuming free-fall is countered by a single impulsive braking burn. Re-ascent from the pit requires a similar thrusting duration, but the overall propellant consumption remains relatively small. For example, for the previously mentioned hydrazine thruster, descent and ascent in-and-out of the MTPC only requires ~ 0.2 kg of propellant, and the overall propellant consumption for the entire micro-hopper mission is just ~ 1 kg. This requires a propellant tank of ~ 2 litres, i.e., a volume comparable with a 2U CubeSat. The attitude control propellant budget is unlikely to alter this finding substantially.

Design Considerations

The design of the micro-hopper depends on the mission requirements. To minimise mission risk, it is arguably better to avoid landing on the unpredictable rubble strewn over the floor of the MTPC (Fig. 1) and to acquire the required lateral lower pit images whilst the micro-hopper remains hovering. On the other hand, the exhaust plume emitted from a micro-hopper of ~ 10 kg from a set of thrusters with ~ 16 N total thrust may result in regolith uplift [28, 29] when operated in close proximity to the surface resulting in obscuration - as well as vibration. Consequently, it may be beneficial for the micro-hopper to deploy a tether carrying a camera/imaging unit hanging below the main bus, see Fig. 4 and 5. In the most extreme case, the tether could be designed to exceed to the MTPC depth by a significant margin (a tether of up to 120 m length), such that the bus would remain hovering above the local lunar surface level - to maintain direct line-of-sight with Earth. Alternatively, the tether might be designed to be as short ~ 2 m, or deleted, assuming that the hover position to surface separation is sufficient to obviate the dust obscuration problem. At ~ 5 m distance the exhaust would have expanded by a factor of $\sim 1000+$, hence the plume dynamic pressure may be insufficient to cause regolith movement.

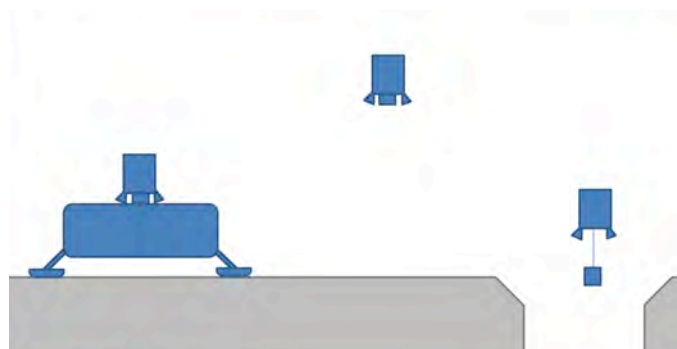


Figure 4: Lunar micro-hopper concept deployed from main lander ~ 2 km from pit crater

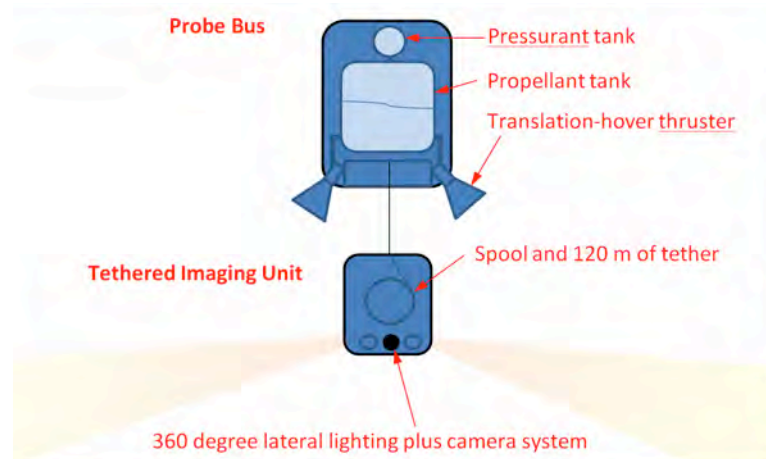


Figure 5: Lunar micro-hopper concept (to obtain internal images of pit crater)

Martian Micro-Hopper Concept

General Considerations

From a performance standpoint, a similar propulsive micro-probe like the one shown in Fig. 4 could be adopted to hop over the Martian surface and then to fly in-and-out of a pit crater. However, reconnaissance of Martian pit craters is likely to be classified as a Class IV mission under COSPAR policy [30]. Assuming that landing is not permitted and re-ascent is required after images from inside the pit crater have been obtained, the higher surface gravity acceleration becomes more challenging: either it leads to larger propellant mass fractions, or it requires the necessary introduction of more complex bi-propellant systems offering higher specific impulse, but then there is the issue of possible biological contamination - especially in the case of the short tether option. Based on the possible existence of subsurface volatiles [8] it would be necessary to avoid possible contamination with hydrogen containing exhaust radicals to avoid corrupting the scientific measurements intended. Consequently, instead of hydrazine or hypergolic bipropellant systems, it seems likely that battery-powered rotorcraft [25-27], or possibly hoppers propelled by inert gas systems [31-33], would have to be selected.

Rotorcraft Performance Considerations

Simple momentum actuator disk (or Rankine-Froude) theory can be used to estimate the power required to hover with a rotor system in the tenuous Martian atmosphere. The total required rotor power input may be estimated as,

$$P_{rotor} = k \sqrt{\frac{(m_{mrc} g_{mars})^3}{2 \rho_{surface} A}} \quad (3)$$

where: m_{mrc} is the micro-rotorcraft mass; g_{mars} 3.71 ms^{-2} is the surface gravitational acceleration; ρ_{mars} 0.02 kg m^{-3} is the surface atmospheric density at the applicable latitude and season; A is total the actuator disk area; the factor k is typically ~ 2.2 when rotor profile power is included as well as the induced power. For example, if $m_{mrc} = 2 \text{ kg}$ and $A = 1 \text{ m}^2$, then $P_{rotor} \sim 220 \text{ W}$. Whilst supply at this power level is feasible using currently available lithium-ion cell pack with a mass of $\sim 0.65 \text{ kg}$, it is roughly double that required for a

similarly-sized rotorcraft operating at sea-level on Earth, suggesting limited but still practically feasible operations.

It should also be noted in this example, the rotor induced downwash velocity, U_i , is ~ 15 m/s, which is substantially less than that of a typical rocket thruster. The rotor induced dynamic pressure, $\frac{1}{2} U_i^2$, is only ~ 2 Pa, suggesting that dust uplift and subsequent lateral view obscuration is unlikely to be a major problem at ~ 2 m surface separation.

Rotorcraft Design Considerations

To achieve a hop range of several kilometers, but avoid contamination as mentioned above, a promising design solution is to employ a ballistic micro-rocket stage that launches from the main lander and carries a micro-rotorcraft in a rotor-folded state, see Fig. 6. Just before the pit entrance is reached, the micro-rocket stage and micro-rotorcraft would separate, and then the rotors would be deployed to decelerate and permit slow hover-descent into the pit crater. The spent micro-rocket stage would then crash land well clear of the pit entrance.

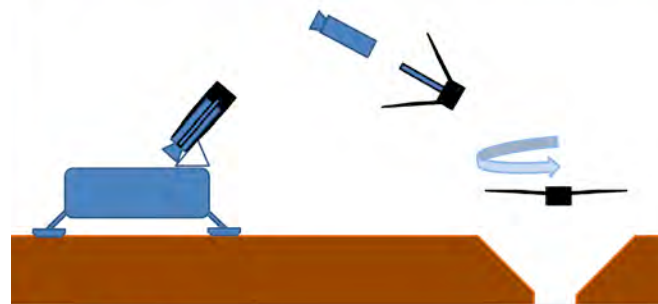


Figure 6: Martian pit crater probe concept with rotor deceleration

Alternative Schemes

It should be noted that when re-ascent is not required (i.e., when transmission via a relay is feasible), instead of using a rotorcraft for deceleration, an imaging unit with parachute may be a simpler option [34], see Fig. 7. To reduce the descent velocity of a 1 kg imaging unit to ~ 10 m/s, requires a parachute of radius ~ 2 m assuming it has a specific area of ~ 6 m²/kg such that the combined unit plus parachute mass is ~ 3 kg. The downside in this case is that the parachute has to be deployed immediately above the entrance, requiring quite a precise lob from the ballistic delivery stage.

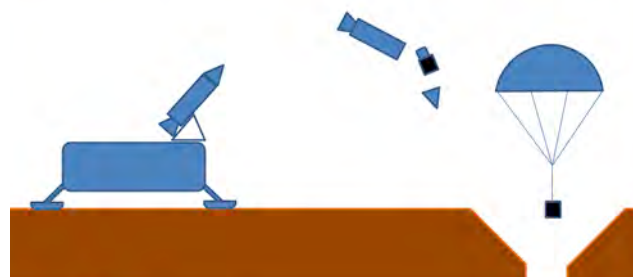


Figure 7: Martian pit crater probe concept with parachute deceleration

Discussion

The above presentation only introduces some of the key issues concerned with pit crater reconnaissance and a few of the options available. There are many other possible *in situ* and remote sensing subsurface void detection methods [e.g., 17-24, 31-37].

One major problem with all the *in situ* methods is the need to decide which feature(s) to select for the first reconnaissance mission(s) and the possible ambiguities arising. For example, at some future date it might be found that the MTPC does not offer any extensive void, but whilst that definite discovery would be a useful negative result, it would not imply that all other lunar pit craters are similarly closed. Similarly, if rubble on the floor of the MTPC blocks openings, then ambiguity will remain. This problem is illustrated by the schematic of the Wood Valley Pit Crater (Fig. 3). In this likely-strong analogue case, it may be seen that positioning a camera (or LIDAR ranging system) immediately above the rubble pile (labelled “collapse”) would probably not permit detection of any open pathway to the lava tubes lying below. An interesting proposed scheme using multiple “microbots” [20, 38] may permit more effective explorative-speleological penetration into such rubble piles. Indeed, it is fully recognised that some of the alternative proposed exploration methods referenced herein (or a combination of them) may eventually be selected in preference to the schemes presented above.

Concluding Remarks

This brief study indicates that the class of propulsive micro-hoppers briefly described here and elsewhere [23, 24, 39] appear to be feasible for both lunar and Martian pit exploration. Based on the simple analysis presented, there is no major propulsive barrier preventing these hop missions, provided at least one agency or private venture elects to place a lander within a few kilometres of one of the selected features. An unresolved issue is the exact sizing of such micro-hoppers. A nominal gross mass of 10 kg was assumed for the lunar micro-hopper example above, but a comprehensive mass breakdown analysis has not yet been performed. Whilst there have been many studies on micro-propulsion systems for micro/nano-spacecraft with thrust-to-weight ratios much less than one, there has been little work on the feasibility of micro-sized propulsion systems for hoppers of ~10 kg [e.g., 24, 39]. In order to perform such studies details on available off-the-shelf components (such as propellant flow valves) are needed, but it is worth pointing-out that there is no fundamental miniaturization constraint, i.e. such small propulsive systems (including attitude control) are perfectly feasible.

The only major downside of the class of *in situ* probes presented here is that the first mission may result in the negative finding that the selected pit crater is closed, without any open access to an extensive void and – in the case of Mars – that it lacks any significant quantities of accessible trapped volatiles. However, without undertaking such curiosity-driven exploration the potential opportunity for subsurface void utilisation will never be realised.

Acknowledgements

Dr. M. Norman (ANU) and S. Barraclough (UNSW Canberra) kindly made some useful comments on the draft of this manuscript, although they are not responsible for any errors or misconceptions that may remain.

References

1. Haruyama J. *et al.*, “Possible Lunar Lava Tube Skylight Observed by Selene Cameras”, *Geophysical Research Letters*, Vol. 36, L21206, doi:10.1029/2009GL040625, 2009.
2. Robinson, M.S. *et al.*, “Confirmation of Sublunarean Voids and Thin Layering in Mare Deposits”, *Planetary and Space Sciences*, Vol. 69, 2012, pp. 18-27.
3. Cushing, G. E., “Candidate Cave Entrances on Mars”. *Journal of Cave and Karst Studies*, Vol. 74, no. 1, pp. 33–47. DOI: 10.4311/ 2010EX0167R
4. Cushing, G. E., Okubo, C.H. and Titus, T. N. “Atypical Pit Craters on Mars: New insights from THEMIS, CTX, and HiRISE observations”, *Journal of Geophysical Research*, Vol. 120, June 2015, pp. 1023-1043.
5. Horz, F., “Lava Tubes: Potential Shelters for Habitats”. *Lunar Bases and Space Activities of the 21st Century*, Ed. Mendell, W.W., pp. 405, Lunar and Planetary Institute, Houston, USA, 1985, pp. 405-412.
6. Daga, A. W., Daga, M. A., and Wendel, W. R., “Evolving Concepts of Lunar Architecture: The Potential of Subselene Development”, *The Second Conference on Lunar Bases and Space Activities of the 21st Century*, Proceedings from a conference held in Houston, TX, April 5-7, 1988. W. W. Mendell, Ed. NASA Conference Publication 3166, 1992, pp. 281-291.
7. Blamont, J., “A Roadmap to Cave Dwelling on the Moon and Mars”, *Advances in Space Research*, Vol. 54, no. 10, 2014, pp. 2140-2149.
8. Williams, K. E., McKay, C. P., Toon, O. B., Head, J. W. “Do Ice Cave Exist on Mars?” *Icarus*, Vol. 209, 2010, pp. 358-368.
9. Atkinson, A, and Atkinson, V. *Undara Volcano and its Lava Tubes*, published by the authors, Brisbane, 1995, ISBN 0957 8828 07.
10. Greeley, R., “Lava Tubes and Channels in the Lunar Marius Hills”, *The Moon*, Vol. 3, 1971, pp. 289-314.
11. Coombs, C.R., and Hawke, B.R., “A Search for Intact Lava Tubes on the Moon: Possible Lunar Base Habitats”, *The Second Conference on Lunar Bases and Space Activities of the 21st Century*, NASA Conf. Publ., NASA CP-3166, vol. 1, 1992, pp. 219– 229.
12. Murase, T. and Mc.Birney, A.R., “Viscosity of Lunar Lavas”, *Science*, Vol. 167, pp. 1491-1493.
13. Okuto, C.H. and Martel, S.J., “Pit Crater Formation on Kilauea Volcano, Hawaii”, *Journal of Volcanology and Geothermal Research*, Vol. 86, 1998, pp. 1-18.
14. Hulme, G., “A Review of Lava Flow Processes Related to the Formation of Sinuous Rilles”, *Geophysical Surveys*, Vol. 5, 1982, pp. 245-279.

15. Favre, G., “Some Observations of Hawaiian Pit Craters and Relations with Lava Tubes”, *Proceedings of the 3rd International Symposium on Vulcanospeleology*, William Halliday (Chairman), Bend, Oregon, July 30-August 1, 1982. International Speleological Foundation, Seattle, p. 37- 41.
16. de Angelis, G. *et al.*, “Lunar Lava Tube Radiation Safety Analysis”, *Journal of Radiation Research*, Vol. 43, 2002, pp. S41-S45.
17. Nosanov, J., Velten, A., Mitchell, K and Arora, N. “*PERISCOPE: PERIapis Subsurface Cave OPTical Explorer*”, NASA Innovative Advanced Concept (NIAC) Phase 1 Final Report, 2015. See also: <https://www.nasa.gov/feature/periscope-periapis-subsurface-cave-optical-explorer>, last updated, Hall. L. (Ed.), July 15 2015.
18. Whittaker, W., *Technologies Enabling Exploration of Skylights, Lava Tubes and Caves*, NASA Innovative Advanced Concepts (NIAC) Phase 1 Final Report, Grant No. NNX11AR42G, September 14 2012.
19. Yoshida, K. “Low-Cost Rovers for Exploration of Lunar Lava Tubes” *11th International Academy of Astronautics (IAA) Low-Cost Planetary Missions Conference*, Berlin, Germany, June 9-11, 2015.
20. Kesner, S.B. *et al.*, “Mobility and Power Feasibility of A Microbot Team System for Extraterrestrial Cave Exploration”, *2007 IEEE International Conference*, Rome, Italy, 10-14 April, 2007, pp. 4893-4898 doi: 10.1109/Robot.2007.364233.
21. Ximenes, S. W., Elliot, J. O. and Bannova, O., “Defining a Mission Architecture and Technologies for Lunar Lava Tube Reconnaissance”, *ASCE Earth and Space 2012 Conference*, Pasadena, USA, April 15-18, 2012.
22. Ximenes, S.W. *et al.* “LEAP2: Development of a Lunar Ecosystem and Architectural Prototype at the Marius Hills Skylight”, paper 6022, *Workshop on Golden Spike Human Lunar Expeditions*, October 3-4, Texas, USA, 2013.
23. Robinson, M.S., Thanga, J., Wagner, R.V. and Hernandez, V.A., “ARNE – Sublunarean Explorer”, Paper 3025, *Annual Meeting of the Lunar Exploration Analysis Group*, Laurel, Maryland, USA, October 22-24, 2014.
24. Dorrington, G. E. “Rationale for and Conceptual Design of a Microprobe Spacecraft for Lunar Pit Reconnaissance”, *Asia-Pacific Symposium on Aerospace Technology (APISAT-2015)*, Cairns, Australia, 25-27 Nov. 2015.
25. Datta, A. *et al.* “Design of a Martian Autonomous Rotary-Wing Vehicle”, *Journal of Aircraft*, Vol. 40, No. 3, May–June 2003, pp. 461-472.
26. Tsuzuki, N. Sato, S. and Abe, T., “Design and Feasibility for a Miniature Mars Exploration Rotorcraft”, *24th International Congress of the Aeronautical Sciences (ICAS)*, 29th August – 3rd September, 2004.
27. Balaram, J. and Tokumar, P., “Rotorcrafts for Mars Exploration” *11th International Planetary Probe Workshop* Pasadena, California, USA, June 19th, 2014.

28. Wagner, S. A., “The Apollo Experience Lessons Learned for Constellation Lunar Dust Management”, *NASA/TP-2006-213726*, September, 2006.
29. Metzger, P. T., Li, X., Immer, C. D. and Lane, J. E., “ISRU Implications for Lunar and Martian Plume Effects, AIAA 2009-1204, *47th AIAA Aerospace Sciences Meeting including the New Horizons Forum and Aerospace Exposition*, Orlando, USA, 5-8 Jan. 2011.
30. Anon. “COSPAR Planetary Protection Policy”, Approved by the Bureau and Council, *World Space Congress*, Houston, Texas USA, Oct. 10-20, 2002, Amended 24 March 2005.
31. Zubrin, R. *et al.* *Report of the Design and Operation of a Mars Gashopper*, NASA Study report no. NAS3-00074, Pioneer Astronautics, 2000.
32. Yu. D.-R., *et al.*, “Preliminary Design Analysis of a Hopper Vehicle for Mars Mission”, *Proceedings of the Institute of Mechanical Engineers*, G, 224, 283 291 doi:10.1243/09544100JAERO615, 2010.
33. Anon. *Mars Hopper Concept Technologies*, Executive Summary, Contract no. 4000107642, GSP Internal No. 2013-2, ESA General Studies Programme, 2013.
34. Costello, M. and Frost, G., “Simulation of a Mortar Launched, Parachute Deployed Battlefield Imaging System”, *Journal of Dynamic Systems, Measurement, and Control* 126, September 2004, pp. 583-593.
35. Rowell, C. R., Pidlisecky, A., Irving, J.D. and Ferguson, R.J., “Characterization of Lava Tubes Using Ground Penetrating Radar of the Moon National Monument, USA” *CREWES Research Report*, Vol. 22, 2010, pp. 1-14.
36. Chappaz, L., Sood, R., Melosh, H. and Howell, K., “Buried Empty Lava Tube Detection with GRAIL Data”, *AIAA/AAS Astrodynamics Specialist Conference*, San Diego, USA, 4-7 August 2014.
37. Carroll K. A. *et al.*, “Exploring Subsurface Lunar Voids Using Gravimetry”, Paper 1351, *46th Lunar and Planetary Science Conference*, The Woodlands, Texas, USA, March 16-20, 2015.
38. Dubowsky, S., Kesner, S., Plante, JS., and Boston, P., “Hopping Mobility Concept for Search and Rescue Robots,” *Industrial Robot, An international Journal*, Vol. 35, 2008, pp. 238-245.
39. Thangavelautham, J. *et al.* “Flying, Hopping Pit-Bots for Cave and Lava Tube Exploration on the Moon and Mars”, *Proceedings of the 2nd International Workshop on Instrumentation for Planetary Missions*, Greenbelt, Maryland, Nov. 4-7, 2014.



APPENDIX A

16ASRC List of Presentations & Posters

List of Presentations

Abstracts are listed in alphabetical order of the Presenter

Andoh Michael Afful: Space Object Characterisation – A Case for Ballistic Coefficient Estimation

Prof. Stuart John Anderson: Space-borne interception of HF radar echoes for environmental intelligence

Dr. Kirco Arsov: High accuracy ionospheric modelling to support GNSS positioning and navigation in Australia

Professor Frances Bagenal: Exploration of the Outer Solar System: New Horizons at Pluto and Juno at Jupiter

Prof Jeremy Bailey: A Large Fully-Online Astrobiology Course

Prof Jeremy Bailey: How did we discover what planetary atmospheres are made of?

Simon Barraclough: Assessment and Verification of the Thermal Performance of the BRMM Spacecraft

Ruken Alac Barut: Analysing Post-Seismic Deformation of Izmit Earthquake with InSAR, GNSS AND Coulomb Stress Change Modelling

Miss Emily Jessica Bathgate: Raman, SEM and EPMA analyses of Australian eucrites

Dr Craig Benson: A Southern Hemisphere Planetary Radar Demonstration

Mr Sanat Biswas: Position and Velocity estimation of Re-entry Vehicles using Fast Unscented Kalman Filters

Dr Z.Bouya: The Australian Region Ionospheric Maps

Dr. Helen E. A. Brand: In Situ studies of Jarosite Formation: From Tasmania to Mars

Prof Iver Cairns: The INSPIRE-2 / AU03 Cubesat for the QB50 Project

Prof Iver Cairns: Prediction and testing of Type II radio emission, white light images, and CME properties from the Sun to Earth

Dr Kathleen Campbell: Astrobiology of Hot Springs on Early Earth and Mars

Mr Christopher Capon: Ionospheric Wake Modelling for Improved Resident Space Object Detection

Francesco Cappello: Navigation and Guidance Systems for Space Transportation Applications

Francesco Cappello: GNSS Attitude Determination and Control for Space Transportation Applications

Dr Graziella Caprarelli: It was a dark and stormy night in Lunae Planum

Dr Graziella Caprarelli: The International Space University Southern Hemisphere Program

Dr Brett Carter: Geomagnetically induced currents around the world during the 2015 St. Patrick's Day storm

Professor Christine Charles: Plasma experiments in the laboratory and space: the emerging role of 'CubeSat' nano-satellites and miniaturised propulsion systems.

Dr Rowena Christiansen: Space Medicine 101 – A Primer on What Happens to the Human Body in Space

Dr Rowena Christiansen: NASA's Human Research Roadmap – The 33 Key Issues for Human Health and Performance in Space

George Coulloupas: A Systems Engineering Approach to Miniaturised Satellite Constellation Design Optimisation 82

Miss Julie Currie: Relationship between HF radar spectral broadening and field aligned currents

Dr Giuseppina Dall'Armi-Stoks: Computational Electromagnetic Modelling to Support Spacecraft Design

Dr Jerome Daquin: Stability, chaos and transport in Earth orbits

Dr Jerome Daquin: Heterogeneous Multiscale Methods for the mean orbital motion: a discussion

Dr Florent Deleflie: Atmospheric reentry prediction for artificial satellites from TLE time series and precise orbit determination

Prof Andrew Dempster: Updates and progress of UNSW-ECO Cubesat

Upulie Divisekera: A New Era of Space Exploration

Lieutenant-Commander Luke Dixon, RAN: Human Factors in Hostile Environments: Projecting 102 Years of experience in Australian Submarines to long haul space missions

Dr Alina Donea: Far side imaging of the Sun for space weather prediction: how many active regions do we miss?

Dr. Graham Dorrington: Rationale and Strategies for Reconnaissance of Lunar

and Martian Pit-Voids

Dr. Graham Dorrington: On the Feasibility of Nanosats for Early Bushfire Detection

Roger Dudziak: Passive Thermal Control System for CubeSats

Dr Bradley Evans: Leveraging “Big Environmental Data” for Modelling Ecosystem Production in Space and Time

Dr Gordon J. Frazer: Wide field-of-view sensing for surveillance-of-space

Robert S. Fuller: Did Aboriginal Australians record a simultaneous eclipse and aurorae in their oral traditions?

Dr Douglas Griffin: DST Group and UNSW Canberra Buccaneer Programme Status and Plans

Dr. Douglas Griffin: The Engineering of Space Flight Programmes in the Australian Context: a sustainable model

Carla B. Guedes: Australian Indigenous Traditions of the Moon and its Relationship to Women

Dr Duane W. Hamacher: How Torres Strait Islanders “Read” the Twinkling of Stars to Predict Weather

Mr Adam Harris: An analysis of short-arc orbit determination for Low Earth Orbit objects comparing batch and Kalman Filter methods

Changyong He: Comparison of atmospheric mass density models and their impact on the orbit propagation of low Earth orbit satellites

Mr Andrew Heitmann: Parameterised modelling of travelling ionospheric disturbances using angle-of-arrival observations on oblique HF propagation paths

Dr Jason Held: Planning missions for large constellations

Dr Tanya Hill: The planetarium - connecting the public to current space research

Dr Steven Hobbs: A4 Rover: First Build to Initial Field Trials of a Small Planetary Science Rover for Mars Surface Exploration

Dr Steven Hobbs: Hands Off Field Work: Comparison of Human and Robotic Methods for Gathering Terrain Data using Structure From Motion

Mrs Gabriela-Nicoleta Hobbs: The Ethics of Working with Robots

Mrs Gabriela-Nicoleta Hobbs: Educational and Scientific Benefits of Extreme Environments

Dr David A Holdsworth: Effects of ionospheric disturbances upon over-the-horizon radar

A/Prof Jonti Horner: Towards the Exo-Earth Era – a Dedicated Australian Exo-planet Observatory

Dr Anthony John Horton: The Australian Space Eye: a CubeSat to study the history of galaxy formation

Changjiang Hu: Contemporary Space-based GNSS Remote Sensing

Mr Garland Hu: Modular and Reusable Flight Software Design for the Buccaneer Risk Mitigation Mission

Noor Huq: Evaluation of Current and Projected CubeSat Propulsion Technologies for Navigating Cislunar Space

Dr Eriita Jones: Inferring the presence of subsurface water on Mars from surface ejecta grain size.

Dr Eriita Jones: Identifying Something Which Can't Be Seen: Holistic Methodologies In The Search For Subsurface Water on Mars and Other Planets.

Rohan Kapoor: Modelling a Rendezvous to Comet Hartley 2 around its Perihelion

Dr Lucyna Kedziora-Chudczer: Auroral emissions of Jupiter

Dr Andrew Lambert: Low Earth Orbit interaction with the atmosphere

Trevor M. Leaman: Sacred Celestial Landscapes: Were Wiradjuri Cultural Sites also used as Astronomical "Observatories"?

Dr Bo Li: Mapping Magnetic Field Lines between the Sun and Earth

Dr Zishen Li: Towards a Two-Layer Ionospheric Delay Model for Real-time Single-frequency PPP over Australian Region

Dr Kurt Liffman: A Unified Framework for Producing CAI Melting, Wark-Lovering Rims and Bowl-Shaped CAIs

Mr Yi Xiang Lim: Cognitive Human Machine Interface for the Ground Pilot Station of an Unmanned Reusable Space Vehicle

Victor Lim: Optimising the launch, deployment and performance of a smallsat constellation

Dr David Lingard: Australian Participation in the Biarri CubeSat Missions

Dr Philippe Lorrain: Buccaneer Risk Mitigation Mission Assembly, Integration and Verification Programme

Dr Kenneth J.W. Lynn: Descending Intermediate layers/Descending Sporadic E

Mr Ronald Maj: Quasi-thermal Noise Spectroscopy on a Cubesat in Earth's Ionosphere

John Le Marshall: Recent and Impending Advances in the Use of Earth Observations from Space for Numerical Weather Prediction

Dr Peter May: Earth Observations from Space: Critical information used by the Bureau for national benefit

Troy McCann: The Melbourne Space Program: Growing Australia's Space Sector

Professor Frederick Menk: Role of Ultra-low Frequency Plasma Waves in Energizing Particles in Earth's Radiation Belts

Dr Franklin Mills: Simulations of time-of-day variability of SO₂ on Venus

Angus Muffatti: Multi-objective Design Optimisation of a small scale Cusped Field Thruster for micro satellite platforms

David Netherway: Measured and Predicted Power Received via HF Ionospheric Propagation

Dr Dave Neudegg: Long term median foF₂ variations in the Antarctic polar cap and the competing effects of solar EUV, magnetospheric precipitation and ionisation transport

Ms. Belinda Nicholson: Stars as proxies for studying the Sun's early history

Karlie Noon: Australian Indigenous uses of Moon Haloes to Predict Weather

Dr Robert Norman: RMIT SPACE Research Centre – overview of past and present research endeavours

Dr Kimberley Norris: Antarctic Behavioural Health as a Space Analogue

Dr. German Olivares-Pulido: CRCSI Project 1.21: Ionospheric Modelling

Ms Natalie Olsen: Ground Segment Software Design and Development for the Buccaneer Risk Mitigation Mission

Lenard Pederick: Observations of Travelling Ionospheric Disturbances with a Network of Quasi-Vertical Incidence Sounders in the Alice Springs region

Dr Li Qiao: Knowledge exploration for CubeSat design trade space using multi-dimensional scaling and clustering

Subramanian Ramasamy: Design and Development of Communication System for Unmanned Reusable Space Vehicles

Subramanian Ramsamy: Astrionics Systems for Unmanned Reusable Space Vehicles

Arunkumar Rathinam: Prospects for Multi-GNSS for Space Service Volume

Igor Rozenberg: Russian New Generation "Federation" Crewed Spacecraft Project Status

Prof Roberto Sabatini: Overview of the ISS Columbus module astronics

Danielle Shean: Created Mars analogues as effective tools for learning

Dr Tracey Sletten: Circadian misalignment and sleep disruption during long-term analog space missions.

Prof Michael Smart: Flyback booster for dedicated launch of small satellites

Mr Brenton Smith: The Impact Of Lift And Drag On dof Motion Of Leo Objects : Formation Control And Debris Behaviour

Jack Soutter: The Long-Term Stability of the Known Neptune Trojans

Dr. Christian Steimle: Bartolomeo – Your All-in-one Mission Solution in Low Earth Orbit

Victoria Tasker: Becoming cyborgs to expand humanity: will the integration of technology and humans reinforce humanity, or redefine it?

Ms. Samira Tasnim: A generalized equatorial model for the accelerating solar wind

Dr Edoardo Tescari: Exploring Indigenous Astronomical Knowledge in Australia and Central America: A Cross-Cultural Collaboration

Dr Matthew Tetlow: The SUSat QB50 mission

Dr Lachlan Thompson: New Capability for Emerald & Mount Burnett Observatories, Victoria for Earth Situational Awareness, Research, Education and Tourism

Dr Anne Unewisse: Airglow Observations from ELOISE

Dr Anne Unewisse: Imagers for Ionospheric Airglow Observations

Ivan Voropaev: Satellite electric drive

Dr Andrew Wabnitz: SpaceLink: A Lightweight, Robust and Secure Communication Link for Small Satellites

Mr Kehe Wang: The Metadata Development of Space Weather Services and a Proposal of a United Australian Space Research Metadata Portal

Prof Colin Waters: Global magnetic signature of the 2015 St Patricks day geomagnetic storm

Ian Whitchurch: The Barsoom Express : Earth orbit to Mars orbit in three months by solar electric propulsion

Dr Yang Yang: Schmidt-Kalman Filter and its Applications to Orbit Determination of Space Objects

Dr Jeanne Young: New Space Weather Services products using observations of the Earth's magnetic field and their relevance to the user community

Prof Kefei Zhang: An Advanced Near Real-Time GNSS Water Vapour Platform for severe weather and Climate Studies

Mr Yang Zhao: New Methods for Improving Two-line Element Outlier Detection Based on a Consistency Check

Posters

Posters are listed in alphabetical order of first author

Mr Akash Arora: Extending the Autonomous Science capabilities of planetary rovers through probabilistic models of domain knowledge

Professor Frances Bagenal: Pluto's interaction with its space environment

Miss Siti Aminah Bahari: Climatology of total electron content over Malaysia for the period of 2003–2014

Mr. Suraj Bijjahalli: A GNSS Integrity Augmentation System for reusable space vehicles

Dr. Helen E. A. Brand: Synchrotron Powder Diffraction for Planetary Sciences

Dr H. E. A. Brand: The Allende Meteorite: An Case Study For All The Family?

Dr Graziella Caprarelli: Results and interpretation of radar sounder MARSIS data over Lucus Planum, Mars.

Dr Graziella Caprarelli: STEM education and outreach activities with the MARVEL project

Dr Brett Carter: Next Generation Space Weather Forecasts

Dr Rowena Christiansen: A fresh look at the role of the human appendix in expeditionary medicine "from the far corners of the Earth to the stars": benivolem aut insidiator?

Prof Andrew Dempster: Low Earth Orbit Equatorial Synthetic Aperture Radar

Dr Steven Hobbs: The Little Blue Rover: Robotic Characterisation of a Mars Analogue Site in Arkaroola 111

Naveen Timothy Kodikara: Assessment on the Efficacy of Global Ionospheric Maps to Improve the Performance of Precise Point Positioning

Dr Vasily Lobzin: Automatic recognition of complex magnetic regions on the Sun

in SDO magnetogram images and prediction of flares: Techniques for the revised Flarecast

Damien J. Melis: Space traveller physique; considerations in commercial spacecraft cabin design

Mr Andrew Michaelson: Re-vitalising Australia's Space Industry

Dr Franklin Mills: Potential Impacts of Heterogeneous Chemistry on Venus' Mesosphere

Dr Dave Neudegg: The Ionosphere of Mars

Siddharth Pandey: Mars Society Australia and Ladakh: Astrobiology Science and Education Expedition in the Himalayas

Dr James Waldie: Further Evaluation of the Performance of Field Science in an Analogue EVA suit

Dr Siqi Zhang: How does prolonged magma-ocean solidification affect lunar evolution